MASTER COPY KEEP THIS COPY FOR REPRODUCTION PURPOSES

REPORT DOCUMENTATION PAGE

Form Approved
OMB No. 0704-0188

1. AGENCY USE ONLY (Leave blank)	2. REPORT DATE	3. REPORT TYPE AND DATES COVERED
	Mar 95	Final 22 Mar 91-21 Sep 94

4. TITLE AND SUBTITLE
Improved Interception Capability Through the Use of Transform Domain Processing

5. FUNDING NUMBERS
DAAL03-91-G-0071

6. AUTHOR(S)
L.B. Milstein

7. PERFORMING ORGANIZATION NAME(S) AND ADDRESS(ES)
University of California, San Diego
La Jolla, CA 92093

8. PERFORMING ORGANIZATION REPORT NUMBER

9. SPONSORING/MONITORING AGENCY NAME(S) AND ADDRESS(ES)
U.S. Army Research Office
P.O. Box 12211
Research Triangle Park, NC 27709-2211

10. SPONSORING/MONITORING AGENCY REPORT NUMBER
ARO 27754.4-EL

11. SUPPLEMENTARY NOTES
The views, opinions and/or findings contained in this report are those of the author(s) and should not be construed as an official Department of the Army position, policy, or decision, unless so designated by other documentation.

12a. DISTRIBUTION/AVAILABILITY STATEMENT
Approved for public release; distribution unlimited.

12b. DISTRIBUTION CODE

13. ABSTRACT *(Maximum 200 words)*

The research conducted during the course of this grant was devoted to two basic problems. The first was that of designing and analyzing an enhanced radiometer possessing the capability of intercepting a signal which is embedded in narrowband interference. The essence of the design was to precede the radiometer with a narrowband interference suppression filter; this allowed the receiver to null out most of the energy of the interference before it entered the radiometer, with the net result being an intercept receiver with much lower false alarm probability. The second major topic that was studied dealt with the design and performance analysis of code division multiple access (CDMA) systems for military communications. This topic was chosen because it complemented the former research area of interception, in the sense that the two together provided coverage of the essence of military communication needs (i.e., knowledge of the enemy's signaling, and security of one's own signaling). The research on CDMA included optimizing the chip rate of a direct sequence system when used over a frequency selective fading channel, and designing an enhanced coarse acquisition system to allow synchronization in the presence of narrowband interference.

SUBJECT TERMS
Intercept receiver, CDMA, Acquisition

15. NUMBER OF PAGES

16. PRICE CODE

17. SECURITY CLASSIFICATION OF REPORT	18. SECURITY CLASSIFICATION OF THIS PAGE	19. SECURITY CLASSIFICATION OF ABSTRACT	20. LIMITATION OF ABSTRACT
UNCLASSIFIED	UNCLASSIFIED	UNCLASSIFIED	UL

IMPROVED INTERCEPTION CAPABILITY THROUGH THE USE OF TRANSFORM DOMAIN PROCESSING

Final Report

1.0 Introduction

The research conducted during the course of this grant was devoted to two basic problems. The first was that of designing and analyzing an enhanced radiometer possessing the capability of intercepting a signal which is embedded in narrowband interference. The essence of the design is to precede the radiometer with a narrowband interference suppression filter; this allows the receiver to null out most of the energy of the interference before it enters the radiometer, with the net result being an intercept receiver with a much lower false alarm probability.

The second major topic that was studied dealt with the design and performance analysis of code division multiple access (CDMA) systems for military communications. This topic was chosen because it complemented the former research area of interception, in the sense that the two together provided coverage of the essence of military communication needs (i.e., knowledge of the enemy's signaling, and security of one's own signaling).

The specific research on CDMA had several components associated with it. These included optimizing the chip rate of a direct sequence system when used over a frequency selective fading channel, designing an enhanced coarse acquisition system to allow synchronization in the presence of narrowband interference (using techniques similar to those employed in the design of the intercept receiver), analyzing a parallel, coarse acquisition system to determine how its performance affects the capacity of a CDMA network, and designing a power control scheme for the base-to-mobile link of a cellular CDMA system.

In Section 2, we present an overview of each of these research areas. Section 3 lists the graduate students who received partial support from this grant, and Section 4 presents a complete listing of publications arising from this research. Finally, the appendices present documentation of the

topics overviewed in the second section.

2.0 Overview of Research Results

2.1 Enhanced Intercept Receiver

2.1.1 Transform Domain Processing

The problem that we address is that of intercepting a direct sequence BPSK waveform which is received in the presence of narrowband interference and thermal noise. The narrowband interference is modeled as a sinewave, and the receiver that we analyze is basically a radiometer, but with one major difference. Because the narrowband interference produces unwanted energy at the output of a classical radiometer, over and above that due to thermal noise, the interference has the effect of increasing the false alarm rate. To remedy this problem, we place a narrowband interference suppression filter in front of the radiometer to reject as much interference as possible before entering the radiometer.

The specific rejection filter that we analyze is known as a compressive receiver, the heart of which is a surface acoustic wave (SAW) device. Indeed, this type of receiver has appeared in the literature in the past. In [1], experimental results on performance are presented, which correspond to a single time segment of the waveform passing through the compressive receiver. In [2], the performance of a discrete-time system using baseband FFT's rather than SAW devices is analyzed. In our research, we analyze the SAW-based receiver of [1], but, as opposed to [1], we accumulate multiple outputs of the analog compressive receiver and make a final decision on whether-or-not the spread spectrum waveform is present on the basis of the cumulative test statistic. We prove that the cumulative test statistic is asymptotically normal.

Our research results corroborate those obtained experimentally in [1] and those obtained analytically in [2]. However, as indicated above, while those of both [1] and [2] correspond to just a single sweep of the real-time Fourier transform device, we have accumulated a test statistic over multiple sweeps. From an operational point-of-view, this means that a system which cannot achieve the desired performance with a single sweep can be designed to achieve its performance

goal by independently choosing the sweep time (typically determined by the technology limitations of whatever Fourier transform device the system employs) and the overall integration time.

Our principal analytical contribution is that the test statistic is asymptotically Gaussian. Our principal system-level contribution is that for a given probability of detection, the enhanced radiometer that we have analyzed exhibits a much smaller false alarm probability than does the classical radiometer. The details are presented in Appendix A.

2.1.2 Wavelet Transform

As described in Section 2.1.1, transform domain processing can be utilized to suppress undesired interference and, consequently, improve system performance. Since traditional applications requiring transform domain processing perform excision only in the Fourier domain, one of the main objectives of this phase of our research was to extend transform domain processing to include wavelets as the basis functions. Specifically, the use of wavelets in the excision of jamming signals from spread spectrum communications systems was investigated. Simulations were performed using several basis functions for a spread spectrum receiver experiencing narrowband jamming, and results were compared with conventional Fourier domain processing. Furthermore, implementation of the exciser using multirate digital filters was considered. An intercept receiver which employed wavelet transform domain excision was also described. The receiver detected DS-BPSK spread spectrum signals in the presence of narrowband interference by employing adaptive interference rejection techniques. The improvement in the system performance over that of conventional radiometric detection was shown by presenting results of probability of detection versus probability of false alarm. Appendix B presents the details of the analysis.

2.2 CDMA for Secure Communications

2.2.1 Optimum Chip Rate for CDMA Systems

2.2.1.1 Channel Characterization and Performance Analysis

This research task emphasized the performance of a direct sequence code division multiple access system operating over a frequency selective fading channel. This topic was chosen because, in recent years, there has been considerable interest in the application of CDMA techniques to wireless communications. CDMA can potentially accommodate more users than either TDMA or FDMA, because as additional users are activated, the system performance as seen by any single user is degraded only slightly; thus, as long as the increase in BER is tolerable, the already - established links remain operational. Another advantage of CDMA is that there are no requirements for precise time or frequency coordination among users as in TDMA or FDMA. Furthermore, CDMA offers the usual benefits associated with spread spectrum systems such as interference rejection/suppression (which is what causes the 'graceful' degradation mentioned above) and multipath mitigation.

While there has been much work on this topic in the past, most authors have assumed either Rayleigh or Rician statistics for the channel. However, empirical data exists which suggests that path fading statistics, especially for the initial (shortest) paths, are more adequately described by a Nakagami, or m-distribution with parameter m=0.75, (which is worse than Rayleigh, for which m=1).

In our research, a channel model incorporating Nakagami multipath fading is developed and the BER performance of a DS - CDMA system operating through it using coherent demodulation is analyzed. For the particular cases of interest (m=1 and m=0.75), the fading statistics do not contain a specular component; therefore, in order to demodulate coherently, the implicit assumption is made that some type of carrier recovery and/or fade-mitigation technique is used. One method that has been found effective in combatting multipath Rayleigh fading (and providing coherent demodulation) is the simultaneous transmission of one or more inband or adjacent-band pilot tones. The receiver considered is a RAKE receiver with a variable number of taps to allow for varying degrees of diversity. The amount of improvement obtainable by channel coding is also investigated using a rate 1/2, constraint length 7 convolutional code and Viterbi

decoding. We modeled the channel as having an exponentially decaying multipath intensity profile, and found that significant improvement in capacity resulted from using the diversity. However, when the multipath intensity profile had a fast decay, the paths with low average strengths provided little information relative to the initial paths. The derivations and results are presented in Appendix C.

2.2.1.2 Comparison of Narrowband versus Broadband CDMA

A hybrid FDMA/CDMA scheme operating over a frequency selective Rayleigh fading channel was analyzed. The performance of the hybrid system was compared with that of a wideband CDMA system occupying the same total bandwidth. Both coherent and noncoherent modulation formats were investigated; it was found that, for coherent modulation with a RAKE receiver, wideband CDMA had greater capacity than did the hybrid. However, for the noncoherent modulation formats (either DPSK or square-law detected orthogonal signaling), a hybrid system can have a greater capacity if a high channel error rate can be tolerated. Otherwise, a wideband system remains optimal.

More specifically, the hybrid system treats each segment, or sub-spectrum, as a stand-alone CDMA system, independent of the other segments, as shown in Figure 1. Using the multipath fading channel model and analysis described in [3], and making some reasonable assumptions on the relationships between signal bandwidth and 1) the number of resolvable paths, 2) the path powers, and 3) the path decay rate, the following set of conclusions can be drawn:

(i) For coherent reception where each system uses as many paths as it is capable of resolving, the wideband system yields greater capacity.

(ii) If the wideband coherent system is limited by complexity constraints so that it cannot make constructive use of all resolvable paths, a hybrid system can yield a larger capacity.

(iii) As the decay rate of the multipath intensity profile (MIP) increases to a sufficiently large value, all systems will perform the same, since only one resolvable path is

available. This implies that the wideband system will only attempt to resolve a single path, since the resolution of additional paths will yield increased noise and multiple access interference.

(iv) For binary noncoherent modulation formats, at high channel error rates and small values of the MIP decay factor, a hybrid yields higher capacity, whereas at low channel rates, wideband CDMA is superior.

Finally, in terms of the most obvious applications, namely voice and data, the above conclusions can be restated in the following manner. For coherent reception, wideband CDMA is superior for either application unless a complexity constraint is imposed so that the receiver cannot take advantage of all the multipath it is capable of resolving. For DPSK with equal-gain combining, a hybrid is superior for voice if the multipath decay factor is small; if the decay factor is large, and each system users the proper number of resolvable paths, there is not much difference in performance. However, for data communications, wideband CDMA yields greater capacity. Appendix D presents the complete analysis.

2.2.2 Enhanced Coarse Acquisition System

The coarse acquisition performance of a CDMA overlay system operating in a mobile communications environment was analyzed. Specifically, a CDMA system, supporting communication between several mobile units and one base station, was overlaid in frequency on an existing narrowband BPSK user. At the CDMA base-station receivers, narrowband interference rejection filters were used to suppress the BPSK interference. It was demonstrated that the presence of BPSK interference did not severely affect the acquisition performance when the ratio of BPSK to CDMA bandwidth was small. As the ratio becomes larger, the acquisition performance degrades, but nonetheless, the use of the interference rejection filter significantly decreases the time to acquire. The details are presented in Appendix E.

2.2.3 Effect of Acquisition on CDMA Capacity

Using a parallel, noncoherent acquisition system, the performance of the reverse link of a CDMA spread spectrum system, incorporating the effects of additive white Gaussian noise and multiple access interference was derived. It was shown that acquisition performance requirements can limit the overall capacity of a CDMA spread spectrum system. Therefore, overall capacity calculations should take into account both acquisition and post acquisition-based performance criteria. It was also shown that the period of the spreading sequence is an important factor in determining acquisition performance. Increasing the observation interval does not significantly improve the performance when integrating over multiple spreading sequence periods. For details of the analysis, see Appendix F.

2.2.4 Forward Link Power Control

Our last topic has to do with the design and analysis of a power control scheme for the forward link (i.e., the base-to-mobile link) of a cellular CDMA system. The power control scheme was designed to ensure that each user in a given cell has nominally the same performance, irrespective of the user's location. Because of the presence of intercell interference, a mobile located at the boundary of a cell experiences more interference than does a mobile near the center of the cell. To equalize the performance, an approximate bit error rate (BER) expression was derived as a function of the mobile's position; the power control law resulted by forcing the BER to be independent of the location. Specific details are presented in Appendix G.

References

[1] J. P. Gevargiz, P. K. Das and L. B. Milstein, Adaptive narrowband interference rejection in a DS spread spectrum intercept receiver using transform domain signal processing techniques. *IEEE Transactions on Communications,* COM-37, pp. 1359-1366, Dec. 1989.

[2] S. Davidovici, and E. G. Kanterakis, Radiometric Detection-Sequence Spread-Spectrum Signals Using Interference Excision. *IEEE Journal on Selected Areas in Communications,* Vol. 7, No. 4, pp. 576-589, May 1989.

[3] T. Eng and L. B. Milstein, "Coherent DS-CDMA Performance in Nakagami Multipath Fading," submitted for publication.

3.0 Graduate Students Supported

3.1 The following graduate students at UCSD received partial support during the course of this grant:

1. Lynn Gottesman (PhD received 6/93)
2. Roland Rick (continuing PhD student)
3. Tom Eng (continuing PhD student)

3.2 The following graduate students at RPI received partial support during the course of this grant:

1. David Eng
2. Kyung J. Han
3. Jeffrey Koay
4. Mike Mettke
5. David Permana
6. Paul Rencibia

4.0 List of Publications

1. Eng, T., and L.B. Milstein, Performance of DS-CDMA in frequency selective Nakagami fading. *1992 IEEE Military Comm. Conf.*, pp. 4.5.1 - 4.5.5, Oct. 1992.
2. Eng, T., and L.B. Milstein, Capacities of hybrid FDMA/CDMA systems in multipath fading. *1993 IEEE Military Comm. Conf.*, pp. 753-757, Oct. 1993.
3. Zorzi, M., and L.B. Milstein, Power control on the forward link in cellular CDMA. *IEEE International Zurich Conference on Communications, March 1994.*

4. Rick, R.R., and L.B. Milstein, Noncoherent parallel acquisition in CDMA spread spectrum system. *1994 International Conference on Communications,* pp. 1422-1426, May 1994.

5. Zorzi, M., and L.B. Milstein, Power control and coding in a cellular CDMA mobile ratio system. *1994 International Conference on Communications,* pp. 1629-1633, May 1994.

6. Medley, M., G. Saulnier, and P. Das, Applications of wavelet transforms in spread spectrum communication systems. *SPIE Vol. 2242, Wavelet Applications,* pp. 54-68, 1994.

7. Eng, T., and L.B. Milstein, Capacities of hybrid FDMA/CDMA systems in multipath fading. *IEEE Journal on Selected Areas in Comm.,* June 1994.

8. Gottesman, L.D., and L.B. Milstein, The coarse acquisition performance of a CDMA overlay system. Accepted in *IEEE Journal on Selected Areas in Comm.*

9. Masry, E., and L.B. Milstein, Enhanced signal interception in the presence of interference. Accepted in *IEEE Trans. Comm.*

10. Zorzi, M., and L.B. Milstein, Optimal power control in a cellular CDMA mobile radio system. Submitted to *Trans. on Vehicular Technology.*

11. Eng, T., and L.B. Milstein, Coherent DS-CDMA performance in Nakagami multipath fading. Submitted to *IEEE Trans. Comm.*

12. Mettke, M., M. Medley G. Saulnier, and P. Das, Wavelet transform excision using IIR filters in spread spectrum communication systems. Accepted in *Proceedings of Globecom, 1994.*

Appendix A

ENHANCED SIGNAL INTERCEPTION IN THE PRESENCE OF INTERFERENCE

Elias Masry Laurence B. Milstein

Department of Electrical and Computer Engineering

University of California, at San Diego

La Jolla, CA 92093

Abstract

In this paper, we consider the problem of intercepting a direct sequence spread spectrum waveform which is embedded in both narrowband interference and additive white Gaussian noise. The receiver we analyze is a broadband radiometer which has been enhanced in the following manner: Prior to entering the square-law device in the radiometer, the received waveform is passed through a transform domain processor which serves as a notch filter to null out the narrowband interference before it can contribute unwanted energy to the output of the radiometer. A central-limit theorem is established for the receiver's output which forms the basis for analyzing the performance of the receiver. For various combinations of system parameters, numerical results are presented in the form of receiver operating characteristics.

This work was partially supported by the Office of Naval Research under Grant N00014-90-J-1175 and by the Army Research Office under Grant DAAL03-91-G-0071.

1. Introduction

The problem that we address in this paper is that of intercepting a direct sequence BPSK waveform which is received in the presence of narrowband interference and thermal noise. The narrowband interference is modeled as a sinewave, and the receiver that we analyze is basically a radiometer, but with one major difference. Because the presence of the narrowband interference produces unwanted energy at the output of a classical radiometer, over and above that due to thermal noise, the interference has the effect of increasing the false alarm rate. To remedy this problem, we place a narrowband interference suppression filter in front of the radiometer to reject as much interference energy as possible before entering the radiometer.

The specific rejection filter that we analyze is known as a compressive receiver, the heart of which is a surface acoustic wave (SAW) device ([1], [2]). Indeed, this type of receiver has appeared in the literature in the past. In [3], experimental results on performance are presented, which correspond to a single time-segment of the waveform passing through the compressive receiver. In [4], the performance of a discrete-time system using baseband FFT's rather than SAW devices is analyzed. In this paper, we analyze the SAW-based receiver of [3], but, as opposed to [3], we accumulate multiple outputs of the analog compressive receiver and make a final decision on whether-or-not the spread spectrum waveform is present on the basis of the cumulative test statistic. We prove that the cumulative test statistic is asymptotically normal which facilities the performance analysis of the proposed system.

2. System Description

A block diagram of the receiver is shown in Fig. 1. The received waveform is given either by

$$H_1\colon\ r(t) = APN(t)\cos\omega_0 t + B\cos(\omega_1 t + \Theta) + n_W(t) \tag{1a}$$

or

$$H_0\colon\ r(t) = B\cos(\omega_1 t + \Theta) + n_W(t)\,. \tag{1b}$$

That is, we assume we receive either a broadband direct sequence (DS) spread spectrum waveform embedded in narrowband interference plus additive white Gaussian noise (AWGN), or just the

interference plus noise; it is the function of the receiver to determine when the DS signal is present.

In (1), $PN(t)$ is the spreading sequence; the data on the signal is ignored because the combination of the data and the spreading sequence is modeled as just another spreading sequence operating at the same chip rate. Also in (1), A and B are constant amplitudes, Θ is a random phase uniformly distributed over $(-\pi, \pi)$ and $n_W(t)$ is AWGN of two-sided spectral density $\frac{\eta_0}{2}$.

The receiver works in the following manner: The input waveform is divided into T second intervals; all odd intervals are processed in the lower branch of the receiver, and all even segments are routed to the upper branch. Consider, for example, the upper branch. The SAW device, whose impulse response is $\cos(\omega_0 t + \beta t^2)\, P_{T_1}(t)$, where β is a constant and

$$P_a(x) = \triangleq \begin{cases} 1 & 0 \le x \le a \\ 0 & \text{elsewhere}, \end{cases} \tag{2}$$

can be envisioned as a tapped-delay line with length T_1 seconds. For reasons detailed in references such as [1] and [5], we set $T_1 = 2T$. Then, if a time-limited waveform of duration T seconds enters the device at say, $t = 0$, the useful output of the SAW device is from $t = T$ to $t = 2T = T_1$, and with $a(t)$ given by (3) below, that output can be shown to be the Fourier transform of the input over the frequency range $\omega \in [2\beta T,\ 2\beta T_1]$. That is, if, for $t \in [0, T]$,

$$a(t) = \cos[\omega_0 t - \beta t^2], \tag{3}$$

then the output of the SAW device can be shown to be ([1], [5])

$$g_0(t) = \frac{1}{2}\cos(\omega_0 t + \beta t^2) \int_0^T r(\tau) h(t) \cos 2\beta t \tau \, d\tau$$

$$+ \frac{1}{2}\sin(\omega_0 t + \beta t^2) \int_0^T r(\tau) h(t) \sin 2\beta t \tau \, d\tau, \; T \le t \le 2T \tag{4}$$

where $h(t)$ is a data tapering window. Note that the two integral expressions represent the real and imaginary parts, respectively, of the tapered Fourier transform of the time-limited segment of $r(t)$ in the interval [0, T]. The reason for the "ping-ponging" of even and odd intervals to the upper and lower branches is that as one given T-second segment is being processed, an adjacent T-second segment is

prevented from causing interference by being routed to the alternate branch.

In light of the above description, the general expressions for $a(t)$ and $b(t)$ are as follows:

$$a(t) = \sum_{i=0}^{\infty} \cos\left[\omega_0(t-2iT) - \beta(t-iT)^2\right] P_T(t-2iT) \tag{5}$$

and

$$b(t) = \sum_{i=1}^{\infty} \cos\left[\omega_0(t-(2i-1)T) - \beta(t-(2i-1)T)^2\right] P_T(t-(2i-1)T) \tag{6}$$

These timing functions are shown in Fig. 2a and Fig. 2b, respectively. Given the Fourier transform interpretation of the outputs of the SAW devices, it is clear that if a wideband DS waveform plus narrowband interference is used as the input to the system, then the output looks qualitatively as shown in Fig. 2c. Further, if one wanted to suppress the narrowband interference, one could multiply the waveform shown in Fig. 2c by that shown in Fig. 2d, thus producing the signal displayed in Fig. 2e. It is the purpose of the function $H_c(t)$ in Fig. 1 to accomplish this interference suppression. Specifically, if we define

$$H_0(t) \triangleq \begin{cases} 0\ , & \dfrac{\omega_1 - \Delta/2}{2\beta} \le t \le \dfrac{\omega_1 + \Delta/2}{2\beta} \\ 1\ , & 0 \le t < \dfrac{\omega_1 - \Delta/2}{2\beta}\ ,\ \dfrac{\omega_1 + \Delta/2}{2\beta} < t \le T\ , \end{cases} \tag{7a}$$

then

$$H_c(t) = \sum_{i=1}^{\infty} H_0(t-iT) \tag{7b}$$

In words, $H_c(t)$ represents the action of a notch filter centered at the carrier frequency of the interference, ω_1, and having a notch-width of Δ rad/sec.

The remainder of components of Figure 1 essentially constitute a classical radiometer. The output $g_1(t)$ of the SAW devices is squared and integrated, and the final test statistic $g(MT)$ is compared to a threshold to determine whether-or-not the DS signal is present.

Notice that the block labelled "LPF" is shown just to explicitly remove double frequency terms at the output of the squaring device. Its presence is not really needed, since the integrator serves as a lowpass filter. From (4), it follows that the input to the integrator, over $[T, 2T]$, is given by

$$g_2(t) = \left\{ \left[\int_0^T h(\tau) r(\tau) \cos 2\beta t \tau \, d\tau \right]^2 + \left[\int_0^T h(\tau) r(\tau) \sin 2\beta t \tau \, d\tau \right]^2 \right\} H_c^2(t)$$

$$= \left| \int_0^T h(\tau) r(\tau) \, e^{-i 2\beta t \tau} \, d\tau \right|^2 H_c^2(t) ,$$

and in general, over the interval $[(j+1)T, (j+2)T]$, we have

$$g_{2,j}(t) = \left| \int_0^T h(\tau) r(\tau + jT) \, e^{-i 2\beta (t - jT)} \, d\tau \right|^2 H_c^2(t), \quad (j+1)T \le t \le (j+2)T, \quad j = 0, 1, \cdots \tag{8}$$

where we used the fact that the data tapering window is assumed periodic with period T. Typical examples for $h(t)$ over $[0, T]$ are

$$h(t) = 1 \quad , \quad h(t) = 1 - \frac{2}{T} \left| t - \frac{T}{2} \right| .$$

The final test statistic is given by

$$g(MT) = \sum_{j=0}^{M-2} \int_{(j+1)T}^{(j+2)T} g_{2,j}(t) \, dt \tag{9}$$

and in a normalized form as

$$S_M = \frac{1}{M-1} \, g(MT) . \tag{10}$$

3. System Analysis

By (9) and (10) we have

$$S_M = \frac{1}{M-1} \sum_{j=0}^{M-2} \int_0^T g_{2,j}(u + (j+1)T) \, du$$

$$= \frac{1}{M-1} \sum_{j=0}^{M-2} \int_0^T \tilde{g}_{2,j}(u)\, du$$

where

$$\tilde{g}_{2,j}(t) = \left| \int_0^T h(\tau)\, r(\tau + jT)\, e^{-i2\beta(t+T)\tau}\, d\tau \right|^2 H_c^2(t), \quad 0 \le t \le T. \tag{11}$$

Let

$$X_j \triangleq \int_0^T \tilde{g}_{2,j}(u)\, du \quad , \quad j = 0, 1, \cdots \tag{12}$$

so that

$$S_M = \frac{1}{M-1} \sum_{j=0}^{M-2} X_j . \tag{13}$$

We need to find the distribution of S_M. Under H_1 write

$$r(t) = c(t, \Theta) + n_W(t) \tag{14}$$

where

$$c(t, \Theta) = A\, PN(t) \cos \omega_0 t + B \cos(\omega_1 t + \Theta). \tag{15}$$

Then

$$\tilde{g}_{2,j}(t) = \left| q_{1,j}(t, \Theta) + q_{2,j}(t) \right|^2 H_c^2(t) \tag{16}$$

where

$$q_{1,j}(t; \Theta) = \int_0^T h(\tau) c(\tau + jT, \Theta)\, e^{-i2\beta(t+T)\tau}\, d\tau \tag{17a}$$

$$q_{2,j}(t) = \int_0^T h(\tau)\, n_W(\tau + jT)\, e^{-i2\beta(t+T)\tau}\, d\tau . \tag{17b}$$

We note that

$$E[q_{2,j}(t)\, q_{2,k}^*(s)] = \frac{\eta_0}{2} \int_0^T h^2(\tau)\, e^{-i2\beta(t-s)\tau}\, d\tau\, \delta_{j,k} \tag{18}$$

so that the processes $\{q_{2,j}(t)\}_{j=0}^{\infty}$ are independent complex-valued Gaussian processes with zero means and a common covariance function

$$R_2(u) = E[q_{2,j}(u+t)q_{2,j}^*(t)] = \frac{\eta_0}{2}\int_0^T h^2(\tau)\, e^{-i2\beta u\tau}\, d\tau\,. \tag{19}$$

For future reference we also note that

$$R_2^+(u,\, v) \triangleq E[q_{2,j}(u)\, q_{2,j}(v)] = \frac{\eta_0}{2}\int_0^T h^2(\tau) e^{-i2\beta(u+v+2T)\tau}\, d\tau \tag{20}$$

which is a function of $u+v$. It follows, that given Θ, the random variables X_j's are conditionally independent.

We now compute the conditional mean and variance of the statistic S_M given Θ. We have by (12) (13) and (16) that

$$E[S_M \mid \Theta=\theta] = \frac{1}{M-1}\sum_{j=0}^{M-2}\mu_j(\theta) \tag{21}$$

where

$$\mu_j(\theta) = E[X_j \mid \Theta=\theta] = \int_0^T \{\mid q_{1,j}(u,\,\theta)\mid^2 + E\mid q_{2,j}(u)\mid^2\}\, H_c^2(u)\, du$$

and by (19)

$$\mu_j(\theta) = \int_0^T \mid q_{1,j}(u,\,\theta)\mid^2 H_c^2(u)\, du + \frac{\eta_0}{2}\int_0^T h^2(\tau)\, d\tau \int_0^T H_c^2(u)\, du$$

$$= \int_0^T \mid q_{1,j}(u,\,\theta)\mid^2 H_c^2(u)\, du + \frac{\eta_0}{2}\left(T - \frac{\Delta}{2\beta}\right)\int_0^T h^2(\tau)\, d\tau\,. \tag{22}$$

Next

$$\sigma_j^2(\theta) = \mathrm{var}[X_j \mid \Theta=\theta]$$

$$= \int_0^T\int_0^T H_c^2(u)\, H_c^2(v)\, \mathrm{cov}\{\mid q_{1,j}(u,\,\theta)+q_{2,j}(u)\mid^2,\ \mid q_{1,j}(v,\,\theta)+q_{2,j}(v)\mid^2\}\, du\, dv \tag{23a}$$

and by the derivations in Appendix A

$$\sigma_j^2(\theta) = \int_0^T \int_0^T H_c^2(u) H_c^2(v) \{2Re[q_{1,j}^*(u,\theta) q_{1,j}^*(v,\theta) R_2^+(u+v)]$$

$$+2\,\mathrm{Re}[q_{1,j}^*(u,\theta) q_{1,j}(v,\theta) R_2(u-v)]$$

$$+[\,|R_2(u-v)|^2 + |R_2^+(u+v)|^2]\}\,du\,dv$$

$$\equiv a_j'(\theta) + a_j''(\theta) + a''' \tag{23b}$$

and since the X_j's are conditionally independent random variables we have

$$\mathrm{var}[S_M \mid \Theta = \theta] = \frac{1}{(M-1)^2} \sum_{j=0}^{M-2} \sigma_j^2(\theta)\,. \tag{24}$$

If we knew the functional form of the conditional distribution of S_M given Θ we could evaluate the performance of the radiometer by

$$P_d = \frac{1}{2\pi} \int_{-\pi}^{\pi} P[S_M > \gamma \mid \Theta = \theta]\,d\theta \tag{25}$$

and

$$P_{f_a} = \frac{1}{2\pi} \int_{-\pi}^{\pi} P[S_M > \gamma \mid \Theta = \theta, A = 0]\,d\theta \tag{26}$$

where γ is the detector's threshold. A closed-form expression for the conditional distribution of S_M given Θ is impossible to obtain since the distributors of the X_j's are not known. Instead we prove that the conditional distribution of S_M given Θ is asymptotically Gaussian for large M. This result, along with the expressions (21) - (22) and (23) - (24) for the conditional mean and variance of S_M, allow us to compute the probability of detection and of false alarm of the radiometer via equations (25) and (26), i.e., if $\Phi(x)$ is the standard normal distribution (with zero mean and unit variance) then, for large M, we have

$$P[S_M > \gamma \mid \Theta = \theta] = 1 - \Phi\left[\frac{\gamma - E[S_M \mid \Theta = \theta]}{\mathrm{var}^{1/2}[S_M \mid \Theta = \theta]}\right]$$

and

$$P[S_M > \gamma \mid \Theta = \theta, A = 0] \simeq 1 - \Phi\left[\frac{\gamma - E[S_M \mid \Theta = \theta, A = 0]}{\text{var}^{1/2}[S_M \mid \Theta = \theta, A = 0]}\right].$$

We now establish the following result.

THEOREM. Given $\Theta = \theta$ we have that the normalized random variable

$$\frac{S_M - E[S_M \mid \Theta = \theta]}{\text{var}^{1/2}[S_M \; \Theta = \theta]}$$

converges in distribution, as $M \to \infty$, to a zero-mean unit variance Gaussian random variable.

Proof. Since the $X_j's$ are conditionally independent (given $\Theta = \theta$) it suffices to show, by Lyapounov's condition [6], that for some $\nu > 2$ we have

$$\frac{\sum_{j=0}^{M-2} E \mid X_j - \mu_j(\theta) \mid^{\nu}}{\left[\sum_{j=0}^{M-2} \sigma_j^2(\theta)\right]^{\nu/2}} \to 0 \quad \text{as } M \to \infty . \tag{27}$$

By the c_r- inequality [6] we have

$$E \mid X_j - \mu_j(\theta) \mid^{\nu} \le 2^{\nu-1} \{E \mid X_j \mid^{\nu} + \mid \mu_j(\theta) \mid^{\nu}\} . \tag{28}$$

By (15) and (17a)

$$\mid q_{1,j}(t, \theta) \mid \le (A+B) \int_0^T \mid h(\tau) \mid d\tau \equiv D_1 < \infty \tag{29}$$

so that by (22)

$$\mu_j(\theta) \le D_1^2 \int_0^T H_c^2(u)\, du + \frac{\eta_0}{2}\,(T - \frac{\Delta}{2\beta}) \int_0^T h^2(\tau)\, d\tau = D_1^2 (T - \frac{\Delta}{2\beta}) + \frac{\eta_0}{2}\,(T - \frac{\Delta}{2\beta}) \int_0^T h^2(\tau)\, d\tau$$

$$\equiv D_2 < \infty \quad \text{for all } j . \tag{30}$$

Next by (12) and (16)

$$X_j = \int_0^T \mid q_{1,j}(u, \theta) + q_{2,j}(u) \mid^2 H_c^2(u)\, du$$

$$\leq 2\{\int_0^T |q_{1,j}(u,\theta)|^2 H_c^2(u)\,du + \int_0^T |q_{2,j}(u)|^2 H_c^2(u)\,du\}$$

and by (29)

$$X_j \leq 2\{TD_1^2 + \int_0^T |q_{2,j}(u)|^2\,du\}. \tag{31}$$

By the c_r- inequality

$$E|X_j|^\nu \leq 2^\nu\{(TD_1^2)^\nu + E(\int_0^T |q_{2,j}(u)|^2\,du)^\nu\}. \tag{32}$$

Now with

$$Y_j \triangleq \int_0^T |q_{2,j}(u)|^2\,du$$

we note that $q_{2,j}(t)$ is a stationary complex-valued Gaussian process with zero mean and covariance function $R_2(u)$ - which does not depend on j -. Thus $E|Y_j|^\nu$ exists for all $\nu > 2$ and does not depend on j. Put $E|Y_j|^\nu = G_\nu < \infty$. It then follows by (32) that

$$E|X_j|^\nu \leq 2^\nu\{(TD_1^2)^\nu + G_\nu\}. \tag{33}$$

Thus by (28), (30), and (33) we have

$$E|X_j - \mu_j(\theta)|^\nu \leq 2^{\nu-1}\{2^\nu[(TD_1^2)^\nu + G_\nu] + D_2^\nu\} \equiv D_3 < \infty$$

for all $j \geq 0$, so that

$$\sum_{j=0}^{M-2} E|X_j - \mu_j(\theta)|^\nu \leq (M-1)D_3. \tag{34}$$

Finally we examine the denominator in (27). By (23) we have

$$\sigma_j^2(\theta) = a'_j(\theta) + a''_j(\theta) + a'''.$$

It is shown in Appendix B that

$$a'_j(\theta) + a''_j(\theta) \geq 0 \tag{35}$$

and thus

$$\sum_{j=0}^{M-2} \sigma_j^2(\theta) \geq (M-1)\, a''' . \tag{36}$$

Thus by (31) and (33)

$$\frac{\sum_{j=0}^{M-2} E\,|X_j - \mu_j(\theta)|^{\nu}}{\left[\sum_{j=0}^{M-2} \sigma_j^2(\theta)\right]^{\nu/2}} \leq \frac{(M-1)D_3}{(M-1)^{\nu/2}\,(a''')^{2/\nu}} \quad \to 0$$

as $M \to \infty$ for every $\nu > 2$. This completes the proof of the theorem. □

4. Numerical Results

The equations presented in the previous section were evaluated numerically, and we present below some results which illustrate the performance of the system. The key parameters were chosen in the following manner: The chip duration T_c was arbitrarily set equal to unity, and the remaining time parameters, as well as the frequency parameters, were defined relative to T_c. For example, we assume the bandwidth of the spread spectrum signal is $2\pi(2/T_c)$ rads/sec. Since we transform from $2\beta T$ to $2\beta T_1 = 4\beta T$, then, with ω_0 the carrier frequency, we want $2\beta T = \omega_0 - \frac{2\pi}{T_c}$ and $4\beta T = \omega_0 + \frac{2\pi}{T_c}$. Therefore ω_0 is equal to $3\beta T$, and $2\beta T = 4\pi/T_c$ or $\beta = \frac{2\pi}{TT_c}$. Since the number of chips per observation interval, n, equals T/T_c, we have $\beta = \frac{2\pi}{(nT_c^2)}$ and $\omega_0 = \frac{6\pi}{T_c}$. Finally, the spreading sequence was a maximal-length shift register sequence corresponding to a 15th degree polynomial.

Before evaluating the general form of these expressions, we set both the interference level B and the notch width Δ to zero. This left us with what is essentially a classical radiometer operating in AWGN, the performance of which is well known ([7]). Indeed, we checked our results for this special case with those existing in the literature and found good agreement, thus giving us confidence as to the accuracy of our numerical results.

Consider now the performance of the system with nonzero interference. We assume that the data tapering window $h(t) = 1$ over $[0, T]$, which does not provide any tapering of the data. Better

performance is expected for smooth $h(t)$ which is symmetric around $T/2$ and vanishes at the end points $\{0, T\}$, e.g. for $h(t) = 1 - \frac{2}{T} \mid t - \frac{T}{2} \mid$. Consider first Fig. 3, which is the receiver operating characteristic (ROC) for the system (i.e., a plot of probability of detection, P_d, versus probability of false alarm, P_{f_a}). There are four curves shown in Fig. 3, parameterized by the ratio of interference power-to-signal power, denoted by JSR, where

$$JSR = \frac{B^2}{A^2}.$$

All curves correspond to $n = 100$ chips per integration interval, $M = 100$ such intervals, $\omega_1 = \omega_0$ (i.e., the interference frequency equals the carrier frequency of the DS waveform), and the notch width $\Delta = \frac{2}{T}(2\pi)$ (e.g., the entire mainlobe of the transformed interference is being suppressed).

By way of comparison, Figure 4 shows the same results for the $JSR = 10\,dB$ curve, but without the suppression filter. For example, if one looks at the point $P_d = 0.9$ on both curves, one finds that without the suppression filter, $P_{f_a} = 10^{-3}$, whereas with the suppression filter, $P_{f_a} = 6\times10^{-7}$, or a decrease of over three orders of magnitude.

If one now looks at the ROC's shown in Fig. 5, which correspond to the same four curves of Fig. 3, except that now $\omega_1 = \omega_0 + \frac{\beta T}{2}$ (i.e., the frequency of the interference is offset from the carrier frequency of the spread spectrum waveform, and thus so is the center of the notch filter), it is seen that there is a relatively slight improvement in performance. This is predictable, since when the interferer is offset from the carrier frequency of the DS waveform, less energy is notched out of the mainlobe of the signal-of-interest in the process of suppressing the interference.

Finally, consider the effect of varying M, and n, but keeping the product Mn constant. That is, the total number of chips over which the received waveform is observed is Mn. Since a radiometer is essentially an energy detector, one would not expect significant variation in performance as n and M vary as long as the product is held constant. To see this, consider Figs. 6 and 7, which correspond to $JSR = 10\,dB$ and $20\,dB$, respectively. Each figure has two curvers on it, one corresponding to $M = 10$, $n = 1000$ and $\omega_1 = \omega_0$, and the other corresponding to $M = 50$, $n = 200$, and $\omega_1 = \omega_0$. It can be seen that

for both values of JSR, the performance of the system is insensitive to changes in either M or n as long as the product is constant. Also, for $JSR = 20\,dB$, if one removes the suppression filter, the curve of Fig. 8 results for either ($M = 10$, $n = 1000$) or ($M = 50$, $n = 200$). Once gain, if one compares the curve of Fig. 8 to those of Fig. 7, one sees the tremendous improvement in system performance which is achievable by employing the suppression filter.

5. Conclusions

In this paper, we have presented an analysis of an enhanced radiometer designed to intercept a direct sequence spread spectrum waveform received in the presence of narrowband interference plus thermal noise. The enhancement over the classical radiometer is a SAW-based narrowband interference suppression filter, which is placed in the system prior to the squaring device. This results in significantly less energy due to the interference affecting the final test statistic. In turn, for a given probability of detection, the enhanced radiometer exhibits a much smaller false alarm probability than does the classical radiometer.

Our current results corroborate those obtained experimentally in [3] and those obtained analytically in [4]. However, while those of both [3] and [4] correspond to just a single sweep of the real-time Fourier transform device, we have accumulated a test statistic over multiple sweeps. From an operational point-of-view, this means that a system which cannot achieve the desired performance with a single sweep can be designed to achieve its performance goal by independently choosing the sweep time (typically determined by the technology limitations of whatever Fourier transform device it employs) and the overall integration time.

Our principal analytical contribution is that the test statistic is asymptotically Gaussian, for any tapering window $h(t)$. We compare this to the analytical results of [3] where a discrete-time transform domain FFT-based radiometer is analyzed: The distribution of the test statistic is given as an infinite Hermite expansion (Gram-Charlier) whose coefficients $\{\alpha_j\}_{j=0}^{\infty}$ are linear combinations of the cumulants of the test statistic [3, eq. (A.22)]. A closed-form expression for the distribution of the test statistic is not available except when the discrete-time tapering window is flat [3, eq. (72)]. By using multiple sweeps M

of the real-time Fourier transform SAW-device, we were able to establish that for large M, the distribution of the test statistic is in fact Gaussian.

APPENDIX A

Proof of (23b). Put

$$C = q_{1,j}(u, \theta) \quad , \quad D = q_{1,j}(v, \theta)$$

$$X = q_{2,j}(u) \quad , \quad Y = q_{2,j}(v)$$

and note that X and Y are jointly Gaussian complex-valued random variables with zero means. Then

$$\mathrm{cov}\{\,|C+X|^2,\ |D+Y|^2\} = E\,|(C+X)(D+Y)|^2 - E\,|C+X|^2\,E\,|D+Y|^2\,. \qquad \text{(A.1)}$$

Using the fact that

$$E[X|Y|^2] = 0\,,\ E[Y|X|^2] = 0$$

and

$$E[\,|X|^2\,|Y|^2] - E\,|X|^2\,E\,|Y|^2 = E[XY]E[X^*Y^*] + E[XY^*]E[X^*Y]$$

we find, by expanding (A.1), that

$$\mathrm{cov}\{\,|C+X|^2,\ |D+Y|^2\} = 2\mathrm{Re}\{(CD)^*\,E[XY]\} + 2\mathrm{Re}\{CD^*\,E[X^*Y]\}$$

$$+\,|E[XY]|^2 + |E[XY^*]|^2$$

and (23b) follows from (23a), (19), and (20). □

APPENDIX B

Proof of (32). By (23b)

$$a_j'(\theta)+a_j''(\theta)=2\int_0^T\int_0^T H_c^2(u)\,H_c^2(v)\,\mathrm{Re}\{q_{1,j}^*(u,\theta)\,q_{1,j}^*(v,\theta)\,R_2^+(u,v)+q_{1,j}^*(u,\theta)\,q_{1,j}^*(v,\theta)\,R_2(u-v)\}\,du\,dv$$

but

$$R_2^+(u,v)=E\,[q_{2,j}(u)\,q_{2,j}(v)]$$

and

$$R_2(u-v)=E\,[q_{2,j}(u)\,q_{2,j}^*(v)]$$

so that

$$a_j'(\theta)+a_j(\theta)=2\int_0^T\int_0^T H_c^2(u)\,H_c^2(v)\,A_j(u,v,\theta)\,du\,dv \qquad \text{(A.2)}$$

where

$$A_j(u,v,\theta)=E\left\{\mathrm{Re}\left[q_{1,j}^*(u,\theta)\,q_{1,j}^*(v,\theta)\,q_{2,j}(u)\,q_{2,j}(v)+q_{1,j}^*(u,\theta)\,q_{1,j}(v,\theta)\,q_{2,j}(u)\,q_{2,j}^*(v)\right]\right\}$$

$$=E\left\{\mathrm{Re}[q_{1,j}^*(u,\theta)\,q_{2,j}(u)(2\,\mathrm{Re}[q_{1,j}^*(v,\theta)\,q_{2,j}(v)])]\right\}$$

$$=2E\left\{\mathrm{Re}[q_{1,j}^*(u,\theta)\,q_{2,j}(u)]\,\mathrm{Re}[q_{1,j}^*(v,\theta)\,q_{2,j}(v)]\right\}.$$

It then follows by (A.2) that

$$a_j'(\theta)+a_j''(\theta)=4E\left[\int_0^T H_c^2(u)\,\mathrm{Re}\left[q_{1,j}^*(u,\theta)\,q_{2,j}(u)\right]du\right]^2\geq 0\,.$$

References

[1] L. B. Milstein, and P. K. Das, An analysis of a real-time transform domain filtering digital communication system, Part I: Narrowband interference rejection. *IEEE Transactions on Communications*, Vol. COM.28, No. 6, pp. 816-824, June 1980.

[2] K. H. Li, and L. B. Milstein, On the use of a compressive receiver for signal detection. *IEEE Transactions on Communications*, COM-39, pp. 557-566, April 1991.

[3] J. P. Gevargiz, P. K. Das and L. B. Milstein, Adaptive narrowband interference rejection in a DS spread spectrum intercept receiver using transform domain signal processing techniques. *IEEE Transactions on Communications*, COM-37, pp. 1359-1366, Dec. 1989.

[4] S. Davidovici, and E. G. Kanterakis, Radiometric Detection of Direct-Sequence Spread-Spectrum Signals Using Interference Excision. *IEEE Journal on Selected Ares in Communications*, Vol. 7, No. 4, pp. 576-589, May 1989.

[5] L. B. Milstein, Interference rejection techniques in spread spectrum communications, *Proceedings of the IEEE*, pp. 657-671, June 1988.

[6] M. Loève, *Probability Theory*. Princeton: Van Nostrand, 1963.

[7] D. J. Nicholson, *Spread Spectrum Signal Design*. Rockville: Computer Science Press, 1988.

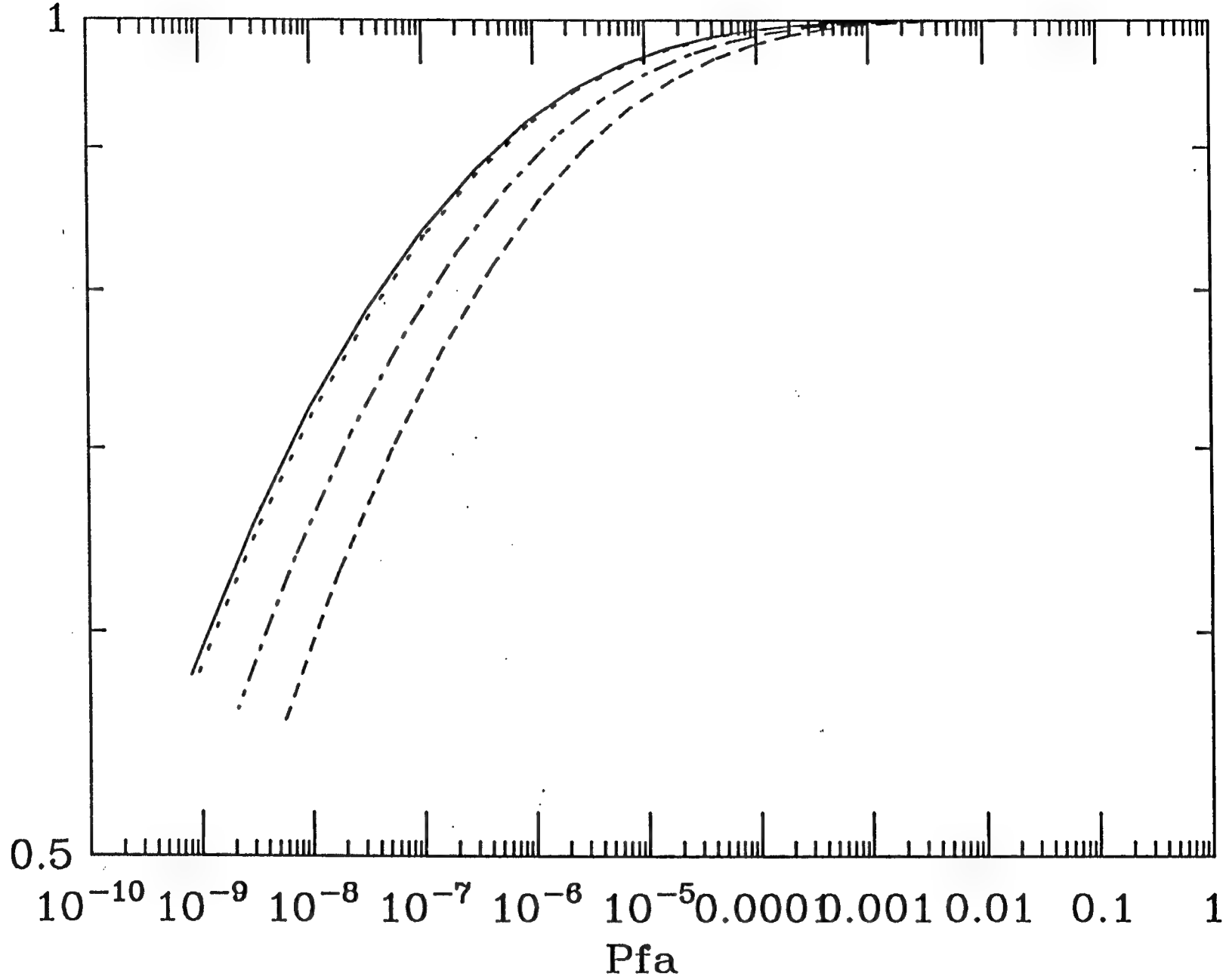

Figure 3

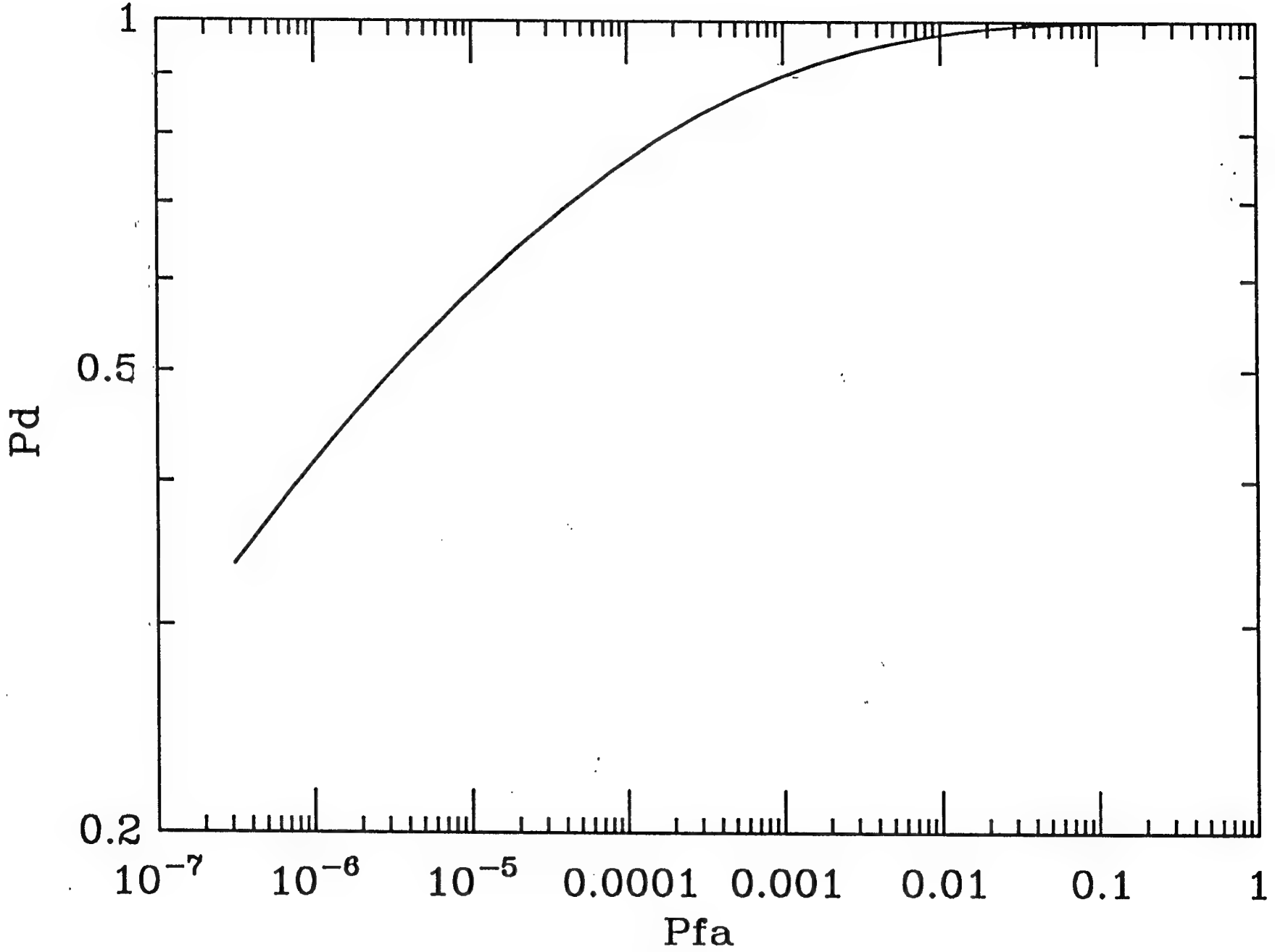

Figure 4

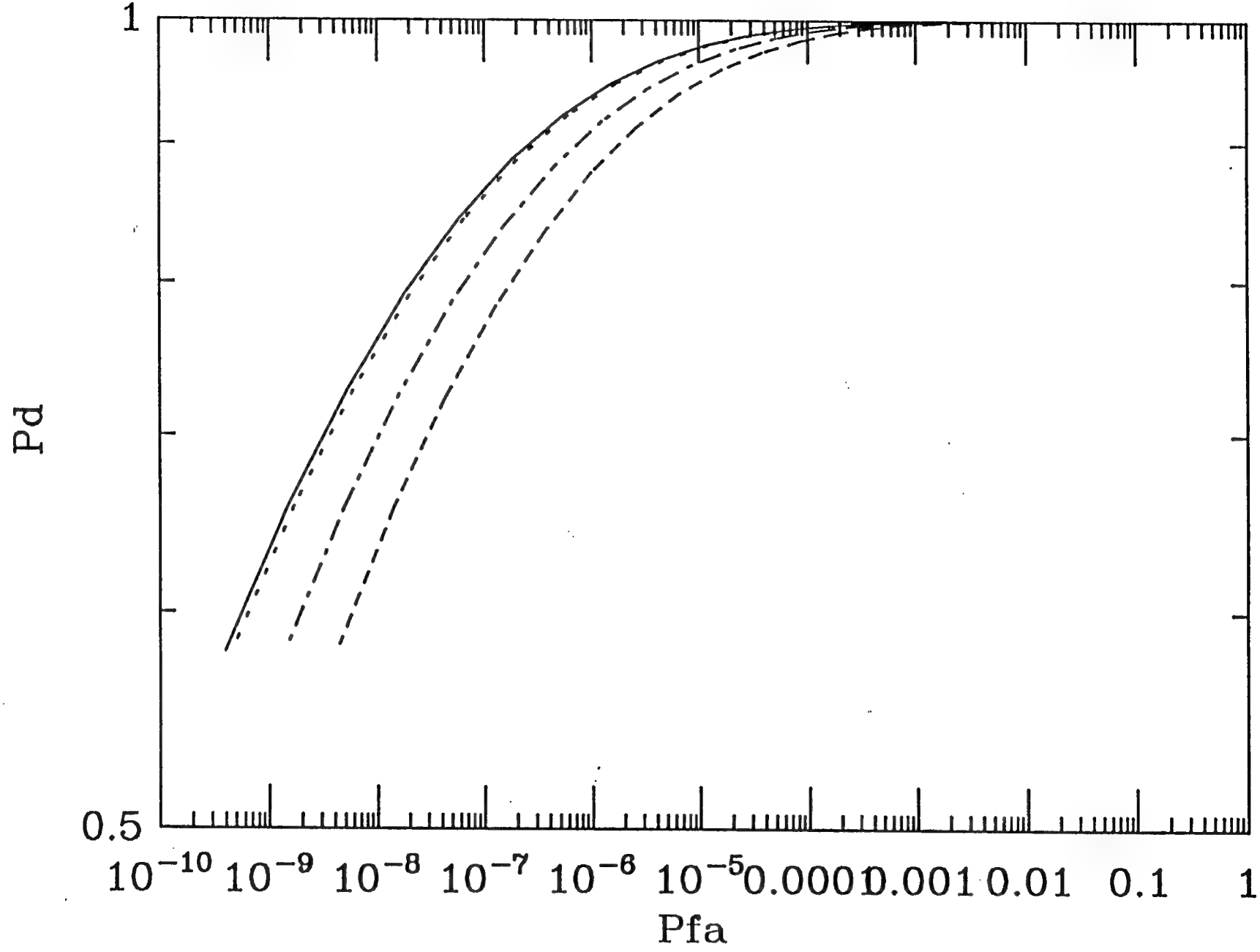

Figure 5

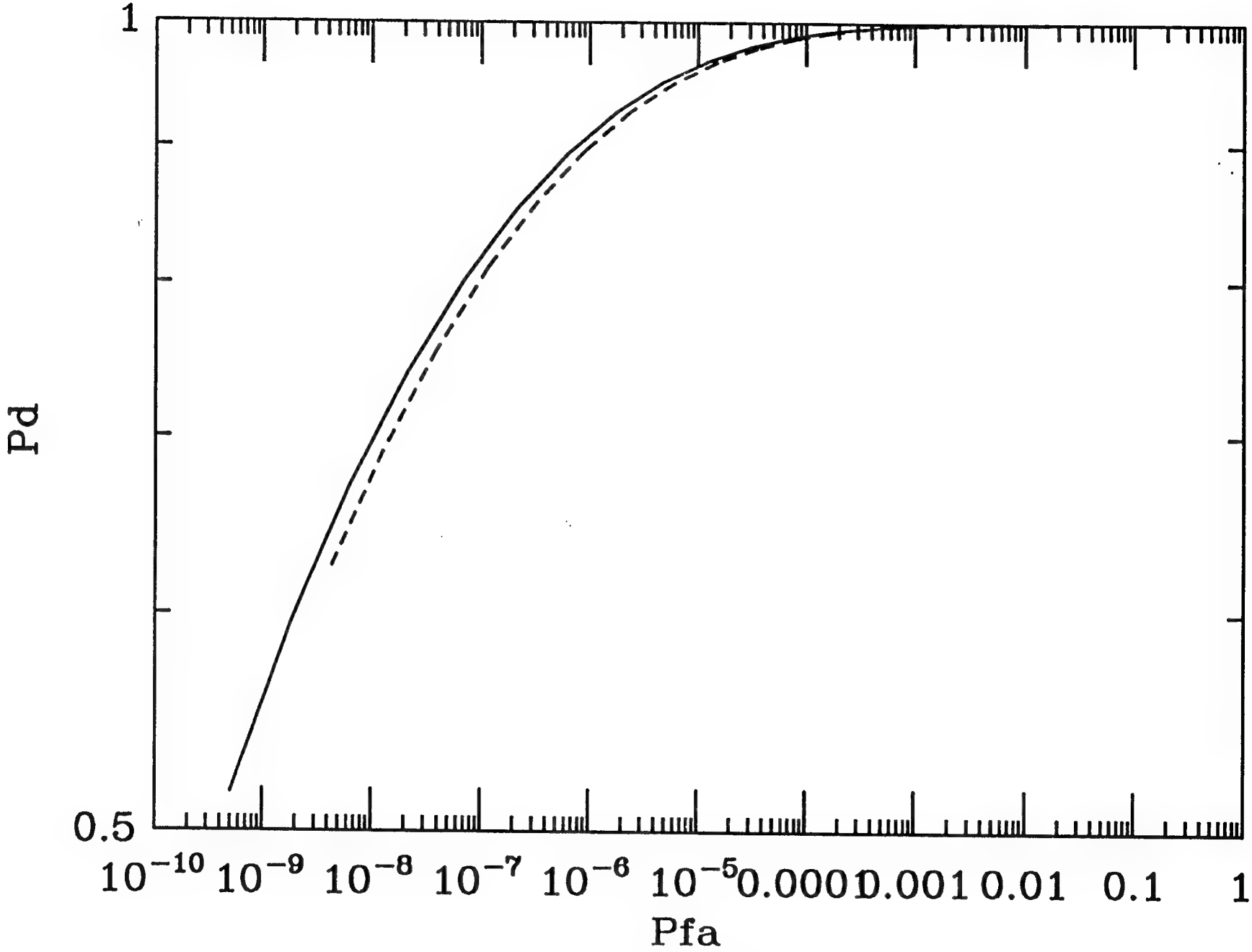

Figure 6

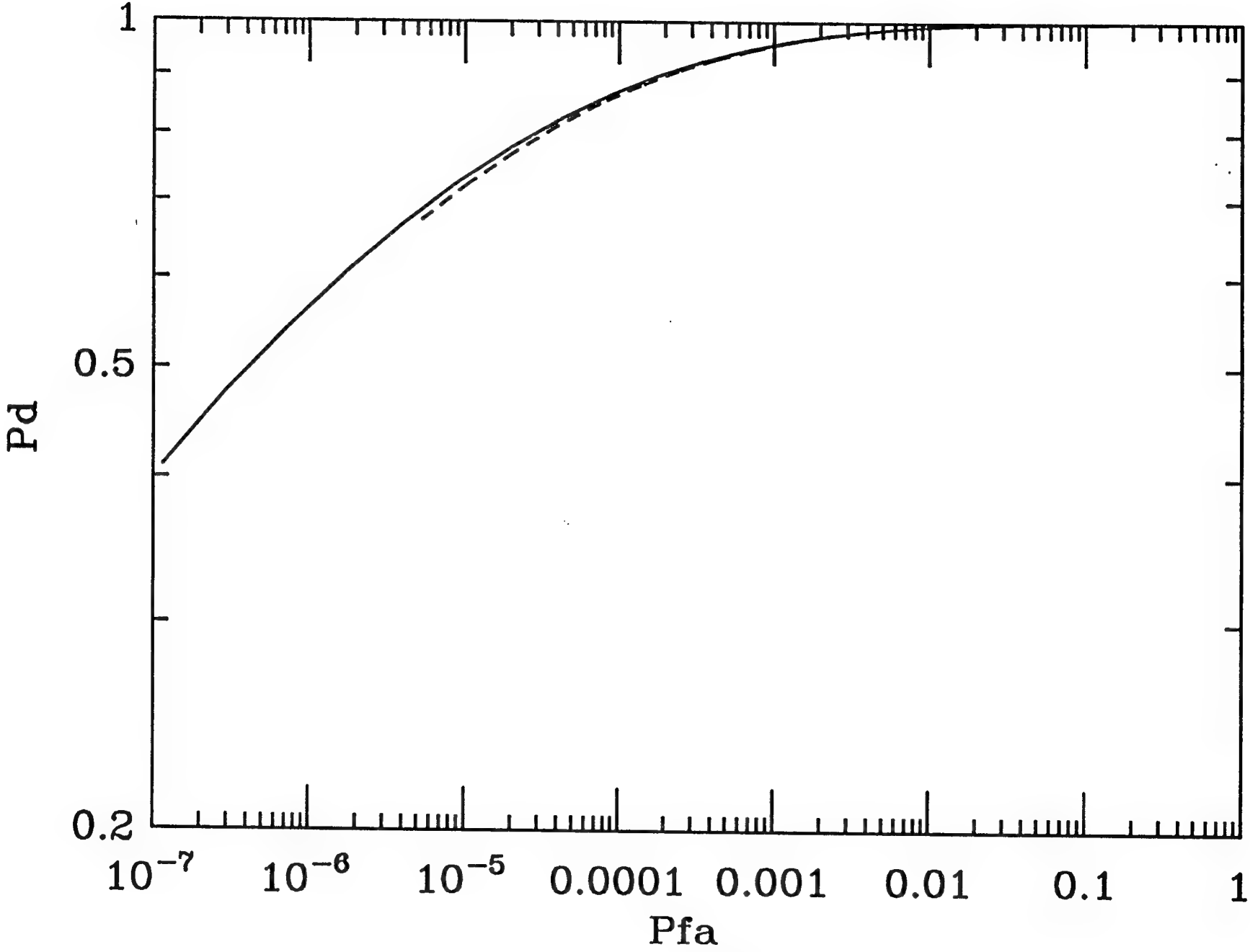

Figure 7

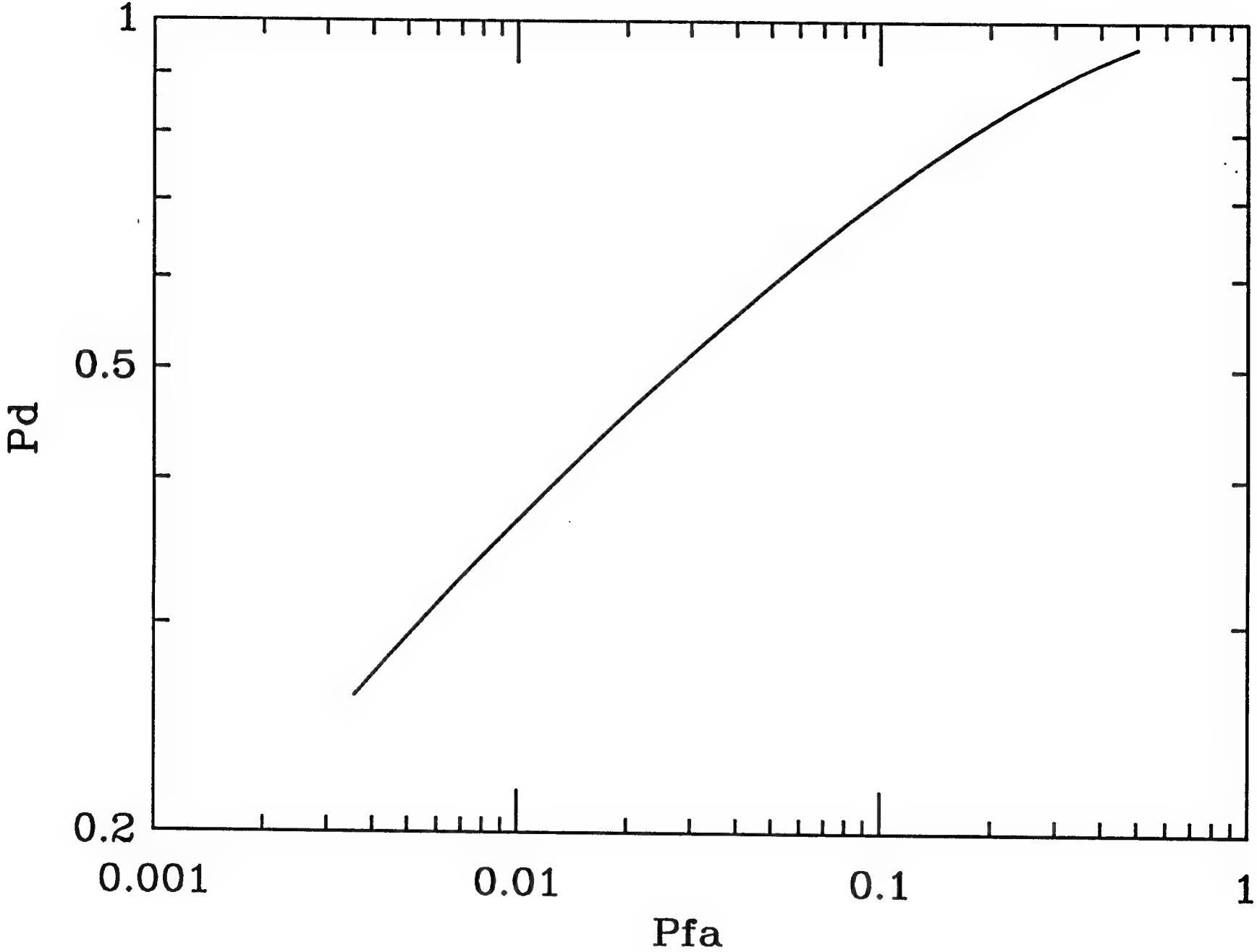

Figure 8

Applications of the wavelet transform in spread spectrum communications systems

Michael Medley, Gary Saulnier and P. Das

Electrical, Computer, and Systems Engineering Department
Rensselaer Polytechnic Institute
Troy, New York 12180-3590

ABSTRACT

In communication applications, particularly ones using spread spectrum (SS) techniques, transform domain processing can be utilized to suppress undesired interference and, consequently, improve system performance. Since traditional applications requiring transform domain processing perform excision only in the Fourier domain, one of the main objectives of this paper is to extend transform domain processing to include wavelets as the basis functions. Specifically, the use of wavelets in the excision of jamming signals from SS communications will be investigated. Simulations have been performed using several basis functions for an SS receiver with narrowband jamming. Results of this simulation are presented, including BER figures, and compared with conventional Fourier domain processing. Implementation of the exciser using multirate digital filtering filters is also discussed. An intercept receiver which employs wavelet transform domain excision is also described. The receiver detects DS-BPSK spread spectrum signals in the presence of narrow-band interference by employing adaptive interference rejection techniques. The improvement in the system performance over that of conventional radiometric detection only is shown by presenting numerical simulation results of probability of detection versus false alarm as the receiver-operating-characteristic (ROC) for an enhanced total power detector.

1 INTRODUCTION

Spread spectrum (SS) communication techniques have become attractive to both the military and civilian communication sectors. Some of the well-known advantages of SS waveforms include their limited immunity to narrow-band interference, transparency to unintended receivers such as intercept receivers, tolerance to multipath effects, and capabiltiy for code division multiple access. These capabilities have made the application of SS communication techniques especially attractive to receivers operating in a hostile environment where low probability of intercept (LPI) as well as immunity to both intentional and unintentional interference is highly desirable.

Although there are several common spread spectrum techniques, such as direct-sequence (DS) modulation, frequency-hopping, time-hopping and related hybrids, the only process considered in this paper is DS, which is generated by modulating the binary information with a wide-band pseudo-noise (PN) sequence and further up-converting the resulting signal to a carrier frequency. Because the interference immunity of a SS system is limited, the performance will suffer if the power of the interfering signal is increased. Signal processing techniques that have the potential of improving the anti-jamming resistance without increasing the transmission bandwidth

are normally employed. If the interference signal is narrow-band, then notch filters can be used to improve performance.

Two classes of methods for suppressing narrow-band jammers in a direct-sequence spread spectrum receiver have been studied and successfully implemented[1-8]. These are LMS based adaptive filters and transform domain excisers. This paper considers the excision of interference in the wavelet transform[9-14] domain. Some properties of wavelet transforms may make the wavelet transform domain better suited for the suppression of some types of interference than the frequency domain.

The following sections provide a brief overview of SS communications and transform domain excision. Later, the wavelet transform is introduced and its application to interference suppression in SS communications and intercept receivers is discussed. Finally, performance results are presented which illustrate the capability of the wavelet transform in suppressing interference.

1.1 Spread spectrum communications

In DS communications, spreading of the information data spectrum is achieved by multiplying the information signal with a reference PN code. In general, PN codes are generated using maximal-length shift registers (MLSR) which produce sequences that have autocorrelation sequences that approximate an impulse function, thus making the signal look like white noise in the frequency domain. More specifically, an N-chip PN sequence produces an autocorrelation value of N with a time lag of zero and -1 for all other time lags. Consequently, the longer the PN sequence (larger N) the more closely the autocorrelation approximates an impulse function.

To send information, the transmitter sends some portion of the PN sequence multiplied by either a ± 1, depending on the polarity of the data bit. In general, the data bit duration is only a fraction of the total PN sequence duration, allowing multiple data bits to be transmitted during the period of a single sequence. However, this paper will only consider the special case where a data bit is a full PN sequence in duration, meaning that a +1 is sent by transmitting an uninverted PN sequence and a -1 is sent by transmitting an inverted PN sequence. In the receiver, the signal is multiplied by a locally-generated copy of the PN sequence and the result is integrated over a data bit period. This process "despreads" the signal back to the original information bandwidth and a simple thresholding operation is used to detect the data. This despreading operation is equivalent to correlating the recieved waveform with the locally-generated PN sequence. Of course, synchronization of the local PN sequence with that in the receive signal is required prior to despreading. In this paper it will be assumed that synchronization has been obtained.

The spreading of the information data results in an increase in the transmitted signal's bandwidth. Specifically, if each information data bit is spread by a PN code of length N, the bandwidth of the transmitted signal is also spread by a factor of N relative to the original information signal bandwidth. This ratio of spread bandwidth to the original information rate is frequently called the *processing gain* of the spread spectrum system and serves as a measure of the amount of interference immunity that is achieved through the use of SS methods.

The goal of SS communications is to improve system performance and reliability while simultaneously providing a data signal that is difficult for unintended receivers to detect. According to the discussion above, it is expected that the signal bandwidth of the spread data signal will be much larger than that of the original information message. Hence, if we limit our discussion to signal representation in the frequency domain, it is not surprising that the spread signal energy spans a large frequency range. Viewing our SS system from this domain, it is easily visualized that a narrow-band interference signal will occupy only a portion of the spread signal's bandwidth and, if the interference energy spectrum is sufficiently small, may be removed without significantly distorting the data signal. Such a scenario naturally leads to the idea of transform domain excision.

1.2 Transform domain excision

When a signal is transformed or mapped to a different "space" and processed, the signal processing is said to have been performed in the transform domain, or, in other words, that one is using transform domain processing. Note that this mapping should be unique and unambiguous, and that an inverse mapping or transformation, which can return the signal to the time domain, should exist. The most widely used transform is the Fourier Transform, but there are many others of importance such as the Hadamard, Fresnel, Hartley, Mellin and Hilbert Transforms, to name but a few. In communications and radar applications, particularly ones using spread spectrum techniques, transform domain processing can be utilized to suppress undesired interference and, consequently, improve performance. Here, the basic idea is to choose a transform such that the jammer or the undesired signal is nearly a delta function in the transform domain, while the desired signal is transformed to a waveform that is very "flat" or "orthogonal", with respect to the transformed interference. A simple exciser can then remove the interferer without removing a significant amount of desired signal energy. An inverse transform then produces the nearly interference-free desired signal. This is the fundamental concept behind transform domain excision. A typical transform domain exciser implementing the wavelet transform is shown in block diagram form in Figure 1.

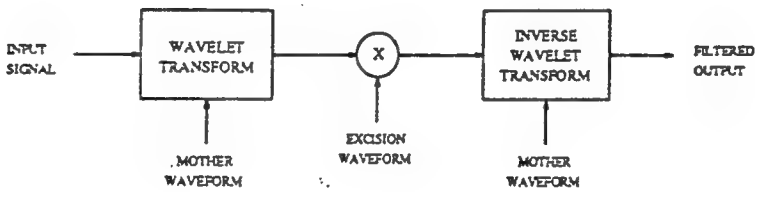

Figure 1: A wavelet excision system

1.3 Wavelet transform

To date, most of the research and development related to transform domain signal processing has been restricted to applications involving the Fourier transform. Most of the practical implementations use *short-time* Fourier transforms which observe only a segment of the input signal to produce an estimate of the transform. While the Fourier transform uses infinite-duration sinusoids as the basis functions for the transformation, the short-time transforms, such as the Fast Fourier Transform (FFT), use truncated or windowed sinusoids.

Since the interfering signals are both time and band limited, the main advantage of using wavelets as opposed to the standard Fourier basis functions is the reduction of sidelobes in the transform domain representation. These sidelobes are the result of the windowing of the input signal that is required to use the short-time transform. The reduction of these sidelobes can improve our ability to remove the interference without distorting the desired signal, with a resultant improvement in performance.

Wavelet transforms are linear and square integrable transforms having a kernel (called the *primitive* or *mother waveform*) which is not fixed. Using this mother wavelet, daughter wavelets are formed by some transformation and, together, in many instances, these wavelets form a complete orthonormal set. The fundamental difference between the wavelet transform and other transforms is that any square integrable function can become the primitive or mother waveform. This ability to choose the function is vital to the success of the wavelet transform in separating desired and undesired components of a signal in a radar or communication system.

If we define $\psi(t)$ as the mother waveform, a complete orthogonal set of daughter wavelets $\psi_{a,b}(t)$ can be

generated from $\psi(t)$ by dilation (by a factor of a) and shift (by an amount b)

$$\psi_{a,b}(t) = \frac{1}{\sqrt{|a|}}\psi(\frac{t-b}{a}).$$

Note that we have replaced t by $t' = \frac{t-b}{a}$ in the above equation. The parameter a also defines the length of the time window and b its location.

By setting $a = a_0^m$ and $b = nb_0a_0^m = anb_0$, where m and n are integers $(\pm1, \pm2, ...)$, one can also define the Discrete Wavelet Transform, DWT, basis functions as follows

$$\psi_{m,n}(t) = a_0^{-m/2}\psi[a_0^{-m}(t - nb_0a_0^m)].$$

Using the above functions, the discrete wavelet transform can be written as

$$X_{DWT}(m,n) = \int x(t)\psi^*_{m,n}(t)dt.$$

The choice of the wavelet basis functions is very important and, for obvious reasons, these functions should be orthonormal. In addition to the orthonormality condition, we would also like the overall system response to be consistent with the perfect reconstruction (PR) property.[13]

One way to perform the wavelet transform while satisfying the perfect reconstruction and orthonormal basis function criteria is to use a filter bank composed of several smaller filter bank structures which each correspond to the analysis section of a two channel paraunitary quadrature-mirror filter (QMF) bank, one of which is shown in Figure 2. Here, the FIR filters $H_0(z)$ and $H_1(z)$ are typically lowpass and highpass digital FIR filters, respectively,

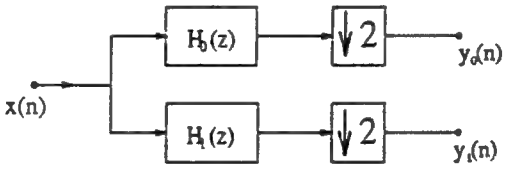

Figure 2: Analysis section of a two-channel paraunitary QMF bank

and have a unique relationship between them.[13] For this paper, $H_0(z)$ was implemented using a 4-tap FIR with the coefficients being set equal to those derived by Daubechies.[9] With respect to figure 2, the wavelet coefficients can be expressed as

$$y_k(n) = \sum_{m=0}^{1} x(m)h_k(2n - m).$$

These values are subsequently converted into vector format and fed into the transform domain processing device. Note that different mother wavelets correspond to different values of the filter coefficients, h_k, used. The input signal can be perfectly reconstructed using a set of 2-channel paraunitary QMF bank synthesis filters, the constraints of which, as well as their relationship to the synthesis filters $G_0(z)$ and $G_1(z)$, are discussed in detail in other texts.[13,14]

In spread spectrum systems, the spectrum of the transmitted signal is expected to be approximately flat throughout the transform domain, thus implying that the discrete wavelet coefficients, $y_k(n)$, have relatively similar magnitudes. If an interference source is present in the channel, then the received signal's spectrum will no longer remain relatively flat, but, instead, will also reflect the energy distribution of the interfering source. For example, if a strong narrow-band jammer interferes with the spread spectrum signal, then the received signal's spectrum will indicate the increased amount of energy, corresponding to the jammer, in the appropriate bands.

Hence, any of the discrete wavelet transform coefficients that exhibit an energy level that is significantly higher than that of its neighbors may be assumed to contain a significant amount of the narrow-band interference energy. As previously stated, such an assumption is the basis of the transform domain exciser.

In transform domain excision, these transform bands, or bins, with high energy content are excised, thus removing a significant portion of the interference energy. The degree of success with which the interference is removed depends on the transform technique's ability to isolate the undesired signal in as few bins as possible.

2 APPLICATION OF THE DWT TO DSSS SYSTEMS

As an alternative to the FFT, the full binary subband tree decomposition, or regular DWT, as shown in Figure 3, can be used for interference excision. As can be seen from the figure, this particular transform method recursively divides the input signal spectrum into separate lowpass and highpass components. Each resulting

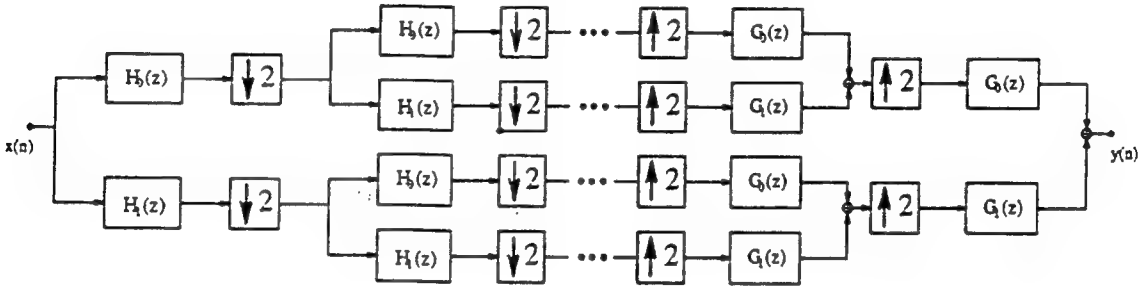

Figure 3: Full binary tree structure of the regular DWT

component is subsequently partitioned into finer resolution lowpass and highpass frequency bands until the desired level of frequency resolution is obtained. For example, if only two stages of the full binary tree were utilized, the transform domain representation of the input signal would consist of four equal bandwidth frequency bins. As a result, the regular DWT provides a uniform partition of the signal's frequency spectrum much like the FFT. However, unlike the FFT, the spectral sidelobes of the DWT are not as large and, hence, fewer bins may need to be excised to achieve the same *bit error rate*, or *BER*, performance, or, equivalently, with the same number of bins removed, the BER performance of the regular DWT may show an improvement over that of the FFT.

Frequency domain excision using the FFT yields satisfactory BER performance if the interference source is stationary. However, when the jammer is pulsed, or generally nonstationary, the sharp transitions induced in the time domain signal are spread or smeared throughout the frequency spectrum thus making the distinction between data signal energy and interference energy very difficult.

To handle such interference. the dyadic binary subband tree structure, which is equivalent to the Discrete Wavelet Transform,[14] shown in Figure 4 is used to mitigate nonstationary interference. The DWT is a transform that partitions the signal spectrum into octave frequency bands, thus providing high frequency resolution at low frequencies while retaining good time resolution at high frequencies. Current research efforts have shown that the DWT is capable of effectively localizing bursty interference to a small portion of the transform domain as shown in Figure 12. This method of isolating pulsed interference using the DWT is not unlike the frequency transform domain methods used to isolate continuous narrow-band interference. Since the interference can be localized in the transform domain, it can also be excised without significantly degrading overall system performance. It will be illustrated in the following section that, for short duration pulses, the FFT is unable to significantly isolate

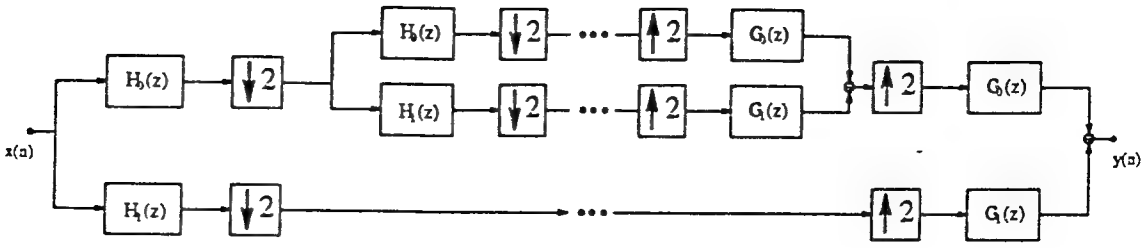

Figure 4: Dyadic binary tree structure of the DWT

the interference to a small number of frequency bins.

2.1 DSSS communications receiver

A block diagram of the DSSS receiver incorporating the wavelet transform is shown in Figure 5. After excision,

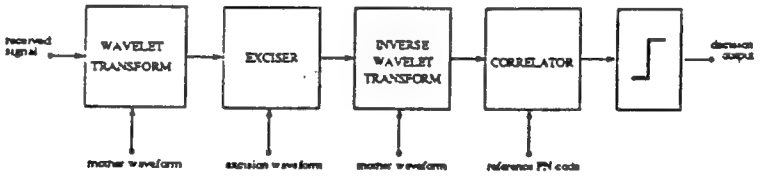

Figure 5: A DSSS communications receiver

the received signal is inverse transformed back into the time domain, correlated with the known reference signal, the PN code, and compared to a threshold to yield the decision output.

Figures 6, 7 and 8 help to illustrate the idea of transform domain excision. These figures show the magnitude responses of the FFT, Full Binary Subband Tree Decomposition (Regular DWT) and Discrete Wavelet Transform (DWT) of a 63-chip PN code. From these figures, it is easily seen that the energy of the PN sequence is distributed throughout most of the bins in each of the transforms. This is expected since one property of pseudo-noise sequences is its nearly uniform distribution of energy throughout the frequency domain and since each of the transform methods represent a different partitioning of this domain. Note that it is implicitly understood that each data bit is sampled 63 times.

Figures 9 and 10 show the magnitude responses of the FFT and Regular DWT of a stationary narrow-band (single-tone) jammer, respectively. As can be seen from the figures, both transforms isolate a significant amount of the jammer energy to a relatively small number of bins. Since the PN sequence energy is spread throughout many bins and since the law of superposition holds with both transforms, these figures support the supposition that it may be possible to excise, or remove, those bins containing significant jammer energy without removing a significant amount of energy from the PN sequence.

Likewise, for nonstationary interference, Figures 11 and 12 illustrate the magnitude responses of the FFT and DWT of a white noise pulsed interferer with a duty cycle of 15%, respectively. It is clear that the DWT is capable of isolating the pulsed interference energy to a small number of bins in the transform domain. As previously mentioned, such energy compaction in the transform domain supports the idea that jammer energy may be removed without significant degradation of the PN sequence. These figures clearly show, however,

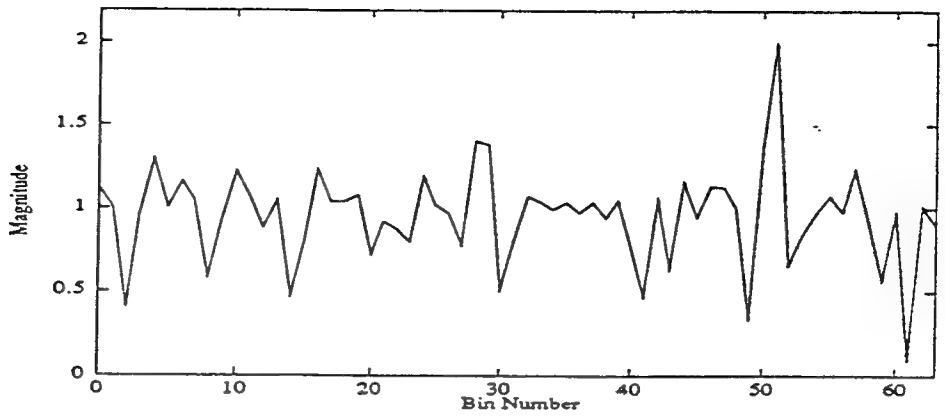

Figure 6: Magnitude response of the FFT of the 63-chip PN code

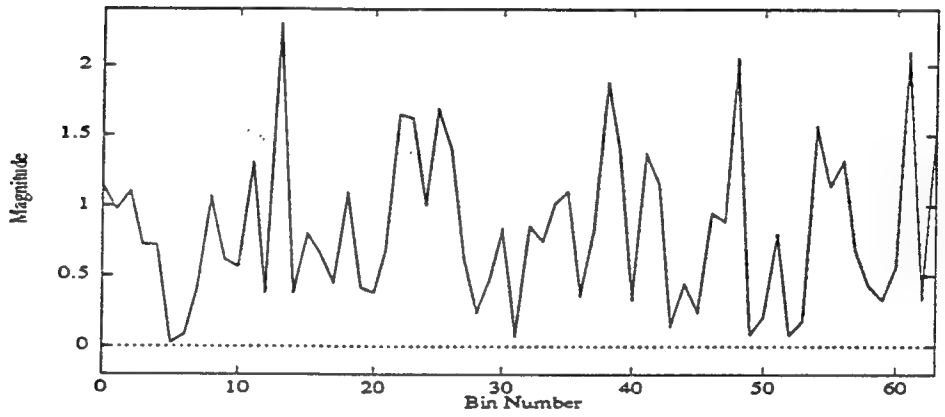

Figure 7: Magnitude response of the full binary subband tree decomposition (Regular DWT) of the 63-chip PN code

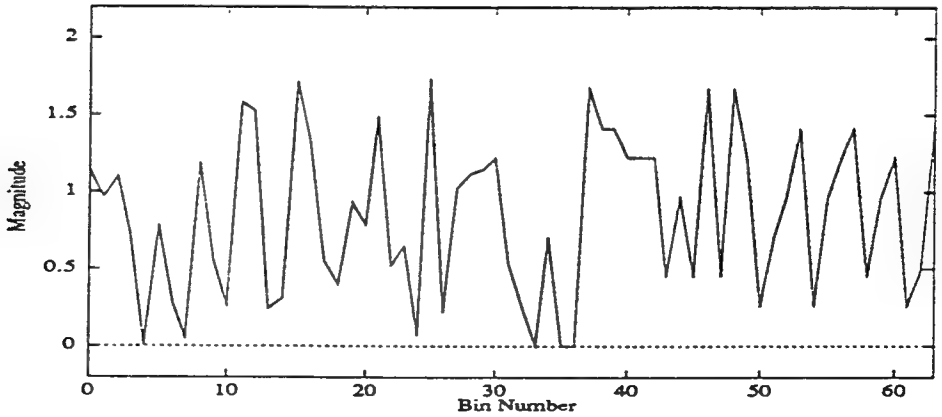

Figure 8: Magnitude response of the DWT of the 63-chip PN code

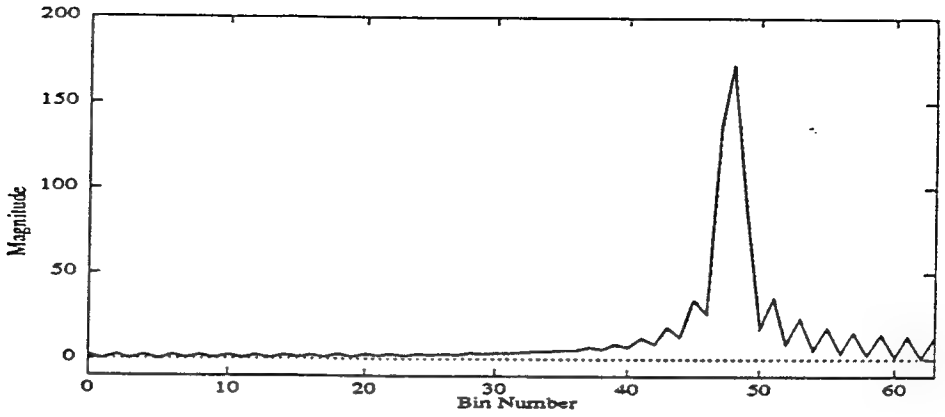

Figure 9: Magnitude response of the FFT of the stationary single-tone jammer

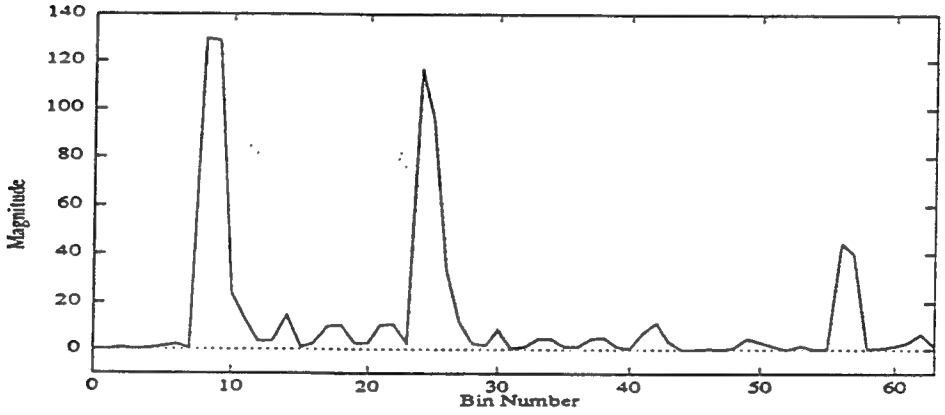

Figure 10: Magnitude response of the full binary subband tree decomposition (Regu lar DWT) of the stationary single-tone jammer

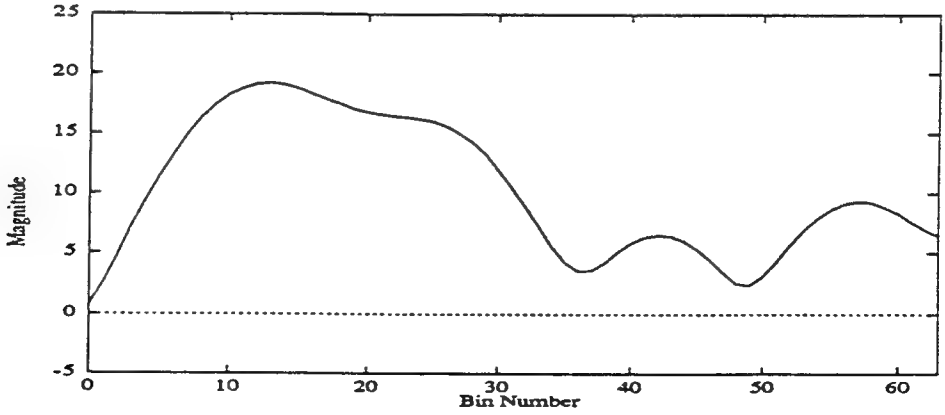

Figure 11: Magnitude response of the FFT of the pulsed jammer

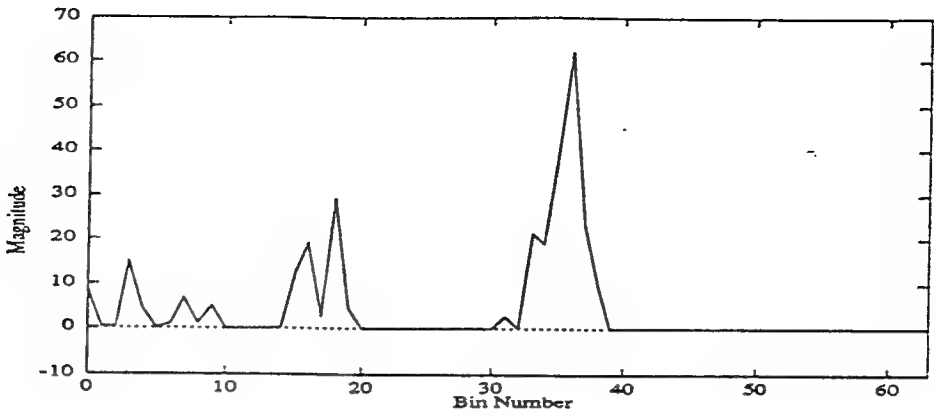

Figure 12: Magnitude response of the DWT of the pulsed jammer

that the FFT is not capable of isolating the pulsed interference energy to as few bins as the DWT. Hence, for applications involving nonstationary interference sources, it is expected that, under certain conditions, using the DWT transform method in place of the FFT may yield improved system performance.

Sometimes, however, it is not necessary to return to the time domain, since one might be able to extract the desired information (e.g. make a bit decision) directly in the transform domain. Figure 7 shows the regular DWT of the 63-chip PN code. The 63-chip PN code could equally, and correctly, be identified as a spread +1 binary data bit. It can be shown that if the polarity of the data bit were reversed, then so to would be the polarity of the PN sequence as well as the regular DWT and DWT of Figures 7 and 8. Hence, unambiguous information regarding the polarity of the data bit transmitted is present in the wavelet transform domain and may be used to make the bit decision directly in that domain. To take advantage of this information, it is necessary to correlate the transform of the received signal with that of the known PN reference code as shown in Figure 13.

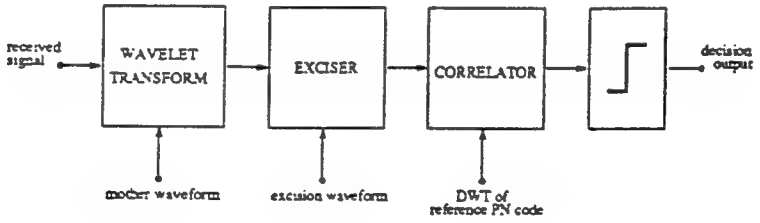

Figure 13: A DSSS transform domain communications receiver

DSSS system performance is often measured in terms of the system's bit error rate performance. The general goal of SS systems is to improve communications reliablility and hence improve the overall BER. The objective of transform domain excision is to further improve on SS system performance when intentional or unintentional interference is present. The above figures illustrate that when using the correct transform method, much of the undesired interference energy may be isolated to a few transform domain bins and subsequently excised and, as a result, communications in the presence of such a source may be maintained or improved. As will be discussed next, the idea of transform domain processing may also be used to improve the performance of traditional radiometric detectors, or intercept receivers.

2.2 Intercept receiver design

The classical technique to detect the presence of a DS-BPSK signal is to use a total power radiometer, which consists of a bandpass filter (BPF), a squaring device and an integrator. The detected power of the received signal is compared to an external threshold, which is a function of the additive white Gaussian Noise (AWGN). The decision on the presence of a DSSS signal is made if the measured detected power exceeds the threshold. The performance of such a detection technique can be illustrated by presenting the probability of detection, P_d, versus the probability of false alarm, P_{fa}, which results in the well-known *receiver-operating-characteristic*, *ROC*, of the detector.

Unfortunately, the operation of the above detection technique in the presence of narrow-band interference typically collapses due to the increase in the probability of false alarm. This is because the receiver typically does not have any apriori knowledge regarding either the presence or the power of either the intercepted signal or the narrow-band interference. As alluded to in the previous section, transform domain excision using the wavelet transform may be used to alleviate this problem. A block diagram of the intercept receiver incorporating transform domain excision is shown in Figure 14. As is evident from the figure, this receiver configuration

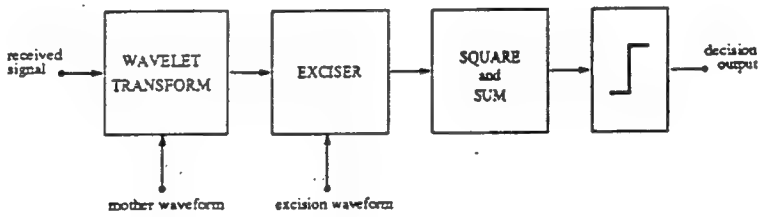

Figure 14: A DWT based intercept receiver

removes the interference energy via excision and subsequently determines the residual energy level by squaring and summing the remaining transform domain components. The result of the summation is then compared to the threshold value to make the determination of P_d and P_{fa}. As with the DSSS receiver, it is expected that using transform domain excision to remove certain stationary and nonstationary interference will result in an overall improvement in system reliability and performance.

3 RESULTS AND CONCLUSIONS

3.1 DSSS receiver performance

To evaluate the performance of the DSSS communications receivers of Figures 5 and 13, a SS communications system was simulated using the Signal Processing WorkSystem, SPW, software by Comdisco Systems Inc. A 63-chip PN sequence was used to perform the DS modulation of the binary input data stream, which was sampled at a rate of 63 samples per bit, and simulations were performed at baseband at a normalized data rate of 1 Hz. The spread data signal was subsequently transmitted over an AWGN channel with interference and, at the receiver, non-windowed 64-point transforms were used to transform the time domain waveform into the frequency domain. To perform the regular and standard DWT transforms, 4-tap FIR filters utilizing the coefficients derived by Daubechies[9] are implemented in the two-channel paraunitary QMF banks of Figures 3 and 4. The effects of system performance in the presence of both stationary and nonstationary interference were studied and are presented in terms of their BER plots.

Specifically, Figure 15 compares the relative performance of the receiver using the FFT and regular DWT transform methods. The interference source present in this system is a stationary 30 dB single-tone, or sinusoidal, jammer at a frequency of 8.0/63.0. For this particular jammer, stationarity simply implies that the jammer characteristics are statistically invariant for an amount of time that is greater than the bit duration, since this makes the jammer stationary over the time period that is processed by a single transform. In this and all subsequent figures "SNR" corresponds to the energy per data bit to one-sided noise spectral density ratio and, as such, does not consider the jammer power. Figure 15a illustrates the BER curves for the DSSS receiver when suppression of the interfering waveform is attempted by removing four of the transform domain bins, whereas, Figure 15b shows a situation in which a system performance is improved by excising eight bins. It is noted from these figures, that when very few bins, such as four, are removed, excision via the FFT generally results in a lower BER for a given SNR as compared to excision via the regular DWT. However, when a sufficiently large number of bins are removed, such as eight, the converse is true.

Since the interference is a continuous sinusoid and the FFT basis functions are well-suited for representing sinusoidal signals with a time duration greater than that of the transform window length, the FFT is better able to isolate a large amount of this energy to a very small number of bins as compared to the regular DWT. Additionally, since there is a non-negligible amount of aliasing between the lowpass and highpass quadrature-mirror filters within the filter bank subband structure of the regular DWT,[14] it is understandable that the regular DWT is not capable of isolating the same amount of jammer energy to so few bins.

There is, however, a limit to this argument. After removing a certain number of bins, each additional bin excised in the Fourier domain results in little, if any, BER improvement. In fact, from the figures, it is clear that the FFT performance with four bins excised is superior to that of the same system with eight bins removed. This result is due to the fact that the rectangular window used in the FFT smears the narrow-band interference spectrum throughout several bins. Since the amount of the resulting sidelobe energy decays so slowly, there is a limit to the number of additional bins that can be removed and still result in an appreciable improvement in system performance. In particular, when performing transform domain excision, it is important to keep in mind that the processing goal is to maximize the amount of interference energy removed while simultaneously minimizing the amount of spread signal energy that is lost. In general, the first bins excised usually remove a very large amount of jammer energy relative to that of the spread signal. However, as more bins are excised, the ratio of jammer to signal energy removed continues to decrease until a point is reached where the benefits of excising one more bin are outweighed by the loss of spread signal energy.

As with the FFT, the regular DWT implementation also divides the frequency spectrum into uniform bandwidth bins. Although aliasing is present between filters in the analysis section of the QMF banks composing the subband tree, this should not imply that every transform domain bin is significantly corrupted with aliased energy. In fact, unlike the FFT, the regular DWT implementation does not suffer from significant energy level sidelobes as shown in Figure 10. As a result, most bins in the regular DWT transform domain contain either a high or low level of jammer to signal energy, with very few midrange values. This is in contrast to the FFT, where, at the bin corresponding to the center frequency of the narrow-band jammer, the jammer to signal energy ratio starts at a very high level and then decays slowly on either side. Thus, when more than a very small number of bins are excised, it is not surprising that the performance of the receiver implementing the regular DWT is better than that of the receiver using FFT based excision. This is evidenced in Figure 15b which shows that when eight bins are excised, the BER corresponding to the regular DWT based receiver for a given SNR is lower than that of the FFT based receiver with the same number of bins removed as well as any of the previously discussed systems. Again, however, it should be noted that if too many bins are removed, system performance will rapidly degrade.

From the BER plots, it is clear that using the regular DWT with eight bins excised yields the best system performance. It should, however, be noted that this system is not necessarily optimal and that further tests must be performed to determine which transform method and how many bins must be excised to yield the best overall system performance.

As previously mentioned, in the presence of a stationary sinusoidal jammer, transform domain excision using either the FFT or regular DWT based receivers significantly improves system performance. As shown in Figure 16, however, the excision capability of the FFT based receiver in the presence of a nonstationary, or pulsed, interference source is far less effective. In particular, Figure 16 compares the relative performance of the DSSS receiver using the FFT and DWT transform methods in the presence of a white noise pulsed jammer. This interference source is modeled as a white noise source with a duty cycle of 5% relative to a period of 70 samples, thus ensuring that the pulse duration is much less than that of the data bit while the pulse period is slightly larger. The noise variance has been specified such that the effective jammer to signal ratio is 23.3 dB. Figure 16a illustrates the BER curves for the DSSS receiver when suppression of the interfering waveform is attempted by removing four of the transform domain bins, and, similarly, Figure 16b shows the situation in which system performance is improved by excising eight bins.

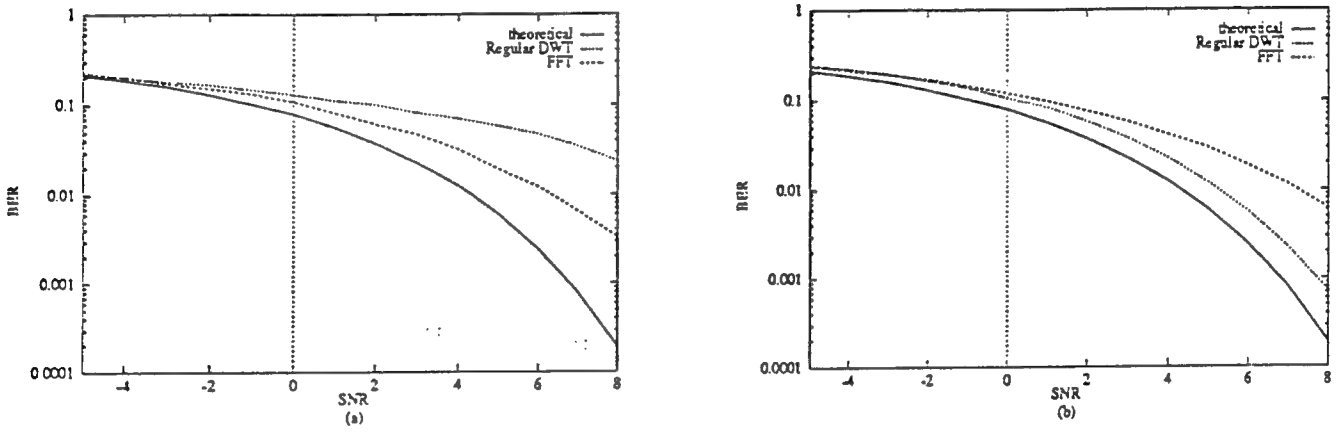

Figure 15: FFT and regular DWT based DSSS receiver performance in the presence of stationary interference: (a) BER with 4 bins excised, (b) BER with 8 bins excised

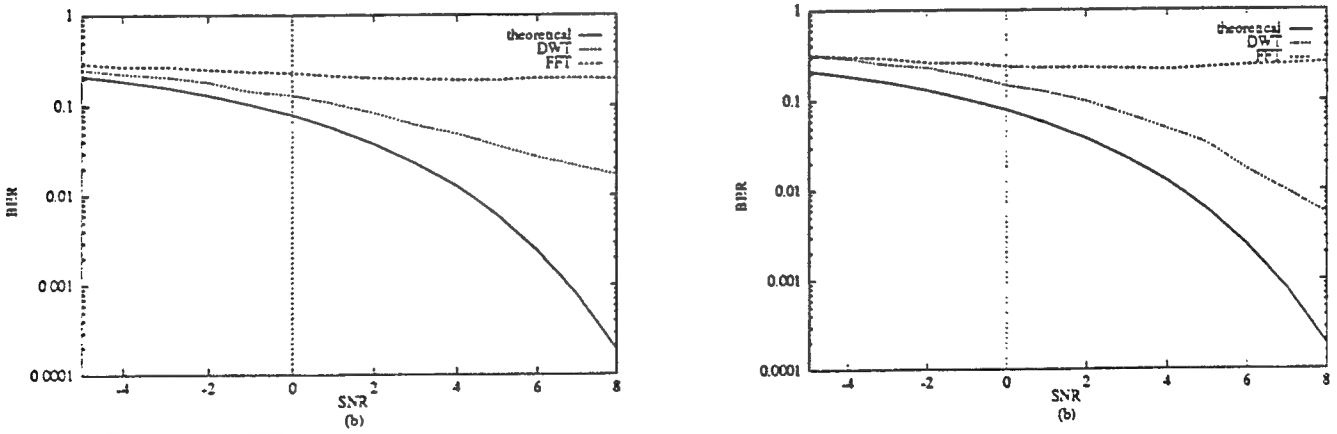

Figure 16: FFT and DWT based DSSS receiver performance in the presence of nonstationary interference: (a) BER with 4 bins excised, (b) BER with 8 bins excised

It is obvious from Figure 11 that the FFT based receiver is incapable of isolating any amount of the jammer energy to a small number of transform domain bins. In this case, the jammer energy is spread throughout the transform domain and, since almost all of the bins are characterized by a relatively large jammer to signal energy ratio, transform domain excision using the FFT is completely ineffective in improving system performance as

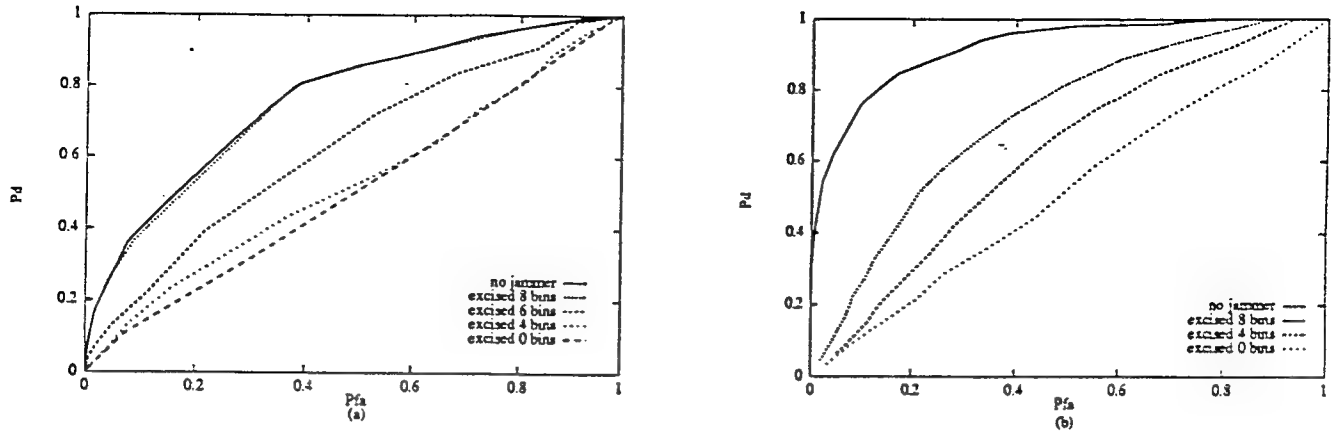

Figure 17: Regular DWT and DWT based intercept receiver performance: (a) ROC for regular DWT based receiver with stationary interference, (b) ROC for DWT based receiver with nonstationary interference

Figure 17a was generated by testing the receiver in the presence of the nonstationary pulsed jammer using the DWT with a SNR = -4 dB. Again, excising two, four or eight bins improves receiver performance, with the removal of eight bins leading to the best results. Using the DWT, this receiver is able to isolate and excise much of the pulsed jammer energy. As before, neither of these receivers claim to be optimal, however, as the figures show, they are quite effective in improving receiver performance in the presence of interference. Again, more analysis must be performed to determine the system parameters that optimize this performance.

3.3 Conclusion

Given the above results, it seems logical to conclude that no one transform method is completely effective at suppressing all types of interference. Often times, the best performance of each receiver, whether it is the DSSS communications receiver or the intercept receiver, depends on both the transform method used and the type of interference present. This paper has demonstrated that either the regular DWT or standard DWT, depending on the interference source, can be used as an alternative to the standard FFT in interference suppression applications using transform domain excision.

In order to use these transforms effectively, their limitations must be understood. Since the regular DWT structure partitions the frequency domain into uniform bands, like the FFT, it would seem to be a natural candidate for an alternative to the FFT that would possess similar strengths and weaknesses. Like the FFT, this transform is effective at isolating and removing stationary narrow-band interference. However, neither transform is particularly good at confining the energy of nonstationary jammers to a small portion of the transform domain.

For these situations, the above results clearly indicate that the DWT performs especially well. In fact, the figures show that the DWT is particularly well suited to transform domain compression and excision of the interference energy for short duration pulsed jammers. The effects of additional system parameters such as transform length, QMF bank filter implementation and jammer frequency were not discussed in this paper, but nonetheless merit further investigation.

4 ACKNOWLEDGEMENTS

P. Das was partially supported by UCSD subcontract under U.S. Army Grant No. DAAL09-91-G-0071.

5 REFERENCES

[1] R. Bijjani and P. Das. Rejection of narrowband interference in pn spread spectrum systems using neural networks. *Proceedings of Globecom*, 1990.

[2] John Gevargiz, Michael Rosenmann, Pankaj Das, and Laurence B. Milstein. A comparison of weighted and non-weighted transform domain processing systems for narrowband interference excision. *Proceedings of IEEE Military Communications Conference*, 1984.

[3] J. Gevargiz, P. Das, and L. B. Milstein. Adaptive narrowband interference rejection in a ds spread spectrum intercept receiver using transform domain signal processing techniques. *IEEE Transactions on Communications*, 37, 1989.

[4] John Guilford and P. Das. The use of the adaptive lattice filter for narrowband jammer rejection in ds spread spectrum systems. *Proc. International Conference on Communications*, 1985.

[5] W. W. Jones and K. R. Jones. Narrowband interference suppression using filterbank analysis/synthesis techniques. *Proceedings MILCOM*, 1992.

[6] L. B. Milstein and P. Das. An analysis of a real-time transform domain filtering digital communication system: Part i: Narrowband interference rejection. *IEEE Trans. on Communications Technology*, COM-28, 1980.

[7] Gary J. Saulnier, P. Das, and Laurence B. Milstein. Suppression of narrow-band interference in a pn spread-spectrum receiver using a ctd-based adaptive filter. *IEEE Transactions on Communications*, Com-32, 1984.

[8] Gary J. Saulnier, Pankaj K. Das, and Laurence B. Milstein. An adaptive digital suppression filter for direct-sequence spread-spectrum communications. *IEEE J. on Selected Areas in Communications*, SAC-3, 1985.

[9] I. Daubechies. Orthonormal basis of compactly supported wavelets. *Comm. Pure and Appl. Math*, XLI, 1988.

[10] O. Rioul and M. Vetterli. Wavelets and signal processing. *IEEE Signal Processing Magazine*, 1991.

[11] C. K. Chui (Ed). *Wavelets: A Tutorial in Theory and Applications.* Academic Press, 1992.

[12] C. K. Chui (Ed). *Wavelets: An Introduction to Wavelets, vol. 1.* Academic Press, 1992.

[13] P. P. Vaidyanathan. *Multirate Systems and Filter Banks.* Prentice Hall, 1993.

[14] Ali N. Akansu and Richard A. Haddad. *Multiresolution Signal Decomposition.* Academic Press, 1992.

Coherent DS - CDMA Performance in Nakagami Multipath Fading.

Thomas Eng and Laurence B. Milstein
Dept. of Electrical and Computer Engineering
University of California at San Diego
La Jolla, CA 92093

Abstract

The coherent reception of direct sequence - code division multiple access (DS - CDMA) signals in a multipath fading channel is considered. The channel model assumes independent paths with Nakagami fading statistics; this model includes the Rayleigh channel as a special case and is a reasonable model for a frequency - selective fading channel. The bit error rate (BER) performance of a RAKE receiver under various multipath fading conditions is derived and evaluated. The results indicate that, when channel coding is employed, over 40 users may access the channel (assuming 127 chips per bit) simultaneously under typical fading conditions, and can achieve a BER of 0.001 with an average received signal - to -noise ratio (SNR) per bit of 10 dB.

This work was partially supported by the Army Research Office under Grant DAAL03-91-G-0071 and by the Office of Naval Research under Grant N00014-91-J-1234.

I. Introduction

In recent years, there has been considerable interest in the application of CDMA techniques to multiple access communications. CDMA can potentially accommodate more users than either TDMA or FDMA, because as additional users are activated, the system performance as seen by any single user is degraded only slightly; thus as long as the increase in BER is tolerable, the already - established links remain operational. Another advantage of CDMA is that there are no requirements for precise time or frequency coordination among users as in TDMA or FDMA. Furthermore, CDMA offers the usual benefits associated with spread spectrum systems such as interference rejection/suppression (which is what causes the 'graceful' degradation mentioned above) and multipath mitigation.

There has been much written on the topic of DS - CDMA performance analysis. Gardner and Orr [1], Borth and Pursley [2], and Geraniotis [3] considered the effects of multiple access interference for a single path channel. Turin [4] analyzed the effects of multipath fading and multiple access noise on the overall average received signal-to-noise ratio (SNR), thus bypassing a detailed analysis based on a specific fading statistic. Similarly, Lehnert and Pursley [5] analyzed SNR performance for a multipath-combining receiver and determined system performance in terms of parameters of the signature sequences. Geraniotis and Pursley [6] and Kavehrad and McLane [7] considered coherent system performance for a Rician and Rayleigh channel, respectively. And Xiang [8] and Ochsner [9] treated the noncoherent case for Nakagami and Rayleigh fading, respectively. Though the approach used by these authors varied widely, most assume either Rayleigh or Rician fading. However, as Turin [10] and Suzuki [11] have pointed out, empirical data suggests that path fading statistics, especially for the initial (shortest) paths, are more adequately described by a Nakagami, or 'm', distribution with parameter m = 0.75 (which is worse than Rayleigh, for which m = 1). The Nakagami-m distribution is also of great interest to ionospheric physicists because amplitude fading due to ionospheric scintillation has been found to follow an m-distribution [12, 13, 14].

In this paper, a channel model incorporating Nakagami multipath fading is developed and the BER performance of a DS - CDMA system operating through it using coherent demodulation is analyzed. For the particular cases of interest (m=1 and m=0.75), the fading statistics do not contain a specular component; therefore, in order to demodulate coherently, the implicit assumption is made that some type of carrier recovery and/or fade-mitigation technique is used. One method that has been found effective in combatting multipath Rayleigh fading (and providing coherent demodulation) is the simultaneous transmission of one or more in-

band or adjacent-band 'pilot' tones [15]. Another method to obtain the coherent reference is via channel-parameter estimation circuits [16]. Since implementation issues are not the main topics of concern here, perfect coherence will be assumed without further justification. The receiver considered is a RAKE receiver with a variable number of taps to allow for varying degrees of diversity. The amount of improvement obtainable by channel coding is also investigated using a rate 1/2, constraint length 7 convolutional code and Viterbi decoding.

II. DS - CDMA System Model

The system model to be considered consists of K+1 simultaneous transmitters (the zeroth user being the reference user whose performance is to be evaluated); each transmitter, or user, is assigned a unique CDMA code sequence (also called a signature sequence) which modulates, along with the carrier, the data sequence. The signature sequence of each user is periodic with period much longer than the processing gain N; the code sequences have a common chip rate of $1/T_c$, where $T_c = T/N$, and $1/T$ is the information bit rate. Let $a_k(t)$ denote the code sequence waveform of the k-th user, and let $\{a_j^{(k)}\}$ be the corresponding sequence of elements of $\{+1,-1\}$. Then

$$a_k(t) = \sum_{j=-\infty}^{\infty} a_j^{(k)} P_{T_c}(t-jT_c) \quad ,$$

where $P_{T_c}(t) = 1$ for $0 < t < T_c$ and equals zero otherwise. Similarly, the data signal waveform may be written as

$$b_k(t) = \sum_{j=-\infty}^{\infty} b_j^{(k)} P_T(t-jT) \quad .$$

The transmitted signal for the k-th user is, therefore,

$$s_k(t) = \mathrm{Re}[S_k(t)e^{j\omega_0 t}],$$

where

$$S_k(t) = \sqrt{2P}a_k(t)b_k(t)e^{j\theta_k}$$

and where P is the average transmitted power, common to all users, ω_0 is the common carrier frequency, and θ_k is the phase of the k-th carrier.

Assuming asynchronous operation, each non-reference-user signal is misaligned relative to the reference signal by an amount τ_k, k=1, 2, ... K; thus, the composite signal at the input to the channel is

$$s_T(t) = \mathrm{Re}[S_T(t)e^{j\omega_0 t}] \quad ,$$

where (1)

$$S_T(t) = \sum_{k=0}^{K} \sqrt{2P}a_k(t-\tau_k)b_k(t-\tau_k)e^{j\phi_k} \quad ,$$

$\phi_k = \theta_k - \omega_0\tau_k$, and $\theta_0 = \tau_0 = 0$. Furthermore, the asynchronous assumption implies that the $\{\phi_k\}_{k=1}^{K}$ are independent identically distributed (iid) random variables uniformly distributed in $(0, 2\pi)$, and likewise $\{\tau_k\}_{k=1}^{K}$ may be taken to be iid random variables uniform in (0, T).

III. Channel Model

A commonly used model for a frequency-selective multipath channel is a finite - length tapped delay line as shown in Figure 1 for the k-th user [9, 16], where the $L_p^{(k)}$ tap weights $\{\alpha_i^{(k)}\}$ are independent Nakagami random variables with probability density functions (pdf)

$$p(\alpha_i^{(k)}) = M(\alpha_i^{(k)}, m, \Omega_i^{(k)}),$$

where (2)

$$M(R, m, \Omega) = \frac{2\, m^m\, R^{2m-1}}{\Gamma(m)\, \Omega^m} e^{-(m/\Omega)R^2} \quad ,$$

and the phases $\{\psi_i^{(k)}\}$ are iid random variables uniform in $(0, 2\pi)$ and are independent of $\{\alpha_i^{(k)}\}$. In (2), m is a fade parameter assumed common for all paths and is equal to the inverse of the 'normalized variance' of $\alpha_i^{(k)}$, i.e., $m = E[(\alpha_i^{(k)})^2] / \mathrm{var}[(\alpha_i^{(k)})^2]$; for this reason, 1/m is termed the 'fading figure' [17]; m is also related to the commonly used scintillation index, S_4, by $m=(S_4)^{-2}$ [14, 18]. The parameter $\Omega_i^{(k)}$ is the second moment of

$\alpha_i^{(k)}$ (i.e. $\Omega_i^{(k)} = E[(\alpha_i^{(k)})^2]$), and is assumed to be related to the second moment of the initial path strength $\Omega_0^{(k)}$ by

$$\Omega_i^{(k)} = \Omega_0^{(k)} e^{-\delta i} \quad , \quad \delta \geq 0 \quad . \tag{3}$$

This functional form for $\Omega_i^{(k)}$ accounts for the decay of average path strength as a function of path delay; the parameter δ reflects the rate at which this decay occurs. The shape of the decay function (3) is sometimes referred to as the multipath intensity profile (MIP). The MIP is assumed to be exponential here, and actual measurements [19] indicate that this is fairly accurate for a congested urban area.

N(t) in Fig. 1 is the complex valued low - pass - equivalent AWGN with two-sided spectral density η_0; therefore, N(t) is a circularly symmetric, zero-mean Gaussian random process with covariance function $E[\, N(t)\, N^*(\tau)\,] = 2\,\eta_0\,\delta(t-\tau)$. The number of paths $L_p^{(k)}$ is related to the maximum delay spread, Δ, of the channel and is assumed known (or measurable). Furthermore, $L_p^{(k)}$ is assumed to be less than N (which is equivalent to assuming that the maximum delay spread is less than T); since Δ is on the order of 5 μs (for urban areas) [10], this is a reasonable assumption for bit rates of 200 KHz or less.

Charash [20] and Xiang [8] used a similar model to analyze the performance of noncoherent orthogonal signalling and noncoherent CDMA respectively; their model is not a tapped delay line but a random delay, discrete 'resolvable' path model with equal average path strengths (i.e., their MIP is a constant). The random delay model seems to be better suited for situations where there are only a few distinct paths, whereas the tapped delay line model is more suitable for situations where the delay profile is more or less continuous and where the propagation is highly frequency - selective [9, 16].

IV. Receiver Model

The receiver structure is shown in Figure 2a for the reference user (k = 0), where the superscript has been omitted for convenience (variables without superscripts will refer to the reference user unless otherwise noted). This receiver is essentially a coherent RAKE receiver [21], where the number of taps, L_R, is a variable parameter less than or equal to L_P. L_R is made a variable so that the effect of diversity may be observed. For the ideal coherent receiver assumed here, the results will show that the optimal value for L_R is L_P, as one might

expect; the same is not necessarily true for incoherent reception, however, as Ochsner [9] has shown for a Rayleigh channel.

The matched filter is matched to the reference user's CDMA code and is assumed to have achieved time synchronization with the intial path of the reference signal. Because the period of the spreading sequence is larger than the bit interval, the matched filter sub-sequence needs to be updated every T seconds. Also, in order to demodulate the multipath, the filter must remain matched to each sub-sequence for $(L_R\text{-}1)T_c$ seconds. Since $L_R \le L_P < N$, $(L_R\text{-}1)T_c < T$ and therefore a single matched filter suffices to serially demodulate each bit.

The tap weights and phases are assumed to be perfect estimates of the channel parameters. In practice, these estimates may be obtained from separate circuits, such as those given in Proakis [16], and then fed to the demodulator; or the estimation and coherent demodulation may be done jointly through tone calibration techniques [e.g., 22, 23, 24], in which case the actual receiver would be different from that shown but the analysis that follows would still apply (transmitting a pilot tone would incur some penalty in power, but this could be accounted for by simply shifting the SNR axis of the results by an appropriate amount).

The sampling times of the receiver are $nT+(L_R\text{-}1)T_c$, where n is an integer index. For example, to detect the zeroth information bit b_0, the sample time would be $T+(L_R\text{-}1)T_c$; the 'T' term is from the usual matched filter sampling time and the '$(L_R\text{-}1)T_c$' term is from the combining of the $(L_R\text{-}1)$ paths following the initial path. Figure 2b shows the chip sequences of each path of the reference signal going into the matched filter.

V. Performance Analysis

With the input to the channel as given in (1), and noting that the channel responds to each user independently, the output of the channel (which is also the input to the receiver) may be written as (in the sequel, only the complex envelope will be given)

$$R_T(t) = \sum_{k=0}^{K} R_k(t) + N(t) \quad ,$$

where

$$R_k(t) = \sqrt{2P} \sum_{n=0}^{L_p^{(k)}-1} a_k(t-nT_c-\tau_k)\, b_k(t-nT_c-\tau_k)\, \alpha_n^{(k)}\, e^{j\xi_n^{(k)}} \quad ,$$

and where $\left\{\xi_n^{(k)}\right\} = \left\{\psi_n^{(k)} + \phi_k\right\}$ are iid and uniformly distributed in $(0, 2\pi)$.

The response of the reference receiver to $R_T(t)$ at any sampling instant, say at $t = T+(L_R-1)T_c$, may be separated into a signal component, denoted by U_s, and three noise components, denoted U_{mp}, U_{ma}, and U_N; the first noise component is due to 'self-noise' from the multipath waveform of the reference signal, the second component is due to 'multiple access' noise from all the other users, and the third component is due to AWGN. Thus the total response is

$$U = U_s + U_{mp} + U_{ma} + U_N \quad .$$

Since both the noise and fading processes are assumed stationary, it is clear that the error probability at only one sampling instant need be evaluated; moreover, as usual in BER calculations, the path strengths and phases are assumed constant during any bit interval.

(A) Conditional Error Probability

From the channel and receiver models, U_N may be represented as

$$U_N = \sqrt{2P} \sum_{n=0}^{L_R-1} \alpha_n \, e^{-j\psi_n} \int_{nT_c}^{T+nT_c} a_0(\tau - nT_c)\, N(\tau)\, d\tau \; .$$

Letting $t = \tau - nT_c$ in the above integral yields the more convenient expression

$$U_N = \sqrt{2P} \sum_{n=0}^{L_R-1} \alpha_n \, e^{-j\psi_n} \int_{0}^{T} a_0(t)\, N(t + nT_c)\, dt \; .$$

Conditioned on $\{\alpha_n\}$ and $a_0(t)$, U_N is a complex Gaussian random variable with zero mean and variance $E[U_N U_N^* \mid \{\alpha_n\}, a_0(t)] = 2P \sum_{n=0}^{L_R-1} \alpha_n^2 \, (2\eta_0 T)$. Since the conditional statistics of U_N do not depend on $a_0(t)$, the conditioning on $a_0(t)$ may be removed without destroying the Gaussian nature of U_N; the conditioning on $\{\alpha_n\}$ is retained, however. Also, conditioned on $\{\alpha_n\}_{n=0}^{L_R-1}$, each term in the above sum (in the expression for U_N) is zero-mean and circularly symmetric (N(t) being zero-mean and circularly symmetric implies that the integrals are

also zero-mean and circularly symmetric; the exponential factor merely adds an independent random phase to each term and does not affect its statistics). Therefore, U_N is Gaussian, zero-mean, and circularly symmetric; furthermore, the terms are pairwise uncorrelated, and thus

$$\sigma_N^2 \equiv \mathrm{var}(U_N) = E\left[U_N U_N^* \mid \{\alpha_n\}\right] = 4\,E\,\eta_0 \sum_{n=0}^{L_R-1} \alpha_n^2 \ , \qquad (4)$$

where $E = PT$ is the average transmitted energy-per-bit.

To determine U_{ma}, consider the receiver response to the k-th ($k \neq 0$) signal, conditioned on $a_0(t)$ and $\{\alpha_n\}$,

$$U_{ma}^{(k)} = \sqrt{2P} \sum_{n=0}^{L_R-1} \alpha_n\, e^{-j\psi_n}\, \widetilde{R_k}(T + nT_c) \ ,$$

where $\widetilde{R_k}(.)$ is the matched filter response to $R_k(.)$; denoting the impulse response of the matched filter as $h(\tau)$, the response to $R_k(.)$ may be written as

$$\widetilde{R_k}(t) = \sqrt{2P} \sum_{i=0}^{L_p^{(k)}-1} \alpha_i^{(k)}\, e^{j\xi_i^{(k)}} \int_{t-T}^{t} h(t-\tau)\, a_k(\tau-\tau_k-iT_c)\, b_k(\tau-\tau_k-iT_c)\, d\tau \ .$$

Substituting in $h(\tau) = a_0(T-\tau)$ and setting $t = T+nT_c$ yields

$$\widetilde{R_k}(T+nT_c) = \sqrt{2P} \sum_{i=0}^{L_p^{(k)}-1} \alpha_i^{(k)}\, e^{j\xi_i^{(k)}} \int_{nT_c}^{T+nT_c} a_0(\tau-nT_c)\, a_k(\tau-\tau_k-iT_c)\, b_k(\tau-\tau_k-iT_c)\, d\tau \ .$$

Changing the dummy variable of integration to $t = \tau-nT_c$, the filter response may now be written as

$$\widetilde{R_k}(T + nT_c) = \sqrt{2P} \sum_{i=0}^{L_p^{(k)}-1} \alpha_i^{(k)}\, e^{j\xi_i^{(k)}} \int_{0}^{T} a_0(t)\, a_k(t-\tau_k + (n-i)T_c)\, b_k(t-\tau_k + (n-i)T_c)\, dt \ . \qquad (5)$$

If the period of the CDMA signature sequence is large relative to the processing gain, then the sequences may be modelled as random binary sequences, where each chip in a sequence is independently determined (by flipping a coin, for example), and the sequences are mutually independent; using this model for the code sequences, the integral in (5), call it $I_{n-i}^{(k)}(\tau_k)$, can be shown to be a zero-mean random variable with conditional variance $\frac{2T^2}{3N}$ $+ \frac{T^2}{6N}\sum_{i=0}^{N-2} a_i\, a_{i+1}$. Note that the second term of this conditional variance is proportional to the (N-1 chip) partial autocorrelation of the spreading sequence, and therefore its magnitude is small relative to the first term for almost all possible sequences. In fact, even though the signature sequences are commonly modelled as being randomly generated, in practice, they are PN sequences that have small partial autocorrelations by design [25]. In light of the relative insignificance of the second term, only the dominant first term will be retained in the subsequent analysis. Thus, from (5), $\widetilde{R_k}(T + nT_c)$ is taken to be zero-mean with conditional variance

$$\sigma_k^2 = 2P\,(\frac{2T^2}{3N}) \sum_{i=0}^{L_p^{(k)}-1} E[(\alpha_i^{(k)})^2] = 2P(\frac{2T^2}{3N}) \sum_{i=0}^{L_p^{(k)}-1} \Omega_i^{(k)} = 2P\,(\frac{2T^2}{3N})\, \Omega_0^{(k)}\, q(L_P^{(k)}, \delta)\ ,$$

where Eq. (3) was used and $q(L_P^{(k)}, \delta) \equiv \left(\frac{1-e^{-\delta L_p^{(k)}}}{1-e^{-\delta}}\right)$; this implies that $U_{ma}^{(k)}$ is also zero-mean with approximate variance $4P^2\,(\frac{2T^2}{3N})\, \Omega_0^{(k)}\, q(L_P^{(k)}, \delta) \sum_{n=0}^{L_R-1} \alpha_n^2$.

Furthermore, conditioned on $a_0(t)$, the $U_{ma}^{(k)}$ are independent for different k, as may be seen by writing $U_{ma}^{(k)}$ as

$$U_{ma}^{(k)} = 2P \sum_{n=0}^{L_R-1} \alpha_n \sum_{i=0}^{L_p^{(k)}-1} \alpha_i^{(k)}\, e^{j(\xi_i^{(k)}-\psi_n)}\, I_{n-i}^{(k)}(\tau_k),$$

where the $\{I_{n-i}^{(k)}(\tau_k)\}$ are independent for different k because the spreading waveforms $\{a_k(t)\}$, as well as the data waveforms $\{b_k(t)\}$, are independent for different k; the $\{\alpha_i^{(k)}\}$ are independent by assumption, and the $\{\xi_i^{(k)}-\psi_n\}$ are independent because the $\{\xi_i^{(k)}\}$ are iid and uniform in $(0, 2\pi)$ [26]. Also, $U_{ma}^{(k)}$ has bounded absolute third moments since $I_{n-i}^{(k)}(\tau_k)$ is bounded by T and $\alpha_i^{(k)}$ has finite absolute moments of all finite order. With these properties of $U_{ma}^{(k)}$, Liapounoff's version of the central-limit-theorem [27] is applicable to the

sequence $\{U_{ma}^{(k)}\}$, and therefore, as the number of users $K \to \infty$, $U_{ma} = \sum_{k=1}^{K} U_{ma}^{(k)}$ is asymptotically normal with zero-mean and conditional variance

$$\sigma_{ma}^2 = \frac{8E^2}{3N} \sum_{k=1}^{K} \Omega_0^{(k)} \, q(L_P^{(k)}, \delta) \sum_{n=0}^{L_R-1} \alpha_n^2 \quad . \tag{6}$$

Note that since σ_{ma}^2 is independent of $a_0(t)$, the conditioning on $a_0(t)$ may be removed as was done for U_N. Thus, for K large, U_{ma} may be approximated as a zero-mean, circularly symmetric, Gaussian random variable with variance given by (6). The use of the Gaussian approximation in BER calculations is well documented and it has been shown to be quite accurate even for small values of K (< 10) when the BER is 10^{-3} or greater [3, 6, 28, 29].

Next, consider the response to $R_0(t)$; recalling that the receiver is in time synchronism with the initial path of $R_0(t)$, and that the sampling time is $T + (L_R-1)T_c$, the response to $R_0(t)$, which by definition is equal to U_s+U_{mp}, may be written as [Appendix A]

$$U_s + U_{mp} = 2PT_c \, x^T A y \quad , \tag{7a}$$

where $$x^T = [\, \alpha_0 e^{j\psi_0}, \alpha_1 e^{j\psi_1}, \ldots, \alpha_{L_P-1} e^{j\psi_{L_P-1}} \,] \quad ,$$

$$y^T = [\, \alpha_0 e^{-j\psi_0}, \alpha_1 e^{-j\psi_1}, \ldots, \alpha_{L_R-1} e^{-j\psi_{L_R-1}} \,] \quad , \qquad L_R \le L_P < N$$

and A is a L_P by L_R matrix with elements $\{a_{ij}\}$ given by

$$a_{ij} = \begin{cases} b_0 \, N & , \; i=j \\ b_{-1} \, c_{-1}(i-j) + b_0 \, c_0(i-j) & , \; i>j \\ b_1 \, c_1(j-i) + b_0 \, c_0(j-i) & , \; i<j \end{cases} \tag{7b}$$

$$c_{-1}(k) = \sum_{n=0}^{k-1} a_n \, a_{n-k} \quad , \quad c_{-1}(0) = 0$$

$$c_0(k) = \sum_{n=0}^{N-k-1} a_n \, a_{n+k}$$

$$c_1(k) = \sum_{n=N-k}^{N-1} a_n \, a_{n+k} \quad .$$

The signal component U_s consists of the contributions from the elements of A for which i=j, thus

$$U_s = b_0 2 E \sum_{n=0}^{L_R-1} \alpha_n^2 \quad . \tag{8}$$

Note that conditioned on $\{\alpha_n\}_{n=0}^{L_R-1}$ and b_0, U_s is a constant.

U_{mp} is slightly more complicated and is dependent on the adjacent bits b_{-1} and b_1, as well as on the assigned signature code and its partial autocorrelation properties. Conditioned on the signature sequence and $\{\alpha_n\}$, U_{mp} is independent of U_{ma}. Furthermore, for large K, the magnitude of U_{mp} is small relative to that of U_{ma}, and as $K\rightarrow\infty$, the sum $U_{mp}+U_{ma}$ is asymptotically normal [27] with zero mean and variance $\sigma_{mp}^2+\sigma_{ma}^2$. The parameter σ_{ma}^2 has already been found and is given in (6), where it is seen that it does not depend on the spreading waveform $a_0(t)$ (or equivalently, the spreading sequence $\{a_i\}$). The parameter σ_{mp}^2, however, is clearly dependent on $\{a_i\}$, as (7b) indicates. This dependence on $\{a_i\}$ implies that, in order to find the average BER, the conditional BER must be averaged over all possible sequences for $\{a_i\}$, which is computationally not feasible. Therefore, some modification for σ_{mp}^2 must be made; one option is to simply ignore it for very large K, since $\sigma_{mp}^2/\sigma_{ma}^2 \rightarrow 0$ as $K\rightarrow\infty$; for moderate values of K, more accurate results could be obtained if a non-zero estimate for σ_{mp}^2 is used. In light of the relatively simple expression obtained for σ_{ma}^2 in (6), and the fact that U_{ma} is the dominant noise term in practical systems, an approximation for σ_{mp}^2, with similar form to σ_{ma}^2, is derived from (6) by noting certain relationships between U_{ma} and U_{mp}. First, the multipath noise may be considered as the (K+1)-st multiple access user, where instead of L_P paths, there would be only (L_P-1) paths at the input to the receiver because one path goes to U_s. This may be accounted for by replacing the first sum in (6) by $\Omega_0[q(L_P, \delta)-1]$ (which equals the total power received from all the paths except the initial path). Second, because the multipath noise is chip synchronized with the receiver, a factor of 3/2 is introduced in σ_{mp}^2 [e.g., 30]. Therefore, combining these two relationships between U_{ma} and U_{mp}, σ_{mp}^2 is approximated as

$$\sigma_{mp}^2 \approx 4 \frac{E^2}{N} \Omega_0 [q(L_P, \delta)-1] \sum_{n=0}^{L_R-1} \alpha_n^2 \quad . \tag{9}$$

Putting the pieces together, U is now modelled as a complex Gaussian random variable with conditional mean U_s and conditional variance given by $\sigma_{mp}^2 + \sigma_{ma}^2 + \sigma_N^2$. Furthermore, the total 'noise' ($U_{mp} + U_{ma} + U_N$) is circularly symmetric, since each of its three components is circularly symmetric; thus, the decision variable Re[U] is a real Gaussian random variable with mean U_s (since U_s is real) and variance

$$\sigma_T^2 = \frac{1}{2}\left(\sigma_{mp}^2 + \sigma_{ma}^2 + \sigma_N^2\right) . \tag{10}$$

From symmetry, the conditional error probability does not depend on the data bit b_0; therefore assume $b_0=1$, denote

$$S \equiv \frac{1}{\Omega_0} \sum_{n=0}^{L_R-1} \alpha_n^2 \tag{11}$$

and, to reduce the number of parameters, let

$$\sum_{k=1}^{K} \Omega_0^{(k)}\, q(L_P^{(k)}, \delta) = K\, \Omega_0\, q(L_P, \delta) . \tag{12}$$

Then the conditional bit error probability may be written as

$$P_b(S) = \phi(-U_s/\sigma_T) = \phi(-\sqrt{\gamma\, S}) . \tag{13a}$$

where $\phi(x) = \frac{1}{\sqrt{2\pi}} \int_{-\infty}^{x} e^{-t^2/2}\, dt$ and γ is given by

$$\gamma = \left(\frac{q(L_P, \delta)-1}{2N} + \frac{K\, q(L_P, \delta)}{3N} + \frac{\eta_0}{2E\Omega_0} \right)^{-1} . \tag{13b}$$

When $L_P=1$ (no multipath), then $q(L_P,\delta)=1$ and the first term of (13b) vanishes; if $\Omega_0=1$ as well (no fading), then γ reduces to the SNR expression derived by Pursley [31] for a one path channel.

(B) Average Error Probability

The average bit error probability is calculated from the conditional error probability by averaging $P_b(S)$ with the pdf of S, p(S). Since, from Eqs.(11) and (3), S is a sum of squares of Nakagami random variables with densities $M(\alpha_i, m, e^{-\delta i})$, S may be approximated [17] as the square of another Nakagami random variable with density

$$p(S) \approx M(\sqrt{S}, m_S, \Omega_S), \text{ where} \tag{14a}$$

$$m_S = \frac{\left(\sum_{i=0}^{L_R-1} e^{-\delta i}\right)^2}{\sum_{i=0}^{L_R-1} \frac{\left(e^{-\delta i}\right)^2}{m}} = m\,\frac{q(L_R, \delta)^2}{q(L_R, 2\delta)} \tag{14b}$$

$$\text{and} \quad \Omega_S = \sum_{i=1}^{L_R} e^{-\delta(i-1)} = q(L_R, \delta) \ . \tag{14c}$$

It is easily verified from (11) and (14) that $\Omega_s = E[S]$ and $m_s = E[S]^2/\text{var}[S]$, which is consistent with the definition of the density $M(\sqrt{S}, m_S, \Omega_S)$. It is also noted that the approximation is exact when $\delta=0$, i.e., when the average path strengths are equal. When $\delta \neq 0$, the approximation in (14a) may be calibrated by numerically calculating the pdf for specific cases. For this purpose, the exact and approximated pdf's for m = 1 (Rayleigh), $L_R = 2$, and $\delta = 0.2$ were calculated and were found to be virtually identical. In fact, the approximated pdf did not deviate from the exact pdf appreciably until δ was increased to about 1.0. Since the values of δ of interest are small fractions of 1, (14a) is an exact relationship for all intents and purposes.

The average bit error probability P_b, then, may be written as

$$P_b = \int_0^\infty P_b(S)\, p(S)\, dS = \int_0^\infty \Phi(-\sqrt{\gamma S})\, M(\sqrt{S}, m_S, \Omega_S)\, d\sqrt{S} \ . \tag{15}$$

The integral in (15) is the usual formulation for the bit error probability of coherent binary signalling in a Nakagami channel and has a known solution [e.g., 32] (for completeness, it is also derived in Appendix B);

$$P_b = \sqrt{\frac{\gamma_S}{1+\gamma_S}} \frac{(1+\gamma_S)^{-m_S}\,\Gamma(m_S+\frac{1}{2})}{2\sqrt{\pi}\,\Gamma(m_S+1)} {}_2F_1(1,\, m_S+\tfrac{1}{2};\, m_S+1;\, \frac{1}{1+\gamma_S}) \quad , \tag{16a}$$

where $$\gamma_S = \frac{\gamma\,\Omega_S}{2m_S} = \frac{\gamma\, q(L_R,\, 2\delta)}{2\, m\, q(L_R,\, \delta)} \tag{16b}$$

is the effective SNR per path, $\Gamma(.)$ is the Gamma function defined as

$$\Gamma(z) = \int_0^\infty e^{-t}\, t^{z-1}\, dt\,, \quad z > 0 \quad ,$$

${}_2F_1(a, b; c; z)$ is the hypergeometric function defined as

$${}_2F_1(a, b; c; z) = \sum_{k=0}^{\infty} \frac{(a)_k\,(b)_k\, z^k}{(c)_k\, k!} \quad ,$$

and

$$(a)_k = a\,(a+1)\,\ldots\,(a+k-1),\ (a)_0 = 1\ .$$

It is also shown in Appendix B that when m_S is an integer, P_b may be further simplified to

$$P_b = \frac{1}{2}\left[1-\mu \sum_{k=0}^{m_S-1} \binom{2k}{k}\left(\frac{1-\mu^2}{4}\right)^k\right], \qquad \mu = \sqrt{\frac{\gamma_S}{1+\gamma_S}} \ . \tag{17}$$

For the particular case of m=1 and L_R=1, then m_S=1 and (17) reduces to the familiar expression for P_b in Rayleigh fading with no diversity. When m=1 and δ=0 (equal average path strengths), then $m_S=L_R$ and (17) is the bit error probability for maximal ratio combining of L_R paths in Rayleigh fading and is equivalent to the expression given in Proakis [16, Eq. 7.4.15].

VI. Numerical Results

For convenience, the various parameters affecting the bit error probability are recapped below.

N	----	processing gain of the CDMA system; number of chips per bit.
K	----	number of users, not including the reference user.
m	----	fading figure of each path, common to all paths and all users.
L_P	----	total number of paths received from the reference user.
L_R	----	total number of paths combined.
δ	----	rate of exponential decay of the MIP.
$E\Omega_0/\eta_0$	---	average received SNR per bit of initial path of reference signal.

The statistics of the K non-reference users affect the bit error probability through their relationship with Ω_0 and L_P as given in Eq. (12).

The processing gain of the spreading sequence N is usually constrained by the available bandwidth and the information rate. In all of the numerical results that follow, N is kept constant at 127.

To show the improvement afforded by diversity, Figures 3a-3d depict P_b as a function of the average received SNR per bit γ_0, defined as

$$\gamma_0 \equiv E\Omega_0/\eta_0$$

for m=1 (Rayleigh fading), K=50, L_P=10, and δ=0, 0.1, 0.2, and 0.4, respectively; the individual curves in each figure are parametrized by L_R=1, 2, ..., 10. From these plots, it is seen that the faster the MIP decays, the faster the incremental improvement of diversity decreases. Moreover, unlike incoherent combining [9], the optimal value of L_R is seen to be its maximum value (= L_P) for maximal ratio combining.

Figures 4a and 4b show essentially the same trend as Figures 3, but in a different format, with m=0.75, L_R=L_P, γ_0 fixed at 10 dB, and δ=0 (Fig. 4a & 4b) and δ=1/L_P (Fig. 4c & 4d); since L_P is a channel model parameter that reflects the degree of frequency selectivity that the signals experience, Figures 4a through 4d show the effect of this channel characteristic on bit error performance.

Eqs. (16) and (17) may be specialized to produce known results by letting K=0 and L_P=1. Figure 5 depicts P_b as a function of γ_0 for K=0 (no other users) and L_P=1 (no multipath), each curve parameterized by m. The first nine curves are for m=1/2 through m=9/2 in increments of 1/2, and the last curve is for the limiting

case of no fading (m=∞). The results contained in Figure 5 are consistent with those obtained by Nesenbergs [32] and Miyagaki, et al [33].

Figure 6 shows P_b vs γ_0 for m=1, $L_P=L_R=1$, and different values of K (K=10, 20, ..., 100); note that the asymptotic values of the different curves are spaced apart logarithmically, just as the vertical axis tick marks are, indicating a proportionality between K and P_b as γ_0 becomes large. This relationship may be verified by approximating the expression for P_b as follows: For $m=L_P=L_R=1$, P_b is obtained from (17) as

$$P_b = \frac{1}{2}\left[1-\sqrt{\frac{\gamma_S}{1+\gamma_S}}\right] = \frac{1}{2}\left[1-\sqrt{\frac{\gamma}{2+\gamma}}\right] ,$$

where the second equality follows because $\gamma_S = \gamma/2$ and γ is as given by (13b) with $q(L_P,\delta)=1$; rewriting $\sqrt{\frac{\gamma}{2+\gamma}}$ as $\left(1+\frac{2}{\gamma}\right)^{-1/2}$ and approximating the latter by $1-1/\gamma$ yields $P_b \approx 1/(2\gamma)$, which has the asymptotic value

$$P_b(\gamma_0 \to \infty) \approx \frac{K}{6N} .$$

Figures 7a and 7b show P_b as a function of K for $L_P=L_R=10$, $\delta=0$, and m=0.75, 1.0, respectively, the individual curves being parameterized by γ_0. From these plots, it is evident that for any fixed P_b, there is a maximum value of K that the system can achieve; also, it is seen that having γ_0 much greater than 10 dB does not increase the capacity by an appreciable amount.

Finally, Figure 8 depicts the required γ_0 to achieve a certain bit error probability as a function of K for $L_P=L_R=10$, $\delta=0$, and m=0.75 and 1.0.

VII. Channel Coding

To further enhance system performance when operating in a stressed environment, some form of channel coding is usually employed. A detailed description of coding techniques is beyond the scope of the present work; the intent here is merely to indicate the performance enhancement possible with coding by examining briefly one particular code. The code selected is one of the most commonly used coding schemes, namely a convolutional, rate 1/2, constraint length 7 code with a Viterbi algorithm (hard decision) decoder. It is

assumed that the input symbol sequence is properly interleaved so that the channel symbol errors may be considered independent. The tap weights of the encoder shift registers are given in Odenwalder [34].

If hard decisions are used in the decoding algorithm, the decoded bit eror probability is dependent only on the channel symbol error probability, which has already been derived in the previous sections. The relationship between the coded bit error probability, P_B, and the channel error probability, P_c, of the selected code has been obtained through simulation and is presented in [34]. If Odenwalder's simulation curve [34, p. 129] is approximated by a straight line, then a functional relationship for this code is

$$P_B = 10^4 (P_c)^5 , \quad 10^{-1} \le P_c \le 10^{-2} , \tag{18}$$

where P_c is obtained from Eq.(16) with E in the expression for γ_S replaced by $E_b/2$, E_b being the transmitted energy per information bit; the factor of 1/2 arises from the rate (=1/2) of the code. The range restrictions of P_c in (18) imply that the range of P_B for which (18) is valid is $10^{-1} \le P_B \le 10^{-6}$, a range that covers almost all cases of interest.

Using (18), curves analogous to those of Figure 8 are shown in Figure 9. The processing gains of the coded curves are reduced by a factor of 1/2 in order for the chip rates to be equal to those of the uncoded cases. It is seen that the effect of channel coding is a 'stretching' of the performance curves to the right. From Figures 8 and 9, it is seen that in some cases, the coded channel can accommodate twice as many users at equal BER and equal $\gamma_b \equiv \Omega_0 E_b/\eta_0$ (average received SNR per information bit) as the uncoded channel. For example, at a BER of 10^{-3} and γ_b at 10 dB, the uncoded channel can tolerate about 23 (K=22) simultaneous transmissions, whereas the coded channel can tolerate about 49.

VIII. Conclusions/Summary

An analysis of the BER performance of coherent DS - CDMA in a Nakagami multipath fading channel has been presented. A RAKE receiver with perfect channel information was assumed. Using an exponentially decaying MIP, it was found that for a fast decaying MIP, the paths with low average strengths provide little information relative to the initial paths; moreover, for any decay rate, increasing the number of available independent paths (L_P) exhibits the usual 'diminishing returns' characteristic of diversity systems. It was also found that increasing the average received SNR of the initial path (γ_0 uncoded, γ_b coded) much beyond 10 dB

only slightly improved the BER performance. Finally, the improvement afforded by channel coding was demonstrated using a rate 1/2, constraint length 7 convolutional encoder with Viterbi decoding.

Appendix A

The receiver response to the reference multipath signal $R_0(t)$ will be examined. Recall that $R_0(t)$ is represented as

$$R_0(t) = \sqrt{2P} \sum_{i=0}^{L_P-1} a_0(t-iT_c)\, b_0(t-iT_c)\, \alpha_i\, e^{j\psi_i} \quad . \tag{A1}$$

Recall also that the matched filter is matched to $a_0(t)$ and is time synchronized with the initial path of $R_0(t)$. Therefore, the output of the matched filter at time t may be written as

$$\widetilde{R_0}(t) = \sqrt{2P} \sum_{i=0}^{L_P-1} \alpha_i\, e^{j\psi_i} \int_{t-T}^{t} a_0(T+\tau-t)\, a_0(\tau-iT_c)\, b_0(\tau-iT_c)\, d\tau \quad . \tag{A2}$$

At the sampling time $T+(L_R-1)T_c$, (A2) is then

$$\widetilde{R_0}(T+(L_R-1)T_c) = \sqrt{2P} \sum_{i=0}^{L_P-1} \alpha_i\, e^{j\psi_i}\, c(i) \quad , \tag{A3}$$

where $$c(i) = \int_{(L_R-1)T_c}^{T+(L_R-1)T_c} a_0(\tau-(L_R-1)T_c)\, a_0(\tau-iT_c)\, b_0(\tau-iT_c)\, d\tau \quad . \tag{A4}$$

Changing the dummy variable in (A4) to $t = \tau - (L_R-1)T_c$ yields

$$c(i) = \int_0^T a_0(t)\, a_0(t+(L_R-1-i)T_c)\, b_0(t+(L_R-1-i)T_c)\, dt \, . \tag{A5}$$

Note that if $a_0(t+(L_R-1-i)T_c)b_0(t+(L_R-1-i)T_c)$ is defined as a single new sequence, then c(i) is the integral of a product of two binary sequences of the same chip rate, where both sequences are chip synchronized with the integration interval, and one sequence (the one containing the data) is shifted relative to the other by an integer number of chips according to the value of L_R-1-i; if i is greater than L_R-1, the data sequence is shifted to the

right (time increases from left to right) of the matched filter (MF) sequence by $i-L_R+1$ chips. and if i is less than L_R-1, the data sequence is shifted to the left of the MF sequence by L_R-1-i chips. Thus the matched filter output consists of a sum of integrals of products of two sequences with relative shifts ranging from L_R-1 to L_R-L_P. It is clear from (A5) that the first tap of the receiver (the one with no delay) 'rakes' the information bit from the (L_R-1)-st path. The purpose of the L_R-1 delays is to similarly rake the information bits embedded in the other paths. For example, at the output of the first delay, 'L_R-1' in (A5) is replaced by 'L_R-2' and the (L_R-2)-nd path is raked.

The response at the output of the summer, call it U_0, may be pictorially depicted as in Figure A1, where the top group of sequences represents the L_R MF sequences, one for each delay (j=0 denotes zero delay, j=1 denotes one chip delay, etc.) and the bottom group of sequences represents the L_P (data) signal paths. The multiplier coefficients for each sequence are shown at the left of the respective sequences. U_0 consists of L_PL_R terms, and each term involves the integral of the product of two sequences, one from the MF group and one from the data group, the integration interval coinciding with the MF sequence; for example, the term for i=2 and j=1 is

$$r_{21} = 2PT_c\,\alpha_1\alpha_2\, e^{j(\psi_2-\psi_1)}\left[b_0 \sum_{n=0}^{N-2} a_n\, a_{n+1} + b_{-1}\, a_0\, a_{-1}\right]$$

and, in general,

$$r_{ij} = \begin{cases} 2PT_c\,\alpha_i\,\alpha_j\, e^{j(\psi_i-\psi_j)}\,[b_{-1}\, c_{-1}(i-j) + b_0\, c_0(i-j)] & i \geq j \\ 2PT_c\,\alpha_i\,\alpha_j\, e^{j(\psi_i-\psi_j)}\,[b_0\, c_0(j-i) + b_1\, c_1(j-i)] & i<j \end{cases}, \qquad \text{(A6)}$$

where $c_{-1}(k) = \sum_{n=0}^{k-1} a_n\, a_{n-k}$, $c_{-1}(0) = 0$

$$c_0(k) = \sum_{n=0}^{N-k-1} a_n\, a_{n+k}$$

and $$c_1(k) = \sum_{n=N-k}^{N-1} a_n\, a_{n+k}\ , \quad k \geq 1. \qquad \text{(A7)}$$

The terms of (A6) for which i=j are the terms that comprise U_s, the signal component of the decision variable; the remaining terms comprise the multipath noise component U_{mp}. It is convenient to express the reponse U_0 in matrix notation. Let

$$x^T = [\alpha_0 e^{j\psi_0}, \alpha_1 e^{j\psi_1}, \ldots, \alpha_{L_P-1} e^{j\psi_{L_P-1}}]$$

$$y^T = [\alpha_0 e^{-j\psi_0}, \alpha_1 e^{-j\psi_1}, \ldots, \alpha_{L_R-1} e^{-j\psi_{L_R-1}}] \quad , \quad L_R \le L_P < N$$

and $A = [a_{ij}], \qquad 1 \le i \le L_P, 1 \le j \le L_R$

where $$a_{ij} = \begin{cases} b_0 N & , i=j \\ b_{-1} c_{-1}(i-j) + b_0 c_0(i-j) & , i>j \\ b_1 c_1(j-i) + b_0 c_0(j-i) & , i<j \end{cases} .$$

Then $$U_0 = \sum_{i=0}^{L_P-1} \sum_{j=0}^{L_R-1} r_{ij} = 2PT_c\, x^T A y \ . \qquad (A8)$$

Appendix B

In the study of coherent reception of fading signals, the following integral frequently arises,

$$P = \frac{a^b}{\Gamma(b)} \int_0^\infty e^{-at}\, t^{b-1}\, \phi(-\sqrt{ct})\, dt \quad , \tag{B1}$$

where $\phi(x) = \frac{1}{\sqrt{2\pi}} \int_{-\infty}^{x} e^{-t^2/2}\, dt$, and a, b, and c are positive real numbers; noting that

$\phi(-x) = 1-\phi(x) = \frac{1}{\sqrt{2\pi}} \int_x^\infty e^{-t^2/2}\, dt$, P may be written as

$$P = \frac{a^b}{\Gamma(b)} \frac{1}{\sqrt{2\pi}} \int_0^\infty e^{-at}\, t^{b-1} \int_{\sqrt{ct}}^\infty e^{-u^2/2}\, du\, dt \tag{B2}$$

Note that the region of integration is the portion of the upper right quadrant above the curve $t = u^2/c$ (t is the horizontal axis, u the vertical axis).

Changing the order of integration, (B2) is written as

$$P = \frac{a^b}{\Gamma(b)} \frac{1}{\sqrt{2\pi}} \int_0^\infty e^{-u^2/2} \int_0^{u^2/c} e^{-at}\, t^{b-1}\, dt\, du \quad .$$

Letting x = at in the inner integral yields

$$P = \frac{1}{\Gamma(b)\sqrt{2\pi}} \int_0^\infty e^{-u^2/2} \int_0^{au^2/c} e^{-x}\, x^{b-1}\, dx\, du \quad , \tag{B3}$$

where the inner integral in (B3) is now recognized as the incomplete Gamma function, which is expressible as a confluent hypergeometric function by the following identity [35, p.220 or 36, pp.253, 266] .

$$\int_0^z x^{b-1}\, e^{-x}\, dx = b^{-1}\, z^b\, e^{-z}\, {}_1F_1(1; b+1; z) \quad . \tag{B4}$$

Using (B4) in (B3) yields

$$P = \frac{(a/c)^b}{b\Gamma(b)\sqrt{2\pi}} \int_0^\infty u^{2b}\, e^{-\alpha u^2}\, {}_1F_1(1; b+1; au^2/c)\, du \quad , \tag{B5}$$

where $\alpha = a/c + 1/2$. Next, let $y = \alpha u^2$, then (B5) becomes

$$P = \frac{(a/c)^b}{\Gamma(b+1)\sqrt{2\pi}} \frac{1}{2} \left(\frac{1}{\alpha}\right)^{b+1/2} \int_0^\infty y^{b-1/2}\, e^{-y}\, {}_1F_1(1; b+1; \frac{a}{\alpha c} y)\, dy \quad . \tag{B6}$$

The integral in (B6) is integrable by the following formula [35, p.59 or 36, p.269], which is easily verified by integrating term by term the power series expansion of ${}_1F_1$.

$$\Gamma(\sigma)\, {}_2F_1(\sigma, p; q; w) = \int_0^\infty e^{-y}\, y^{\sigma-1}\, {}_1F_1(p; q; wy)\, dy \quad . \tag{B7}$$

Eq. (B7) is valid whenever the LHS converges, a sufficient condition for which is $w<1$ [35, p.59].

Using (B7) in (B6) yields

$$P = \sqrt{\frac{\gamma}{1+\gamma}}\, \frac{(1+\gamma)^{-b}\, \Gamma(b+\frac{1}{2})}{2\sqrt{\pi}\, \Gamma(b+1)}\, {}_2F_1(1, b+\tfrac{1}{2}; b+1; (1+\gamma)^{-1}) \quad , \tag{B8}$$

where $\gamma = c/(2a)$. Note that since a and c are both assumed positive, the argument of the hypergeometric function in (B8), $(1+\gamma)^{-1}$, is less than one; hence (B8) converges for all permissible values of a, b, and c.

Next, the special case of b equalling a positive integer is examined; let $b = n$, $n\varepsilon\{1, 2, ...\}$, then (B1) may be evaluated by integrating by parts repeatedly. Alternatively, (B8) may be specialized to yield the desired result; the latter calculation is described in the remainder of this appendix.

By definition,

$$ {}_2F_1(1,\ n+\tfrac{1}{2};\ n+1;\ z) = \sum_{k=0}^{\infty} \frac{(1)_k \left(n+\frac{1}{2}\right)_k}{(n+1)_k} \frac{z^k}{k!} \quad , \tag{B9} $$

where $(a)_k = \Gamma(a+k)/\Gamma(a) = a\ (a+1)\ \ldots\ (a+k-1)$. (B10)

From (B10), it is seen that $(1)_k = k!$, $(n+1)_k = (n+k)!/n!$ and $(n+1/2)_k = (1/2)_{n+k}/(1/2)_n$. Thus, (B9) may be rewritten as

$$ \begin{aligned} {}_2F_1(1,\ n+\tfrac{1}{2};\ n+1;\ z) &= \sum_{k=0}^{\infty} \frac{\left(\frac{1}{2}\right)_{n+k}}{\left(\frac{1}{2}\right)_n} \frac{n!}{(n+k)!} z^k \\ &= \frac{n!\ z^{-n}}{\left(\frac{1}{2}\right)_n} \sum_{k=0}^{\infty} \frac{\left(\frac{1}{2}\right)_{n+k}}{(n+k)!} z^{n+k} \\ &= \frac{n!}{\left(\frac{1}{2}\right)_n} z^{-n} \left[\sum_{k=0}^{\infty} \left(\frac{1}{2}\right)_k \frac{z^k}{k!} - \sum_{k=0}^{n-1} \left(\frac{1}{2}\right)_k \frac{z^k}{k!} \right] . \end{aligned} \tag{B11} $$

The infinite sum in the last line of (B11) is recognized as the Taylor series expansion of $(1-z)^{-1/2}$; thus, substituting in $z = (1+\gamma)^{-1}$ and using (B11) in (B8), one obtains

$$ P = \sqrt{\frac{\gamma}{1+\gamma}} \frac{(1+\gamma)^{-n}\ \Gamma(n+\frac{1}{2})\ n!\ (1+\gamma)^n}{2\sqrt{\pi}\ \Gamma(n+1)\ (1/2)_n} \left[\sqrt{\frac{1+\gamma}{\gamma}} - \sum_{k=0}^{n-1} \frac{(1/2)_k}{k!} \left(\frac{1}{1+\gamma}\right)^k \right] . $$

Noting that $\sqrt{\pi}\left(\frac{1}{2}\right)_n = \Gamma(n+\frac{1}{2})$, $\Gamma(n+1) = n!$, and $\frac{(1/2)_k}{k!} = \binom{2k}{k}\left(\frac{1}{4}\right)^k$, and cancelling terms in the above equation, yields

$$ P = \frac{1}{2} \left[1 - \sqrt{\frac{\gamma}{1+\gamma}} \sum_{k=0}^{n-1} \binom{2k}{k} \left(\frac{1}{4(1+\gamma)}\right)^k \right] . \tag{B12} $$

Finally, letting $\mu = \sqrt{\frac{\gamma}{1+\gamma}} = \sqrt{\frac{c}{c+2a}}$, (B12) may also be written as

$$P = \frac{1}{2}\left[1 - \mu \sum_{k=0}^{n-1} \binom{2k}{k} \left(\frac{1-\mu^2}{4}\right)^k\right]. \qquad \text{(B13)}$$

References

[1] C. S. Gardner and J. A. Orr, "Fading Effects on the Performance of a Spread Spectrum Multiple Access Communication System," IEEE Trans. on Comm., vol. COM-27, pp. 143-149, Jan. 1979.

[2] D. E. Borth and M. B. Pursley, "Analysis of Direct-Sequence Spread Spectrum Multiple-access Communication Over Rician Fading Channels," IEEE Trans. on Comm., vol. COM-27, pp. 1566-1577, Oct. 1979

[3] E. Geraniotis, "Direct-Sequence Spread-Spectrum Multiple-Access Communications Over Nonselective and Frequency-Selective Rician Fading Channels," IEEE Trans. on Comm., vol. COM-34, pp. 756-764, Aug. 1986.

[4] G. L. Turin, "The Effects of Multipath and Fading on the Performance of Direct-Sequence CDMA Systems," IEEE Journal Sel. Areas Comm., vol. SAC-2, pp. 597-603, July 1984.

[5] J. S. Lehnert and M. B. Pursley, "Multipath Diversity Reception of Spread-Spectrum Multiple-Access Communications," IEEE Trans. on Comm., vol. COM-35, pp. 1189-1198, Nov. 1987.

[6] E. A. Geraniotis and M. B. Pursley, "Performance of Coherent Direct-Sequence Spread-Spectrum Communications Over Specular Multipath Fading Channels," IEEE Trans. on Comm., vol. COM-33, pp. 502-508, June 1985.

[7] M. Kavehrad and P. J. McLane, "Performance of Low-Complexity Channel Coding and Diversity for Spread Spectrum in Indoor, Wireless Communication," AT&T Tech. Journal, vol. 64, pp. 1927-1965, Oct. 1985.

[8] H. Xiang, "Binary Code-Division Multiple-Access Systems Operating in Multipath Fading, Noisy Channels," IEEE Trans. on Comm., vol. COM-33, pp. 775-784, Aug. 1985.

[9] H. Ochsner, "Direct-Sequence Spread-Spectrum Receiver for Communication on Frequency-Selective Fading Channels," IEEE Journal Sel. Areas Comm., vol. SAC-5, pp. 188-193, Feb. 1987.

[10] G. L. Turin, "Introduction to Spread-Spectrum Antimultipath Techniques and Their Application to Urban Digital Radio," Proc. IEEE, vol. 68, pp. 328-353, Mar. 1980.

[11] H. Suzuki, "A Statistical Model for Urban Radio Propagation," IEEE Trans. on Comm., vol. COM-25, pp. 673-680, July 1977.

[12] H. E. Whitney, et al, "Estimation of the Cumulative Amplitude Probability Distribution Function of Ionospheric Scintillation," Radio Science, vol. 7, pp.1095-1104, Dec. 1972.

[13] H. E. Whitney, "Amplitude and Fade Rate Statistics for Equatorial and Auroral Scintillation," in *Effect of the Ionosphere on Space Systems and Communication*, J. M. Goodman (editor), 1975.

[14] E. J. Fremouw, et al, "On the Statistics of Scintillating Signals," Journal of Atmospheric and Terrestial Physics, vol. 42, pp.717-731, 1980.

[15] J. P. McGeehan and A. J. Bateman, "Theoretical and Experimental Investigation of Feedforward Signal Regeneration as a Means of Combating Multipath Propagation Effects in Pilot-Based SSB Mobile Radio Systems," IEEE Trans. on Veh. Tech., vol. VT-32, pp. 106-120, Feb. 1983.

[16] J. G. Proakis, *Digital Communications*, McGraw Hill, 1983.

[17] M. Nakagami, "The m-Distribution - A General Formula of Intensity Distribution of Rapid Fading," reprinted from *Statistical Methods of Radio Wave Propagation* (W. C. Hoffman ,editor), Pergamon Press, Oxford, England; 1960.

[18] P. D. Shaft, "On the Relationship Between Scintillation Index and Rician Fading," IEEE Trans. on Comm., vol. COM-22, pp. 731-732, May 1974.

[19] G. L. Turin, et al, "A Statistical Model of Urban Multipath Propagation," IEEE Trans. Veh. Tech., vol. VT-21, pp. 1-9, Feb. 1972.

[20] U. Charash, "Reception Through Nakagami Fading Multipath Channels with Random Delays," IEEE Trans. on Comm., vol. COM-27, pp. 657-670, April 1979.

[21] R. Price and P. E. Green, Jr., "A Communication Technique for Multipath Channels," Proc. IRE, vol. 46, pp. 555-570, March 1958.

[22] M. Yokoyama, "BPSK System with Sounder to Combat Rayleigh Fading in Mobile Radio Communication," IEEE Trans. Veh. Tech., vol. VT-34, pp. 35-40, Feb. 1985.

[23] F. Davarian, "Comments on 'BPSK System with Sounder to Combat Rayleigh Fading in Mobile Radio Communication'," IEEE Trans. Veh. Tech., vol. VT-34, pp. 154-156, Nov. 1985.

[24] F. Davarian, "Mobile Digital Communication Via Tone Calibration," IEEE Trans. Veh. Tech., vol. VT-36, pp. 55-62, May 1987.

[25] G. L. Stüber and C. Kchao, "Analysis of a Multiple-Cell Direct-Sequence CDMA Cellular Mobile Radio System," IEEE Journal Sel. Areas Comm., vol. SAC-10, pp. 669-679, May 1992.

[26] F. J. Scire, "A Probability Density Function Theorem for the Modulo y Values of the Sum of Two Statistically Independent Processes," Proc. IEEE, vol. 56, pp. 204-205, Feb. 1968.

[27] D. A. S. Fraser, *Nonparametric Methods in Statistics*, Wiley, 1957.

[28] K. Yao, "Error Probability of Asynchronous Spread Spectrum Multiple Access Communication Systems," IEEE Trans. on Comm., vol. COM-25, pp.803-809, Aug. 1977.

[29] J. S. Lehnert and M. B. Pursley, "Error Probabilities for Binary Direct-Sequence Spread-Spectrum Communications with Random Signature Sequences," IEEE Trans. on Comm., vol. COM-35, pp. 87-98, Jan. 1987.

[30] H. F. A. Roefs and M. B. Pursley, "Correlation Parameters of Random Sequences and Maximal Length Sequences for Spread-Spectrum Multiple Access Communications," Proc. IEEE Canadian Conf. on Comm. & Power, pp. 141-143, 1976.

[31] M. B. Pursley, "Performance Evaluation for Phase-Coded Spread Spectrum Multiple-Access Communications - Part I : System Analysis," IEEE Trans. on Comm., vol. COM-25, pp. 795-799, Aug. 1977.

[32] M. Nesenbergs, "Binary Error Probability Due to an Adaptable Fading Model," IEEE Trans. on Comm. Sys., vol. CS-12, pp. 64-73, March 1964.

[33] Y. Miyagaki, et al, "Error Probability Characteristics for CPSK Signal Through m-Distributed Fading Channel," IEEE Trans. on Comm., vol. COM-26, pp. 88-100, Jan. 1978.

[34] J. P. Odenwalder, *Error Control Coding Handbook*, Linkabit Corp., July 15, 1976. See also J. P. Odenwalder, "Optimal Decoding of Convolutional Codes," Ph. D. Dissertation, UCLA, 1970.

[35] Y. L. Luke, *The Special Functions and Their Approximations, Vol. I*, Academic Press, 1969.

[36] A. Erdelyi, et al, *Higher Transcendental Functions, Vol. I*, McGraw Hill, 1953.

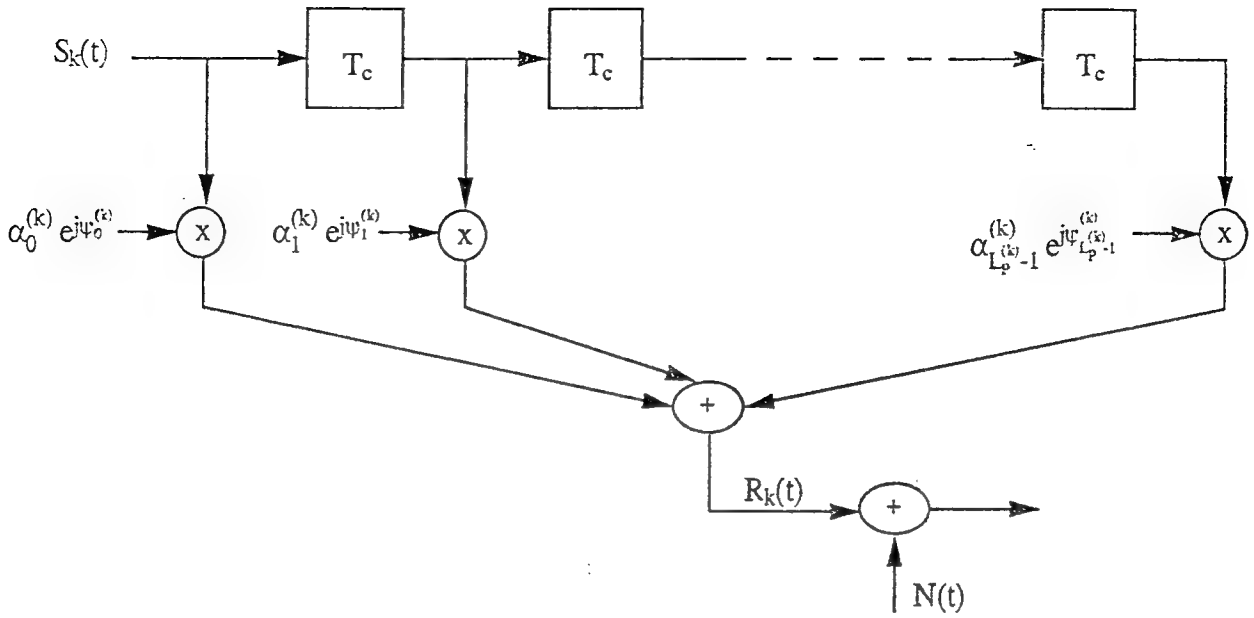

Fig. 1. Multipath Channel Model. (Complex Baseband Representation).

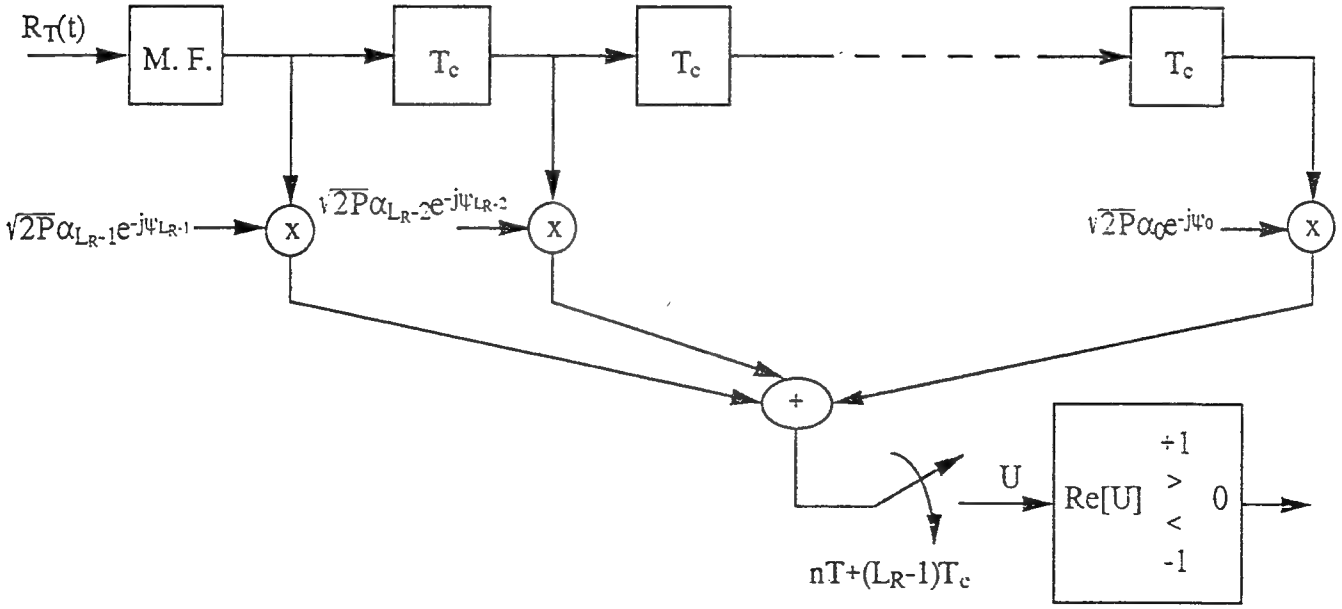

Fig. 2a. RAKE Receiver Model.

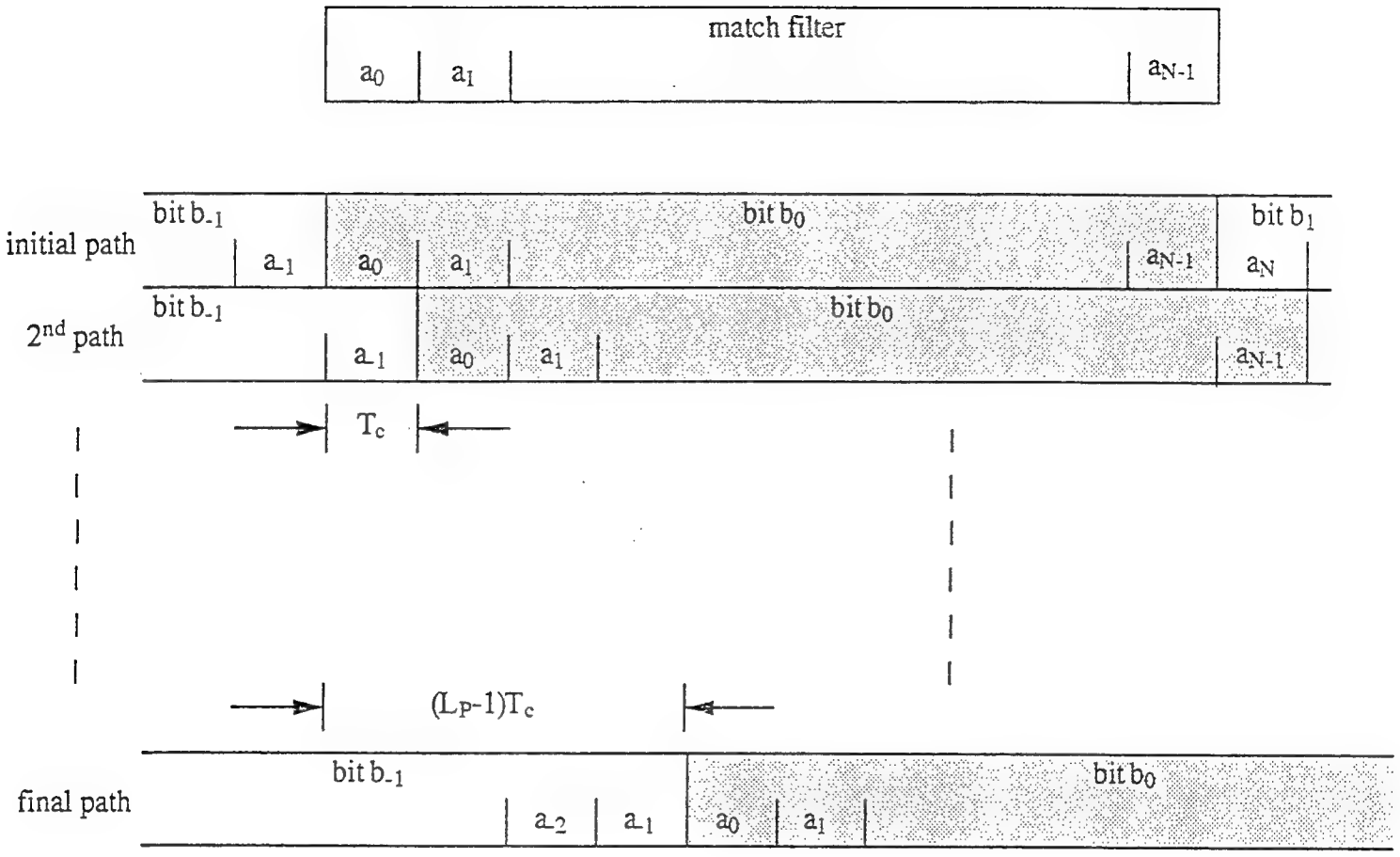

Fig. 2b. Chip sequences of the reference signal with respect to the chip sequence of the matched filter at time $T=NT_c$. The signal chip sequences may be visualized as moving from right to left as time increases, while the matched filter sequence remains stationary; the response is then the integral of the product of the filter sequence with everything under its span.

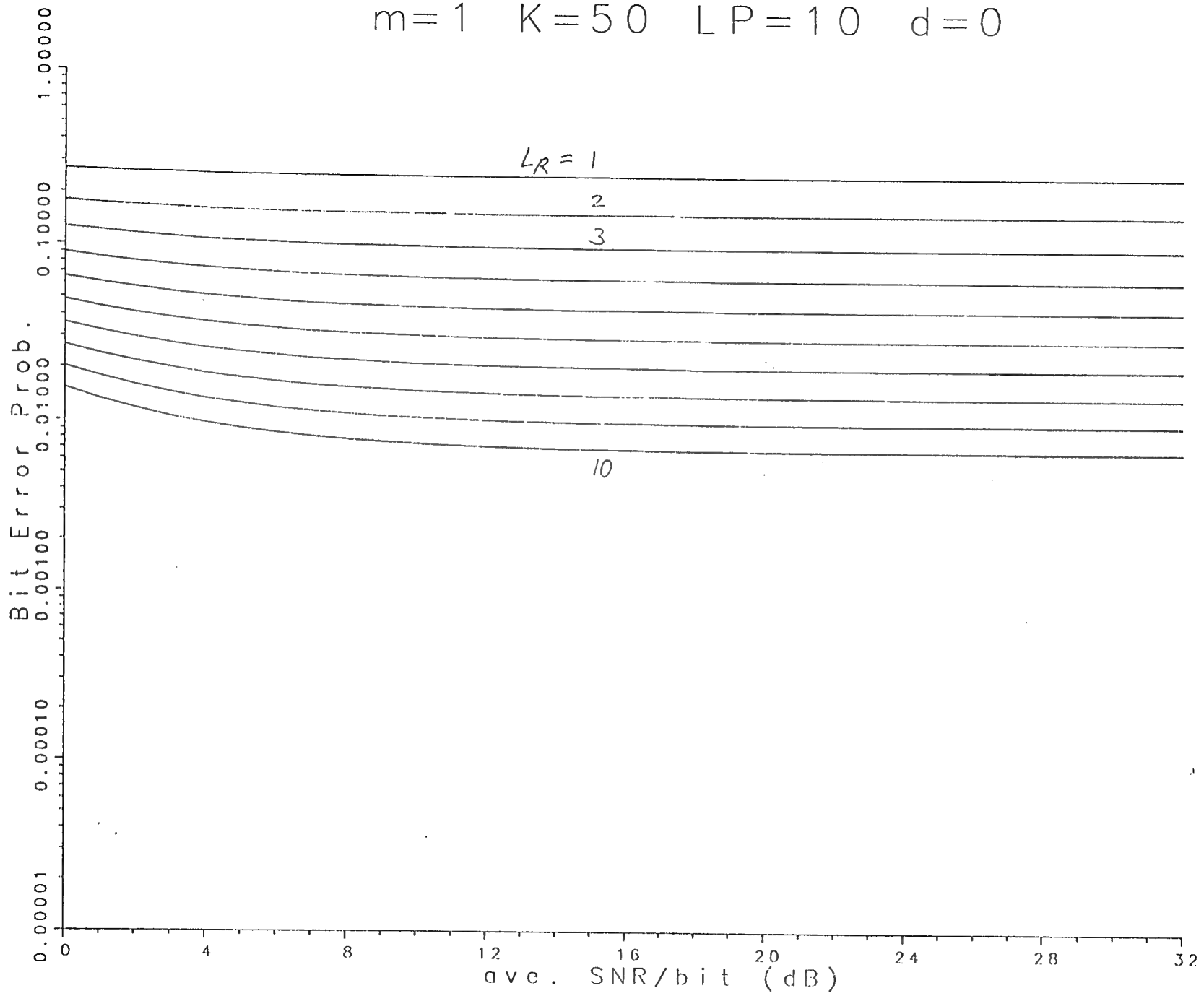

Fig. 3a. P_b vs γ_0 : $\delta = 0$

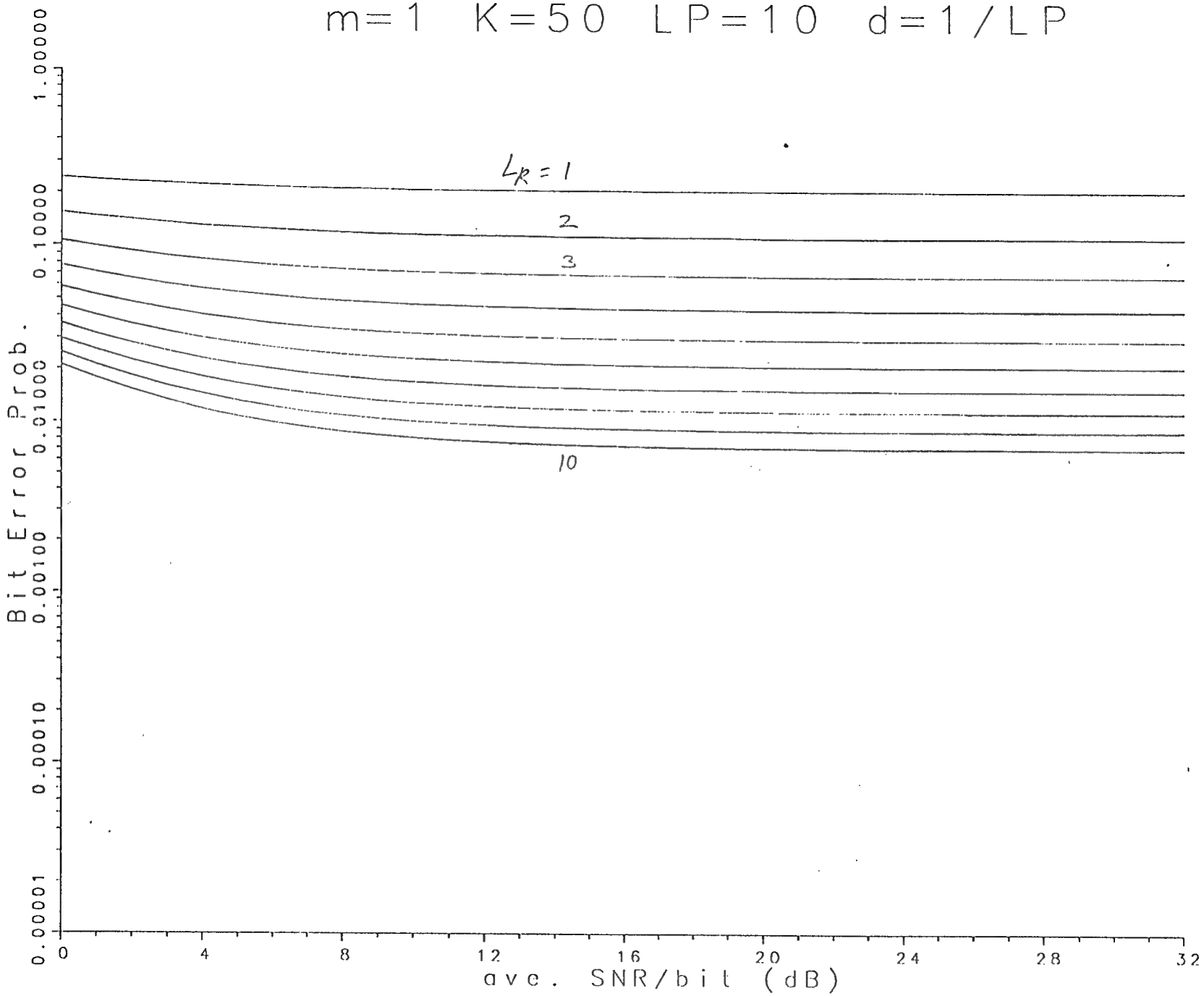

Fig. 3L. P_L vs γ_0 : $\delta = 0.1$

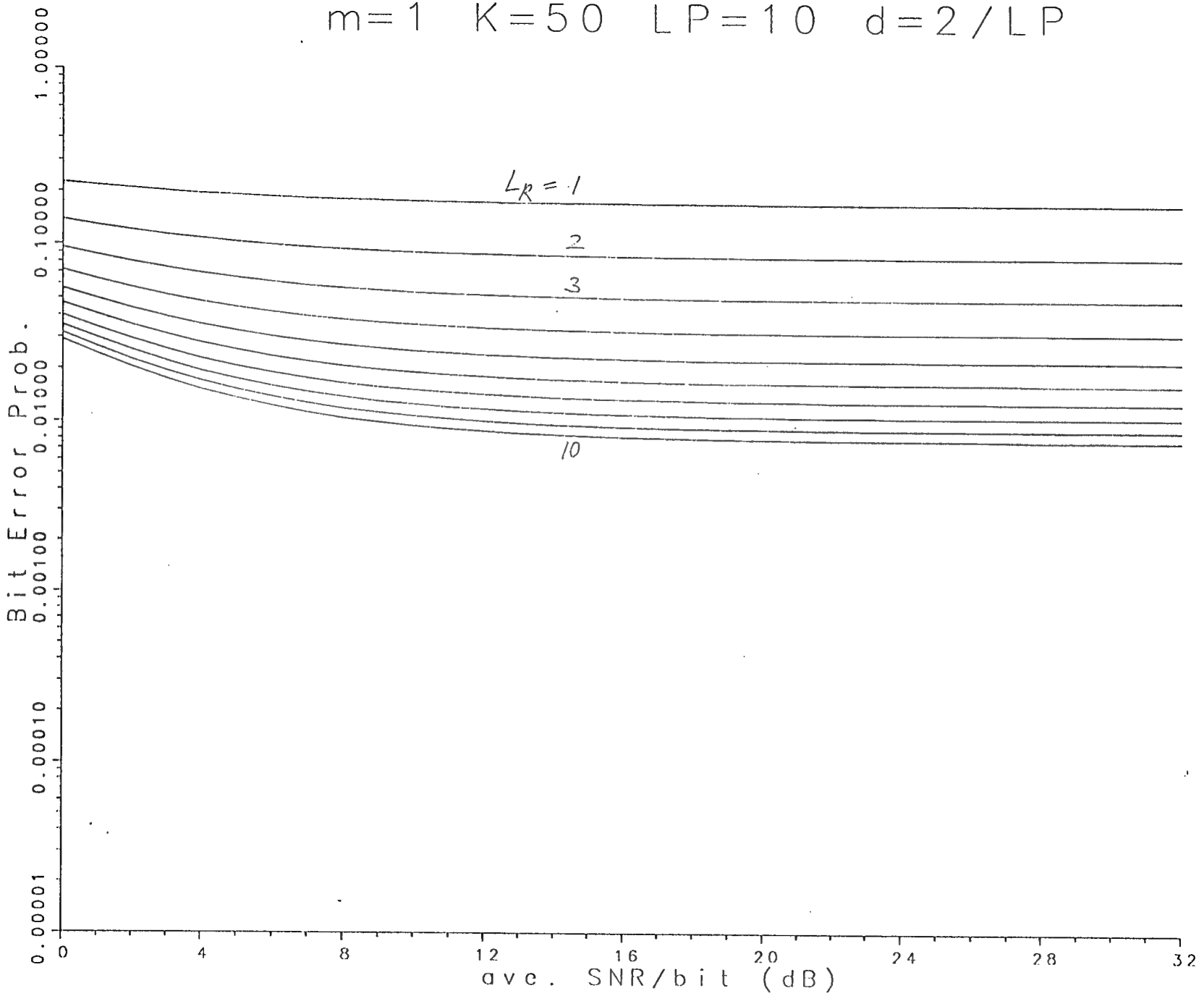

Fig. 3c. P_b vs γ_0 : $\delta = 0.2$

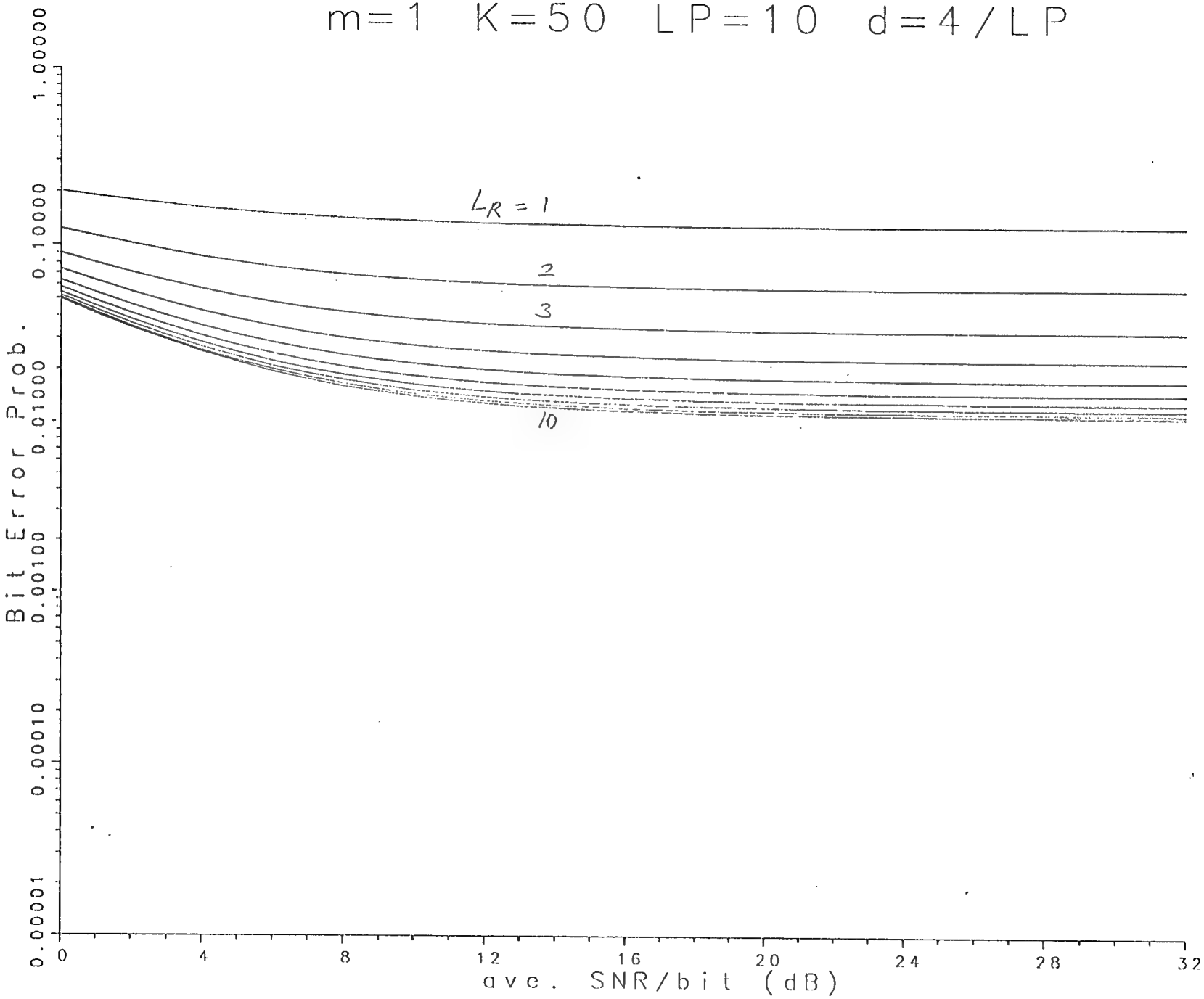

Fig. 3d. P_b vs γ_0 ; $\delta = 0.4$

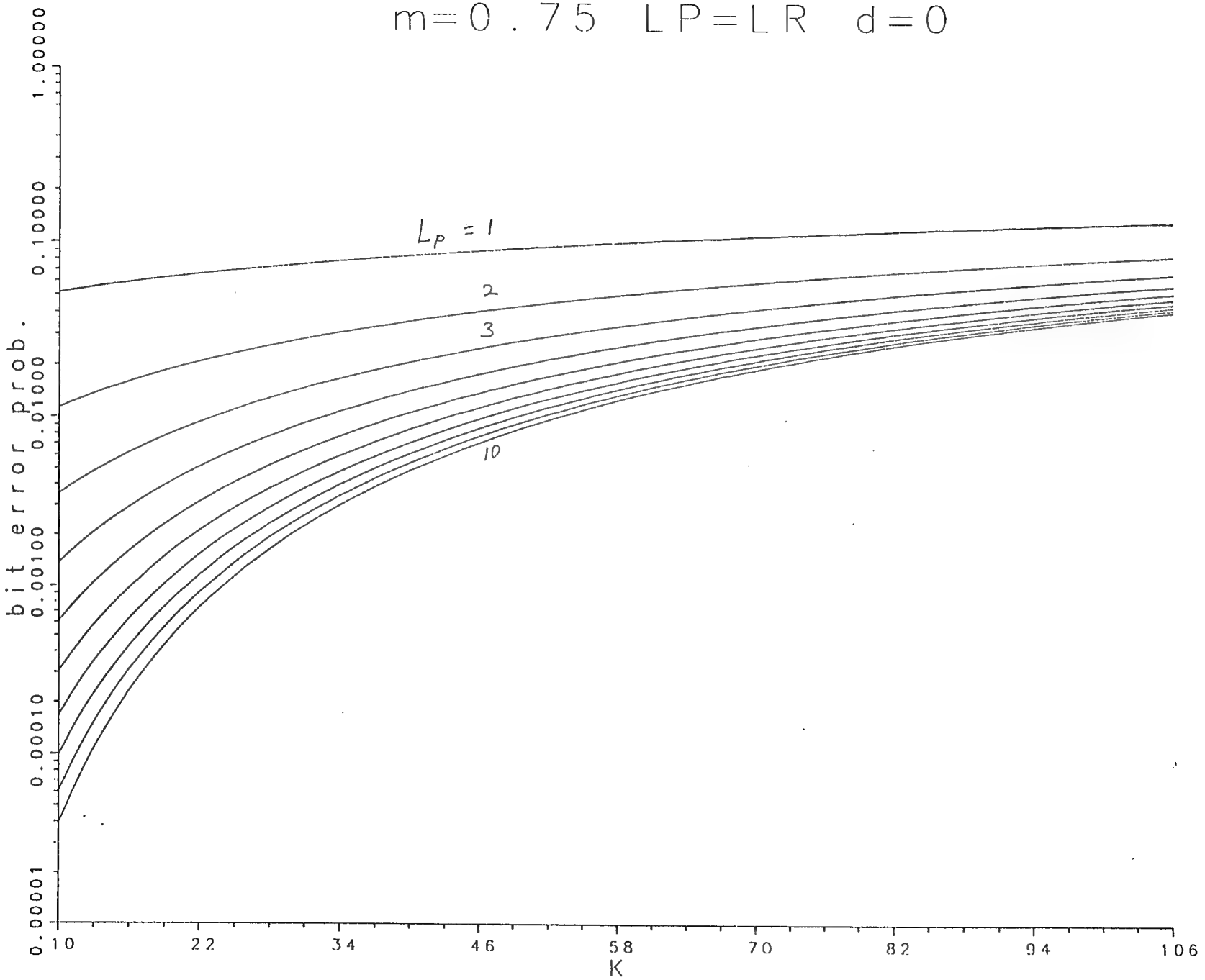

Fig. 4a. P_b vs K ; $\varepsilon = 0$

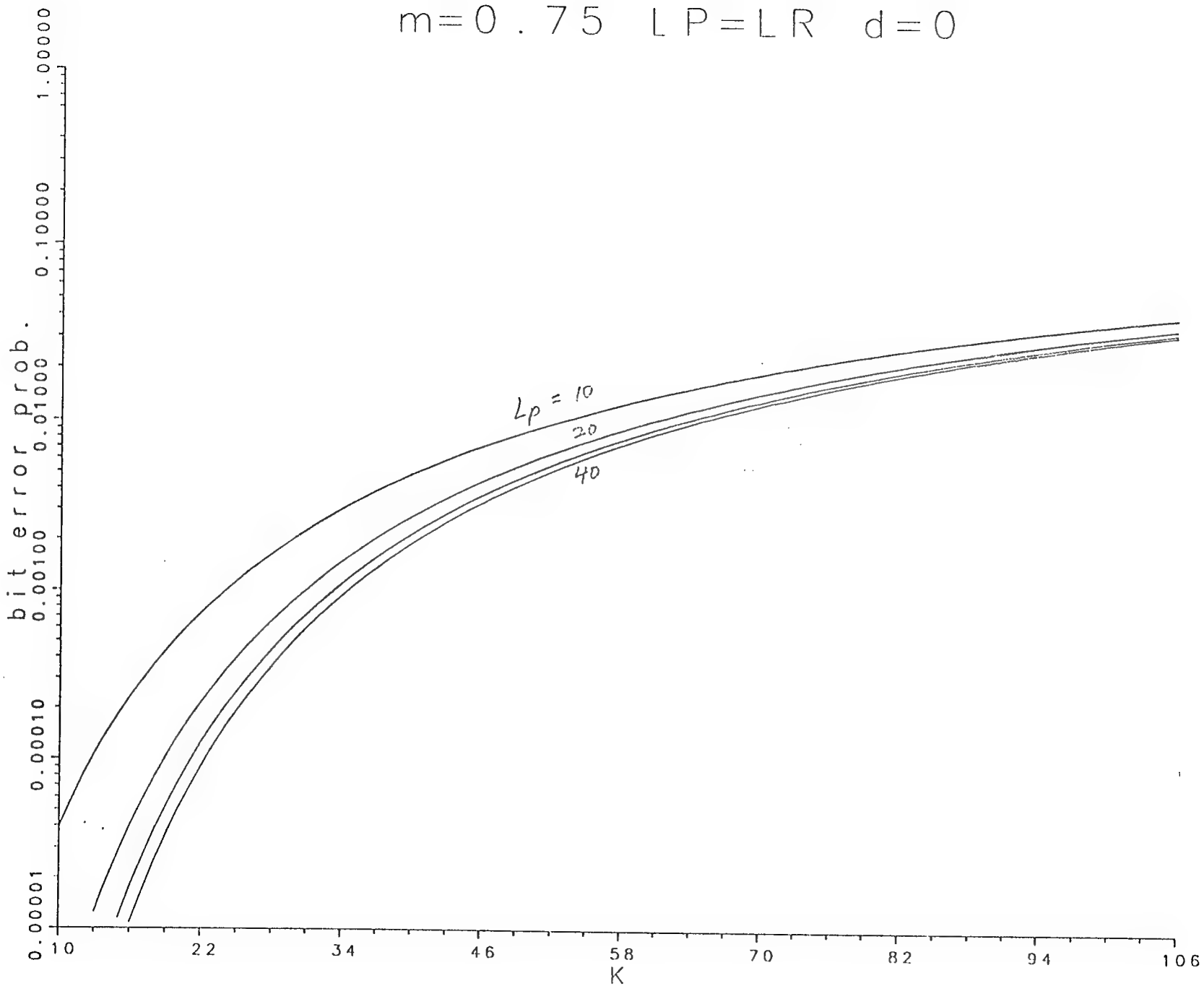

Fig. 4b. P_b vs K : $\delta = 0$

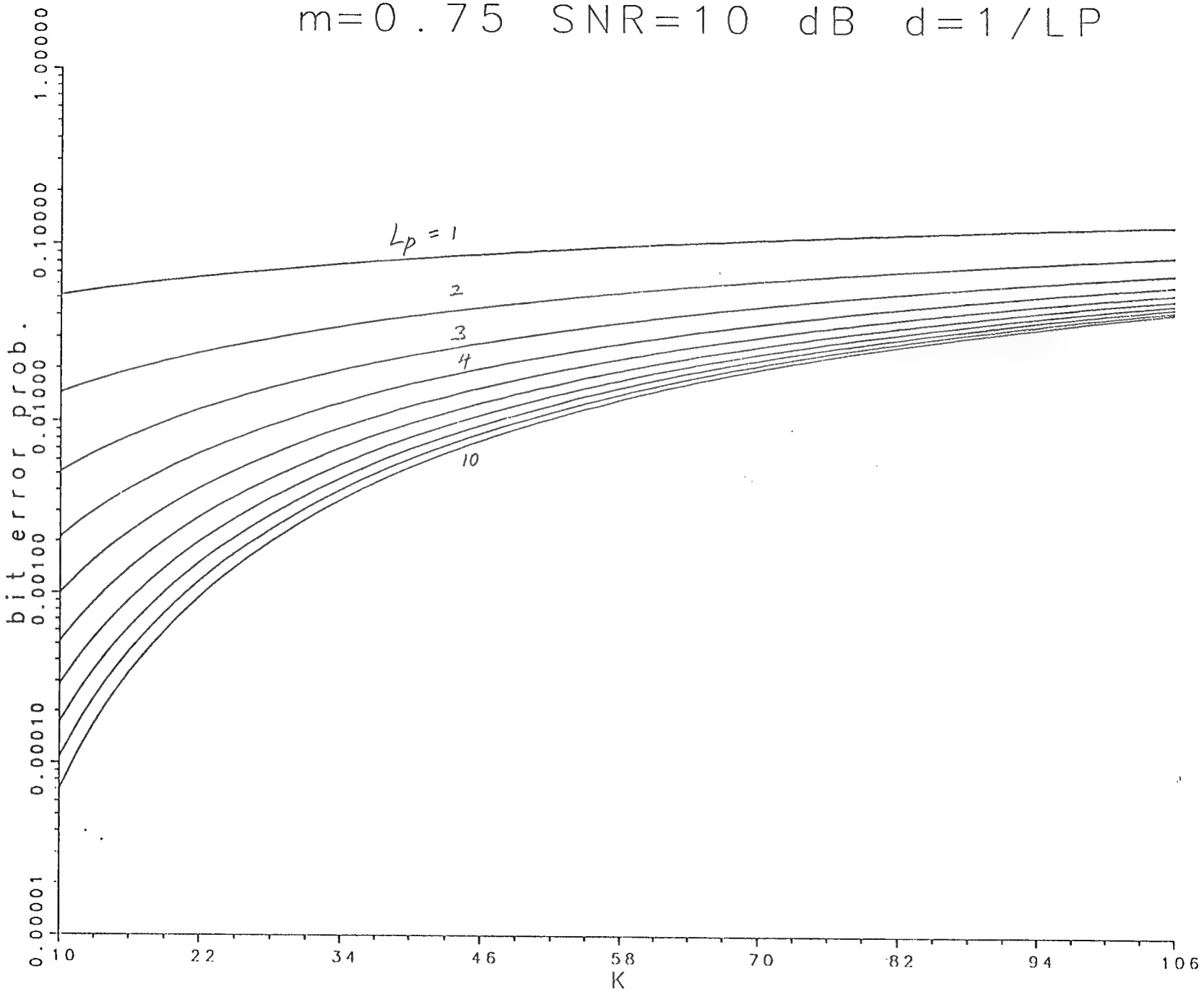

Fig. 4c. P_b vs K : $\delta = 0.1$

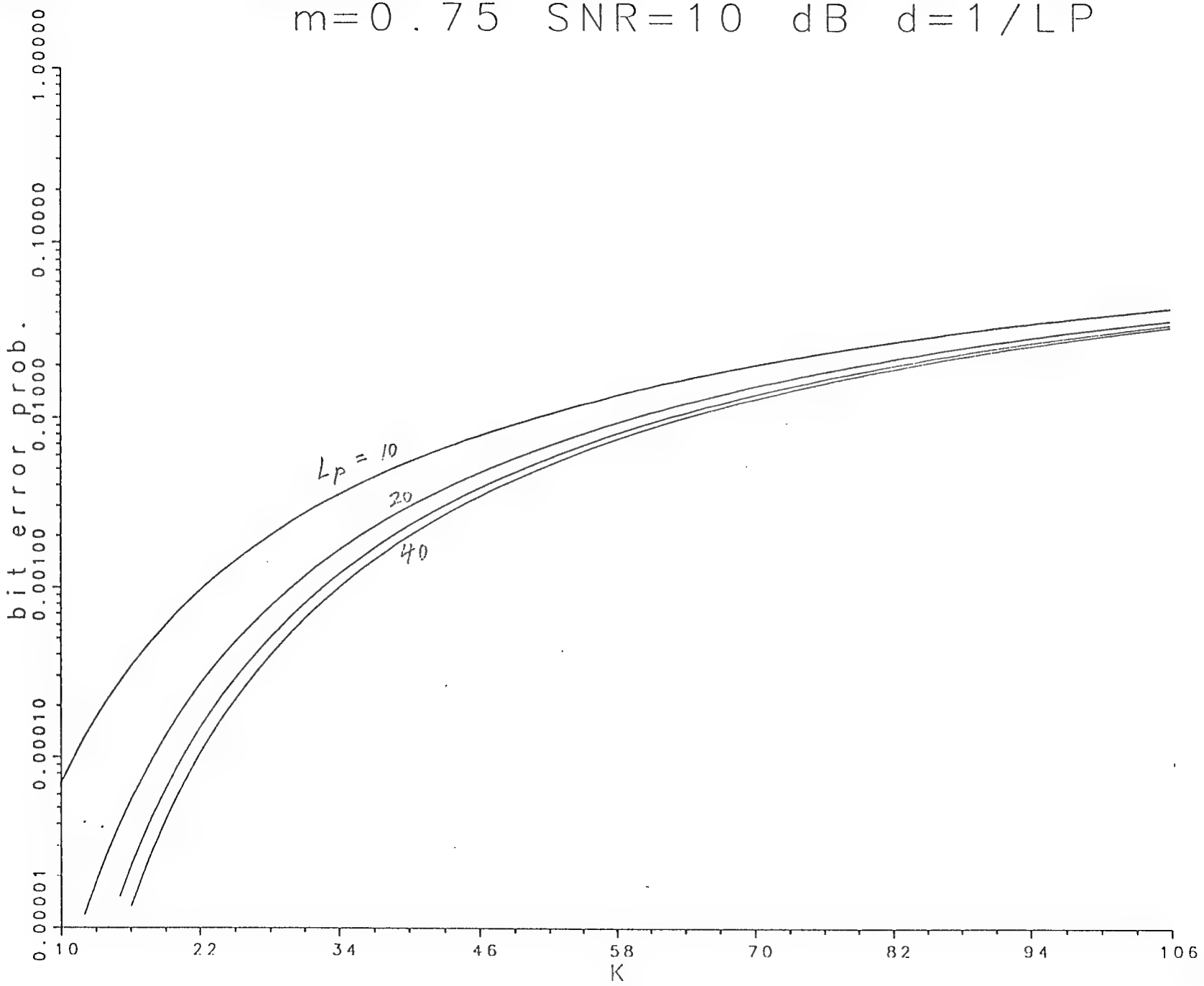

Fig. 4d. P_b vs K ; $\delta = 0.1$

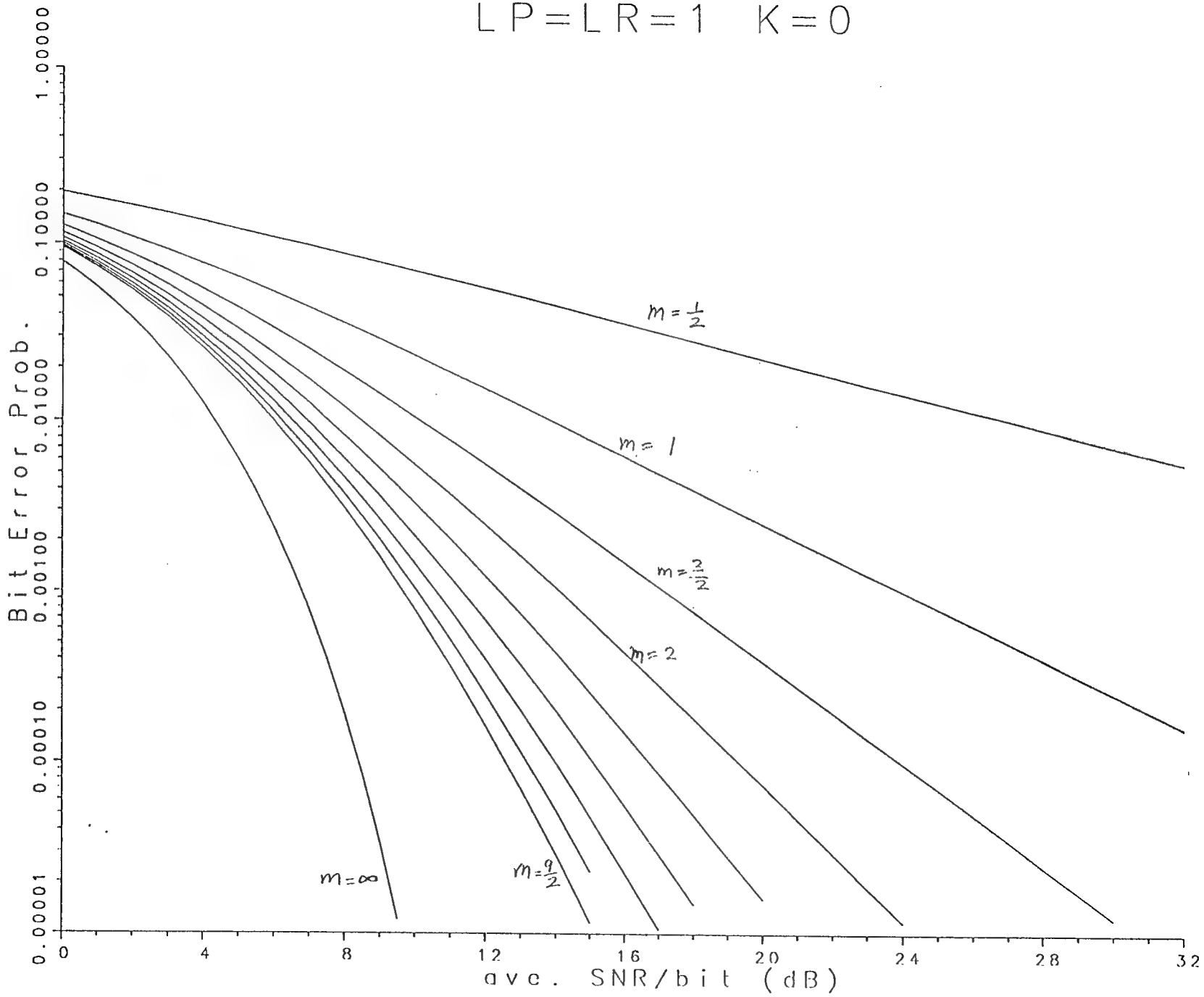

Fig. 5. P_b vs γ_0

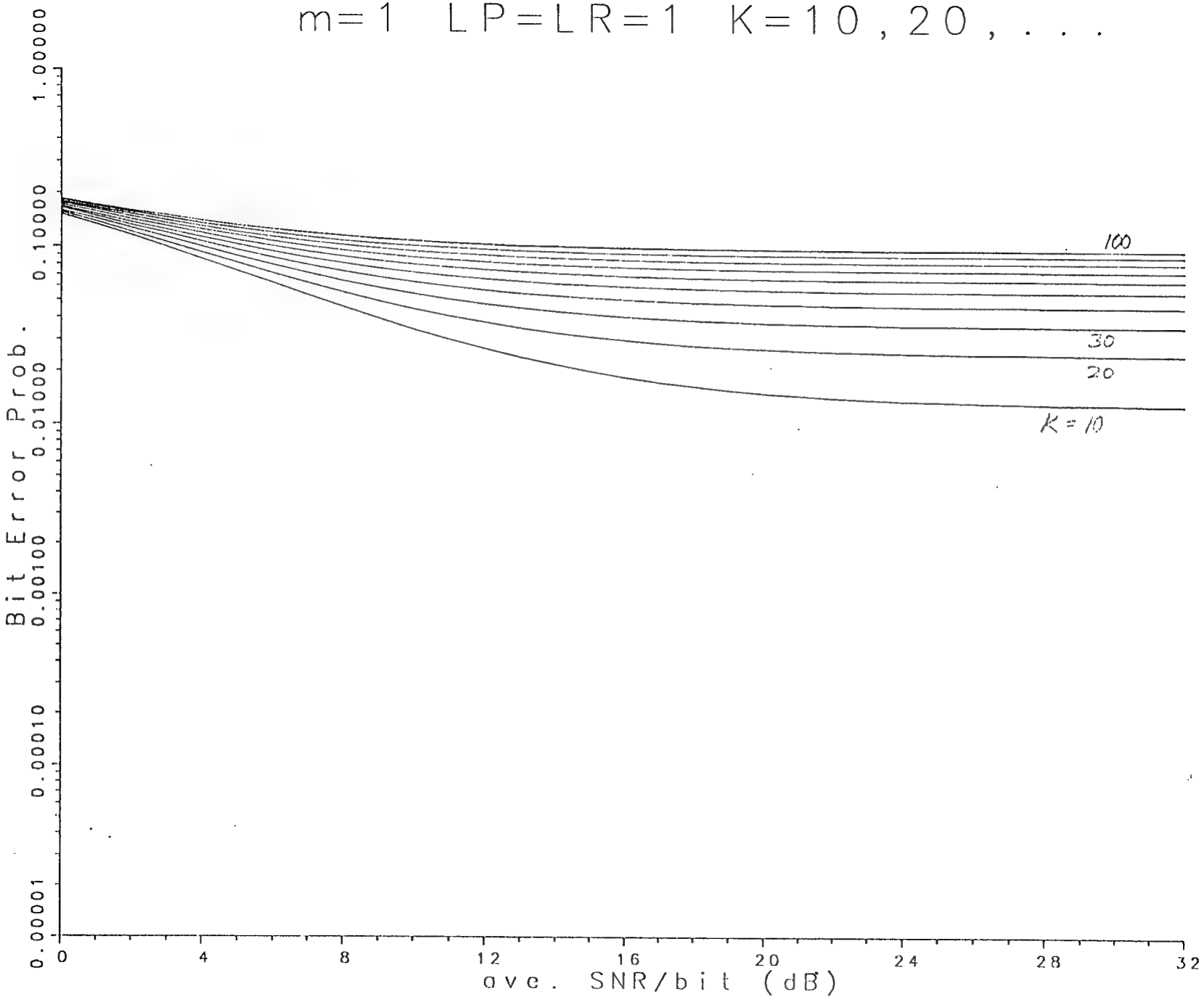

Fig. 6. P_b vs γ_0

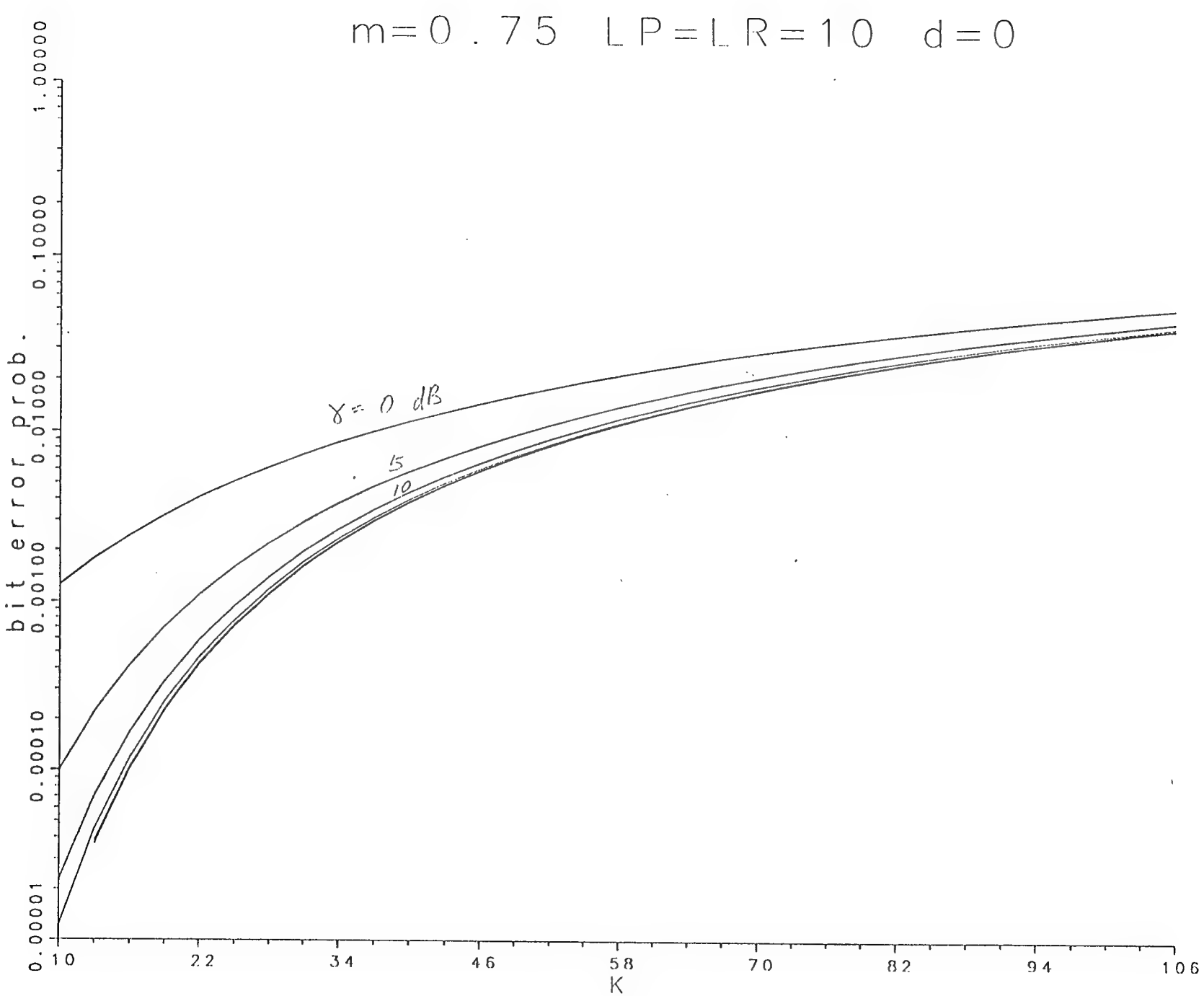

Fig. 7a. P_b vs K, $m = 0.75$

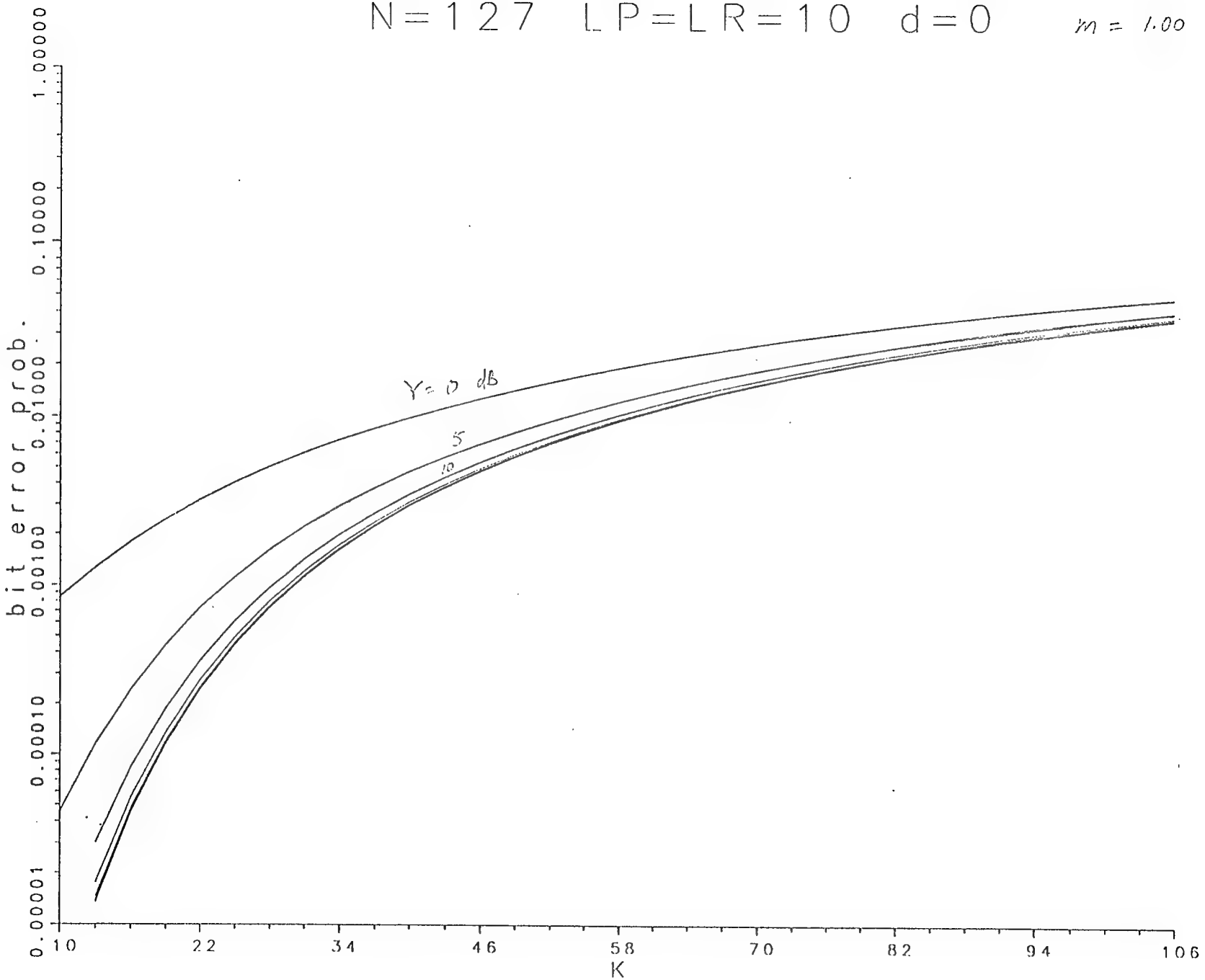

Fig. 76. P_b vs K, $m = 1.00$

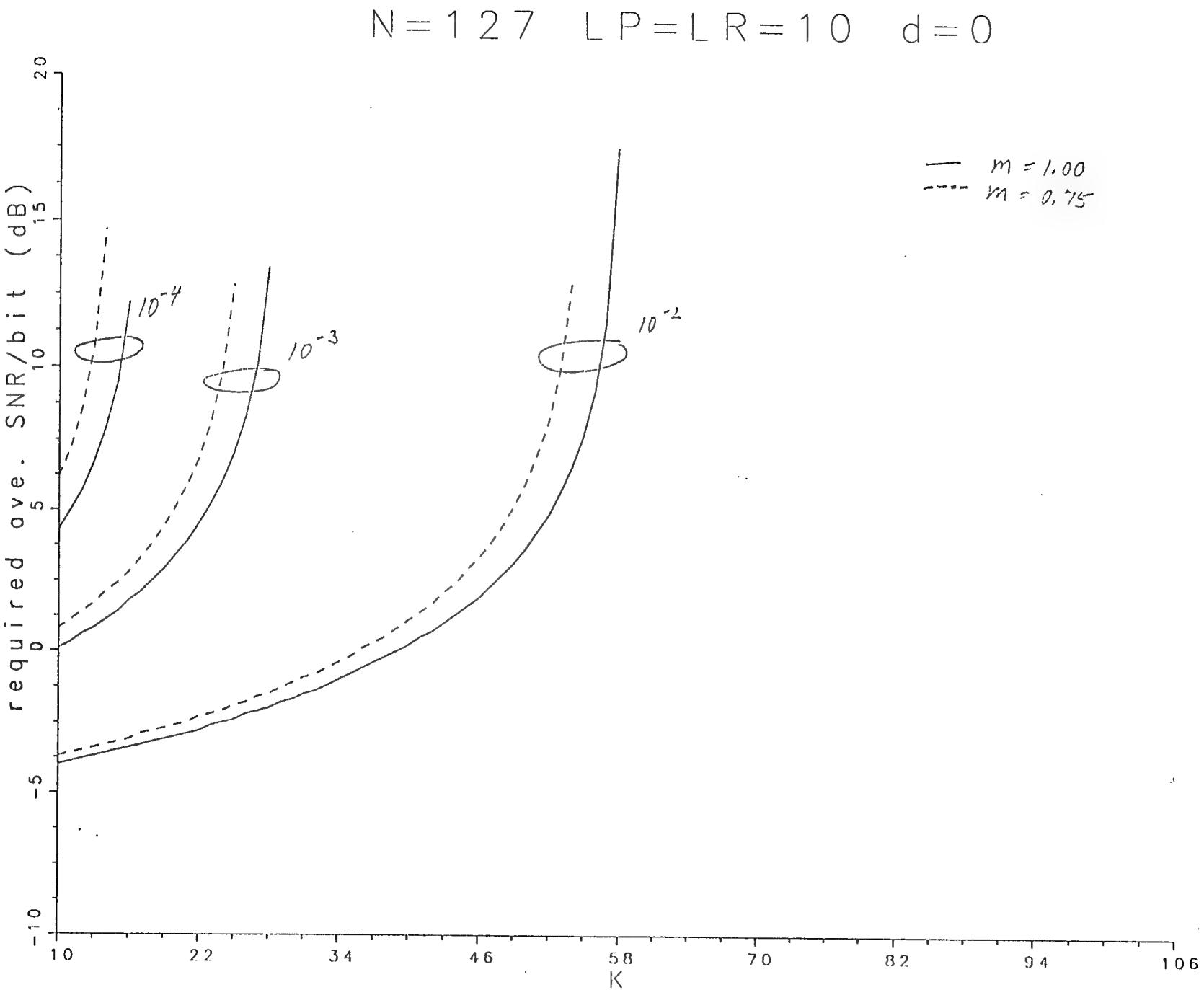

Fig. 8. Required γ_0 vs K.

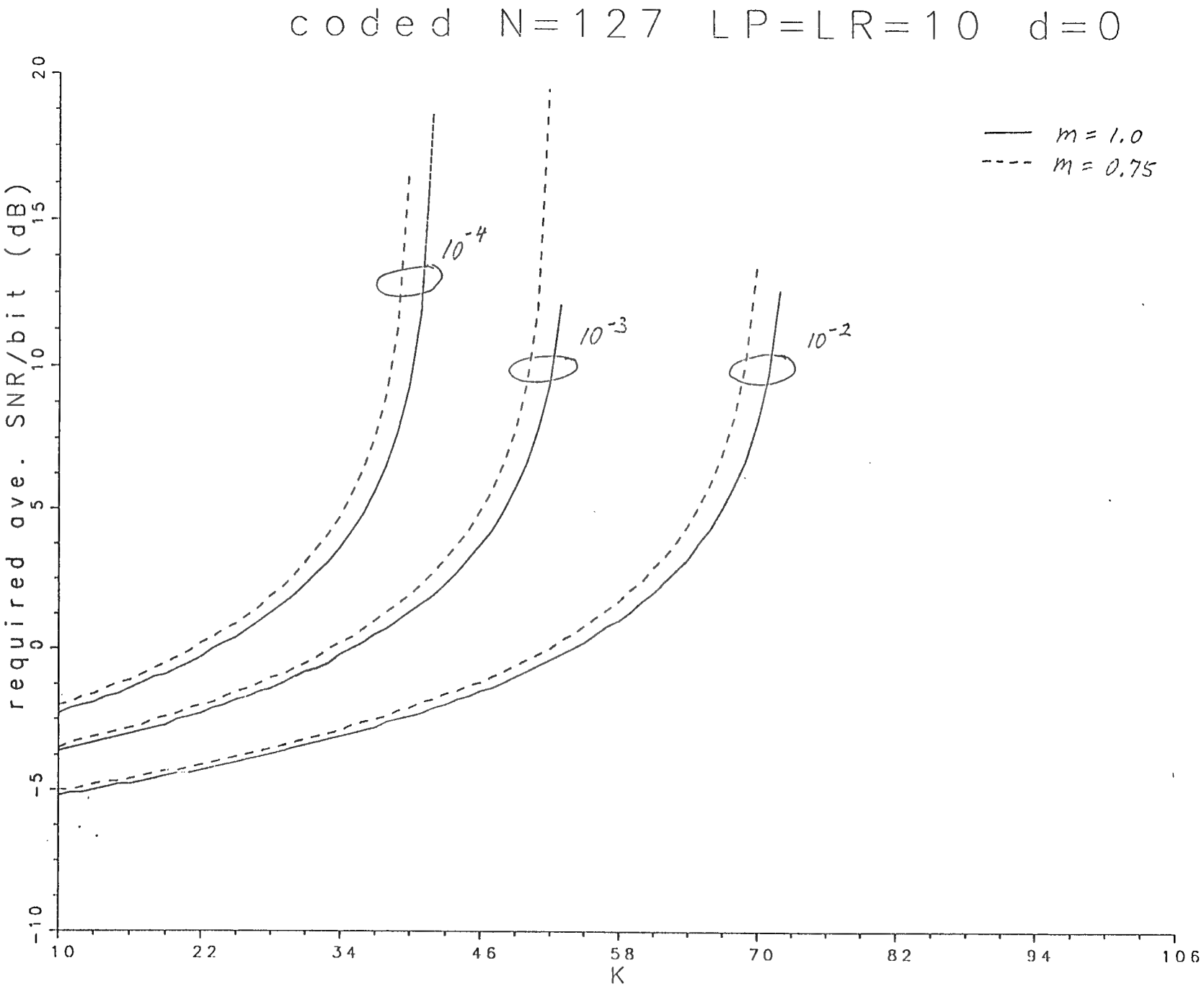

Fig. 9. Required γ_b vs K.

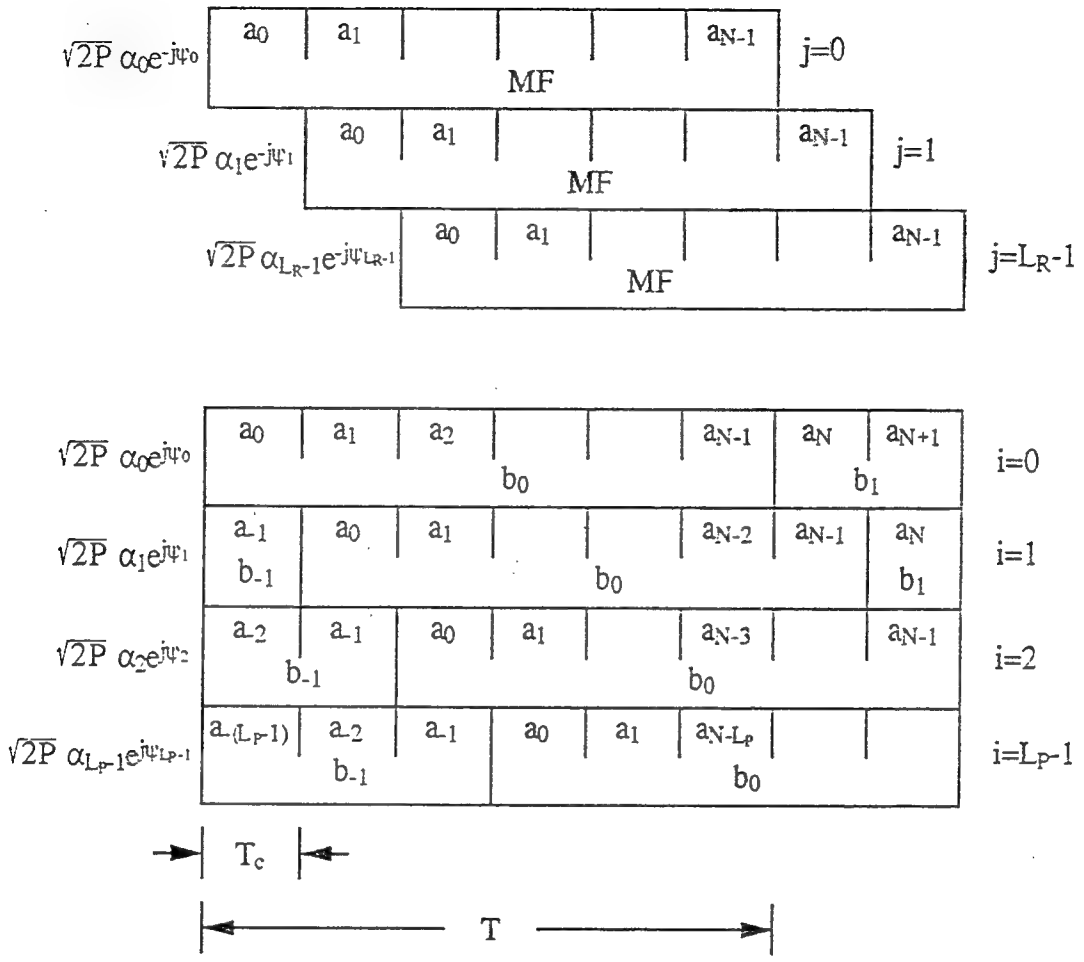

Fig. A1. Pictorial representation of receiver response to reference signal. In this example, the number of paths received is four, and the number of paths combined is three. The response is obtained as follows: For each (i,j) combination, superimpose the two segments by sliding the j-segment down (or by sliding the i-segment up) and integrating the portion that overlaps. Each segment is multiplied by the factor shown to the left of it. Since all the segments are chip synchronized, the integration reduces to a sum of N chips. The response is obtained by summing the contributions from all (i,j) combinations.

Comparison of Hybrid FDMA/CDMA Systems in Frequency Selective Rayleigh Fading

Thomas Eng and Laurence B. Milstein
Dept. of Electrical and Computer Engineering
University of California at San Diego
La Jolla, CA 92093

Abstract

A hybrid FDMA/CDMA scheme operating over a frequency selective Rayleigh fading channel is described and analyzed. The performance of the hybrid system is then compared with that of a wideband CDMA system occupying the same total bandwidth. Both coherent and noncoherent modulation formats are investigated; it is found that, for coherent modulation with a RAKE receiver, wideband CDMA has greater capacity than does the hybrid. However, for the noncoherent modulation formats (either DPSK or square-law detected orthogonal signalling), a hybrid system can have a greater capacity if a high channel error rate can be tolerated. Otherwise, a wideband noncoherent system remains optimal.

This work was partially supported by the Army Research Office under Grant DAAL03-91-G-0071, by the Office of Naval Research under Grant N00014-91-J-1234, and by the National Science Foundation under Grant NCR-9213140.

I. Introduction

It is well known that direct sequence-code division multiple access (DS-CDMA) is a feasible alternative to frequency division multiple access (FDMA) or time division multiple access (TDMA) for multi-user communications, and numerous papers have been written on its performance [e.g., 1-11]. One stringent requirement that all DS-CDMA systems must meet is that the available bandwidth be contiguous. However, in certain situations, it may not be feasible or practical to satisfy this requirement (e.g., the allocated frequency band might have gaps in it).

As an alternative, one can consider using a hybrid FDMA/CDMA scheme. The spectrum of the original 'wideband' CDMA is shown in Fig. 1, and the spectrum of the hybrid scheme is shown in Fig. 2. In the hybrid scheme, the available wideband spectrum is divided into a number of sub-spectra of smaller bandwidths; for convenience, the bandwidths of each sub-spectrum are assumed equal. Each sub-spectrum facilitates a separate 'narrowband' CDMA system, whose signals employ DS spreading with reduced processing gain (relative to the original wideband signal) and are transmitted in one and only one sub-spectrum. The capacity of this FDMA/CDMA (FCDMA) system is calculated as the sum of the capacities of the sub-spectra.

This paper is organized as follows: In Sections II and III, the CDMA system model and the channel model, respectively, are described, and in Sections IV and V, the bit error rate (BER) expressions for coherent and noncoherent modulation formats, respectively, are derived. In Section VI, the method of calculating the capacities is described and the results are discussed, and finally, in Section VII, the main points are summarized and conclusions restated.

II. CDMA System Model

The system model to be considered consists of K+1 simultaneous transmitters (the zeroth user being the reference user whose performance is to be evaluated); each transmitter, or user, is assigned a CDMA code sequence (also called a signature sequence) which modulates, along with the carrier, the data sequence. For either coherent PSK or DPSK modulation, each user is assigned a unique spreading sequence; for orthogonal-code modulation, each user is assigned two spreading sequences which are orthogonal to one-other (orthogonal in the sense that their chip-by-chip correlation is zero). In either case, the signature sequences are periodic with period much longer than the processing gain N; the sequences of all users have a common chip rate of $1/T_c$, where $T_c = T/N$, and $1/T$ is the information bit rate.

Let $a_k(t)$ denote the code sequence waveform of the k-th user, and let $\{a_j^{(k)}\}$ be the corresponding sequence of elements of $\{+1,-1\}$. Then

$$a_k(t) = \sum_{j=-\infty}^{\infty} a_j^{(k)} P_{T_c}(t-jT_c) \ ,$$

where $P_{T_c}(t) = 1$ for $0 < t < T_c$ and equals zero otherwise. Similarly, the data signal waveform may be written as (the data bits are differentially encoded for DPSK)

$$b_k(t) = \sum_{j=-\infty}^{\infty} b_j^{(k)} P_T(t-jT) \quad .$$

The transmitted signal for the k-th user is, therefore,

$$s_k(t) = \mathrm{Re}[S_k(t)e^{j\omega_0 t}], \text{ where } S_k(t) = \sqrt{2P}\, a_k(t) b_k(t) e^{j\theta_k},$$

and where P is the average transmitted power, common to all users, ω_0 is the common carrier frequency, and θ_k is the phase of the k-th carrier.

Assuming asynchronous operation, each non-reference-user signal is misaligned relative to the reference signal by an amount τ_k, k=1, 2, ... K; thus, the composite signal at the input to the channel is

$$s_T(t) = \mathrm{Re}[S_T(t)e^{j\omega_0 t}], \text{ where } S_T(t) = \sum_{k=0}^{K} \sqrt{2P}\, a_k(t-\tau_k) b_k(t-\tau_k) e^{j\phi_k},$$

$\phi_k = \theta_k - \omega_0\tau_k$, and $\theta_0 = \tau_0 = 0$. Furthermore, the asynchronous assumption implies that the $\{\phi_k\}_{k=1}^{K}$ are independent identically distributed (IID) random variables uniformly distributed in [0, 2π), and likewise $\{\tau_k\}_{k=1}^{K}$ may be taken to be IID random variables uniform in [0, T).

III. Channel Model

A commonly used model for a frequency-selective multipath channel is a finite - length tapped delay line as shown in Figure 3 for the k-th user [9, 12], where the $L_p^{(k)}$ tap weights $\{\alpha_i^{(k)}\}$ are independent Nakagami random variables with probability density functions (pdf)

$$p(\alpha_i^{(k)}) = M(\alpha_i^{(k)}, m, \Omega_i^{(k)}), \quad \text{where } M(R, m, \Omega) = \frac{2\, m^m\, R^{2m-1}}{\Gamma(m)\, \Omega^m} e^{-(m/\Omega)R^2}, \qquad (2)$$

and the phases $\{\psi_i^{(k)}\}$ are IID random variables uniform in [0, 2π) and are independent of $\{\alpha_i^{(k)}\}$. In (2), m is a fade parameter assumed common for all paths and is equal to the inverse of the 'normalized variance' of $\alpha_i^{(k)}$, i.e., $m = E[(\alpha_i^{(k)})^2] / \mathrm{var}[(\alpha_i^{(k)})^2]$; for this reason, 1/m is termed the 'fading figure' [13]; m is also related to the commonly used scintillation index, S_4, by $m=(S_4)^{-2}$ [14, 15]. The parameter $\Omega_i^{(k)}$ is the second moment of $\alpha_i^{(k)}$ (i.e. $\Omega_i^{(k)} = E[(\alpha_i^{(k)})^2]$), and is assumed to be related to the second moment of the initial path strength $\Omega_0^{(k)}$ by

$$\Omega_i^{(k)} = \Omega_0^{(k)} e^{-\delta i}, \quad \delta \geq 0 \quad . \qquad (3)$$

This functional form for $\Omega_i^{(k)}$ accounts for the decay of average path strength as a function of path delay; the parameter δ reflects the rate at which this decay occurs. The shape of the decay function (3) is sometimes referred to as the multipath intensity profile (MIP). The MIP is assumed to be exponential here, and actual measurements [16] indicate that this is fairly accurate for a congested urban area.

N(t) in Fig. 3 is the complex valued low - pass - equivalent AWGN with two-sided spectral density η_0; therefore, N(t) is a circularly symmetric, zero-mean Gaussian random process with covariance function $E[\, N(t)\, N^*(\tau)\,] = 2\, \eta_0\, \delta(\, t - \tau\,)$. The number of paths $L_p^{(k)}$ is related to the maximum delay spread, Δ, of the channel and is assumed known (or measurable). Furthermore, $L_p^{(k)}$ is assumed to be less than N (which is equivalent to assuming that the maximum delay spread is less than T); since Δ is on the order of 5 μs (for urban areas) [10], this is a reasonable assumption for bit rates of 200 KHz or less.

Charash [17] and Xiang [8] used a similar model to analyze the performance of noncoherent orthogonal signalling and noncoherent CDMA (using orthogonal spreading codes) respectively; their model is not a tapped delay line but a random delay, discrete 'resolvable' path model with equal average path strengths (i.e., their MIP is a constant). The model used here may also be interpreted as a discrete-path model, where the delays are assumed to be spaced T_c apart for convenience. Since the random delays in the model are assumed known (i.e., they are assumed to be learned by the receiver), the performance analysis is not affected by the particular set of chosen delay values.

IV. Coherent Modulation

The coherent BER performance using a RAKE receiver as shown in Fig. 4 has been analyzed in [11], where it is shown that if the spreading sequences are modelled as independent random binary sequences, then the test statistic at the receiver may be approximated as a conditional Gaussian random variable with mean (assuming +1 was sent)

$$U_s = 2E\sum_{n=0}^{L_R-1} \alpha_n^2 \text{ , and variance } \sigma^2 = \left(\frac{4E^2\Omega_0\left[q(L_P,\,\delta)-1\right]}{N} + \frac{8E^2\Omega_0 K q(L_P,\,\delta)}{3N} + 4E\eta_0\right)\sum_{n=0}^{L_R-1} \alpha_n^2 \text{ ,}$$

where $q(a,\, b) = \frac{1-e^{-ab}}{1-e^{-b}}$.

The conditional probability of error is then $\phi(-U_s/\sigma)$, where $\phi(x) = \frac{1}{\sqrt{2\pi}}\int_{-\infty}^{x} e^{-t^2/2}\, dt$, and the average probability of error (averaged over the pdf of $\Sigma\alpha_n^2$) may be shown to be

$$P_b = \sqrt{\frac{\gamma_S}{1+\gamma_S}}\,\frac{(1+\gamma_S)^{-m_S}\,\Gamma\left(m_S+\frac{1}{2}\right)}{2\sqrt{\pi}\,\Gamma(m_S+1)}\,{}_2F_1\left(1,\, m_S+\frac{1}{2};\, m_S+1;\, \frac{1}{1+\gamma_S}\right) \text{ ,} \qquad (4a)$$

where $\gamma_S = \dfrac{\gamma\, q(L_R, 2\delta)}{2m\, q(L_R, \delta)}$, $\quad m_S = m\dfrac{q(L_R, \delta)^2}{q(L_R, 2\delta)}$, (4b)

and $\gamma = \left(\dfrac{q(L_P, \delta)-1}{2N} + \dfrac{Kq(L_P, \delta)}{3N} + \dfrac{\eta_0}{2E\Omega_0}\right)^{-1}$. (4c)

In (4a), $\Gamma(.)$ is the Gamma function defined as $\Gamma(z) = \int_0^\infty e^{-t}\, t^{z-1}\, dt$, $z > 0$,

and ${}_2F_1(a, b; c; z)$ is the hypergeometric function defined as

$${}_2F_1(a, b; c; z) = \sum_{k=0}^{\infty} \frac{(a)_k\,(b)_k\, z^k}{(c)_k\, k!}, \quad (a)_k = a\,(a+1)\ldots(a+k-1),\ (a)_0 = 1.$$

The parameter Ω_0 in (4c) is the second moment of the random amplitude attenuation of the first path. This parameter, together with the decay rate δ, completely specifies the powers of each path by the equation $\Omega_i = \Omega_0\, e^{-\delta i}$.

V. Noncoherent Modulation

Two noncoherent receivers are considered, DPSK with differential encoding, and square-law detection with orthogonal signalling.

A. DPSK Receiver Model

The DPSK receiver structure is shown in Figure 5. This receiver is a realization of an equal-gain combining DPSK receiver, where the number of taps (or the number of paths being combined), L_R, is a variable parameter less than or equal to $L_P/2$. L_R is made a variable so that the effect of diversity may be observed. The tap spacing of the receiver is 2Tc (instead of Tc as for the coherent receiver) because it can be shown [Appendix A] that the matched filter response to adjacent paths are correlated, and are uncorrelated for non-adjacent paths. Therefore, to maximize the benefits of diversity for a given number of taps, only every other path is combined.

The matched filter is matched to the reference user's CDMA code and is assumed to have achieved time synchronization with the intial path of the reference signal. Because the period of the spreading sequence is larger than the bit interval, the matched filter sub-sequence needs to be updated every T seconds. Also, in order to demodulate the multipath, the filter must remain matched to each sub-sequence for $2(L_R-1)T_c$ seconds. Since $2L_R \le L_P < N$, $2(L_R-1)T_c < T$ and therefore a single matched filter suffices to serially demodulate each bit.

The multiplier following the matched filter is a dot-product multiplier, whereby the in-phase and quadrature components (relative to the matched filter reference phase) of the matched filter output are treated as vector components. The dot-product multiplication ($\mathbf{x}\cdot\mathbf{y}$), when x and y are treated as

vectors, is equivalent to the operation $Re[xy^*]$ when they are treated as complex numbers; the test statistic U, therefore, is real.

The sampling times of the receiver are $nT+2(L_R-1)T_c$, where n is an integer index. For example, to detect the zeroth information bit b_0, the sample time would be $T+2(L_R-1)T_c$; the 'T' term is from the usual matched filter sampling time and the '$2(L_R-1)T_c$' term is from the combining of (L_R-1) additional paths.

B. DPSK Performance Analysis

With the input to the channel as given in (1), and noting that the channel responds to each user independently, the output of the channel (which is also the input to the receiver) may be written as (in the sequel, only the complex envelope will be given)

$$R_T(t) = \sum_{k=0}^{K} R_k(t) + N(t) \quad , \qquad R_k(t) = \sqrt{2P} \sum_{n=0}^{L_p^{(k)}-1} a_k(t-nT_c-\tau_k)\, b_k(t-nT_c-\tau_k)\, \alpha_n^{(k)}\, e^{j\xi_n^{(k)}} ,$$

where $\left\{\xi_n^{(k)}\right\} = \left\{\psi_n^{(k)} + \phi_k\right\}$ are IID and uniformly distributed in $[0, 2\pi)$.

The response of the reference receiver to $R_T(t)$ at any sampling instant, say at $t = T+2(L_R-1)T_c$, may be written as

$$U = \sum_{i=0}^{L_R-1} U_i \, , \qquad U_i = Re[Z_i(0)Z_i^*(-1)], \tag{5}$$

where

$$Z_i(n) = \int_{nT-2iT_c}^{(n-1)T+2iT_c} R_T(\tau)\, a_0(\tau-2iT_c)\, d\tau .$$

The statistics of random variables of the same type as the $\{U_i\}$ have been investigated by Kavehrad and Ramamurthi [18] in their analysis of DPSK in Rayleigh fading, where U_i is shown to be of the form

$$U_i = Re[(\sqrt{2PT}\alpha_i b_0+N_{1i})(\sqrt{2PT}\alpha_i b_{-1}+N_{2i})^*] \, ,$$

and where N_{1i} and N_{2i} are the matched filter responses to the K interfering users and AWGN. For example, with i = 0, and n = 0,

$$N_{10} = \int_0^T a_0(t)\left[\sum_{k=1}^{K} R_k(t)+N(t)\right] dt \, , \text{ and } \; N_{20} = \int_{-T}^0 a_0(t)\left[\sum_{k=1}^{K} R_k(t)+N(t)\right] dt \, .$$

Also, b_0 and b_{-1} are the differentially encoded data bits, and $\{N_{1i}\}$ and $\{N_{2i}\}$ are modelled as independent zero-mean Gaussian random variables, with identical variances given by

$$\sigma_N^2 = 2\eta_0 T + \sum_{k=1}^{K} \frac{4PT^2}{3N} \Omega_0^{(k)} q(L_p^{(k)}, \delta) . \qquad (6)$$

The Gaussian approximation of the noise variables is based on the assumption of random spreading sequences for all users and is conditioned on the spreading sequence of the intended user (k = 0). Gaussian approximations have been used in the study of similar models [e.g., 6, 19, 20] and have been found to be accurate even for moderate values of K. The variance of the multiple-access interference is given by the second term of (6) and is an approximation which is valid when the spreading sequence of the intended user has small partial autocorrelations [11]. Note that the variance expression of (6) does not depend on the conditioned spreading sequence, therefore averaging over the spreading sequence is not necessary. The independence assumption consists of two parts; first, for each i, N_{1i} is independent of N_{2i}, and second, the pair (N_{1i}, N_{2i}) is independent of the pair (N_{1j}, N_{2j}) for $i \neq j$. The first part of the assumption has been verified by simulation as reported in [18]. For the second part, it can be shown [Appendix B] that if the AWGN is ignored, which is reasonable when $K >> 1$, both components of (N_{1i}, N_{2i}) and (N_{1j}, N_{2j}) consist of sums of K independent quantities; furthermore, the linear combination $\alpha_1 N_{1i} + \alpha_2 N_{2i} + \alpha_3 N_{1j} + \alpha_4 N_{2j}$, where $\{\alpha_i\}$ are arbitrary real constants, is also a sum of K independent quantities. As K increases without bound, the above linear combination can be shown to be asymptotically Gaussian for all sets of constants $(\alpha_1, \alpha_2, \alpha_3, \alpha_4)$. Hence, $(N_{1i}, N_{2i}, N_{1j}, N_{2j})$ is a Gaussian random vector [21], and thus the (N_{1i}, N_{2i}) for different i are jointly Gaussian; since they are uncorrelated [Appendix B], they are independent.

In the variance calculations of (6), the effect of self-interference from the multipath of the reference signal has not been included. For appropriately chosen spreading sequences, the effect of self-interference on BER calculations has been shown to be negligible [22, 23].

With $\{U_i\}$ modelled as above, the conditional probability of error (conditioned on $\{\alpha_n\}$) is given in Proakis [12, eq. (4.4.13)] as

$$P_b = \frac{1}{2^{2L_R-1}} e^{-\gamma_b} \sum_{n=0}^{L_R-1} C_n \gamma_b^n , \qquad (7)$$

where, by definition,

$$C_n = \frac{1}{n!} \sum_{k=0}^{L_R-1-n} \binom{2L_R-1}{k},$$

and

$$\gamma_b = \frac{\gamma}{\Omega_0} \sum_{n=0}^{L_R-1} \alpha_n^2 , \quad \gamma = \left(\frac{\eta_0}{\Omega_0 E} + \frac{2K\, q(L_P,\delta)}{3N} \right)^{-1} . \tag{8}$$

The effective signal-to-noise ratio, γ, follows from (6), with the addition of the following relationship to minimize the number of parameters:

$$\sum_{k=1}^{K} \Omega_0^{(k)}\, q(L_P^{(k)},\delta) = K\, \Omega_0\, q(L_P,\delta) . \tag{9}$$

The average probability of error, P_1, is obtained by averaging P_b with the pdf of γ_b, which for small values of δ (<1.0), is well approximated (exact when $\delta = 0$) by [11, 13]

$$p(\gamma_b) = \frac{\mu^\mu \gamma_b^{\mu-1} e^{-(\mu/\Omega)\gamma_b}}{\Gamma(\mu)\, \Omega^\mu} , \tag{10}$$

where

$$\mu = \frac{\left(\sum_{i=0}^{L_R-1} e^{-2\delta i} \right)^2}{\sum_{i=0}^{L_R-1} \frac{\left(e^{-2\delta i}\right)^2}{m}} = m \frac{q(L_R,2\delta)^2}{q(L_R,4\delta)} , \tag{11}$$

and $$\Omega = \sum_{i=0}^{L_R-1} \gamma\, e^{-2\delta i} = \gamma\, q(L_R, 2\delta) . \tag{12}$$

Thus, $$P_1 = \int_0^\infty P_b\, p(\gamma_b)\, d\gamma_b$$

$$= \int_0^\infty \frac{1}{2^{2L_R-1}} e^{-\gamma_b} \sum_{n=0}^{L_R-1} C_n\, \gamma_b^n \frac{\mu^\mu \gamma_b^{\mu-1}}{\Gamma(\mu)\, \Omega^\mu} e^{-(\mu/\Omega)\gamma_b}\, d\gamma_b$$

$$= \frac{\mu^\mu}{2^{2L_R-1}\, \Gamma(\mu)\, \Omega^\mu} \sum_{n=0}^{L_R-1} C_n \int_0^\infty \gamma_b^{\mu+n-1} \exp\left(-\gamma_b \left(\frac{\mu}{\Omega} + 1 \right) \right) d\gamma_b$$

$$= \frac{\mu^\mu}{2^{2L_R-1}\, \Gamma(\mu)\, \Omega^\mu} \sum_{n=0}^{L_R-1} \frac{C_n\, \Gamma(\mu+n)}{\left(\frac{\mu}{\Omega} + 1 \right)^{\mu+n}} .$$

After some algebraic manipulations, P_1 may be expressed by the relatively simple form

$$P_1 = \frac{1}{2^{2L_R-1}\left(\frac{\Omega}{\mu}+1\right)^{\mu}} \sum_{n=0}^{L_R-1} \frac{C_n\,(\mu)_n}{\left(\frac{\mu}{\Omega}+1\right)^{n}}, \tag{13}$$

where

$$(\mu)_k = \Gamma(\mu+k) / \Gamma(\mu) = \mu\,(\mu+1)\ldots(\mu+k-1), \quad (\mu)_0 = 1.$$

For the special case of $\delta = 0$ (constant MIP) and $m = 1$ (Rayleigh fading),

$$P_1 = \frac{1}{2^{2L_R-1}\,(1+\gamma)^{L_R}} \sum_{n=0}^{L_R-1} \frac{C_n\,(L_R)_n}{\left(\frac{1}{\gamma}+1\right)^{n}}, \tag{14}$$

which is equivalent to the result listed in Proakis [12, eq. (7.4.26)]. And for the case of $L_R = 1$ (single path), (13) reduces to

$$P_1 = \frac{1}{2(1+\gamma)^{m}}, \tag{15}$$

a well known result usually attributed to Barrow [24].

C. Orthogonal Spreading Sequences

Noncoherent CDMA performance using binary orthogonal spreading sequences, whereby each user sends one of two orthogonal PN codes (codes of different users are not necessarily orthogonal), has been examined by Xiang [8] for a random delay channel with a constant MIP (i.e., δ=0). Xiang's results may be readily extended to include exponentially decaying MIP's by modifying certain parameters in his equations.

The receiver block diagram is shown in Fig. 6, which consists of a bank of two matched filters (matched to the orthogonal codes) followed by envelope detectors and squarers. The tap spacing here is $2T_c$, just as for DPSK, because the response at the output of the matched filters is the same as in the DPSK receiver. Assuming the matched filters are in time synchronization with the initial path, the tapped delay lines accumulate the demodulated outputs of L_R-1 subsequent paths. If the interference at each path of each branch is assumed Gaussian and independent of one another (i.e., the same assumptions made previously and in [8]), then the analysis is identical to that of Charash [17], from which the conditional bit error probability may be shown to be

$$P_b(\gamma_b) = \frac{e^{-\gamma_b}}{2^{L_R}\Gamma(L_R)} \sum_{i=0}^{L_R-1} \frac{\Gamma(L_R+i)}{2^i\,\Gamma(i+1)}\,{}_1F_1\left(L_R+i; L_R; \frac{\gamma_b}{2}\right),$$

where γ_b is as defined in (8) with pdf $p(\gamma_b)$ as given in (10), and ${}_1F_1(a;c;x)$ is the confluent hypergeometric function defined as ${}_1F_1(a;c;x) = \sum_{k=0}^{\infty} \frac{(a)_k\, x^k}{(c)_k\, k!}$.

The average bit error probability, P_2, then may be written as

$$P_2 = \int_0^{\infty} P_b(\gamma_b)\, p(\gamma_b)\, d\gamma_b$$

$$= \frac{\left(\frac{\mu}{\Omega}\right)^{\mu}}{2^{L_R}\,\Gamma(L_R)\Gamma(\mu)} \sum_{i=0}^{L_R-1} \frac{\Gamma(L_R+i)}{2^i\,\Gamma(i+1)} \int_0^{\infty} \exp\left(-\gamma_b\left(1+\frac{\mu}{\Omega}\right)\right) \gamma_b^{\mu-1}\, {}_1F_1\left(L_R+i;L_R;\frac{\gamma_b}{2}\right) d\gamma_b .$$

The integral in the last expression is a Laplace transform and may be expressed as [25, p. 269]

$$\int_0^{\infty} \exp\left(-\gamma_b\left(1+\frac{\mu}{\Omega}\right)\right) \gamma_b^{\mu-1}\, {}_1F_1\left(L_R+i;L_R;\frac{\gamma_b}{2}\right) d\gamma_b = \Gamma(\mu)\left(1+\frac{\mu}{\Omega}\right)^{-\mu} {}_2F_1\left(L_R+i;\mu;L_R;\frac{1}{2}\left(1+\frac{\mu}{\Omega}\right)^{-1}\right),$$

where ${}_2F_1(a,b;c;z) = \sum_{k=0}^{\infty} \frac{(a)_k\,(b)_k\, z^k}{(c)_k\, k!}$.

Using the above formula and noting that $\frac{\Gamma(L_R+i)}{\Gamma(L_R)\,\Gamma(i+1)} = \binom{L_R+i-1}{i}$, P_2 is written in the final form

$$P_2 = \frac{1}{2^{L_R}\left(1+\frac{\Omega}{\mu}\right)^{\mu}} \sum_{i=0}^{L_R-1} \frac{1}{2^i} \binom{L_R+i-1}{i}\, {}_2F_1\left(L_R+i;\,\mu;\,L_R;\,\frac{1}{2}\left(1+\frac{\mu}{\Omega}\right)^{-1}\right). \qquad (16)$$

For the single-path dedicated-channel case, $L_R = 1$ and $K = 0$; using the identity ${}_2F_1(a,b;a;z) = (1-z)^{-b}$, (16) reduces to

$$P_2 = \frac{1}{2}\left(\frac{2}{2+\gamma}\right)^m, \qquad (17)$$

which is identical to (15) if 'γ' in (17) is replaced by '2γ'. This is because for $L_R = 1$, the conditional bit error probability for both DPSK and orthogonal signalling are of the same exponential form with $\gamma_{DPSK} = 2\,\gamma_{ortho}$, and thus no matter what type of fading they are subjected to, they would have the same performance characteristics with a 3 dB SNR difference in DPSK's favor. For the special case of

$L_R = 1$ and $m = 1$, (17) reduces to the familiar expression for orthogonal binary signalling in Rayleigh fading, $P = (2+\gamma)^{-1}$ [12, eq. (7.3.12)].

Figures 7a-7c show the BER performance of coherent PSK, DPSK, and orthogonal signalling with square-law detection, respectively, for $N = 511$, $\delta = 0$, and $m = 1$. The individual curves in each plot are parameterized by $L_R = 1, 2, ..., 10$, with $L_P = L_R$ for the coherent case, and $L_P = 2L_R$ for the noncoherent cases* . From these plots, it is seen that for noncoherent modulation, when L_R increases beyond an optimal value, the performance begins to degrade; this is a clear illustration of the so called 'noncoherent combining loss' observed in all noncoherent systems.

VI. FCDMA Capacity Calculations

There are two properties of FCDMA that make it potentially attractive. First, a contiguous band of spectrum is not required; the spectrum of FCDMA may be 'tailored' to fill the available frequency resources. Second, having several sub-spectra allows flexibility in frequency assignments. For example, users with similar BER requirements could be assigned to the same sub-spectrum to maximize capacity.

In order to analyze the performance of FCDMA quantitatively, a model must be used which relates the sub-spectrum bandwidth to the relevant system parameters. The results of the previous sections may then be applied directly to determine BER performance. It was shown above that the system parameters that determine BER performance are the processing gain N, the number of other users (with the same center frequency) K, the fading figure m, the number of resolvable paths L_P, the number of paths that are actually used L_R ($\leq L_P$), the rate of path-strength decay δ, and the average received SNR (of the strongest path) $E\Omega_0/\eta_0$, where E is the received signal energy per bit, Ω_0 is the second moment of the amplitude fading statistic, and η_0 is the single-sided density of the AWGN. In the model used here, the receiver parameters that are presumed bandwidth-dependent are N and L_P. In particular, if T_{c1} and T_{c2} denote the chip times of systems 1 and 2 respectively, then it is assumed that

$$\frac{N_1}{N_2} = \frac{T_{c2}}{T_{c1}} = \frac{L_{P1}}{L_{P2}} \quad . \tag{18}$$

Using (18), the system parameters of each sub-spectrum of FCDMA may be determined from the corresponding parameters of a wideband CDMA of the same total bandwidth. For example, if there are L sub-spectra in the FCDMA system, then the processing gain and the number of resolvable paths of each sub-spectrum are reduced (relative to that of wideband CDMA) by a factor of L, while the other parameters remain unchanged.

The tapped delay line channel model used here has tap spacing equal to the chip time (which is inversely proportional to the signal bandwidth); as a result, a signal with narrower bandwidth not only

---

* Note that, because the number of received paths for the coherent and noncoherent modulation formats are not the same, we do not make any attempt to compare, say, coherent BPSK with DPSK. Rather, we only compare each modulation format to itself as various parameter values are changed.

will have fewer resolvable paths, but each path that is resolvable will have greater power because a number of paths which were individually resolvable for the wideband system are now modelled as being lumped together to form a single path as seen by the narrowband receiver. To model this effect quantitatively, refer to Fig. 8, where an example of a wideband multipath profile with 6 paths is shown; now, if a narrowband signal (say, with half the bandwidth) with the same energy per bit is sent through the channel, and if the received energy is equal in both cases, then a reasonable model for the narrowband channel response is shown in Fig. 9, where the number of taps is halved, the tap spacing is doubled, and the powers of each path are obtained by summing powers of adjacent paths from the wideband model. This makes the total available power at the receiver a constant value independent of the receiver structure. The notion of constant total received power is not only intuitive for our model (since we are summing discrete multipath returns with random RF phases), but is also consistent with Ochsner's channel model [9] derived from a continuous MIP.

In addition to the parameters already discussed, the exponent of the path-strength decay rate for the narrowband model (i.e., δ_2) is also doubled due to the merging of paths. Thus, using notation analogous to (18), the following general relationships are obtained:

$$\frac{\Omega_{02}}{\Omega_{01}} = q\left(\frac{T_{c2}}{T_{c1}}, \delta_1\right), \qquad \frac{\delta_2}{\delta_1} = \frac{T_{c2}}{T_{c1}}, \tag{19}$$

where subscript 1 refers to wideband CDMA and subscript 2 refers to FCDMA.

Let the capacity be defined as the largest K such that $P_b \le P_{req}$ for some P_{req}, and be denoted by $C(L_P, N)$, where only parameters of interest (the ones that are bandwidth-dependent) are explicitly written. The capacity of FCDMA then may be written as $L \times C(L_P/L, N/L)$, where L is the number of sub-spectra of equal bandwidth. Table I lists the coherently demodulated capacities for L = 1, 2, 3, 4, 6, and 12, N = 1023, L_P = 12, $L_R = L_P$, δ = 0, $E\Omega_{01}/\eta_0$ = 10 dB and 50 dB, and m = 1 (which corresponds to Rayleigh fading). Table II lists the capacities with the same parameters except that δ = 0.1. From the results in Tables I and II, it is seen that for both δ = 0 and δ = 0.1, the total capacity decreases as the available spectrum is more finely divided. Thus, the penalty for the increased flexibility of FCDMA is a decrease in system performance.

The results of Tables I and II assume that L_R, the number of resolvable paths used by the RAKE receiver, is constant (L_R = 12) for L = 1, while L_R decreases with L (L_R = 12/L) for L > 1. In presenting the results this way, it is implicitly assumed that the receivers for all cases have as many taps as needed to demodulate all available paths; i. e., for L = 1, the receiver has 12 taps, for L = 2, the receiver has 12/2 = 6 taps, etc. Since the receiver complexity is greatest for L = 1, one can consider an alternate comparison in which complexities are kept constant. Therefore, consider Tables III and IV, which list the capacities for wideband CDMA (N = 1023) with L_R = 12/L, L_P = 12, m = 1, and δ = 0 and 0.1, respectively. Thus, an equal-complexity comparison (between wideband CDMA and FCDMA, using the same number of taps, not among FCDMA's of different L's) may be made by comparing one entry from Table III or IV with the corresponding entry from Table I or II.

From Tables I through IV, it is seen that if the receivers are required to be of equal complexity, FCDMA can now have a significant advantage over wideband CDMA. That is, if the wideband CDMA system does not take advantage of its wider bandwidth, its performance can be surpassed by that of a narrower bandwidth system. However, in light of the continual technological advances made in VLSI design and fabrication, receiver complexity may not be a dominant issue. Further, note that the wideband system does not necessarily have to use all of the resolvable paths to outperform the FCDMA system. For example, from Table II, when $E\Omega_0/\eta_0 = 10$ dB and the probability of error is 10^{-2} (in the absence of coding), a narrowband system corresponding to L = 6 (or two resolvable paths) can support 174 users. From Table IV, it is seen that the wideband system can support a greater number of users by resolving six or more paths. That is, when L = 2 (or six paths being used), the wideband system can support 194 subscribers, or an increase in capacity of 11%. Of course, the wideband system has the option of increasing capacity by 267% if all twelve resolvable paths are used.

Consider now the performance of the noncoherent modulation formats. Tables V through VIII show the capacities for DPSK, and are analogous to Tables I through IV, respectively, except that $L_P = 24$ for the noncoherent modulations (the maximum L_R is still 12 because for noncoherent modulations, no adjacent paths are combined). Similarly, Tables IX through XII show the corresponding capacities for orthogonal signalling. It is seen that the general conclusions reached regarding coherent modulation do not carry over to the noncoherent modulation formats. For example, from Table V, at a BER of 10^{-1}, the capacity first increases and then decreases as the spectrum is more finely divided; the wideband CDMA has the least capacity in this case. At a BER of 10^{-2}, wideband CDMA compares more favorably against FCDMA, but is still inferior to the L = 2 and L = 3 cases. Only at the lower BER requirements of 10^{-3} and 10^{-4} does wideband CDMA begin to manifest a clear advantage over narrowband CDMA. This behavior is consistant with the data shown in Figures 7a, 7b, and 7c, where it is seen that for the noncoherent modulation formats, a larger diversity often performs worse than a smaller diversity at relatively large BER's such as 10^{-1}, and vice versa for small BER's such as 10^{-3}.

Another trend that can be inferred from the tables (for noncoherent modulation formats) is that as fewer and fewer users are connected to the system, the improvement in BER is much more pronounced for wideband CDMA than for narrowband CDMA. For example, from Table VI, at an SNR of 10 dB, the BER for wideband CDMA improves from 10^{-1} to 10^{-4} as the number of users decrease from 169 to 11; at the other extreme, when L = 12, the BER never gets better than 10^{-2} no matter how few users are active. Thus, if the system is required to transmit data, which normally requires an uncoded BER of 10^{-3} or less, then wideband CDMA is clearly superior.

A third interesting comparison that can be made is between the performance corresponding to different values of δ. For all detection schemes, increasing δ has two effects on system parameters, 1) the effective order of diversity, m_s, decreases, and 2) the total interference also decreases. These two factors affect performance in opposite directions, and the final result depends on which factor dominates for the given detection scheme and the given set of system parameters. From Tables I and II, it is seen that for coherent modulation, performance is degraded for all cases when δ is increased

from 0.0 to 0.1. This indicates that the useful properties of each resolvable path out-weigh the destructive properties of the increased interference. When some of the available paths are not used in the demodulation, however, as is shown in the $L > 1$ cases of Tables III and IV, the $\delta = 0.1$ performance is sometimes better than the $\delta = 0.0$ performance, because the tail-end of the MIP is not contributing to the detection process and acts only as interference. Since increasing δ suppresses the tail end of the MIP more rapidly than the front end, the net result is better performance for the larger δ. A similar comparison of the entries of Tables V and VI for DPSK (Tables XI and X for square-law detected orthogonal signalling) reveals that changing δ from 0.0 to 0.1 improves performance in some cases, and degrades performance in other cases. This is in contrast with the coherent detection comparison, where the effect on performance was uniform. The uniformity of performance change for coherent reception may be explained by noting that each path of the MIP is combined optimally (the RAKE receiver performs maximal-ratio combining, which achieves the maximum post-detection SNR possible), and therefore suppressing the MIP (by increasing δ), which decreases the effective order of diversity, always degrades performance. On the other hand, the noncoherent modulation formats use equal-gain combining, which is not an optimal combining technique and which causes the 'noncoherent combining loss' exhibited in Figures 7b and 7c. Therefore, varying δ (which, as noted above, changes m_s) may enhance or degrade performance, depending on the values of the other system parameters.

This same mechanism may also explain the lack of uniformity in an entry-by-entry comparison of Tables VII and VIII (Tables XI and XII), which show the capacities for DPSK wideband CDMA (square-law detected wideband CDMA) with varying degrees of receiver complexity. As an illustration of a limiting case of noncoherent combining loss, it is shown in Appendix C that, for $\delta \rightarrow \infty$, the DPSK P_b for $L_R = 1$ is less than the P_b for $L_R > 1$. In fact, δ does not have to be very large for the above property to hold, as Table XIII shows for both $\delta = 1.6$ and $\delta = 10.0$, with $E\Omega_0/\eta_0 = 50$ dB. Another interesting observation is that when $\delta \rightarrow \infty$, the MIP is effectively reduced to a single path, i.e., $q(L_P, \delta) = 1$, and from Eqs. (4) and (8), the effective SNR is then (ignoring the AWGN term) $\gamma = 3N/K$ and $\gamma = 3N/2K$, for coherent and noncoherent modulation formats, respectively. Noting from Eqs. (4a), (13), and (16) that, if L_R is held constant, the BER is a function only of γ, it follows that the capacity (the capacity of a sub-spectrum in the case of FCDMA) is proportional to the processing gain for any BER. This implies that in an equal-complexity comparison, where L_R for both the wideband and hybrid systems are required to be equal, wideband CDMA capacity should equal FCDMA capacity. This is because the processing gain of each sub-spectra of FCDMA is 1/L times that of the wideband system; therefore, the capacity of each 'narrowband' sub-system of FCDMA is 1/L times that of wideband CDMA, and, since there are L such sub-spectra, the total FCDMA capacity is equal to the wideband CDMA capacity. Table XIV shows the DPSK wideband CDMA capacities for both $\delta = 1.6$ and $\delta = 10.0$, with $E\Omega_0/\eta_0 = 50$ dB. Comparing corresponding entries from Tables XIII and XIV, it is seen that for $\delta = 10.0$, the capacities are equal to within the truncation error. For example, letting $L = 6$, the entry from Table XIII indicates a capacity of 300 at 10^{-1}; this implies that each segment capacity is 50. Now take the corresponding entry from Table XIV, 304, and divide by $L = 6$; the integer portion of the quotient, 50, is equal to the segment capacity.

VII. Conclusions

A hybrid FDMA/CDMA system is described and analyzed. The hybrid system treats each segment, or sub-spectrum, as a stand-alone CDMA system, independent of the other segments. Using the multipath fading channel model and analysis described in [11], and making some reasonable assumptions on the relationships between signal bandwidth and 1) the number of resolvable paths, 2) the path powers, and 3) the path decay rate, the following set of conclusions can be drawn:

(i) For coherent reception where each system uses as many paths as it is capable of resolving, the wideband system yields greater capacity.

(ii) If the wideband coherent system is limited by complexity constraints so that it cannot make constructive use of all resolvable paths, an FCDMA system can yield a larger capacity.

(iii) As the decay rate of the multipath intensity profile (MIP) increases to a sufficiently large value, all systems will perform the same, since only one resolvable path is available. This implies that the wideband system will only attempt to resolve a single path, since the resolution of additional paths will only yield increased noise and multiple access interference.

(iv) For binary noncoherent modulation formats, at high channel error rates and small values of the MIP decay factor, FCDMA yields higher capacity, whereas at low channel rates, wideband CDMA is superior.

Finally, in terms of the most obvious applications, namely voice and data, the above conclusions can be restated in the following manner: For coherent reception, wideband CDMA is superior for either application unless a complexity constraint is imposed so that the receiver cannot take advantage of all the multipath it is capable of resolving. For DPSK with equal-gain combining, FCDMA is superior for voice if the multipath decay factor is small; if the decay factor is large, and each system uses the proper number of resolvable paths, there is not much difference in performance. However, for data communications, wideband CDMA yields greater capacity.

Appendix A

In this appendix, the matched filter response to the received signal is examined. The aim is to show that, for noncoherent demodulation, adjacent tap outputs of a tap delay line with T_c tap spacing, placed after the matched filter, are correlated due to the multiple access interference, and that those of non-adjacent taps are uncorrelated.

Consider first the output of the n-th tap in response to the k-th user, where the matched filter is matched to the code of the zero-th user and $k \neq 0$.

$$Y_n^{(k)} = \mu_n \int_{nT_c}^{nT_c+T} a_0(t-nT_c) \sum_{i=0}^{L_p^{(k)}-1} \alpha_i^{(k)} e^{j\xi_i^{(k)}} a_k(t-\tau_k-iT_c)\, dt$$

$$= \mu_n \sum_{i=0}^{L_p^{(k)}-1} \alpha_i^{(k)} e^{j\xi_i^{(k)}} \int_0^T a_0(t)\, a_k(t-\tau_k-(i-n)T_c)\, dt\,. \qquad \text{(A1)}$$

The parameter μ_n in (A1) is different for coherent and noncoherent modulations, and may be expressed as [11]

$$\mu_n = \begin{cases} \alpha_n^{(0)} e^{-j\xi_n^{(0)}}, \text{ coherent} \\ 1, \text{ noncoherent} \end{cases}. \qquad \text{(A2)}$$

For convenience, denote the integral in the last line of (A1) as

$$c_k(\tau_k,(i-n)T_c) = \tau_k \sum_{j=0}^{N-1} a_j^{(0)} a_{j-i+n-1}^{(k)} + (T_c-\tau_k) \sum_{j=0}^{N-1} a_j^{(0)} a_{j-i+n}^{(k)}\,, \qquad \text{(A3)}$$

where $\{a_i^{(0)}\}$ and $\{a_j^{(k)}\}$ are the chip sequences (for convenience, data bits are not included) of the intended 0-th user and the interfering k-th user, respectively. If the code sequences are modelled as independent random binary sequences, then it is clear that $c_k(\tau_k, iT_c)$ is correlated with $c_k(\tau_k, jT_c)$ if and only if $|i-j| \leq 1$. This fact is easily seen by noting that the two sums in (A3) differ only by a one-chip shift of the $a^{(k)}$-sequence. Now consider the output of the m-th tap, which, using the notation of (A3), may be written as

$$Y_m^{(k)} = \mu_m \sum_{j=0}^{L_p^{(k)}-1} \alpha_j^{(k)} e^{j\xi_j^{(k)}} c_k(\tau_k, (j-m)T_c)\,.$$

The correlation between the outputs of the m-th and n-th tap is then

$$E\{Y_n^{(k)} Y_m^{(k)*}\} = E\{\mu_n \mu_m^*\} \sum_{i=0}^{L_p^{(k)}-1} \sum_{j=0}^{L_p^{(k)}-1} E\left\{\alpha_i^{(k)} \alpha_j^{(k)} e^{j(\xi_i^{(k)} - \xi_j^{(k)})} c_k(\tau_k, (j-m)T_c)\, c_k(\tau_k, (i-n)T_c)\right\}$$

$$= E\{\mu_n \mu_m^*\} \sum_{i=0}^{L_p^{(k)}-1} \sum_{j=0}^{L_p^{(k)}-1} E\left\{\alpha_i^{(k)} \alpha_j^{(k)}\right\} E\left\{ e^{j(\xi_i^{(k)} - \xi_j^{(k)})}\right\} E\{ c_k(\tau_k, (j-m)T_c)\, c_k(\tau_k, (i-n)T_c)\}$$

Considering coherent modulation first, from the independence and uniform distribution of the path phases $\left\{\xi_i^{(k)}\right\}$, it is clear that $E\{\mu_n \mu_m^*\}$ is zero for $m \neq n$; therefore, outputs from different taps are uncorrelated. For noncoherent modulation, $E\{\mu_n \mu_m^*\} = 1$, and from the correlation properties of $c_k(.,.)$, it is clear that $E\{Y_n^{(k)} Y_m^{(k)*}\}$ is zero for $|m-n| > 1$ and non-zero otherwise. And finally, since the receiver response to different users are assumed independent, the same property holds true for the total response to the K interfering users, which was to be shown.

Appendix B

In this appendix, some properties of the noise variables $\{N_{1i}, N_{2i}\}$ are examined. Note first that if AWGN is ignored, both N_{1i} and N_{2i} are of the form

$$N_i(n) = \int_{nT+2iT_c}^{(n+1)T+2iT_c} \left[a_0(t-2iT_c) \sum_{k=1}^{K} R_k(t)\right] dt$$

$$= \sum_{k=1}^{K} \int_{nT+2iT_c}^{(n+1)T+2iT_c} a_0(t-2iT_c)\, R_k(t)\, dt = \sum_{k=1}^{K} N_i^{(k)}(n)\ .$$

The difference between N_{1i} and N_{2i} is that N_{1i} equals $N_i(n)$ for some n, and N_{2i} equals $N_i(n-1)$ for the same n. Conditioned on $a_0(t)$, the $\{N_i^{(k)}(n)\}$ are independent for different k because the $\{R_k(t)\}$ are independent for different k. Furthermore, the independence holds for any value of i and n. Also, from the result of Appendix A, $N_i^{(k)}(n)$ is uncorrelated with $N_j^{(k)}(m)$ if the limits of integration corresponding to one are seperated from those corresponding to the other by at least $2T_c$. Given that $i \neq j$, the seperation requirement is satisfied for any values of m and n, so long as $|i-j| < (N-1)/2$. For large N, (N-1)/2 may be substituted with N/2 with negligible error; then $|i-j| < (N-1)/2$ is equivalent to $L_R < N/2$, which is satisfied by the earlier assumptions that L_P is less than N and $L_R \leq L_P/2$.

Now consider the linear combination

$$\alpha_1 N_{1i} + \alpha_2 N_{2i} + \alpha_3 N_{1j} + \alpha_4 N_{2j} = \sum_{k=1}^{K} \left[\alpha_1 N_i^{(k)}(n) + \alpha_2 N_i^{(k)}(n-1) + \alpha_3 N_j^{(k)}(m) + \alpha_4 N_j^{(k)}(m-1)\right],$$

where $\{\alpha_i\}$ are arbitrary real constants. Since each term inside the square bracket is independent for different k, the sum of the four terms is also independent for different k, and therefore the right hand

side of the above equation consists of a sum of K independent terms. As described in the text, this establishes that (N_{1i}, N_{2i}) and (N_{1j}, N_{2j}) are asymptotically jointly Gaussian [21], and, because they are uncorrelated as discussed above, they are asymptotically independent.

Appendix C

The DPSK probability of error for the limiting case of $\delta \to \infty$ is examined in this appendix.

Letting m=1 and $\delta \to \infty$ in (11) and (12) yields $\mu = 1$ and $\Omega = \gamma = (2K/3N + \eta_0/E\Omega_0)^{-1}$. From (13),

$$P_b = \frac{1}{2^{2L_R-1}(1+\gamma)} \sum_{n=0}^{L_R-1} \frac{C_n\, n!}{(1+\gamma)^n}.$$

When $L_R = 1$, $P_b = \frac{1}{2(1+\gamma)}$, since $C_0 = 2^{2L_R-2}$. When $L_R > 1$, P_b may be rewritten as

$$P_b = \frac{1}{2^{2L_R-1}(1+\gamma)} \left[C_0 + \sum_{n=1}^{L_R-1} \frac{C_n\, n!}{(1+\gamma)^n} \right]$$

$$= \frac{1}{2(1+\gamma)} \left[1 + \frac{1}{C_0} \sum_{n=1}^{L_R-1} \frac{C_n\, n!}{(1+\gamma)^n} \right].$$

Since the term in the square brackets of the last line is greater than 1 for all $L_R > 1$, it follows that $P_b(L_R = 1) < P_b(L_R > 1)$. The physical interpretation of this is simply that (equal-gain) combining additional paths with little or no energy will only degrade performance.

References

[1] C. S. Gardner and J. A. Orr, "Fading Effects on the Performance of a Spread Spectrum Multiple Access Communication System," IEEE Trans. on Comm., vol. COM-27, pp. 143-149, Jan. 1979.

[2] D. E. Borth and M. B. Pursley, "Analysis of Direct-Sequence Spread Spectrum Multiple-access Communication Over Rician Fading Channels," IEEE Trans. on Comm., vol. COM-27, pp. 1566-1577, Oct. 1979

[3] E. Geraniotis, "Direct-Sequence Spread-Spectrum Multiple-Access Communications Over Nonselective and Frequency-Selective Rician Fading Channels," IEEE Trans. on Comm., vol. COM-34, pp. 756-764, Aug. 1986.

[4] G. L. Turin, "The Effects of Multipath and Fading on the Performance of Direct-Sequence CDMA Systems," IEEE Journal Sel. Areas Comm., vol. SAC-2, pp. 597-603, July 1984.

[5] J. S. Lehnert and M. B. Pursley, "Multipath Diversity Reception of Spread-Spectrum Multiple-Access Communications," IEEE Trans. on Comm., vol. COM-35, pp. 1189-1198, Nov. 1987.

[6] E. A. Geraniotis and M. B. Pursley, "Performance of Coherent Direct-Sequence Spread-Spectrum Communications Over Specular Multipath Fading Channels," IEEE Trans. on Comm., vol. COM-33, pp. 502-508, June 1985.

[7] M. Kavehrad and P. J. McLane, "Performance of Low-Complexity Channel Coding and Diversity for Spread Spectrum in Indoor, Wireless Communication," AT&T Tech. Journal, vol. 64, pp. 1927-1965, Oct. 1985.

[8] H. Xiang, "Binary Code-Division Multiple-Access Systems Operating in Multipath Fading, Noisy Channels," IEEE Trans. on Comm., vol. COM-33, pp. 775-784, Aug. 1985.

[9] H. Ochsner, "Direct-Sequence Spread-Spectrum Receiver for Communication on Frequency-Selective Fading Channels," IEEE Journal Sel. Areas Comm., vol. SAC-5, pp. 188-193, Feb. 1987.

[10] G. L. Turin, "Introduction to Spread-Spectrum Antimultipath Techniques and Their Application to Urban Digital Radio," Proc. IEEE, vol. 68, pp. 328-353, Mar. 1980.

[11] T. Eng and L. B. Milstein, "Coherent DS-CDMA Performance in Nakagami Multipath Fading," Submitted for publication.

[12] J. G. Proakis, *Digital Communications*, McGraw Hill, 1983.

[13] M. Nakagami, "The m-Distribution - A General Formula of Intensity Distribution of Rapid Fading," reprinted from *Statistical Methods of Radio Wave Propagation* (W. C. Hoffman editor), Pergamon Press, Oxford, England; 1960.

[14] E. J. Fremouw, et al, "On the Statistics of Scintillating Signals," Journal of Atmospheric and Terrestial Physics, vol. 42, pp.717-731, 1980.

[15] P. D. Shaft, "On the Relationship Between Scintillation Index and Rician Fading," IEEE Trans. on Comm., vol. COM-22, pp. 731-732, May 1974.

[16] G. L. Turin, et al, "A Statistical Model of Urban Multipath Propagation," IEEE Trans. Veh. Tech., vol. VT-21, pp. 1-9, Feb. 1972.

[17] U. Charash, "Reception Through Nakagami Fading Multipath Channels with Random Delays," IEEE Trans. on Comm., vol. COM-27, pp. 657-670, April 1979.

[18] M. Kavehrad and B. Ramamurthi, "Direct-Sequence Spread Spectrum with DPSK Modulation and Diversity for Indoor Wireless Communications," IEEE Trans. on Comm., vol. COM-35, pp. 224-236, Feb. 1987.

[19] K. Yao, "Error Probability of Asynchronous Spread Spectrum Multiple Access Communication Systems," IEEE Trans. on Comm., vol. COM-25, pp.803-809, Aug. 1977.

[20] J. S. Lehnert and M. B. Pursley, "Error Probabilities for Binary Direct-Sequence Spread-Spectrum Communications with Random Signature Sequences," IEEE Trans. on Comm., vol. COM-35, pp. 87-98, Jan. 1987.

[21] Personal communications, Prof. M. Rosenblatt, UCSD.

[22] D. L. Noneaker and M. B. Pursley, "The Effects of Spreading Sequence Selection on DS Spread-spectrum with Selective Fading and Two Forms of Rake Reception," Proc. 1992 Global Telecommunications Conf., vol. 4, pp. 66-70, Dec. 1992.

[23] G. L. Stüber and C. Kchao, "Analysis of a Multiple-Cell Direct-Sequence CDMA Cellular Mobile Radio System," IEEE Journal Sel. Areas Comm., vol. SAC-10, pp. 669-679, May 1992.

[24] B. Barrow, "Error Probabilities for Data Transmission Over Fading Radio Paths," SHAPE Air Defence Tech. Cen., Tech. Rep., 1962.

[25] A. Erdelyi, et al, *Higher Transcendental Functions, Vol. I*, McGraw Hill, 1953.

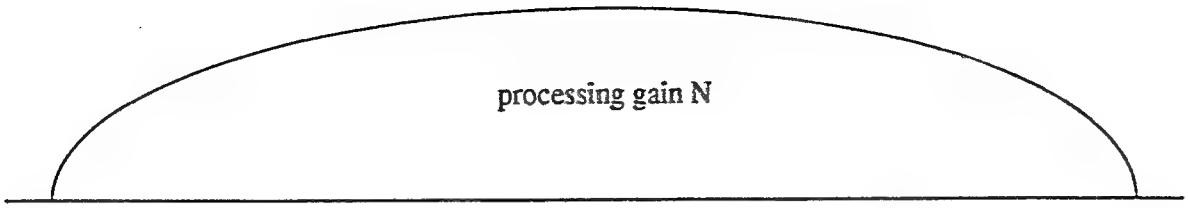

Fig. 1. Spectrum of wideband CDMA.

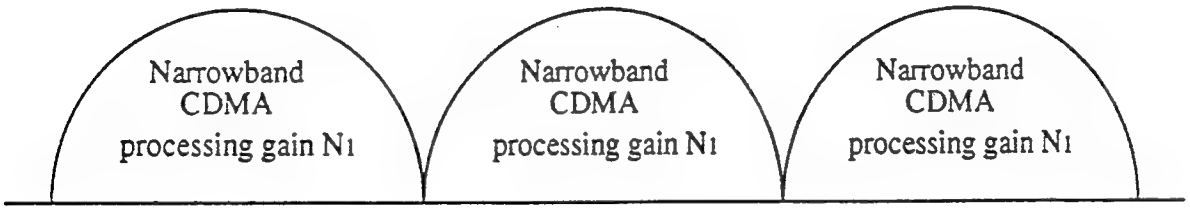

Fig. 2. Spectrum of FDMA/CDMA hybrid scheme.

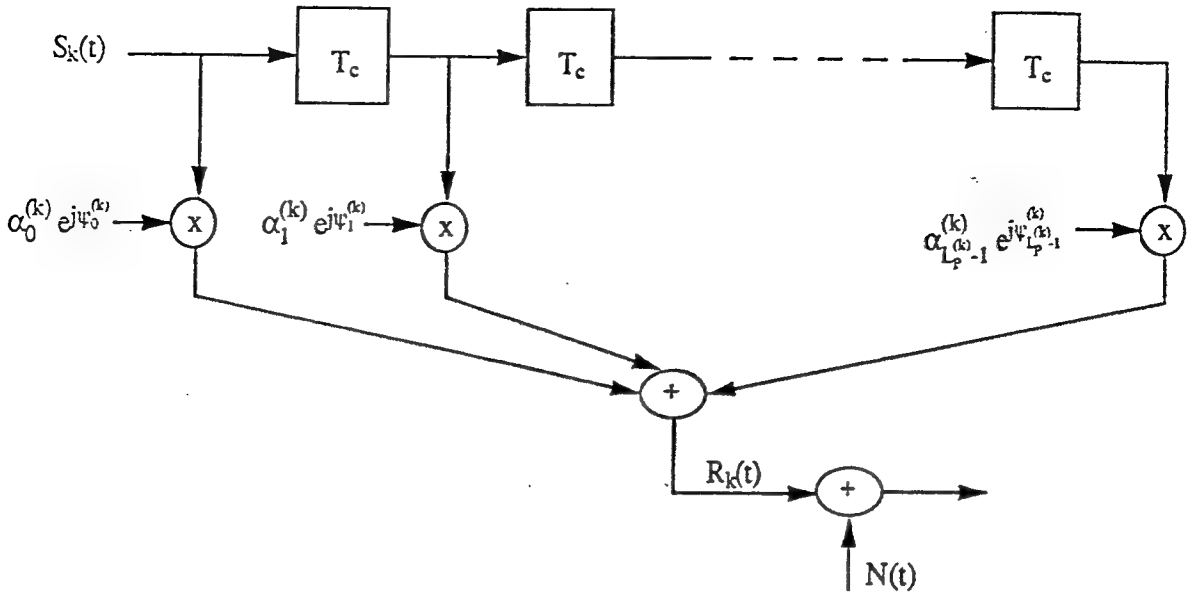

Fig. 3. Multipath Channel Model. (Response to k-th user.)

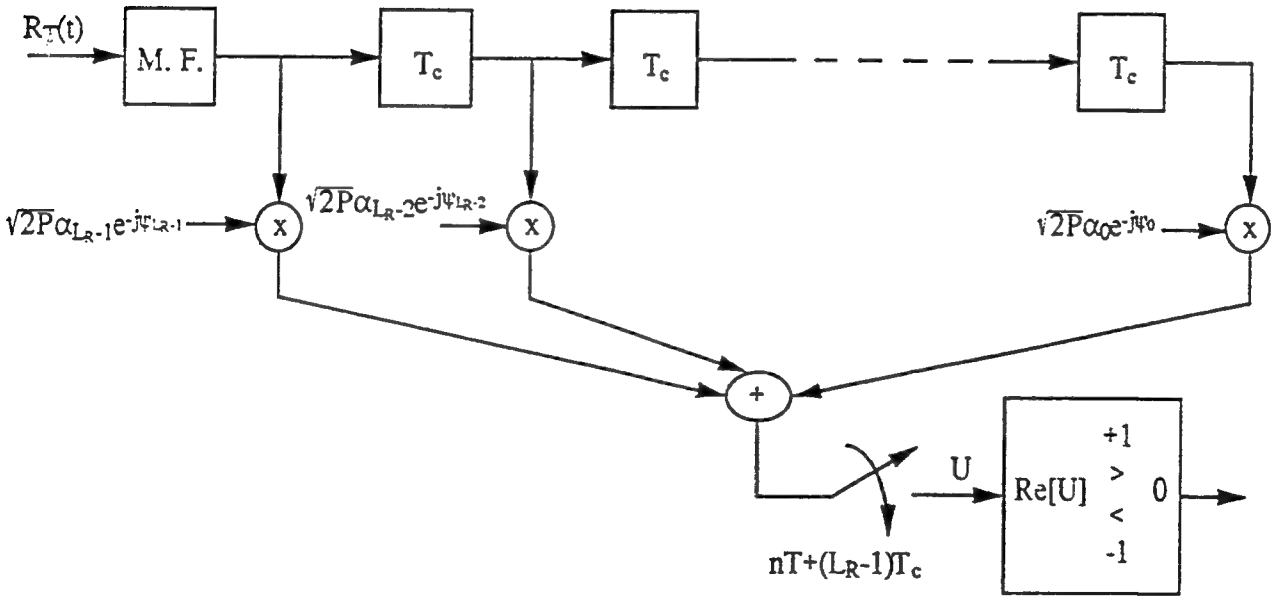

Fig. 4. RAKE Receiver Model.

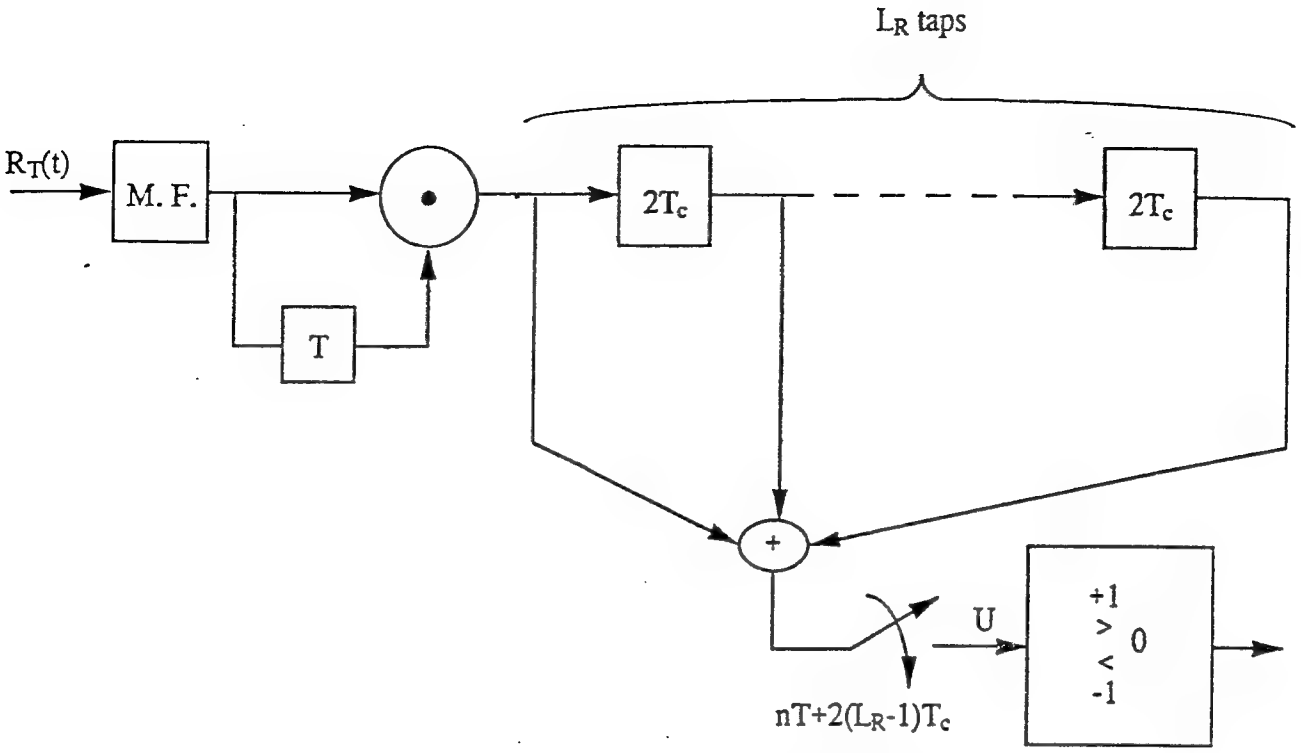

Fig. 5. Equal-gain combining DPSK receiver.

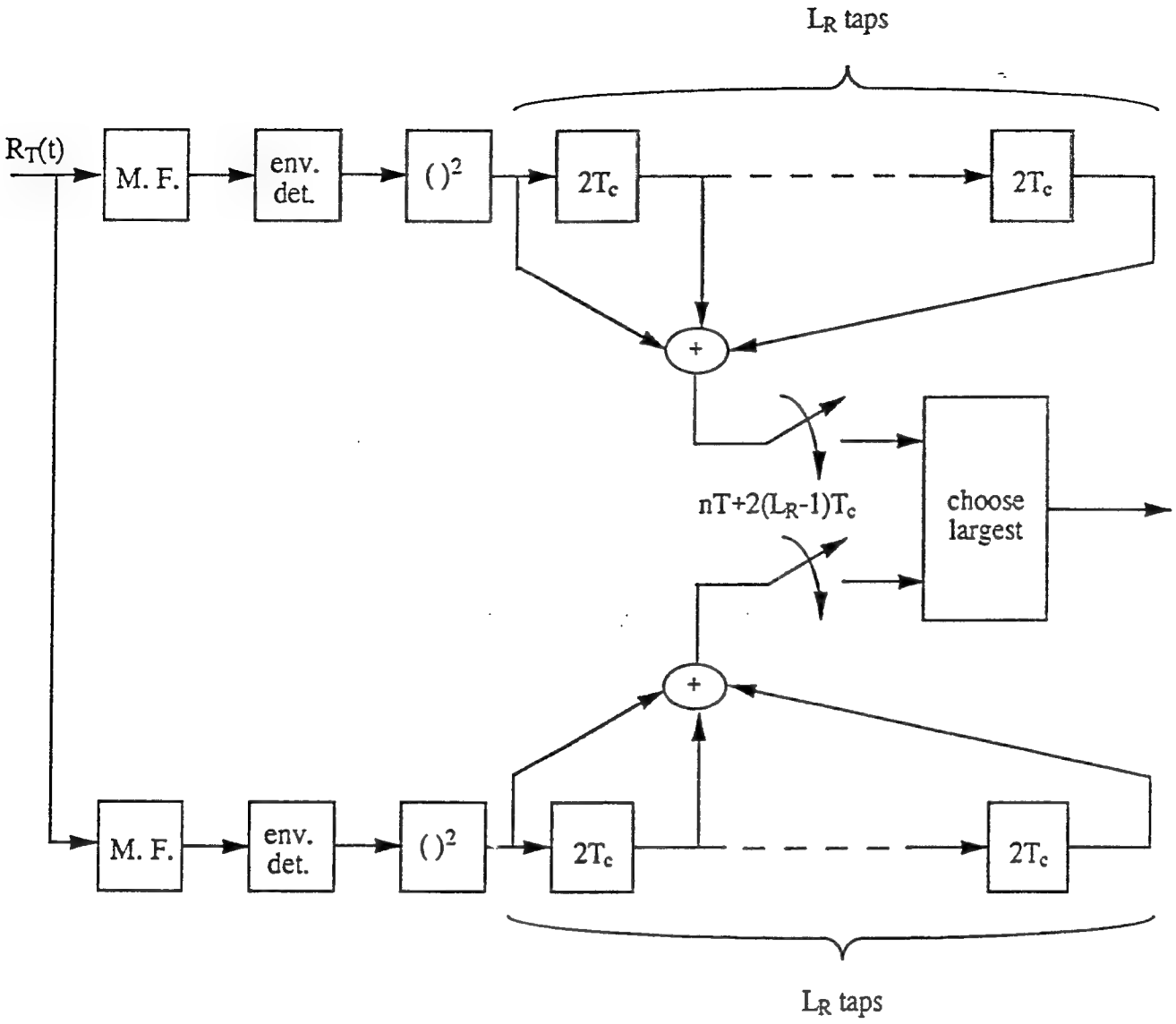

Figure 6. Equal-gain combining square-law receiver.

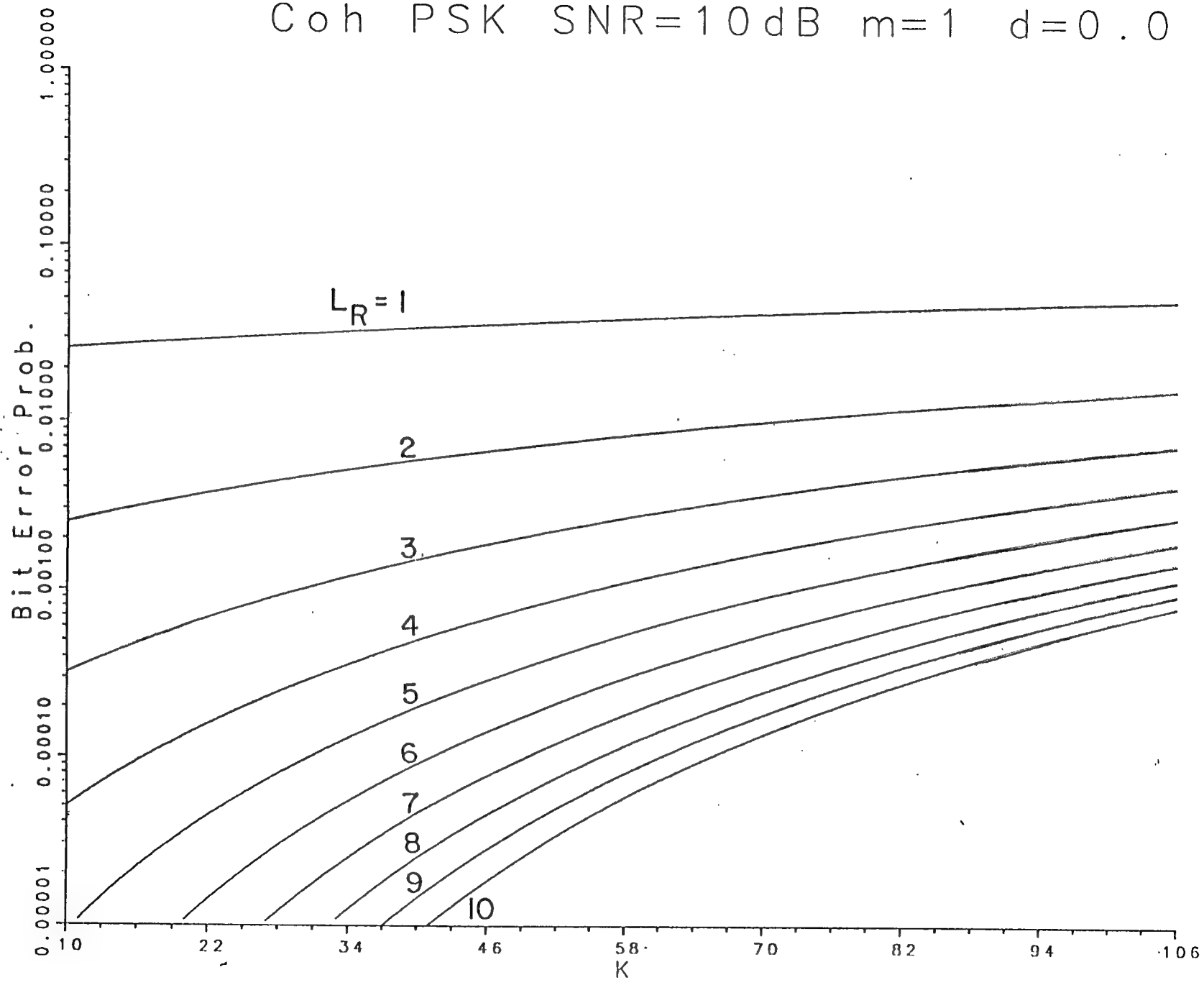
Coh PSK SNR=10dB m=1 d=0.0
Bit Error Prob.
1.00000
0.10000
0.01000
0.00100
0.00010
0.00001
L_R=1
2
3
4
5
6
7
8
9
10
10
22
34
46
58
70
82
94
106
K

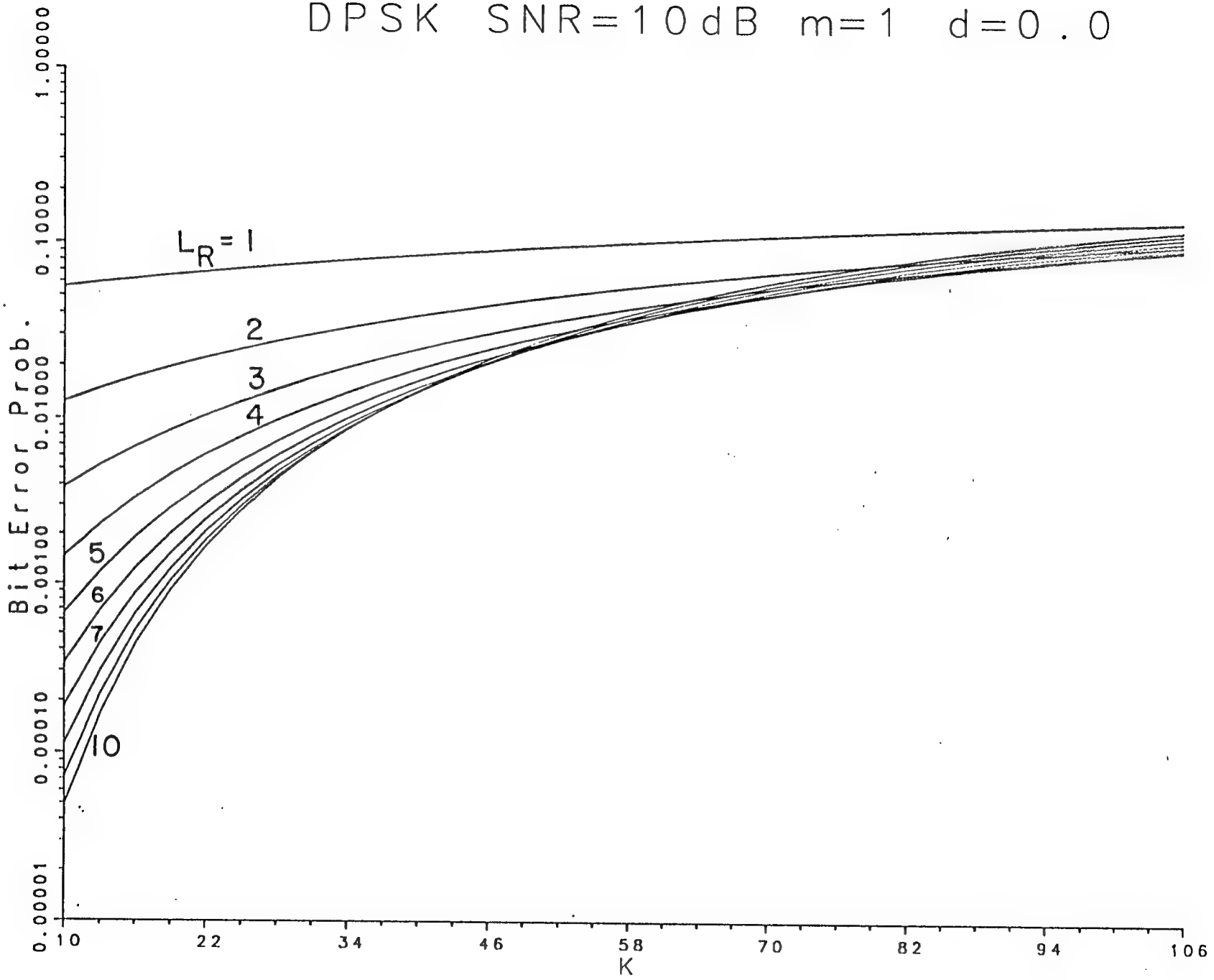
DPSK SNR=10dB m=1 d=0.0
Bit Error Prob.
1.00000
0.10000
0.01000
0.00100
0.00010
0.00001
L_R=1
2
3
4
5
6
7
10
10
22
34
46
58
70
82
94
106
K

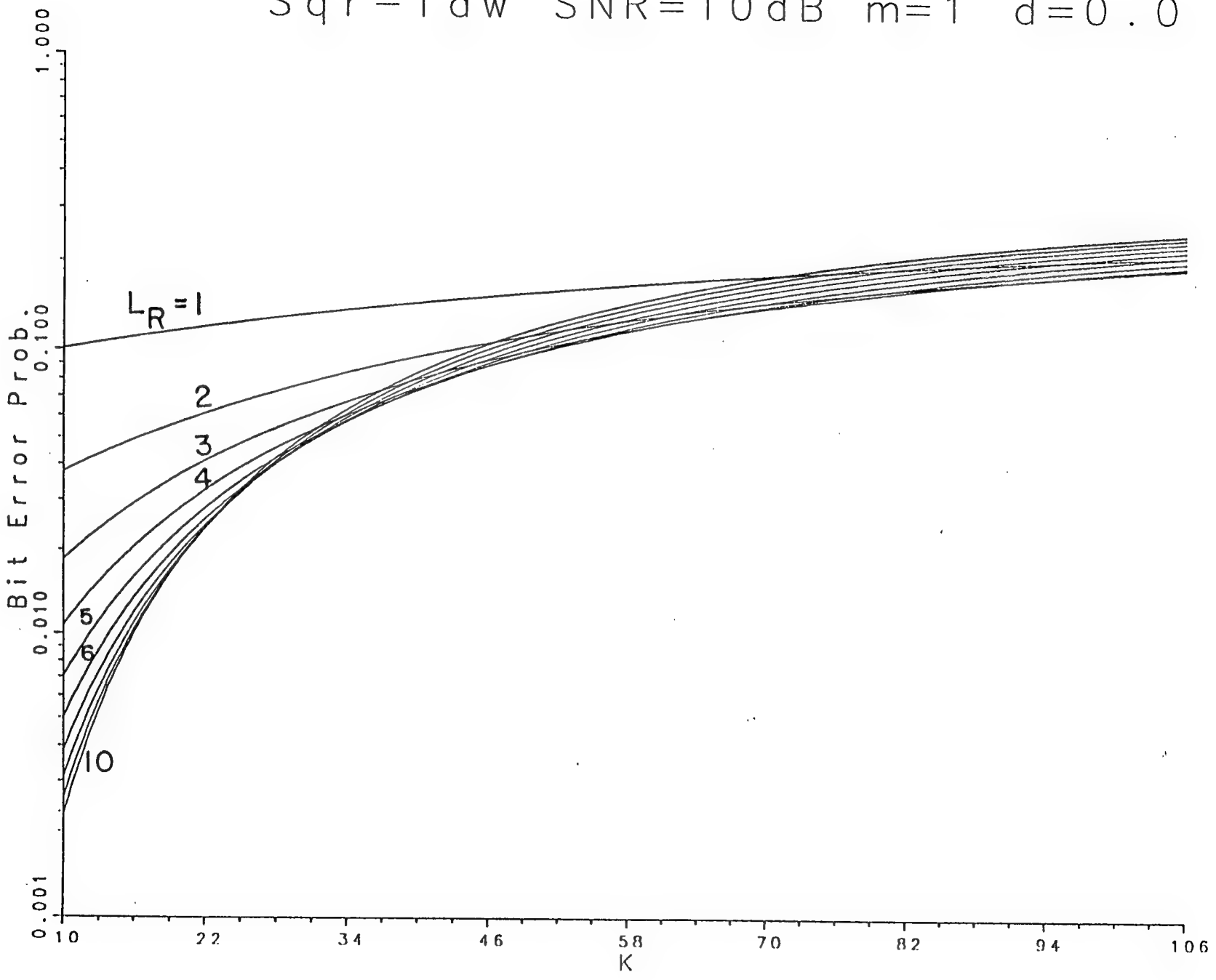
Sqr-law SNR=10dB m=1 d=0.0
Bit Error Prob.
1.000
0.100
0.010
0.001
L_R=1
2
3
4
5
6
10
10
22
34
46
58
70
82
94
106
K

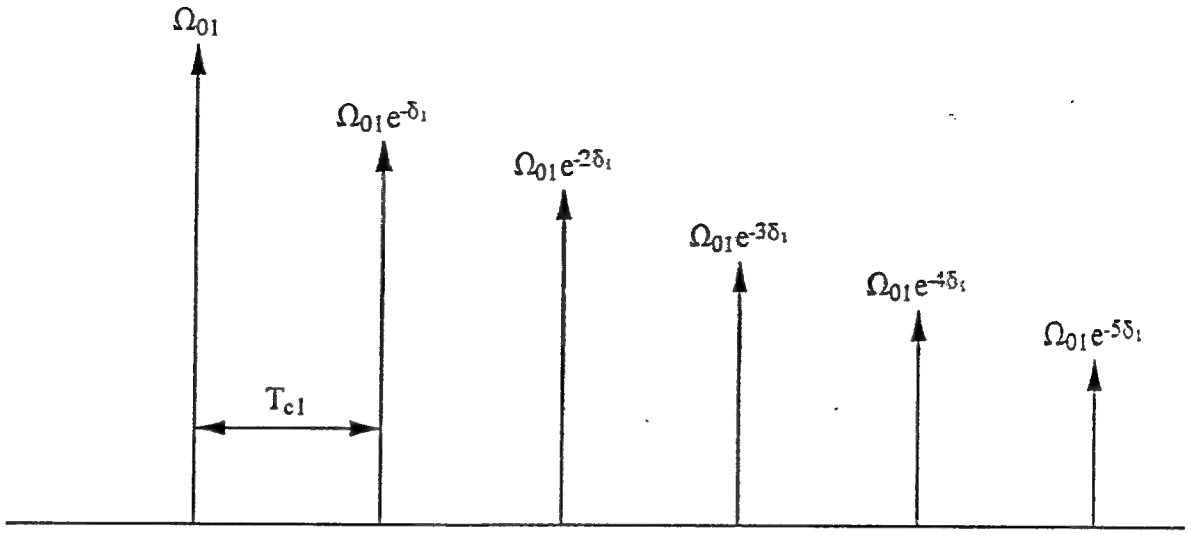

Figure 8. Example of a wideband multipath profile.

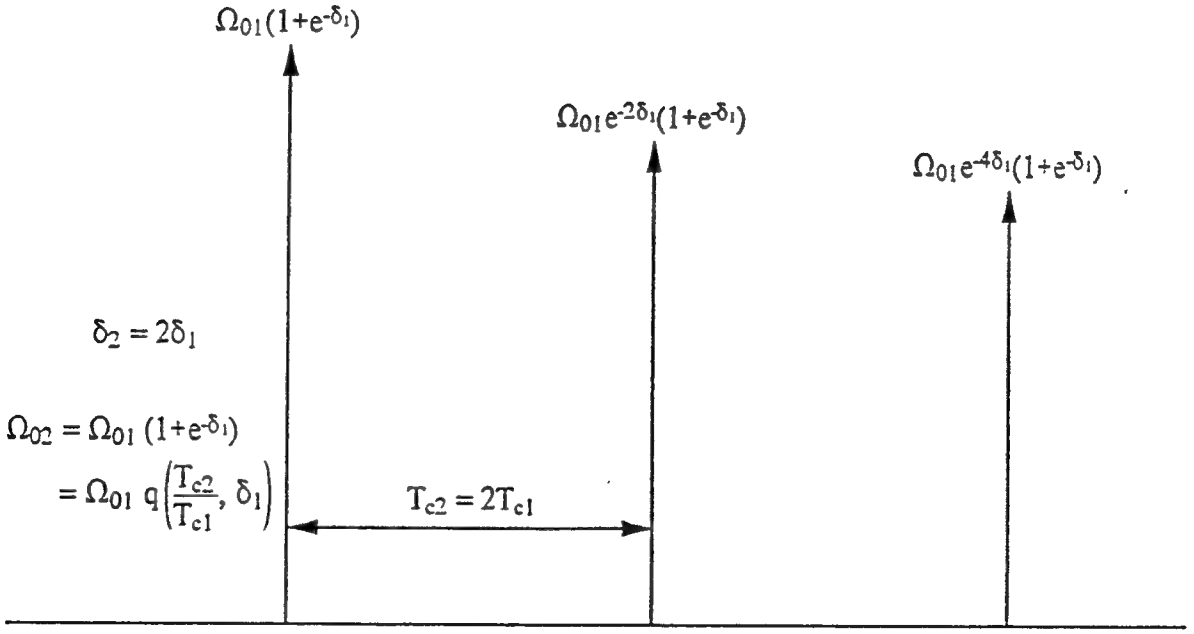

Figure 9. Narrowband multipath profile derived from wideband model of Fig. 8 with L = 2.

	$\frac{E\Omega_0}{\eta_0} = 10dB$				$\frac{E\Omega_0}{\eta_0} = 50dB$			
L	10^{-1}	10^{-2}	10^{-3}	10^{-4}	10^{-1}	10^{-2}	10^{-3}	10^{-4}
1	1758	480	241	145	1770	493	254	158
2	1656	412	182	94	1670	424	196	108
3	1560	348	135	57	1572	360	147	69
4	1464	292	96	28*	1476	304	108	40
6	1290	198	42*	0	1302	210	54*	12*
12	840	48*	0	0	864	60*	0	0

Table I: Capacities of coherent FDMA/CDMA with N = 1023, m =1, $\delta = 0$, and $L_P = 12$.

	$\frac{E\Omega_0}{\eta_0} = 10dB$				$\frac{E\Omega_0}{\eta_0} = 50dB$			
L	10^{-1}	10^{-2}	10^{-3}	10^{-4}	10^{-1}	10^{-2}	10^{-3}	10^{-4}
1	1738	464	226	131	1759	485	247	152
2	1628	390	164	78	1648	410	184	98
3	1521	321	114	39	1542	342	135	60
4	1420	264	72	12*	1444	284	96	36*
6	1236	174	24*	0	1260	192	42*	6*
12	840	36*	0	0	864	60*	0	0

Table II: Capacities of coherent FDMA/CDMA with N = 1023, m =1, $\delta = 0.1$, and $L_P = 12$.

*** Small (segment) capacity values are of questionable accuracy because the central limit theorem is being applied with a relatively small number of terms (i.e., less than ten); however, they do accurately reflect relative SNR.**

L	$\frac{E\Omega_0}{\eta_0} = 10dB$				$\frac{E\Omega_0}{\eta_0} = 50dB$			
	10^{-1}	10^{-2}	10^{-3}	10^{-4}	10^{-1}	10^{-2}	10^{-3}	10^{-4}
1	1758	480	241	145	1770	493	254	158
2	822	199	85	41	835	212	98	54
3	511	107	36	10	524	120	49	23
4	356	63	14	0	369	76	26	10
6	203	22	0	0	216	35	8*	1*
12	57	0	0	0	70	3*	0	0

Table III: Capacities of coherent Wideband CDMA with N=1023, δ=0, L_P=12, and m=1.

L	$\frac{E\Omega_0}{\eta_0} = 10dB$				$\frac{E\Omega_0}{\eta_0} = 50dB$			
	10^{-1}	10^{-2}	10^{-3}	10^{-4}	10^{-1}	10^{-2}	10^{-3}	10^{-4}
1	1738	464	226	131	1759	485	247	152
2	844	194	76	31	865	215	97	51
3	545	105	28	1*	566	126	49	22
4	395	61	6*	0	416	82	27	10
6	244	19	0	0	265	40	9*	1*
12	95	0	0	0	116	7*	0	0

Table IV: Capacities of coherent Wideband CDMA with N=1023, δ=0.1, L_P=12, and m=1.

* Small (segment) capacity values are of questionable accuracy because the central limit theorem is being applied with a relatively small number of terms (i.e., less than ten); however, they do accurately reflect relative SNR.

L	$\frac{E\Omega_0}{\eta_0} = 10dB$				$\frac{E\Omega_0}{\eta_0} = 50dB$			
	10^{-1}	10^{-2}	10^{-3}	10^{-4}	10^{-1}	10^{-2}	10^{-3}	10^{-4}
1	175	70	40	25	182	77	46	31
2	216	74	36	18*	222	80	42	24
3	234	69	27*	9*	240	75	33	15*
4	240	60	20*	4*	248	68	24*	8*
6	240	42*	6*	0	246	48*	12*	0
12	180	0	0	0	180	12*	0	0

Table V: Capacities of DPSK demodulated FDMA/CDMA with N=1023, m=1, δ=0, L_P=24.

L	$\frac{E\Omega_0}{\eta_0} = 10dB$				$\frac{E\Omega_0}{\eta_0} = 50dB$			
	10^{-1}	10^{-2}	10^{-3}	10^{-4}	10^{-1}	10^{-2}	10^{-3}	10^{-4}
1	169	58	26	11	185	74	42	27
2	214	58	18*	2*	230	74	34	18
3	237	51	9*	0	252	66	24*	9*
4	248	44	0	0	264	60	16*	4*
6	258	24*	0	0	276	42*	6*	0
12	276	0	0	0	288	24*	0	0

Table VI: Capacities of DPSK FDMA/CDMA with N=1023, δ=0.1, L_P=24, and m=1.

* Small (segment) capacity values are of questionable accuracy because the central limit theorem is being applied with a relatively small number of terms (i.e., less than ten); however, they do accurately reflect relative SNR.

L	$\frac{E\Omega_0}{\eta_0} = 10dB$				$\frac{E\Omega_0}{\eta_0} = 50dB$			
	10^{-1}	10^{-2}	10^{-3}	10^{-4}	10^{-1}	10^{-2}	10^{-3}	10^{-4}
1	175	70	40	25	182	77	46	31
2	105	34	14	6*	111	40	21	12
3	74	19	5*	0	80	25	11	5*
4	55	10	0	0	62	17	6*	2*
6	34	2*	0	0	41	8*	2*	0
12	9*	0	0	0	15	1*	0	0

Table VII: Capacities of DPSK Wideband CDMA with N=1023, δ=0, L_P=24, and m=1.

L	$\frac{E\Omega_0}{\eta_0} = 10dB$				$\frac{E\Omega_0}{\eta_0} = 50dB$			
	10^{-1}	10^{-2}	10^{-3}	10^{-4}	10^{-1}	10^{-2}	10^{-3}	10^{-4}
1	169	58	26	11	185	74	42	27
2	105	23	2*	0	121	39	18	9*
3	77	9*	0	0	93	25	9*	4*
4	61	1*	0	0	77	17	5*	1*
6	42	0	0	0	58	9*	2*	0
12	24	0	0	0	40	3*	0	0

Table VIII: Capacities of DPSK Wideband CDMA with N=1023, δ=0.1, L_P=24, and m=1.

*** Small (segment) capacity values are of questionable accuracy because the central limit theorem is being applied with a relatively small number of terms (i.e., less than ten); however, they do accurately reflect relative SNR.**

L	$\frac{E\Omega_0}{\eta_0} = 10dB$				$\frac{E\Omega_0}{\eta_0} = 50dB$			
	10^{-1}	10^{-2}	10^{-3}	10^{-4}	10^{-1}	10^{-2}	10^{-3}	10^{-4}
1	84	32	16	9	91	38	23	15
2	104	34	14	6*	110	40	20	12*
3	114	30	9*	0	120	36	15*	6*
4	116	24*	4*	0	124	32*	12*	4*
6	114	18*	0	0	120	24*	6*	0
12	84	0	0	0	84	0	0	0

Table IX: Capacities of square-law detected FDMA/CDMA with N=1023, δ=0, L_P=24, and m=1.

L	$\frac{E\Omega_0}{\eta_0} = 10dB$				$\frac{E\Omega_0}{\eta_0} = 50dB$			
	10^{-1}	10^{-2}	10^{-3}	10^{-4}	10^{-1}	10^{-2}	10^{-3}	10^{-4}
1	76	21	5*	0	92	37	21	13
2	98	20	0	0	114	36	16*	8*
3	108	18*	0	0	126	33	12*	3*
4	116	12*	0	0	132	28	8*	0
6	120	6*	0	0	138	18*	0	0
12	120	0	0	0	144	12*	0	0

Table X: Capacities of square-law detected FDMA/CDMA with N=1023, δ=0.1, L_P=24, and m=1.

* Small (segment) capacity values are of questionable accuracy because the central limit theorem is being applied with a relatively small number of terms (i.e., less than ten); however, they do accurately reflect relative SNR.

L	$\frac{E\Omega_0}{\eta_0} = 10dB$				$\frac{E\Omega_0}{\eta_0} = 50dB$			
	10^{-1}	10^{-2}	10^{-3}	10^{-4}	10^{-1}	10^{-2}	10^{-3}	10^{-4}
1	84	32	16	9*	91	38	23	15
2	49	13	4*	0	55	20	10	6*
3	33	6*	0	0	40	12	5*	2*
4	24	2*	0	0	31	8*	3*	1*
6	14	0	0	0	20	4*	1*	0
12	1*	0	0	0	7	0	0	0

Table XI: Capacities of square-law detected Wideband CDMA with N=1023, δ=0, L_P=24, and m=1.

L	$\frac{E\Omega_0}{\eta_0} = 10dB$				$\frac{E\Omega_0}{\eta_0} = 50dB$			
	10^{-1}	10^{-2}	10^{-3}	10^{-4}	10^{-1}	10^{-2}	10^{-3}	10^{-4}
1	76	21	5*	0	92	37	21	13
2	44	3*	0	0	60	19	9*	4*
3	30	0	0	0	46	12	4*	2*
4	22	0	0	0	38	8*	2*	0
6	13	0	0	0	29	4*	1*	0
12	4*	0	0	0	20	1*	0	0

Table XII: Capacities of square-law detected Wideband CDMA with N=1023, δ=0.1, L_P=24, and m=1.

*** Small (segment) capacity values are of questionable accuracy because the central limit theorem is being applied with a relatively small number of terms (i.e., less than ten); however, they do accurately reflect relative SNR.**

L	δ = 1.6				δ = 10.0			
	10^{-1}	10^{-2}	10^{-3}	10^{-4}	10^{-1}	10^{-2}	10^{-3}	10^{-4}
1	138	13	1*	0	153	12	1*	0
2	194	16*	0	0	202	16*	0	0
3	234	18*	0	0	234	18*	0	0
4	260	20*	0	0	260	20*	0	0
6	300	24*	0	0	300	24*	0	0
12	372	24*	0	0	372	24*	0	0

Table XIII: Capacities of DPSK FDMA/CDMA with N=1023, $E\Omega_0/\eta_0$ = 50 dB, L_P=24, and m=1.

L	δ = 1.6				δ = 10.0			
	10^{-1}	10^{-2}	10^{-3}	10^{-4}	10^{-1}	10^{-2}	10^{-3}	10^{-4}
1	138	13	1*	0	153	12	1*	0
2	162	13	1*	0	202	16	1*	0
3	188	15	1*	0	236	19	1*	0
4	210	17	1*	0	263	21	2*	0
6	242	19	1*	0	304	25	2*	0
12	306	24	2*	0	383	31	3*	0

Table XIV: Capacities of DPSK Wideband CDMA with N=1023, $E\Omega_0/\eta_0$ = 50 dB, L_P=24, and m=1.

* Small (segment) capacity values are of questionable accuracy because the central limit theorem is being applied with a relatively small number of terms (i.e., less than ten); however, they do accurately reflect relative SNR.

The Coarse Acquisition Performance of a CDMA Overlay System

Lynn D. Gottesman and Laurence B. Milstein
Department of Electrical and Computer Engineering
University of California, California
Mail Code 0407
La Jolla, Ca. 92093

Abstract

The coarse acquisition performance of a CDMA overlay system operating in a mobile communications environment is considered. Specifically, a CDMA system, supporting communication between several mobile units and one base station, is overlaid in frequency on an existing narrowband BPSK user. At the CDMA base-station receivers, narrowband interference rejection filters are used to suppress the BPSK interference. It is demonstrated that the presence of the BPSK interference does not severely affect the acquisition performance when the ratio of BPSK to CDMA bandwidth is small. As the ratio becomes larger, the acquisition performance degrades, but nonetheless, the use of the interference rejection filter significantly decreases the time to acquire. We also demonstrate that severe performance degradation results when there is flat Rayleigh fading, both with and without an overlay. When there is a line-of-sight component, of course, performance is much better.

This work was supported in part by the Office of Naval Research under contract ONR N00014-91-J-1234, the Army Research Office under contract ARO DAAL03-91-0071, and the NSF Center for Ultra-High Speed Circuits and Systems (ICAS).

I Introduction

Direct sequence spread spectrum (DS-SS) technology is expected to play a key role in the next generation of digital mobile telephones. Aside from providing multiple accessing capability, DS-SS provides increased privacy, increased multipath suppression, and narrowband interference rejection [1]. In the context of improving the bandwidth efficiency of a multiple access spread spectrum system, we consider the coarse acquisition performance of a so-called CDMA overlay system [2]. In such a system, a set of mobile CDMA users communicate with a base station, while other narrowband users simultaneously transmit in the same frequency band.

The overlay system works because the CDMA power is diffused over a much wider bandwidth than that of the narrowband users. This leaves only a fraction of the CDMA power in any given sub-band occupied by a given narrowband user. If so desired, additional CDMA energy may even be notched out at the CDMA transmitters, without too much degradation to the CDMA system[3]. Correspondingly, the CDMA users may notch out the narrowband interference at their receivers, the idea being that notching a narrow portion from the CDMA spectrum will not critically degrade performance.

A performance analysis of the CDMA overlay system [4] demonstrated its feasibility from the point of view of the bit-error-rate. However, one of the most critical components of any DS-SS system is the code acquisition system. Since, in general, the receiver may know little about the delay or *phase* of the spreading code, the system must acquire this knowledge from the incoming signal. Specifically, the coarse acquisition system determines this phase to within a fraction of a chip duration and a subsequent tracking system finely aligns a locally generated version of the spreading code with the received spreading code. Without initial coarse alignment, tracking cannot be initiated, and hence data demodulation is not possible.

Therefore, in determining the feasibility of a CDMA overlay system, the initial code acquisition performance must be evaluated. Our analysis considers the coarse acquisition performance of the mobile-to-base station link of a CDMA overlay system. In particular, we consider the performance of the base station receivers when one narrowband BPSK user transmits at the CDMA carrier frequency. Both non-fading and flat fading environments are considered.

The remainder of this paper is structured as follows: In Section II we describe the system model and in Section III we evaluate the coarse acquisition performance. In Section IV we provide numerical evaluations of the performance and compare the results to a simulation. Conclusions are then presented in Section V.

II System Description

We consider the coarse acquisition performance of the mobile-to-base station link of a CDMA system, in which there are K_u simultaneous users. At the carrier frequency is one strong narrowband BPSK signal. The CDMA receiver attempts to reject the energy of this waveform with a linear prediction filter, which we describe below. It is assumed that the CDMA signals are relatively narrowband, in the sense that their spread bandwidth is less than the coherence bandwidth of the channel. In particular, we assume that the CDMA channels, including that of the desired user, fade slowly, independently, and in a frequency non-selective manner, according to a Rician distribution. The Rician model enables us to easily consider certain limiting cases such as no fading and Rayleigh fading by appropriately adjusting the parameters of the distribution. We assume power control is employed to compensate for propagation loss from the mobiles to the base station, and for simplicity, we neglect interference from neighboring cells. Exact signal descriptions are given in the next section.

The coarse acquisition portion of the receiver is shown in Figure 1 and is similar to that introduced in [5]. The prefiltering stage consists of a RF-bandpass filter and a linear prediction filter; the latter is illustrated in Figure 2. The linear prediction filter is an N-tap delay line whose tap weights are chosen such that a minimum mean-square error estimate of the current value of its input, based on the last N samples, is subtracted from the actual current value of the input. Since samples of the signal and noise components of the filter's input are approximately uncorrelated from tap to tap, the estimate will be essentially that of the narrowband BPSK interference alone. The subtraction of the estimate from the input thus yields the desired interference suppression. The linear prediction filter has been often proposed for narrowband interference rejection in DS-SS systems [6]-[10]. One reason is that the filter can be easily made adaptive using, say, the well known LMS algorithm, which produces tap weights that are asymptotically unbiased.

Next, after the linear prediction filter is a parallel bank of matched filters, each followed by an envelope detector. There are a total of U_o such branches, where U_o is the length of the uncertainty region. Each matched filter is matched to one particular phase of the desired user's spreading code. In actual systems, the spacing between the matched filter phases is usually a fraction of a chip, typically one half. However, to simplify the mathematics, our model assumes full chip spacing. Note that if L denotes the length of the spreading code, then $U_o \leq L$. We assume the matched filters are partially matched to the distortion caused by the prefiltering stages; that is, they are matched to the distortion to the signal component due to the interference rejection filter, but are not matched to the distortion produced by the front-end bandpass filter. It is demonstrated in [10], in the context of a single user DS-SS system, that this is the most judicious matching strategy. Specifically, it is shown that performance degrades if the matched filters are matched to

just the spreading code, and does not improve much when the matched filters are matched both to the linear prediction filter and the RF-bandpass filter.

The system operates as follows: In the initial search mode, the output of each envelope detector is sampled at time $t=T=MT_c$, where M is the number of chips in the observation interval. The samples are compared, and the phase of the branch with the largest sample is chosen as the "correct" one. Subsequent comparisons of the "correct" matched filter/envelope detector output with some predetermined threshold may further corroborate this choice. The analysis to follow determines an upper bound to the probability of error in the initial search mode.

III Performance Analysis

The receiver of interest (Receiver #1) at the base station receives the sum of four components; the desired signal, multiple-access interference, narrowband BPSK interference, and thermal noise. This can be written as

$$r(t) = s(t) + u(t) + i(t) + n_w(t) . \tag{1}$$

In (1), $s(t)$, the CDMA signal of interest, can be expressed as

$$s(t) = A_1 \sum_{k=-\infty}^{\infty} c^{(1)}_{k+i} \; P_{T_c}(t - kT_c)\cos\omega_o t , \tag{2}$$

where A_1 is a fading amplitude, with a density function described below, the $\{c^{(1)}_k\}$ are the chip values corresponding to the desired user's (user #1) pseudo noise code, and

$$P_a(t) = \begin{cases} 1 & 0 < t \le a \\ 0 & \text{otherwise} \end{cases} . \tag{3}$$

The parameters T_c and ω_o are the chip duration and carrier frequency, respectively. Note that the subscript i in (2) denotes that the i^{th} phase of the spreading code is present, where for convenience of notation, we assume that $0 \le i \le U_o\text{-}1$. We assume the desired user's chip timing is perfectly synchronized and that no data is present. The latter condition corresponds to assuming that a

training period is available to facilitate achieving acquisition. In addition, we assume $\omega_o T_c = 2\pi l$, for some integer l.

The multiple access interference from the interfering K_u-1 CDMA users is given by

$$u(t) = \sum_{\rho=2}^{K_u} A_\rho \sum_{k=-\infty}^{\infty} c^{(\rho)}_k P_{T_c}(t - kT_c - \tau_\rho) \cos(\omega_o t + \phi_\rho) \ . \tag{4}$$

The random amplitudes, $\{A_\rho\}$, including A_1, the amplitude associated with the desired user, are assumed independent and identically distributed. They are governed by the following Rician probability density function:

$$f_{A_\rho}(A_\rho) = \frac{A_\rho}{\sigma^2} exp\left(-\frac{A_\rho^2 + m^2}{2\sigma^2}\right) I_o\left(\frac{mA_\rho}{\sigma^2}\right), \tag{5}$$

where $m^2/2$ is the power in the direct component and $2\sigma^2/2$ is the power in the diffused component. The total power, P_T, is given by $(m^2+2\sigma^2)/2$. When σ^2 is zero, there is no diffused power, corresponding to no fading, and when m is zero, the fading is Rayleigh. The $\{c^{(\rho)}_k\}$, $\rho>1$, are the chip values associated with the ρ^{th} user. They are assumed to be random binary variables, taking on the values of either 1 or -1 with equal probability, and are assumed independent for all ρ and k. The $\{\tau_\rho\}$ are random time delays, uniformly distributed in $[0,T_c]$, and the $\{\phi_\rho\}$ are random carrier phases, uniformly distributed in $[0,2\pi]$. Note that we have not included data in (4) since the $\{c^{(\rho)}_k\}$ are assumed random.

The narrowband BPSK interference can be expressed as

$$i(t) = \alpha \sum_{k=-\infty}^{\infty} d_k P_{T_b}(t - kT_b - \tau_b) \cos(\omega_o t + \phi_b) \ , \tag{6}$$

where α is a deterministic amplitude. (This corresponds to a worst-case situation, since the BPSK signal does not experience fading, but the desired signal does fade.) The $\{d_k\}$ are the data values, and are assumed independent binary random variables, taking on the values 1 and -1 with equal probability. The bit duration is T_b, the variable τ_b is a random time delay, uniformly distributed in $[0,T_b]$, and ϕ_b is a random carrier phase, uniformly distributed in $[0,2\pi]$. Note that for $i(t)$ to be

narrowband, we require $T_b >> T_c$. Finally, we model the thermal noise, $n_w(t)$, as a stationary Gaussian random process with a constant two-sided spectral density $\eta_o/2$.

We next give mathematical descriptions for each block of the acquisition system shown in Figure 1.

The RF-bandpass filter has a rectangular-brickwall characteristic with unity amplitude and bandwidth $2\omega_c$. Hence, its impulse response given by

$$h_{bp}(t) = \frac{2\sin\omega_c t}{\pi t}\cos\omega_o t\,. \tag{7}$$

The linear prediction filter assumes a tap delay line form with the impulse response:

$$h_{lpf}(t) = \delta(t) - \sum_{n=1}^{N} b_n \delta(t - nT_c)\,. \tag{8}$$

Note that by defining a new set of scaler variables $\{a_n\}$, such that a_n=-b_n for $1 \le n \le N$ and a_o=1, the impulse response of the linear prediction filter is equivalently expressed as

$$h_{lpf}(t) = \sum_{n=0}^{N} a_n \delta(t - nT_c)\,. \tag{9}$$

To obtain the tap weights, the Wiener-Hopf equations for linear prediction are solved. They are given by

$$\sum_{n=1}^{N} b_n R((l-n)T_c) = R(lT_c)\,, \qquad l = 1, \ldots, N\,, \tag{10}$$

where is $R(\tau)$ is the autocorrelation function of the output of the RF-BPF (input to the linear prediction filter). If we assume a random form for $s(t)$ and $u(t)$ to be given below, and assume all components of the input are independent, $R(\tau)$ can be expressed

$$R(\tau) = R_{s_1}(\tau) + R_{u_1}(\tau) + R_{i_1}(\tau) + R_{n_1}(\tau)\,, \tag{11}$$

where $R_{s_1}(\tau)$, $R_{u_1}(\tau)$, $R_{i_1}(\tau)$, and $R_{n_1}(\tau)$, are the autocorrelation functions of the desired signal, the multiple access interference, the narrowband BPSK interference, and the thermal noise, respectively, at the output of the RF bandpass filter.

As indicated in the previous section, for the purpose of performance analysis, we model the spreading sequence of user #1 as being deterministic (e.g., a PN sequence), but model the spreading sequences of the other users as being random. However, for the purpose of deriving the tap coefficients of the rejection filter, we model each of the K_u spreading waveforms (i.e., including that of user #1) by an independent random binary process, $c_\rho(t)$, with autocorrelation function

$$R_c(\tau) = \begin{cases} A^2\left(1 - \dfrac{|\tau|}{T_c}\right) & |\tau| \le T_c \\ 0 & \text{otherwise} \end{cases} . \tag{12}$$

Then, we can model the sum of the desired user and multiple access components as the stationary random process

$$s(t) + u(t) = \sum_{\rho=1}^{K_u} A_\rho c_\rho(t) \cos(\omega_o t + \phi_\rho) , \tag{13}$$

where the ϕ_ρ are independent random phases uniformly distributed between 0 and 2π. With the power control assumption, $E[A_\rho^2]$ is the same for all ρ, and equals $2P_T$. The autocorrelation function of the output of the RF-BPF due to the signal plus multiple access interference is straightforwardly determined to be

$$R_{s_1}(\tau) + R_{u_1}(\tau) = \frac{P_T K_u}{\pi \omega_c T_c} \tag{14}$$

$$\cdot \Big(\omega_c(\tau + T_c)\, Si(\omega_c(\tau + T_c)) - 2\omega_c \tau\, Si(\omega_c \tau) + \omega_c(\tau - T_c)\, Si(\omega_c(\tau - T_c)) \Big)$$

$$+ \cos(\omega_c(\tau + T_c)) - 2\cos\omega_c \tau + \cos(\omega_c(\tau - T_c)) \Big) \cos\omega_o \tau \ ,$$

where $Si(x)$ is the sine integral, given by

$$Si(x) = \int_0^x \frac{\sin y}{y} dy. \tag{15}$$

The baseband portion of the BPSK signal given in (6) is also modelled as a random binary process. The autocorrelation function of this random binary process is

$$R_b(\tau) = \begin{cases} \alpha^2 (1 - \frac{|\tau|}{T_b}) & |\tau| \le T_b \\ 0 & \text{otherwise} \end{cases} \tag{16}$$

Then, in a similar fashion, the autocorrelation function of the output of the RF-BPF due to this BPSK signal is

$$R_{i_1}(\tau) = \frac{\alpha^2}{2\pi\omega_c T_b} \tag{17}$$

$$\cdot \Big(\omega_c(\tau + T_b)\, Si(\omega_c(\tau + T_b)) - 2\omega_c \tau\, Si(\omega_c \tau) + \omega_c(\tau - T_b)\, Si(\omega_c(\tau - T_b))$$

$$+ \cos(\omega_c(\tau + T_b)) - 2\cos\omega_c\tau + \cos(\omega_c(\tau - T_b)) \Big) \cos\omega_o\tau .$$

Finally, autocorrelation of the thermal noise component is

$$R_{n_1}(\tau) = \frac{\eta_o \sin\omega_c\tau}{\pi\tau} \cos\omega_o\tau . \tag{18}$$

Inserting the above autocorrelation functions into (10) and solving for the $\{a_n\}$ yields the desired set of filter tap weights. Using the definitions $E=P_T M T_c$ and $J/S=\alpha^2/2P_T$, and assuming $\omega_c T_c=2\pi$, the explicit form of the Wiener-Hopf equations for the CDMA overlay system is

$$\sum_{n=1}^{N} b_n \{K_u [\,(l-n+1)\,Si\,(2\pi\,(l-n+1)) - 2\,(l-n)\,Si2\pi\,(l-n) \tag{19}$$

$$+\,(l-n-1)\,Si\,(2\pi\,(l-n-1))\,] + \frac{J}{S}\frac{T_c}{T_b}\left[\left(l-n+\frac{T_b}{T_c}\right)Si\left(2\pi\left(l-n+\frac{T_b}{T_c}\right)\right)\right.$$

$$\left.-2\,(l-n)\,Si\,(2\pi\,(l-n)) + \left(l-n-\frac{T_b}{T_c}\right)Si\left(2\pi\left(l-n-\frac{T_b}{T_c}\right)\right)\right]\} + 2\pi b_l M\left(\frac{E}{\eta_0}\right)^{-1}$$

$$= K_u [\,(l+1)\,Si\,(2\pi\,(l+1)) - 2lSi\,(2\pi l) + (l-n-1)\,Si\,(2\pi\,(l-n-1))\,]$$

$$+\frac{J}{S}\frac{T_c}{T_b}\left[\left(l+\frac{T_b}{T_c}\right)Si\left(2\pi\left(l+\frac{T_b}{T_c}\right)\right) - 2lSi\,(2\pi l) + \left(l-\frac{T_b}{T_c}\right)Si\left(2\pi\left(l-\frac{T_b}{T_c}\right)\right)\right]$$

$$l = 1, \ldots, N.$$

Next we consider the form of the matched filters. Assuming the matched filters are matched to both the spreading sequence of the desired user (#1) and the distortion due to the interference suppression filter, as described above, the impulse response of the j^{th} matched filter is

$$h_{mf}(t) = \sum_{l=0}^{N} a_l \sum_{m=0}^{M-1} c^{(1)}_{m-l+j}\; P_{T_c}(T-t-mT_c)\cos\,(\omega_o t+\psi)\;, \tag{20}$$

where M is the number of chips contained in the observation interval.

As described above, the set of outputs of Figure 1 are compared to determine the "correct" phase. The set can be denoted as $\{r(i,j)\}$, where $j \in [0, U_o\text{-}1]$. Specifically, $r(i,j)$ is the output of the j^{th} branch when the i^{th} phase of the spreading code is present at the input. It is derived by computing the output of the j^{th} matched filter due to each component in (1), then taking the envelope. The result is

$$r\,(i,j) = \{\,[S_c\,(i,j) + U_c\,(j) + I_c\,(j) + N_c\,(j)\,]^2 \tag{21}$$

$$+\,[U_s\,(j) + I_s\,(j) + N_s\,(j)\,]^2\,\}^{1/2},$$

where

$$S_c(i,j) = \frac{A_1}{2\pi} \sum_{n=0}^{N} a_n \sum_{k=-\infty}^{\infty} c^{(1)}{}_{k-n+i} \sum_{l=0}^{N} a_l \sum_{m=0}^{M-1} c^{(1)}{}_{m-l+j} \tag{22}$$

$$\cdot \{K_m(\omega_c, k) - K_m(\omega_c, k+1)\} ,$$

$$\begin{pmatrix} U_c(j) \\ U_s(j) \end{pmatrix} = \frac{1}{2\pi} \sum_{\rho=2}^{K_*} A_\rho \begin{pmatrix} \cos\phi_\rho \\ \sin\phi_\rho \end{pmatrix} \sum_{n=0}^{N} a_n \sum_{k=-\infty}^{\infty} c^{(\rho)}{}_{k-n} \sum_{l=0}^{N} a_l \sum_{m=0}^{M-1} c^{(1)}{}_{m-l+j} \tag{23}$$

$$\cdot \{K_m(\omega_c, k+\tau_\rho) - K_m(\omega_c, k+1+\tau_\rho)\} ,$$

$$\begin{pmatrix} I_c(j) \\ I_s(j) \end{pmatrix} = \begin{pmatrix} \cos\phi_b \\ \sin\phi_b \end{pmatrix} \frac{\alpha}{2\pi} \sum_{k=-\infty}^{\infty} d_k \sum_{n=0}^{N} a_n \sum_{l=0}^{N} a_l \sum_{m=0}^{M-1} c^{(1)}{}_{m-l+j} \tag{24}$$

$$\cdot \left\{K_m\left(\omega_c, (k+\tau_b)\frac{T_b}{T_c}+n\right) - K_m\left(\omega_c, (k+\tau_b+1)\frac{T_b}{T_c}+n\right)\right\} ,$$

and

$$\begin{pmatrix} N_c(j) \\ N_s(j) \end{pmatrix} = \tag{25}$$

$$\frac{1}{\pi} \sum_{n=0}^{N} a_n \sum_{l=0}^{N} a_l \sum_{m=0}^{M-1} c^{(1)}{}_{m-l+j} \int_{-\infty}^{\infty} n(\tau) \begin{pmatrix} \cos\omega_o\tau \\ -\sin\omega_o\tau \end{pmatrix} I(\tau, \omega_c, m-n) d\tau .$$

In (22)-(25), $K_m(\omega k)$ and $I(t,\omega l)$ are defined by

$$K_m(\omega, k) \triangleq \tag{26}$$

$$\frac{1}{\omega} [\omega T_c(m-k+1) Si(\omega T_c(m-k+1)) - \omega T_c(m-k) Si(\omega T_c(m-k))$$

$$+ \cos(\omega T_c(m-k+1)) - \cos(\omega T_c(m-k))]$$

and

$$I(t,\omega,l) \triangleq Si(\omega(t-lT_c)) - Si(\omega(t-(l-1)T_c)), \tag{27}$$

respectively.

To determine the statistics of $r(i,j)$, consider each component of (21). Aside from the fading amplitude, A_1, the desired signal component, $S_c(i,j)$, is deterministic. To determine a suitable model for the terms $U_c(j)$ and $U_s(j)$, we rewrite (23) as

$$\begin{pmatrix} U_c(j) \\ U_s(j) \end{pmatrix} = \sum_{\rho=2}^{K_u} A_\rho \begin{pmatrix} \cos\phi_\rho \\ \sin\phi_\rho \end{pmatrix} g_\rho, \tag{28}$$

where,

$$g_\rho = \frac{1}{2\pi} \sum_{n=0}^{N} a_n \sum_{k=-\infty}^{\infty} c^{(\rho)}{}_{k-n} \sum_{l=0}^{N} a_l \sum_{m=0}^{M-1} c^{(1)}{}_{m-l+j} \cdot \{K_m(\omega_c, k+\tau_\rho) - K_m(\omega_c, k+1+\tau_\rho)\}. \tag{29}$$

Recall that we have modelled the $\{c^{(1)}{}_k\}$ deterministically, and thus for $\rho \in [2,K_u]$, the $\{c^{(\rho)}{}_k\}$ and τ_ρ are the only random components of g_ρ. Additionally, these random component are statistically independent for different ρ. Therefore the $\{g_\rho\}$'s are independent and identically distributed, and it is clear from (28) that $U_c(j)$ and $U_s(j)$ are sums of the independent and identically distributed random variables $A_\rho \cos\phi_\rho g_\rho$ and $A_\rho \sin\phi_\rho g_\rho$, respectively. Then, by the Central Limit Theorem [11], the terms $U_c(j)$ and $U_s(j)$ are asymptotically Gaussian for a large number of CDMA users, K_u. In addition, is straightforward to verify from (28) that $U_c(j)$ and $U_s(j)$ are zero mean, have equal variances and are uncorrelated.

The remaining terms are $I_c(j)$, $I_s(j)$, $N_c(j)$, and $N_s(j)$. The narrowband interference components $I_c(j)$ and $I_s(j)$ can be taken as deterministic by conditioning on τ_b, ϕ_b, and the data values $\{d_k\}$, and $N_c(j)$ and $N_s(j)$ are Gaussian, as they result from linear operations on a Gaussian process. Imposing the aforementioned conditioning, and assuming the Gaussian model for $U_c(j)$ and $U_s(j)$, the quadrature components $S_c(i,j) + U_c(j) + I_c(j) + N_c(j)$ and $U_s(j) + I_s(j) + N_s(j)$ of (21) are also Gaussian. It is readily verified that these components have equal variances, are uncorrelated, and because of the Gaussian assumption, we take them to be independent. Therefore, we can take $r(i,j)$'s to be Rician random variables. Note that the random

variables $r(i,j)$, $j \in [0, U_o\text{-}1]$ are, in general, correlated, as they result from operations on the same segment of the input waveform.

The probability of error in the initial search mode is the probability that any output due to an incorrect phase exceeds the output due to the correct phase. This is given by

$$P_e = Pr\left(\bigcup_{\substack{j=0 \\ j \neq i}}^{U_o - 1} (r(i,j) \geq r(i,i)) \right). \tag{30}$$

We can upper bound this expression using the union bound, obtaining

$$P_e \leq \sum_{\substack{j=0 \\ j \neq i}}^{U_o - 1} Pr(r(i,j) \geq r(i,i)) , \tag{31}$$

and to evaluate this expression, we consider

$$Pr(r(i,j) \geq r(i,i)) , \tag{32}$$

where, as mentioned above, $r(i,j)$ and $r(i,i)$ are correlated Rician random variables. We use the transformation given by Stein, [12], to determine (32), which yields

$$Pr(r(i,j) \geq r(i,i)) = \frac{1}{2}\left[1 - Q(\sqrt{b_{ij}}, \sqrt{a_{ij}}) + Q(\sqrt{a_{ij}}, \sqrt{b_{ij}})\right] - \frac{A_{ij}}{2} e^{-\frac{(a_{ij} + b_{ij})}{2}} I_o(\sqrt{a_{ij} b_{ij}}), \tag{33}$$

where $Q(\alpha,\beta)$ is Marcum's Q function, given by

$$Q(\alpha, \beta) = \int_{\beta}^{\infty} x e^{-\frac{\alpha^2 + x^2}{2}} I_o(\alpha x) dx , \tag{34}$$

and $I_o(x)$ is the zeroth order modified Bessel function of the first kind, given by

$$I_o(x) = \frac{1}{2\pi}\int_0^{2\pi} e^{x\cos\theta}d\theta\,. \tag{35}$$

The parameters a_{ij}, b_{ij}, and A_{ij} are simple functions of the first and second order moments of the quadrature components of the transformed random variables and can be expressed in terms of the first and second order moments of the quadrature components of $r(i,j)$ and $r(i,i)$. They are

$$\begin{pmatrix} a_{ij} \\ b_{ij} \end{pmatrix} = \tag{36}$$

$$\frac{1}{2}\Bigg[\frac{(\tilde{U}_{ii}+\tilde{N}_{ii}+\tilde{U}_{jj}+\tilde{N}_{jj})\,((S_c(i,i)+I_c(i))^2+I_s(i)^2)}{(\tilde{U}_{ii}+\tilde{N}_{ii}+\tilde{U}_{jj}+\tilde{N}_{jj})^2-4(\tilde{U}_{ij}+\tilde{N}_{ij})^2}$$

$$+\frac{(\tilde{U}_{ii}+\tilde{N}_{ii}+\tilde{U}_{jj}+\tilde{N}_{jj})\,((S_c(i,j)+I_c(j))^2+I_s(j)^2)}{(\tilde{U}_{ii}+\tilde{N}_{ii}+\tilde{U}_{jj}+\tilde{N}_{jj})^2-4(\tilde{U}_{ij}+\tilde{N}_{ij})^2}$$

$$-\frac{4(\tilde{U}_{ij}+\tilde{N}_{ij})\,(S_c(i,i)+I_c(i))\,(S_c(i,j)+I_c(j))}{(\tilde{U}_{ii}+\tilde{N}_{ii}+\tilde{U}_{jj}+\tilde{N}_{jj})^2-4(\tilde{U}_{ij}+\tilde{N}_{ij})^2}$$

$$-\frac{4(\tilde{U}_{ij}+\tilde{N}_{ij})\,I_s(i)\,I_s(j)}{(\tilde{U}_{ii}+\tilde{N}_{ii}+\tilde{U}_{jj}+\tilde{N}_{jj})^2-4(\tilde{U}_{ij}+\tilde{N}_{ij})^2}$$

$$\mp\frac{(S_c(i,i)+I_c(i))^2+I_s(i)^2}{\left[(\tilde{U}_{ii}+\tilde{N}_{ii}+\tilde{U}_{jj}+\tilde{N}_{jj})^2-4(\tilde{U}_{ij}+\tilde{N}_{ij})^2\right]^{1/2}}$$

$$\pm\frac{(S_c(i,j)+I_c(j))^2+I_s(j)^2}{\left[(\tilde{U}_{ii}+\tilde{N}_{ii}+\tilde{U}_{jj}+\tilde{N}_{jj})^2-4(\tilde{U}_{ij}+\tilde{N}_{ij})^2\right]^{1/2}}\Bigg]$$

and

$$A_{ij} = \frac{(\tilde{U}_{ii} + \tilde{N}_{ii}) - (\tilde{U}_{jj} + \tilde{N}_{jj})}{\left[(\tilde{U}_{ii} + \tilde{N}_{ii} + \tilde{U}_{jj} + \tilde{N}_{jj})^2 - 4(\tilde{U}_{ij} + \tilde{N}_{ij})^2 \right]^{1/2}}, \tag{37}$$

and are given in terms of the following second moments:

$$\tilde{U}_{uv} = E[U_c(u)\,U_c(v)] = E[U_s(u)\,U_s(v)] = \tag{38}$$

$$\frac{P_T}{4\pi^2} \sum_{\rho=2}^{K_u} \sum_{k=-\infty}^{\infty} \sum_{n_1=0}^{N} a_{n_1} \sum_{n_2=0}^{N} a_{n_2} \sum_{m_1=0}^{M-1} c^{(1)}_{m_1-n_1+u} \sum_{m_2=0}^{M-1} c^{(1)}_{m_2-n_2+v} \sum_{l_1=0}^{N} a_{l_1} \sum_{l_2=0}^{N} a_{l_2}$$

$$\cdot E[\{K_{m_1}(\omega_c, k+n_1+\tau_\rho) - K_{m_1}(\omega_c, k+n_1+\tau_\rho+1)\}$$

$$\cdot \{K_{m_2}(\omega_c, k+n_2+\tau_\rho) - K_{m_2}(\omega_c, k+n_2+\tau_\rho+1)\}\,]$$

and

$$\tilde{N}_{uv} = E[N_c(u)\,N_c(v)] = E[N_s(u)\,N_s(v)] = \tag{39}$$

$$\frac{\eta_o}{4\pi} \sum_{n_1=0}^{N} a_{n_1} \sum_{n_2=0}^{N} a_{n_2} \sum_{l_1=0}^{N} a_{l_1} \sum_{m_1=0}^{M-1} c^{(1)}_{m_1-l_1+u} \sum_{l_2=0}^{N} a_{l_2} \sum_{m_2=0}^{M-1} c^{(1)}_{m_2-l_2+v}$$

$$\cdot \{K_{m_1-n_1}(\omega_c, m_2-n_2) - K_{m_1-n_1}(\omega_c, m_2-n_2+1)\}\ .$$

Note that in order to numerically evaluate (22) and (38), the summations in k must be truncated. Note also that the probabilities derived in this section are conditional and must be numerically averaged over the random variables A_1, $\{d_k\}$, τ_b, and ϕ_b.

IV Numerical Results and Discussion

We now evaluate the acquisition performance of the CDMA overlay system. First, we assess the validity of our Gaussian assumption for various numbers of CDMA users in the absence of any overlay. For this, we provide simulation results for which either random binary sequences or actual PN codes are used to model the spreading codes of the K_u-1 interfering users. After verifying the Gaussian assumption for a given number of users, we examine the analytical

acquisition performance when the overlay is introduced. The performance is determined when either a linear prediction filter or an infinite notch filter, also implemented by a tapped delay line, is used to reject the BPSK interference. Finally, we determine the performance of the overlay system under the condition of either Rayleigh or Rician fading.

In the following figures, we choose both the length of the spreading sequence and the length of the observation interval to be 127 chips, and the length of the uncertainty region to be 7. The size of the uncertainty region was chosen to be relatively small to decrease otherwise long run times of the program used to evaluate the analytical probabilities and the simulation. Also, ω_c, the half bandwidth of the RF bandpass filter, is set equal to the chip rate, $2\pi/T_c$.

Figure 3 compares analytical and simulation results when there is no overlay and no fading. The analytical upper bound to the probability of error (31) is compared to a simulation of the upper bound. For the purpose of verifying the Gaussian assumption, the simulation uses random binary sequences to model the spreading codes of the interfering CDMA users. From the figure, for a single user system the analytical and simulation results match closely. This is to be expected because there no CDMA interference, and hence no Gaussian assumption. For a seven user system, the Gaussian assumption is only valid at high error rates. As the number of users increases to 11 and 15, however, we observe considerably more agreement between the analytical and simulation results over a wide range of error rates.

Consider now the actual performance levels. Figure 3 predicts relatively poor performance when the number of CDMA users is larger than 11 and in Figure 4, we demonstrate that these levels are not due to looseness of the upper bound. The figure compares the simulated upper bound to the simulated probability of error for 1,3,7,11, and 15 users. Note that for all values of E/η_0, the upper bound closely approximates the true performance. Another possibility is that by using random binary sequences to model the PN codes of the interfering users, the power of the CDMA interference is over-estimated. In an attempt to minimize the cross-correlation interference, we replaced the random binary sequences with actual PN codes corresponding to m-sequences. We found by simulation, however, that the performance is about the same when either random binary sequences or m-sequences are used.

Performance improvement can, of course, be improved at the expense of a longer observation interval. This is demonstrated in Figure 5 for a system of 15 users. In this figure, the actual probability of error (obtained via simulation) is plotted for observation intervals of either 127, 254, or 381 chips. The figure shows that the performance improves quite dramatically as the length of the observation interval is doubled, then tripled.

Having demonstrated the validity of the Gaussian assumption for a large enough number of users, we now use our analytical expressions to demonstrate the performance of the overlay system. Using a 12 user CDMA system with a processing gain of 127, we introduce strong BPSK

interference to the input and insert the linear prediction filter. With the understanding that a longer observation interval will yield better performance, we use an interval of 127 chips to decrease the numerical load. (A larger observation interval necessitates averaging over more BPSK bits, and the number of possible bit patterns increases by a factor of 2 with each additional bit.) The uncertainty region spans 7 phases and we initially assume that there is no fading. In Figure 6, we display the performance of the overlay system when an 8 tap linear prediction filter is used. As a reference, we show in a dashed line the performance of the CDMA system when there is no overlay and no interference rejection filter. We define the BPSK bandwidth relative to the bandwidth of the CDMA system. In particular, we consider .1%, .5%, 1%, and 5% BPSK bandwidths.

At small interference bandwidths, the presence of the BPSK interference does not significantly degrade the acquisition performance. Note the performance for very small bandwidth interference (.1%) is indeed very close to the "no overlay" case. There is, however, substantial performance degradation when the bandwidth of the interference increases to, say, 5%. This is partially because the linear prediction filter is less able to estimate the wider bandwidth BPSK signal and partially because of the distortion to the desired signal due to the filter's wider notch.

To emphasize the utility of the interference rejection filter, we present in Figure 7 the performance of the overlay system when there is no interference rejection filter. We begin with an observation length of $127T_c$ (M=127), and increase it until the performance is comparable to the performance with the interference rejection filter. All curves are upper bounds and the bandwidth of the interference is taken to be 5% of the spreading bandwidth. The figure demonstrates that without a filter, the observation length has to be about 5 times longer to attain the same performance level as when the filter is used. We note that the curves corresponding to larger observation lengths were generated by simulation, again because larger observation lengths increase the number of possible BPSK bit patterns, making averaging the analytical probabilities a difficult task. The curve corresponding to the case the linear prediction filter system with M=127 was generated through our analytical expressions, and is taken from Figure 6.

In Figure 8, we demonstrate the sensitivity of the overlay performance when J/S is varied. We also demonstrate the effect of changing the number of taps between 4 and 8. The figure shows that the acquisition performance is quite dependent on J/S at all interference bandwidths, however, more so when the interference bandwidth is larger. This is again due to the inability of the linear prediction filter to predict wider bandwidth processes. We note that for small BPSK bandwidths, the performance improves somewhat when an 8 tap filter is used instead of a 4 tap filter.

Having demonstrated the performance of the overlay system for the ideal case of no fading, we now demonstrate how the system behaves when the channel is fading. In Figure 9, we plot the performance versus the ratio of direct-to-diffused power of the Rician distribution. From the Rician density function given in (5), this ratio, which we denote P_s/P_d, is $m^2/2\sigma^2$. When P_s/P_d is zero, there is Rayleigh fading, and when P_s/P_d is infinity, there is no fading. We show the performance either when there is no overlay or when the 1% BPSK interference is present. The flat lines under each curve demonstrate the performance when there is no fading. First consider flat Rayleigh fading, which is often the worst case. The figure demonstrates that even before the overlay is introduced, flat Rayleigh fading has an extremely adverse affect on the system performance. The performance improves quite appreciably, however, when P_s/P_d increases and note that the slopes are large at small P_s/P_d. This indicates that a small increase in this ratio will produce a large improvement in performance.

V Conclusion

In this paper, we have modelled and evaluated the coarse acquisition performance of a CDMA overlay system. In the absence of an overlay, we verified the validity of the Gaussian assumption for a given number of CDMA users. We next computed the performance when BPSK interference is added to the system along with a linear prediction filter for narrowband interference suppression. When the bandwidth of the BPSK interference is small, there is only a small amount of performance degradation with the addition of the overlay. When the bandwidth is larger, the performance can be much worse for the same *J/S*. Our most significant conclusion, however, is that the use of the suppression filter results in a large decrease in acquisition time relative to a system operating in the absence of the interference rejection filter.

We also determined that the overlay performance is very dependent on the BPSK power, even when the BPSK bandwidth is small. This behavior implies that a considerable amount of BPSK power is passed by the linear prediction filter to the matched filtering stages. One possibility is that the linear prediction filter does not provide a deep enough notch. To test this theory, in Figure 10 we show the performance when, instead of a linear prediction filter, an infinitely deep notch is implemented by the transversal filter. The performance is shown for a variety of interference bandwidths for a 4 tap notch filter. This figure indicates, however, that the system performs better when the linear prediction filter is used rather than an infinite notch. Performance was worse when an 8 tap infinite notch filter was used. Therefore, the more likely scenario is that the filter is not implementing a wide enough notch, and thus, it may be that an interference rejection filter designed under a strategy other than linear prediction may improve the

performance, especially when J/S is large. As an example, a filter whose notch width is chosen to optimize performance, such as a transform domain rectangular notch filter [5], may be of interest.

Finally, we found that in a Rayleigh fading channel, the acquisition performance degrades drastically, even in the absence of an overlay. When there is a direct component, however, performance can improve considerably, depending on its power. As is the case in most fading channels, diversity will improve the performance, although we did not attempt to quantify the extent of this improvement.

VI Figures

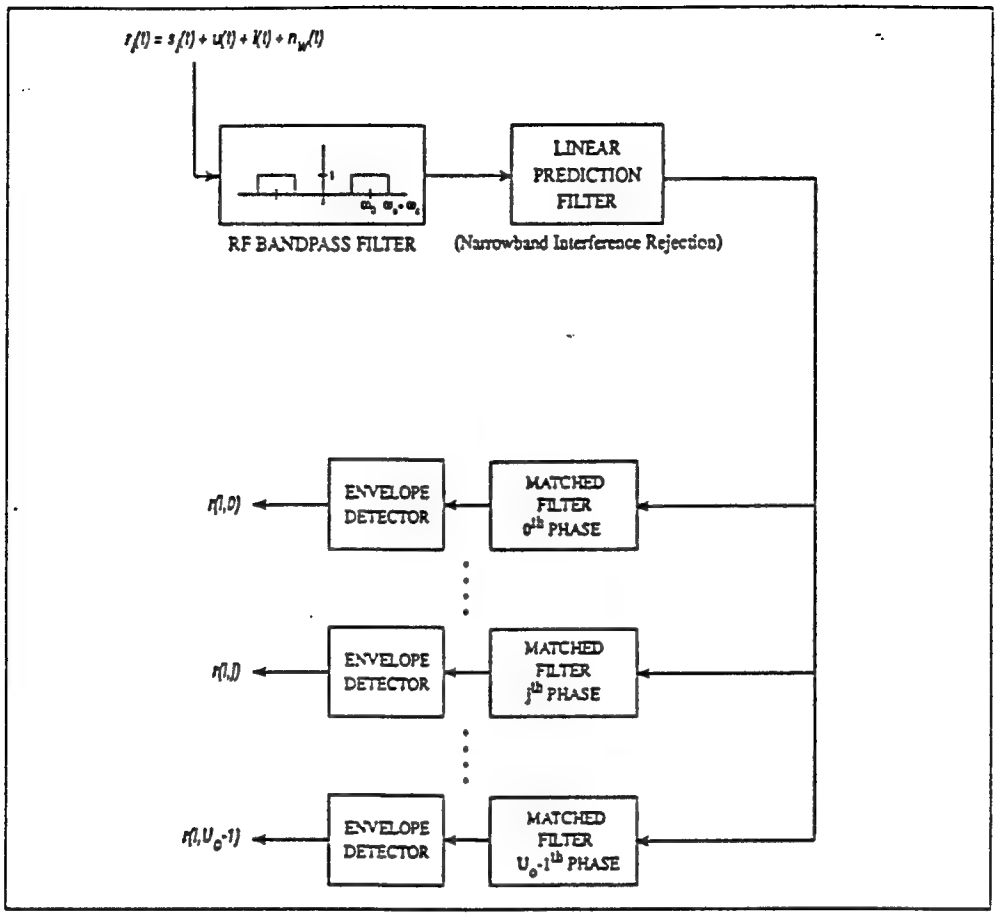

Figure 1 : Parallel Coarse Acquisition System Block Diagram

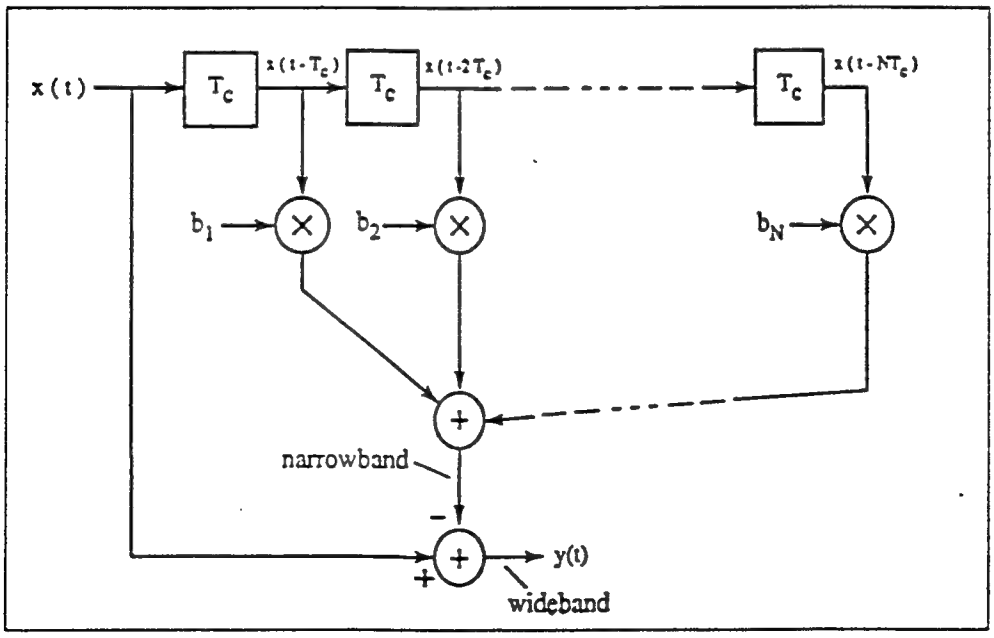

Figure 2 : Linear Prediction Filter

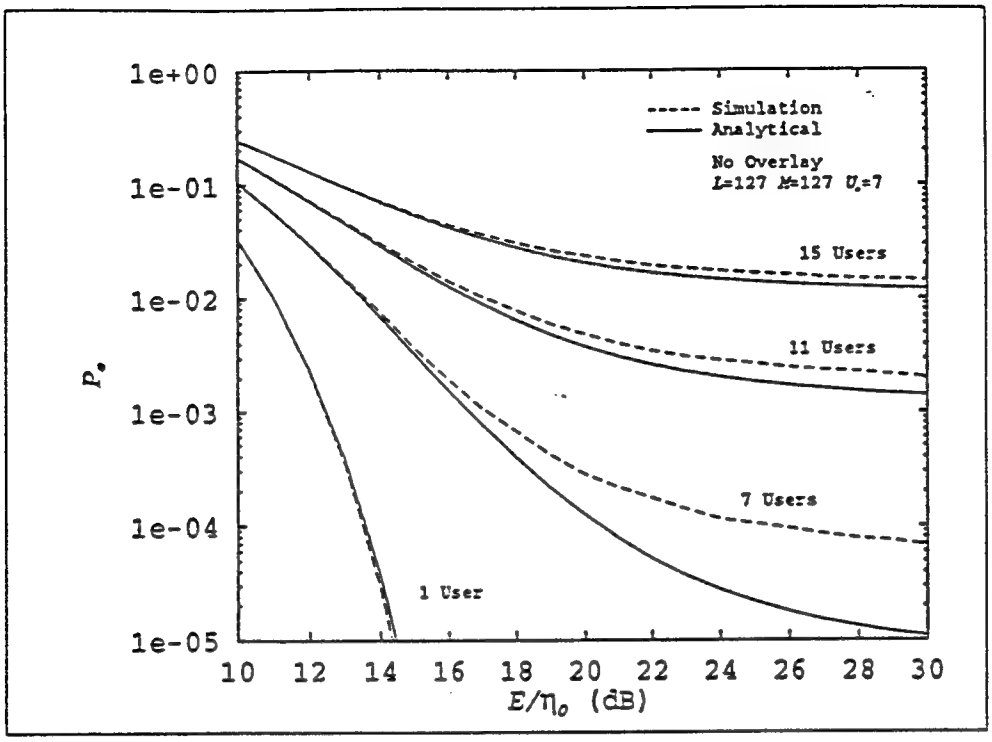

Figure 3 : Analytical and Simulated Performance in the Search Mode

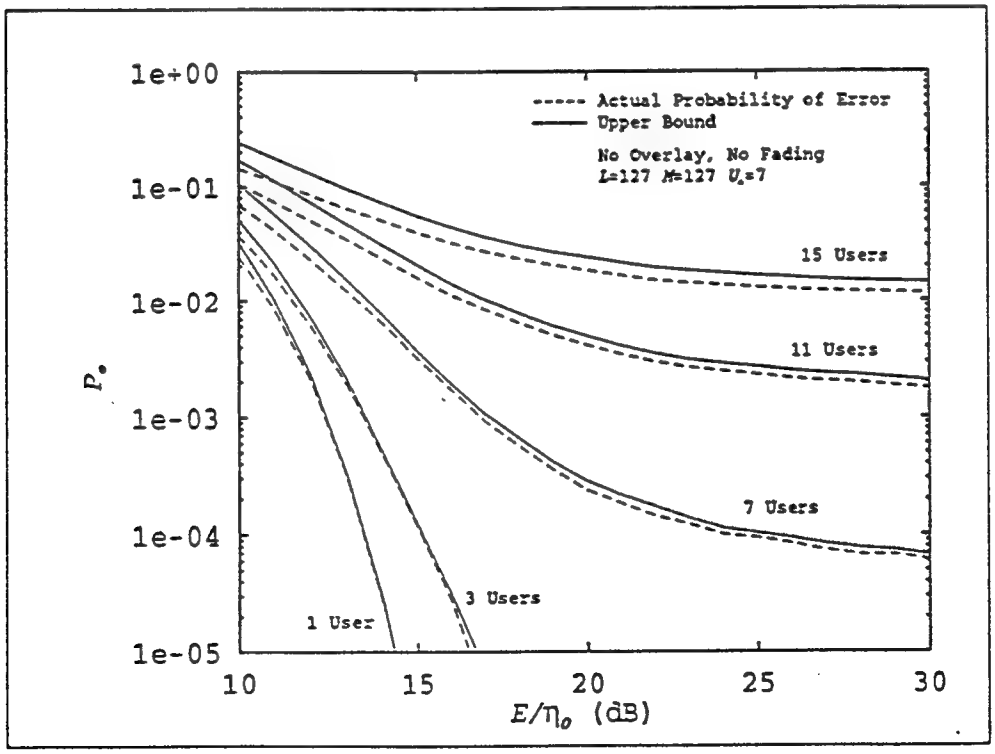

Figure 4 : Simulated Upper Bound versus Simulated Actual Performance

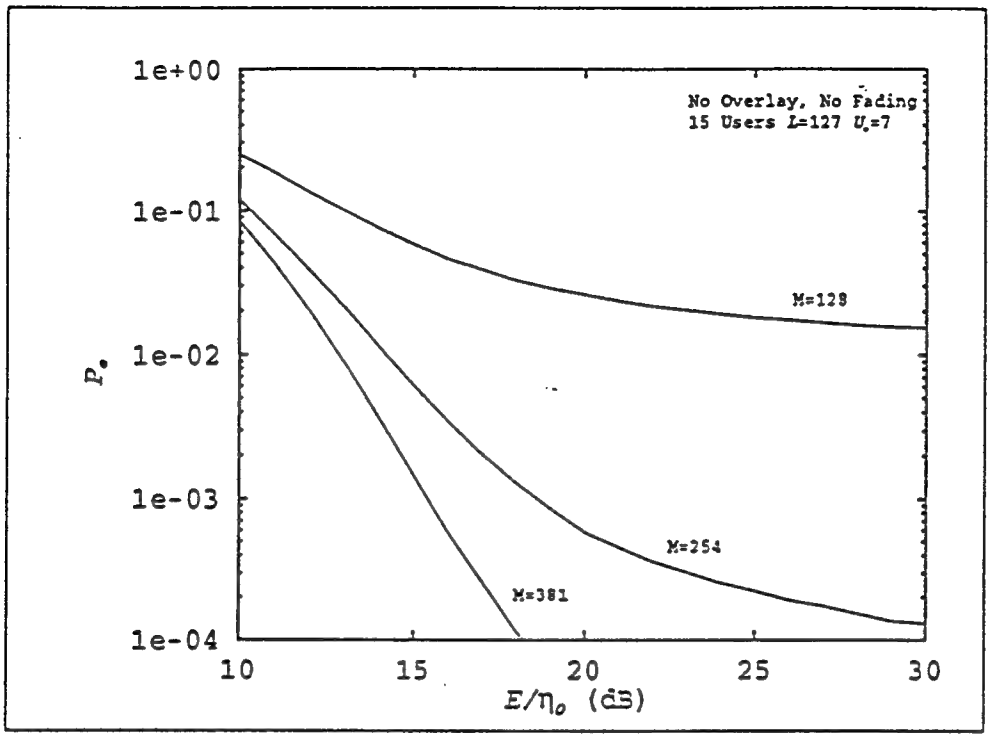

Figure 5 : Simulation of the Effect of Increasing the Observation Interval

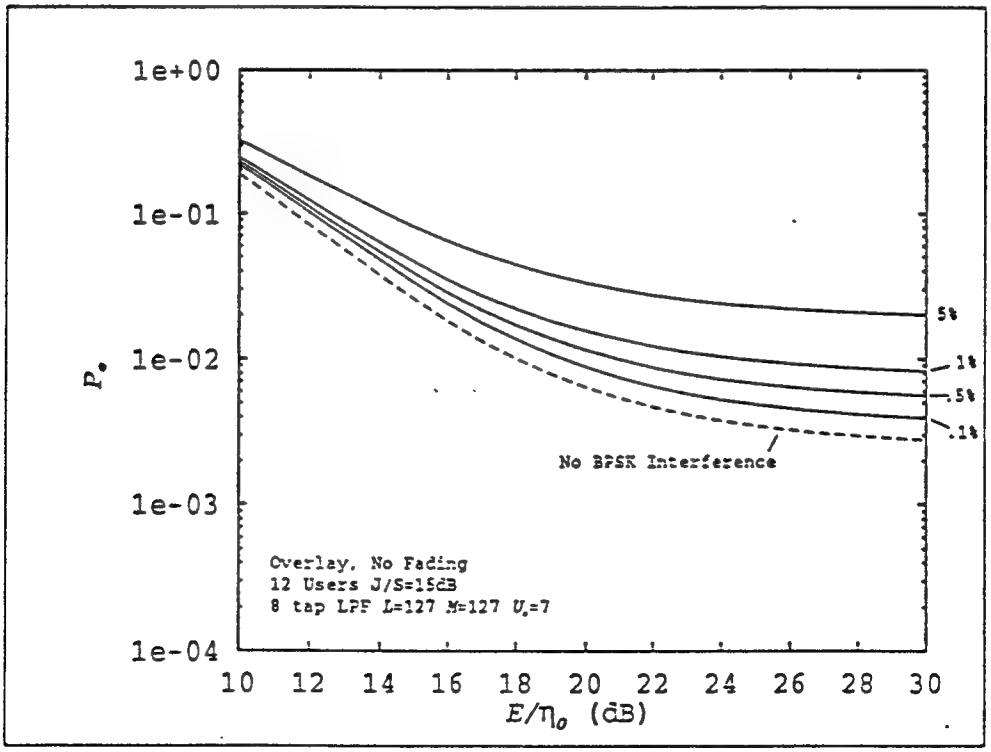

Figure 6 : Analytical Performance of Overlay System, 8 taps

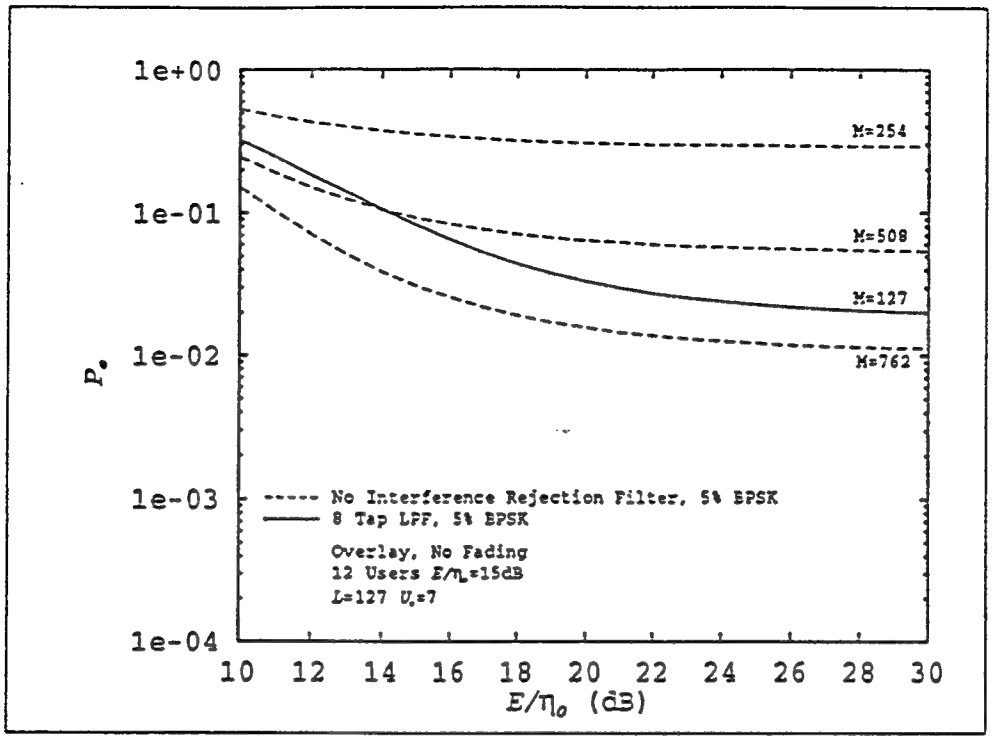

Figure 7 : Simulation of the Effect of Increasing the Observation Interval

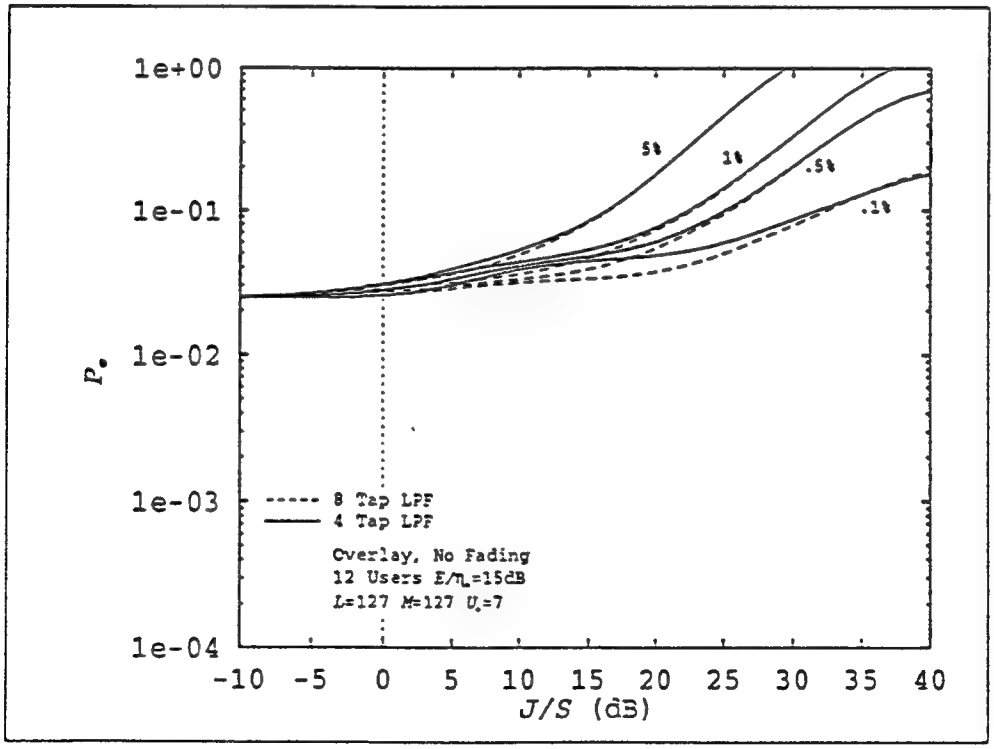

Figure 8 : Analytical Overlay Performance vs *J/S*, 4 and 8 Taps

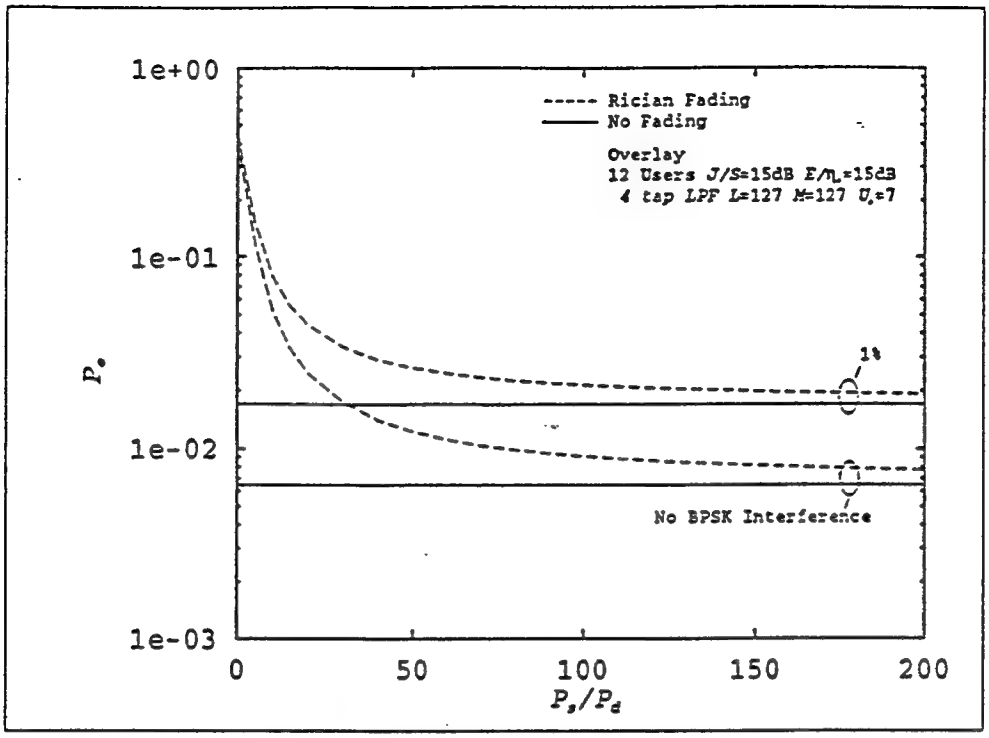

Figure 9 : Analytical Overlay Performance vs the Ratio of Direct-to-Diffused Power, Frequency Non-Selective Rician Fading

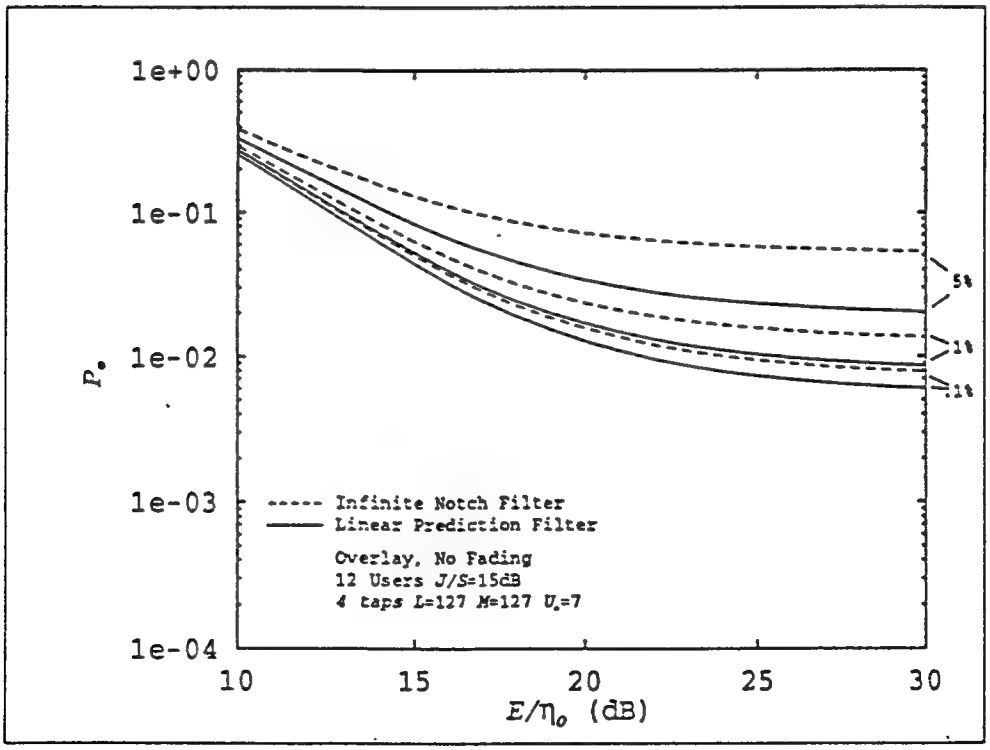

Figure 10 : Analytical Overlay Performance of 4 Tap Infinite Notch System

VII References

[1] R. L. Pickholtz, D. L. Schilling, and L. B. Milstein, "Theory of spread-spectrum communications - a tutorial", IEEE Trans. Commun., vol. COM-30, May 1982, pp. 855-884.

[2] L. B. Milstein, D. L. Schilling, R. L. Pickholtz, V. Erceg, M. Kullback, E. G. Kanterakis, D. S. Fishman, W.H. Biederman, and D. C. Salerno, "On the Feasibility of a CDMA Overlay for Personal Communications Networks" IEEE JSAC, vol. 10, number 4, May 1992, pp. 655-668.

[3] M. Davis and L. B. Milstein, "Filtered spreading sequences for interference avoidance", Proc. International Conference on Universal Personal Communication, Oct 1992.

[4] H. Wang and L. B. Milstein, "Microcellular CDMA mobile communications in frequency overlay situations", IEEE Global Telecomm. Conf., pp. 874-878, Dec. 1992.

[5] L. B. Milstein, "Interference suppression to aid acquisition in direct-sequence spread-spectrum communications," IEEE Trans. Commun.,vol. COM-36, pp. 1200-1207, Nov. 1988.

[6] F. M. Hsu and A. A. Giordano, "Digital whitening techniques for improving spread-spectrum communications performance in the presence of narrow-band jamming and interference", IEEE Trans. Commun., vol. COM-26, February 1978, pp. 209-216.

[7] J. W. Ketchum and J. G. Proakis, "Adaptive algorithms for estimating and suppressing narrow-band interference in PN spread-spectrum systems", IEEE Trans. Commun., vol COM-30, May 1982, pp. 913-924.

[8] L. Li and L. B Milstein, "Rejection of narrow-band interference in PN spread-spectrum systems using transversal filter", IEEE Trans. Commun., vol. COM-30, May 1982, pp.925-928.

[9] R. A. Iltis and L. B. Milstein, "Performance analysis of narrow-band interference rejection techniques in DS spread-spectrum systems," IEEE Trans. Commun.,vol. COM-32, pp. 1169-1177, Nov. 1984.

[10] L. D. Gottesman and L. B. Milstein, "The Performance of a Direct-Sequence Spread-Spectrum Acquisition System Using a Linear Prediction Filter for Narrowband Interference Suppression," to be submitted to IEEE Trans. on Communications

[11] C. W. Helstrom, *Probability and Stochastic Processes for Engineers*, New York: Macmillan, 1984.

[12] M. Schwartz, W. R. Bennett, and S. Stein, *Communication Systems and Techniques*, Chapter 8, New York: McGraw Hill, 1966.

Noncoherent Parallel Acquisition in CDMA Spread Spectrum Systems

Roland R. Rick* Laurence B. Milstein
Electrical and Computer Engineering Department
University of California, San Diego
La Jolla, CA 92093-0407

Abstract

This paper derives the performance of a direct sequence spread spectrum acquisition scheme. The effect of multiple access interference on acquisition performance is determined. Noncoherent acquisition performance is of interest because the system can acquire before it achieves carrier phase lock, and parallel schemes are of interest because they significantly reduce acquisition time over serial schemes. The analysis presented is applicable to the reverse link (mobile to base station) of a mobile communications system which employs code division multiple access (CDMA). By deriving results for both long and short spreading sequences, it is also shown that the periodicity of the spreading sequences has a significant effect on acquisition performance. Finally, the issue of capacity determined by acquisition performance criteria is addressed. The results show that, under certain conditions, the capacity is limited by acquisition, thus indicating the importance of the acquisition problem.

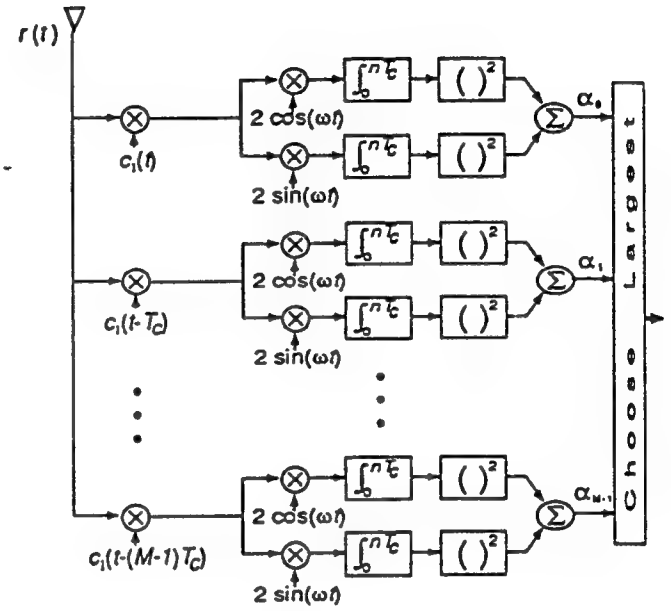

Figure 1: Coarse Acquisition Circuitry: A bank of I-Q noncoherent detectors is used to simultaneously test the spreading sequence phases within the uncertainty region.

1 Introduction

One basic limitation of direct sequence spread spectrum systems is synchronization time, the time it takes to align the locally generated spreading sequence with the received one. Synchronization is divided into two steps, labeled initial acquisition (coarse alignment) and tracking (fine alignment). The focus in this paper is on initial acquisition. The effect of multiple access interference on the acquisition performance is determined. The receiver utilizes a purely parallel search strategy and a fixed dwell noncoherent detection scheme (Figure 1). A purely parallel search strategy is used because it significantly reduces acquisition time compared to serial or partially parallel strategies. Furthermore, noncoherent detection is of interest because it allows initial synchronization to occur before carrier phase synchronization and, therefore, a bank of parallel inphase-quadrature (I-Q) noncoherent detectors is utilized (Figure 1). Typically, the spacing between branches in the receiver is a fraction of a chip, but, for simplicity, full chip spacing is used, and it is assumed that the uncertainty region is confined to M chips (Figure 1). The performance is derived for both long and short spreading sequences to determine the effect of the periodicity of the spreading sequences on acquisition. Long spreading sequences are defined as periodic sequences with a period of N_l chips, where it is assumed that the observation interval, n, also known as the acquisition window length, is less than the sequence period ($n < N_l$). Short spreading sequences are defined as periodic sequences with a period of N_s chips, where it is assumed that the observation interval is an integer multiple of the sequence period ($n = pN_s$). Finally, the analysis of the system performance is presented for the reverse link of a mobile communication system. The analysis of the forward link can be found in [1].

2 Received Signal Model

For the reverse link, it is assumed that there are L users which arrive with independent random carrier phases and

*This work was partially supported by the NSF University/Industry corporation Research Center on Integrated Circuits and Systems at UCSD, and the Army Research Office under Grant DAAL03-91-G-0071.

0-7803-1825-0/94 $4.00 © 1994 IEEE

independent random time delays. Since the focus is on multiple access interference, the effects of data, doppler shifts, and fading are not examined. For simplicity, it is assumed that each user arrives with the same signal power. Then, the received signal is

$$r(t) = A\sum_{i=1}^{L} c_i(t-\tau_i)\cos(\omega t+\theta_i)+\eta_w(t), \qquad (1)$$

where $c_i(t)$ is the spreading waveform of the i^{th} user and $\eta_w(t)$ is additive white Gaussian noise with two sided power spectral density $\frac{\eta_o}{2}$. The spreading waveform $c_i(t)$ is an infinite sequence of rectangular pulses, called chips, of duration T_c, where the height of the j^{th} pulse is denoted by $c_{i,j}$ and is either $+1$ or -1. The user of interest, assumed to be the first user, has a deterministic spreading sequence, $c_{1,j}$, with a period of N chips, and the other users' spreading sequences, also with periods of N chips, are modeled as independent random sequences of equally likely ± 1's. Since, for $i \geq 2$, $c_{i,j}$ are random sequences, the random time delays can be written as $\tau_i = u_i T_c$, where the u_i are, for $i = 2,\ldots,L$, independent and identically distributed (i.i.d.) random variables with uniform probability distributions on the interval $[0,1]$. For simplicity, it is assumed that the receiver is chip synchronized with the user of interest. In other words, $\tau_1 = dT_c$, where d takes on any integer value from 0 to $M-1$ with equal probability.

3 Analysis

In this section, the probability of false lock is derived for the reverse link. The probability of false lock, P_f, is the probability that the receiver chooses an incorrect phase (Figure 1). The mean and variance of the acquisition time, T_{acq}, as a function of P_f, are derived in [2].

3.1 Test Statistics

The test statistics are first derived for long spreading sequences ($N = N_l$), where it is assumed that the observation interval is less than the code period ($n < N_l$). Using the receiver in Figure 1 and the received signal in (1), the output of the r^{th} branch of the receiver is defined as

$$\alpha_r \triangleq \alpha_{r_c}^2+\alpha_{r_s}^2 \triangleq (S_{r_c}+N_{r_c}+I_{r_c})^2+(S_{r_s}+N_{r_s}+I_{r_s})^2, \quad (2)$$

where S_{r_c} and S_{r_s} are, conditioned on the phase, deterministic signal components dependent on the autocorrelation function of $c_1(t)$, and are given by

$$S_{r_{(s)}} = AT_c\begin{pmatrix}\cos\theta_r\\ -\sin\theta_r\end{pmatrix}\sum_{j=0}^{n-1} c_{1,j-r}c_{1,j-d}. \qquad (3)$$

The self-interference terms ($r \neq d$) are assumed to be negligible due to the out-of-phase autocorrelation. The white noise contributions, N_{r_c} and N_{r_s}, are given by

$$N_{r_{(s)}} = \int_0^{nT_c} 2c_1(t-rT_c)\begin{pmatrix}\cos\omega t\\ \sin\omega t\end{pmatrix}\eta_w(t)\,dt, \qquad (4)$$

and have a Gaussian distribution with mean 0 and variance $\sigma_n^2 = \eta_o n T_c$. The elements in the set $\{\{N_{r_c}\}_{r=0}^{M-1},\{N_{r_s}\}_{r=0}^{M-1}\}$ are jointly Gaussian, because they consist of linear functions of a Gaussian process. Assuming the double frequency term is zero, the correlation between any element in $\{N_{r_c}\}_{r=0}^{M-1}$ and any element in $\{N_{r_s}\}_{r=0}^{M-1}$ is zero due to the orthogonality between the sine and cosine channels. Therefore, because uncorrelated jointly Gaussian random variables are independent, the set $\{N_{r_c}\}_{r=0}^{M-1}$ is independent of the set $\{N_{r_s}\}_{r=0}^{M-1}$. Furthermore, the correlation between any two elements in either the cosine set or the sine set is approximately zero compared to the variance of any one of the elements [2]. Therefore, since the elements of $\{N_{r_c}\}_{r=0}^{M-1}$ are jointly Gaussian and approximately uncorrelated, they are approximately independent Gaussian random variables. The same is true for the elements of $\{N_{r_s}\}_{r=0}^{M-1}$.

The interference terms from the other users, I_{r_c} and I_{r_s}, are given by

$$I_{r_{(s)}} = AT_c\sum_{i=2}^{L}\begin{pmatrix}\cos\theta_i\\ -\sin\theta_i\end{pmatrix}F_{r,i}, \qquad (5)$$

where

$$F_{r,i} \triangleq (1-u_i)\sum_{j=0}^{n-1} c_{1,j-r}c_{i,j}+u_i\sum_{j=0}^{n-1} c_{1,j-r}c_{i,j-1} \qquad (6)$$

is the cross-correlation of the r^{th} phase shift of the locally generated sequence and the i^{th} user's received spreading sequence. From Equation (6), and because $c_{1,j}$ is modeled as deterministic and $c_{i,j}$ is modeled as a random binary sequence of equally likely ± 1's for any $i \neq 1$, the random variables $F_{r,i}$, for $i = 2,\ldots,L$, are i.i.d.. Using the central limit theorem for i.i.d. random variables, I_{r_c} and I_{r_s} are asymptotically Gaussian as the number of users grows large. It can also be shown that the set $\{\{I_{r_c}\}_{r=0}^{M-1},\{I_{r_s}\}_{r=0}^{M-1}\}$ is asymptotically jointly Gaussian [2]. Using this and the fact that the correlation between any element in $\{I_{r_c}\}_{r=0}^{M-1}$ and any element in $\{I_{r_s}\}_{r=0}^{M-1}$ is zero due to the random phases, the set $\{I_{r_c}\}_{r=0}^{M-1}$ is independent of the set $\{I_{r_s}\}_{r=0}^{M-1}$. The correlation between two interference terms within a set (or the variance of a given interference term) is given by

$$\mathrm{E}\left[I_{r_{(s)}}I_{q_{(s)}}\right] = (AT_c)^2\sum_{i=2}^{L}\sum_{k=2}^{L}\mathrm{E}\left[\begin{pmatrix}\cos\theta_i\cos\theta_k\\ \sin\theta_i\sin\theta_k\end{pmatrix}\right]\mathrm{E}[F_{r,i}F_{q,k}], \qquad (7)$$

where the last term is given by [2]

$$\mathrm{E}[F_{r,i}F_{q,i}] \simeq \frac{2}{3}n\delta_{r,q}+\frac{1}{6}n\delta_{|r-q|,1}, \qquad (8)$$

and $\delta_{j,k}$ is the Kronecker delta function defined as one when $j = k$ and zero otherwise. After evaluating the first expectation in (7) and substituting (8), Equation (7) becomes

$$\mathrm{E}\left[I_{r_{(s)}}I_{q_{(s)}}\right] = \frac{(AT_c)^2}{3}(L-1)n\left\{\delta_{r,q}+\frac{1}{4}\delta_{|r-q|,1}\right\}. \qquad (9)$$

As a result, adjacent branch test statistics are correlated due to the random time delays of the interfering users.

Lastly, the set $\{\{N_{r_c}\}_{r=0}^{M-1},\{N_{r_s}\}_{r=0}^{M-1}\}$ is independent of the set $\{\{I_{r_c}\}_{r=0}^{M-1},\{I_{r_s}\}_{r=0}^{M-1}\}$, because they are functions of independent random variables.

For short spreading sequences, the observation interval, n, is equal to an integer, p, times the spreading sequence period, N_s. The effect of this change on the signal and noise components is negligible [2]. The interference terms from the other users, I_{r_c} and I_{r_s}, are still given by (5) where, for short spreading sequences,

$$F_{r,i} \triangleq p\left\{(1-u_i)\sum_{j=0}^{N_s-1} c_{1,j-r}c_{i,j} + u_i\sum_{j=0}^{N_s-1} c_{1,j-r}c_{i,j-1}\right\}. \tag{10}$$

The set $\{\{I_{r_c}\}_{r=0}^{M-1},\{I_{r_s}\}_{r=0}^{M-1}\}$ is still asymptotically jointly Gaussian and the set $\{I_{r_c}\}_{r=0}^{M-1}$ is still independent of the set $\{I_{r_s}\}_{r=0}^{M-1}$. Equation (9) becomes

$$\mathrm{E}\left[I_{r_{(i)}}I_{q_{(i)}}\right] = \frac{(AT_c)^2}{3}(L-1)pn\left\{\delta_{r,q} + \frac{1}{4}\delta_{|r-q|,1}\right\}. \tag{11}$$

In summary, it has been shown that $\{N_{r_c}\}_{r=0}^{M-1}$, $\{N_{r_s}\}_{r=0}^{M-1}$, $\{I_{r_c}\}_{r=0}^{M-1}$, and $\{I_{r_s}\}_{r=0}^{M-1}$ are independent sets of zero mean Gaussian random variables, where the variance of the noise terms, σ_n^2, is $\eta_o nT_c$, and the variance of the interference terms, σ_i^2, for long and short spreading sequences are $\frac{(AT_c)^2}{3}(L-1)n$ and $\frac{(AT_c)^2}{3}(L-1)pn$, respectively. Therefore, from (2), α_r, for $r \neq d$, is a central chi-square distributed random variable with 2 degrees of freedom. Conditioned on θ_d, α_d is a noncentral chi-square distributed random variable with 2 degrees of freedom. From (3), the noncentrality parameter in the distribution of α_d is $(AnT_c)^2$. Furthermore, as a result of (9) and (11), and because noise terms within a set are approximately independent, α_r is approximately independent of α_q for $|r-q|>1$. For $|r-q|=1$, the normalized complex cross-correlation between adjacent branch test statistics for both long and short spreading sequences is

$$\rho = \frac{\sigma_i^2}{4(\sigma_n^2+\sigma_i^2)}. \tag{12}$$

3.2 False Lock Probability

Using the union bound, the probability of false lock can be written as

$$P_f = \Pr\left[\bigcup_{\substack{i=0\\ i\neq d}}^{M-1}\alpha_i > \alpha_d\right] \leq \sum_{\substack{i=0\\ i\neq d}}^{M-1}\Pr[\alpha_i > \alpha_d]. \tag{13}$$

In what follows, the bound of (13) will be treated as an approximate equality. For long spreading sequences, it is assumed that the uncertainty region is less than the spreading sequence period ($M < N_l$). In this case, α_0 is independent of α_{M-1}. Therefore, when the received phase corresponds to the first or last branch in the receiver, only one term in the summation in (13) involves correlated test statistics. Otherwise, two terms in (13) involve correlated test statistics. Since each test statistic is equally likely to correspond to the correct phase, the probability of the former case is $\frac{2}{M}$ and the probability of the latter case is $\frac{M-2}{M}$. Therefore, the probability of false lock is given by

$$P_f = \frac{2}{M}\left\{\Pr[\alpha_{(d+1)} > \alpha_d] + (M-2)\Pr[\alpha_q > \alpha_d]\right\} + \frac{M-2}{M}\left\{2\Pr[\alpha_{(d+1)} > \alpha_d] + (M-3)\Pr[\alpha_q > \alpha_d]\right\} \tag{14}$$

for $|q-d|>1$. After some algebra and using [3], the false lock probability becomes

$$P_f = \frac{2(M-1)}{M}\left\{Q_m\left(\sqrt{a},\sqrt{b}\right) - \frac{1}{2}\exp\left[-\frac{a+b}{2}\right]I_0\left(\sqrt{ab}\right)\right\} + \frac{(M-1)(M-2)}{2M}\exp\left[-\frac{(AnT_c)^2}{4(\sigma_n^2+\sigma_i^2)}\right], \tag{15}$$

where $Q_m(u,v)$ is the Marcum Q-function defined as

$$Q_m(u,v) \triangleq \int_v^\infty x\exp\left\{-\frac{x^2+u^2}{2}\right\}I_0(ux)\,dx, \tag{16}$$

and

$$\left\{\begin{array}{c} a \\ b \end{array}\right\} = \frac{(AnT_c)^2}{4(\sigma_n^2+\sigma_i^2)}\;\frac{1\mp\sqrt{1-\rho^2}}{1-\rho^2}, \tag{17}$$

where ρ is given by (12). Lastly, when $\frac{A^2T_c}{3\eta_o}(L-1) \gg 1$, the white noise is negligible compared to the multiple access interference, and (15) can be approximated by

$$P_f \simeq \frac{2(M-1)}{M}\left\{Q_m\left(\sqrt{a},\sqrt{b}\right) - \frac{1}{2}\exp\left[-\frac{a+b}{2}\right]I_0\left(\sqrt{ab}\right)\right\} + \frac{(M-1)(M-2)}{2M}\exp\left[-\frac{3n}{4(L-1)}\right], \tag{18}$$

where

$$\left\{\begin{array}{c} a \\ b \end{array}\right\} = \left\{\begin{array}{c} .0254 \\ 1.5746 \end{array}\right\}\frac{n}{L-1}. \tag{19}$$

For short spreading sequences, it is assumed that the uncertainty region is equal to the period of the spreading sequence ($M = N_s$). In this case, α_0 is dependent on α_{M-1}. Therefore, there are always two terms in the summation in (13) which involve correlated test statistics, and the probability of false lock is given by

$$P_f = 2\Pr[\alpha_{(d+1)} > \alpha_d] + (M-3)\Pr[\alpha_q > \alpha_d] \tag{20}$$

for $|q-d|>1$. Using [3] as above, the false lock probability becomes

$$P_f = 2\left\{Q_m\left(\sqrt{a},\sqrt{b}\right) - \frac{1}{2}\exp\left[-\frac{a+b}{2}\right]I_0\left(\sqrt{ab}\right)\right\} + \frac{M-3}{2}\exp\left[-\frac{(AnT_c)^2}{4(\sigma_n^2+\sigma_i^2)}\right], \tag{21}$$

where a and b are given by (17) and ρ is given by (12). Also, the white noise is negligible compared to the multiple

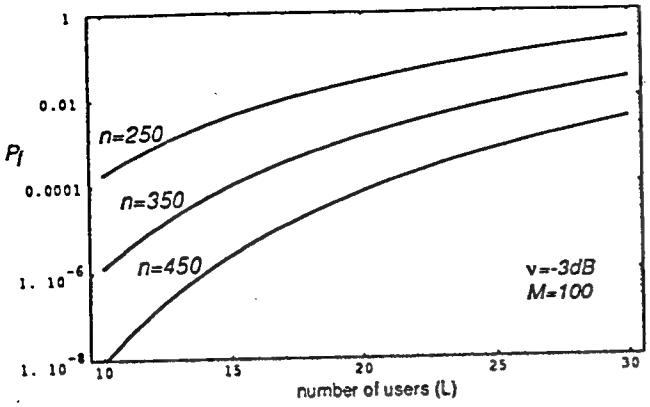

Figure 2: False lock probability versus the number of users for the reverse link of a CDMA mobile communication system. For comparison, the performance is shown for observation intervals of 250, 350, and 450 chips.

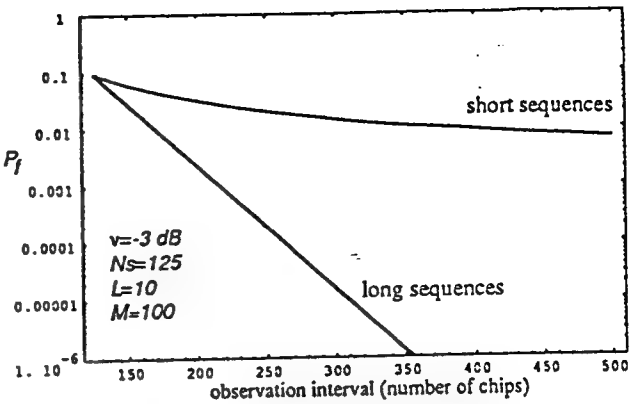

Figure 3: Comparison of the performance of long and short spreading sequences for the reverse link of a CDMA mobile communication system. The false lock probability is plotted versus the observation interval. The period of the short spreading sequence is 125 chips.

access interference when $\frac{A^2T_c}{3\eta_o}(L-1)p \gg 1$. Then, (21) can be approximated by

$$P_f \simeq 2\left\{Q_m\left(\sqrt{a},\sqrt{b}\right) - \frac{1}{2}\exp\left[-\frac{a+b}{2}\right] I_0\left(\sqrt{ab}\right)\right\} + \frac{M-3}{2}\exp\left[-\frac{3N_s}{4(L-1)}\right], \quad (22)$$

where

$$\left\{\begin{array}{c} a \\ b \end{array}\right\} = \left\{\begin{array}{c} .0254 \\ 1.5746 \end{array}\right\} \frac{N_s}{L-1}. \quad (23)$$

Notice that, when the white noise becomes negligible, the performance for short sequences is determined by the sequence period, N_s, not the observation interval.

4 Results

All of the major approximations, as well as the overall system performance, were verified by simulation [2]. In this section, the effects of various parameters on the false lock probability are plotted. Twice the chip energy-to-noise power spectral density ratio is represented by

$$\nu \triangleq \left(\frac{2E_c}{\eta_o}\right)_{dB} = 10\log_{10}\frac{A^2T_c}{\eta_o}. \quad (24)$$

In order to see the effect of the observation interval and the number of users on acquisition performance, the false lock probability, for long spreading sequences, is plotted versus the number of users with the observation interval as a parameter (Figure 2). In Figure 3, the performance of both long and short spreading sequences is plotted for comparison. When the observation interval is equal to one period of the short spreading sequence, the performance is the same for long and short sequences. For short spreading sequences, increasing the observation interval increases the signal-to-noise ratio but does not affect the signal-to-interference ratio because the cross-correlation between the interfering users and $c_{1,j}$ is the same for each period and, therefore, integrating over successive periods multiplies both the signal and interference by the same constant. For long spreading sequences, increasing the observation interval increases both the signal-to-noise ratio and the signal-to-interference ratio. Therefore, the curve for short spreading sequences decreases at a much slower rate. Thus, for long spreading sequences, the most important parameters are the observation interval and the number of users and, for short spreading sequences, the most important parameters are the spreading sequence period and the number of users.

5 Capacity

Since the multiple access interference is what typically limits capacity, it is reasonable to assume that the white noise is negligible. Then, it is known that an estimate, based on a Gaussian approximation, of the uncoded bit error rate is

$$P_e \simeq Q\left(\sqrt{\frac{3N_b}{L-1}}\right), \quad (25)$$

where N_b is defined as the bandwidth expansion or the number of chips-per-bit. The post-acquisition-based capacity is defined as the maximum permissible number of users, L, as a function of N_b, such that the uncoded bit error rate does not exceed 10^{-2}. For our example, the capacity is 142 users when $N_b = 256$. The acquisition-based capacity is defined as the maximum permissible number of users, as a function of the observation interval, n, such that the false lock probability does not exceed a certain threshold, ε. For simplicity, this discussion will be limited to long spreading sequences. In order to minimize the average acquisition time, the threshold should be chosen such that $m_p P_f \simeq .1T_d$, where m_p is the penalty time for false lock and T_d is the observation interval in seconds, $T_d = nT_c$ [2]. Because $M \gg 1$ and the correlated pairwise false lock probability is on the same order of

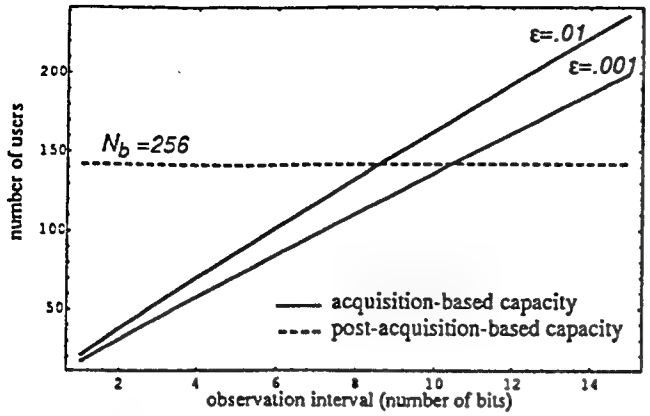

Figure 4: Comparison of the capacity based on acquisition and post acquisition performance criteria. The uncoded bit error rate needs to be less than or equal to 10^{-2}. The probability of false lock needs to be less than or equal to ϵ. The maximum number of users is plotted versus the observation interval in bits. For comparison, the results are shown for $\epsilon = .01, .001$. The number of chips per bit is 256.

magnitude as the uncorrelated pairwise false lock probability, Equation (18) can be approximated by

$$P_f \simeq \frac{M-1}{2} \exp\left[-\frac{3n}{4(L-1)}\right]. \qquad (26)$$

If there is no apriori information, the uncertainty region, M, is equal to the sequence period, N_l, which must be greater than or equal to the observation interval for (26) to be valid. Therefore, setting $M = n$ gives an optimistic estimate of P_f and an optimistic capacity estimate. Then, the capacity is, for large n and L, given by

$$L \simeq \frac{3n}{4 \log \frac{n}{2\epsilon}}, \qquad (27)$$

where the constraint is that $P_f \leq \epsilon$. The conclusion that the capacity is dependent on $n/\log n$ was also obtained in [4], where the capacity was defined as the maximum permissible number of users as a function of the observation interval subject to the constraint that the probability of acquisition failure tends to zero as $n \rightarrow \infty$. In Figure 4, the capacity is presented for various thresholds. The curve for the post-acquisition-based capacity is flat because N_b is held fixed. For an observation interval of less than 8 bits, the capacity is limited by acquisition. On the other hand, with a reasonable observation interval of about 10 bits, the acquisition-based capacity is equivalent to the bit error rate-based capacity. This is a significant advantage of using a parallel search strategy. If, however, the test statistics needed to be obtained serially, a much larger observation interval would be required. Overall, acquisition performance criteria can significantly affect the capacity of a CDMA system. Therefore, any valid capacity calculation requires taking into account both acquisition and post-acquisition-based capacity calculations.

6 Conclusion

This paper has derived the acquisition performance of the reverse link of a CDMA spread spectrum system, incorporating the effects of additive white Gaussian noise and multiple access interference. It has been shown that acquisition performance requirements can limit the overall capacity of a CDMA spread spectrum system. Therefore, overall capacity calculations should take into account both acquisition and post acquisition-based performance criteria. It has also been shown that the period of the spreading sequence is an important factor in determining acquisition performance. Increasing the observation interval does not significantly improve the performance when integrating over multiple spreading sequence periods. Future research should incorporate the effects of interference from surrounding cells, power control, shadowing, chip shapes, and lack of chip synchronization, as well as incorporating previous work on the effects of data [5], doppler shift [6], and fading [7, 8].

References

[1] R. R. Rick, L. B. Milstein, "Forward Link Acquisition Performance in CDMA Mobile Communications Systems," Submitted to *IEEE Third Comm. Th. Mini-Conf. in conjunction with Globecom '94.*

[2] R. R. Rick, "Noncoherent Parallel Acquisition in CDMA Spread Spectrum Systems," Ph.D. Dissertation, University of California, San Diego. To be submitted.

[3] S. Stein, "Unified analysis of certain coherent and noncoherent binary communications systems," *IEEE Trans. Info. Theory*, vol. IT-10, no. 1, January 1964, pp.43-51.

[4] U. Madhow, M. B. Pursley, "Acquisition in Direct-Sequence Spread-Spectrum Communication Networks: An Asymptotic Analysis," *IEEE Trans. Info. Theory*, vol. 39, no. 3, May 1993, pp.903-912.

[5] U. Cheng, "Performance of a class of parallel spread spectrum code acquisition schemes in the presence of data modulation," *IEEE Trans. Commun.*, vol. 36, no. 5, May 1988, pp.596-604.

[6] U. Cheng, W. J. Hurd, J. I. Statman, "Spread spectrum code acquisition in the presence of doppler shift and data modulation," *IEEE Trans. Commun.*, vol. 38, no. 2, February 1990, pp.241-250.

[7] E. A. Sourour, S. C. Gupta, "Direct sequence spread spectrum parallel acquisition in a fading mobile channel," *IEEE Trans. Commun.*, vol. 38, no. 7, July 1990, pp.992-998.

[8] E. A. Sourour, S. C. Gupta, "Direct sequence spread spectrum parallel acquisition in nonselective and frequency selective rician fading channels," *IEEE Journal on Selected Areas in Communications*, vol. 10, no. 3, April 1992, pp.535-544.

Appendix G

Optimal Power Control in a Cellular CDMA Mobile Radio System [1]

M. Zorzi and L.B. Milstein

Department of Electrical and Computer Engineering
University of California, San Diego
La Jolla, CA 92037

May 1993

[1]This work was partially supported by the Office of Naval Research under Grant N00014-91-J-1234, and by the Army Research Office under Grant DAAL03-91-G-0071.

Abstract

In this paper, the base-to-mobile link in a cellular CDMA mobile radio system, in the presence of Rayleigh fading, is considered, and an analytical approach is developed which enables us to find the optimal form of the power control law and to evaluate its performance in terms of the system utilization, i.e., the ratio of the number of admitted users and the spreading factor per information bit. The use of both block and convolutional codes is considered, and the average probability of error of the system is presented for both types of codes.

1 Introduction

For the new mobile communications services, spread spectrum modulation techniques are being considered because they exhibit various features which are desirable in such an environment. Perhaps the most important is the capability to offer multiple access to a common transmission medium, i.e., the frequency band, to a population of uncoordinated users, by assigning to each user a unique spreading sequence which allows the receiver to recognize the intended signal and to reject the interfering messages [1]. This technique of code division multiple access (CDMA) has proven to be very efficient in terms of bandwidth utilization [2]; this is basically due to the possibility, in a cellular environment, of reusing the same frequency band in every cell, whereas in systems using FDMA or TDMA it is necessary to devise a clustered structure in order to guarantee sufficient separation between cells operating in the same band and therefore to have tolerable interference levels [3].

The problem of evaluating the performance of CDMA systems has been extensively studied in the recent literature, with application to both terrestrial and satellite systems [2,4,5]. Due to the complexity of the statistical models by which the propagation is described (including the near-far effect and random attenuations such as fading), combined with the necessity of taking into account the interference both from the cell in which the intended user is located and from the surrounding cells, an accurate analysis of the performance is always a difficult task. In particular, the forward link, i.e., the communication from the base station to the mobile unit, has been studied under the restrictive assumption of deterministic propagation [3]; in the presence of Rayleigh fading, a simplified analysis is presented in [4]. In this latter paper, a worst-case approach is taken, assuming the intended user is located on the cell boundary; this does not account for the fact that, in reality, the user's location is randomly distributed within the cell, and thus the near-far problem and the associated power control effects were not considered. The need for a more complete and realistic approach is therefore clear. The forward link, in the presence of frequency selective fading, has been studied in [6], in which results are obtained mainly via computer simulation. A simulation approach is also taken in [2], in which Rayleigh fading is not taken into account, but log normal shadowing is considered instead. In this paper, we set up an analytical framework which enables us to study the performance of the forward link under fairly general conditions.

A key feature for a CDMA system to operate properly is power control, which is an effective way to combat the near-far problem, and in particular to ensure that users near the boundary of the cell do not experience severe impairments. This has previously been studied by Nettleton and Alavi [7]. Also, in [3], a simpler class of power control laws has been proposed, and Gejji [8] has presented an analytical approach for optimizing power control. Neither paper accounts for fading, and both consider interference from only a limited number of surrounding cells. In this paper, we give an analytical formulation to the problem of finding the optimum power control scheme in the presence of fading. Also, coded performance is considered, using both block codes and convolutional codes. For the latter, due to complexity considerations, an approximate approach is proposed, and a simulated approach is developed as well. Finally, an analysis of the sensitivity of

the results with respect to some parameters, such as noise, number of interfering cells considered, power loss exponent, degree of orthogonality between different spreading sequences and imperfect interleaving, concludes the paper.

2 System Model

In this section, we describe a model for our cellular CDMA system in which the envelope of the received signal is a Rayleigh distributed random variable. This model is widely accepted in the literature for a narrowband CDMA waveform, even though the propagation phenomena are much more complex to describe, and lends itself to a tractable analysis.

In our analysis, we focus on the forward link, i.e., the base-to-mobile path. The base station (BS) transmits to its own users, using direct sequence spread spectrum modulation. Each mobile, along with the desired signal, picks up interfering signals. These signals come both from the BS's of the surrounding cells (intercell interference) and from the BS of the cell in which the user is located (intracell interference). We assume that the total average transmitted power P_T be the same for each BS.

In considering the effect of the surrounding cells, we will limit ourselves to the first two tiers, i.e., to the 18 cells closest to the cell 0, in which the intended receiver is located. In each cell, we assume an average number of M active users, whose positions are independent of each other and uniformly distributed within the cell itself.

In order to combat the near-far effect, a power control (PC) scheme must be used. This technique results in different transmitted powers to different users, based on an estimate of the performance experienced by the users themselves. We assume that this compensation is possible only for the attenuation due to the distance of the users from its BS, since the fluctuations due to the Rayleigh fading are too rapid to be tracked. The ideal criterion used in devising a PC strategy is to provide an equal service quality to any user, regardless of its position. This means that an optimal PC law should result in the same error probability for all users in the system.

More precisely, let BS_j denote the base station of the cell j, and let r_{ji} be the distance of the user ji (i.e., the ith user in cell j) from its base station, BS_j. The power $P_{T_{ji}}$ that the BS_j transmits to the user ji is given by

$$P_{T_{ji}} = P_0 \varphi(r_{ji}), \tag{1}$$

in which the function φ is the *power control law (PCL)*. The mean value of this function, when averaged over the random distance r_{ji}, is taken equal to 1, so that the total average power transmitted by BS_j is

$$P_{T_j} = E\left[\sum_{i=1}^{M} P_0 \varphi(r_{ji})\right] = M P_0, \tag{2}$$

and is the same for all j. Following [4,9], we model the global effect of t as Gaussian noise.

3 Analysis

With the above model, the received waveform at the mobile is [4]

$$r(t) = \sum_{j=0}^{18} \alpha_j A_j \sum_{i=1}^{M} d_{ji}(t - \tau_{ji}) PN_{ji}(t - \tau_{ji}) \cos(\omega_0 t + \theta_{j}$$

where A_j is the unfaded amplitude of the signal from BS_j, the α_j's distributed r.v.'s with unit power, $d_{ji}(t)$ and $PN_{ji}(t)$ are the binary data a of the ith user in cell j, respectively, τ_{ji} and θ_{ji} are the corresponding t phase, respectively, and $n_w(t)$ is additive white Gaussian noise. Due to t in each cell, we assume that the power transmitted by each BS is given b Since we will consider only the position of the intended receiver, for si $r_j, j = 0, \ldots, 18$, be its distance from BS_j. Then the useful signal power

$$S = \frac{\alpha_0^2 A_0^2}{2} = \alpha_0^2 K r_0^{-\eta} \varphi(r_0) P_0,$$

in which α_0^2, the fading loss, is an exponentially distributed r.v. with unit me distributed. The factor $Kr_0^{-\eta}$ accounts for the deterministic path loss, whic inverse η^{th} power of the distance; η can take values between 2 and 4 in the and larger values if blockage is present. The analysis will be carried out fc dependence of the results on the value of η will be investigated.

The interference power from BS_j is given by

$$I_j = \frac{\alpha_j^2 M A_j^2}{2} = \alpha_j^2 K r_j^{-\eta} P_T.$$

If P_N is the noise power and L is the processing gain of the spread spectrum error probability, conditioned on the α_j^2's, is computed as in [4]:

$$\begin{aligned} P_e &= \Phi\left(-\sqrt{\frac{S}{P_N + \frac{7}{3L} I_0 + \frac{1}{3L}\sum_{j=1}^{18} I_j}}\right) \\ &= \Phi\left(-\sqrt{\frac{\alpha_0^2 K r_0^{-\eta} \varphi(r_0) P_0}{P_N + \frac{7}{3L}\alpha_0^2 K r_0^{-\eta} P_T + \frac{1}{3L}\sum_{j=1}^{18} \alpha_j^2 K r_j^{-\eta} P_T}}\right) \\ &= \Phi\left(-\left[\frac{M}{3L\varphi(r_0)}\left(\frac{W + \sum_{j=1}^{18} \alpha_j^2 \left(\frac{r_j}{r_0}\right)^{-\eta}}{\alpha_0^2} + \gamma\right)\right]^{-\frac{1}{2}}\right) \end{aligned}$$

$$= \Phi\left(-\sqrt{\frac{\Lambda}{\gamma+\nu}}\right) \triangleq P_e(\Lambda, r_0, \nu),$$

where

$$W \triangleq \frac{P_N}{P_0 K r_0^{-\eta}} \frac{3L}{M}$$

$$\Lambda(r_0) \triangleq \frac{3L}{M}\varphi(r_0)$$

$$\nu \triangleq \frac{W + \sum_{j=1}^{18} \alpha_j^2 \left(\frac{r_j}{r_0}\right)^{-\eta}}{\alpha_0^2}$$

$$\Phi(x) \triangleq \int_{-\infty}^{x} \frac{e^{-\frac{t^2}{2}}}{\sqrt{2\pi}} dt,$$

and γ is defined below. Note that, due to the PCL, Λ is a function of r_0. A later, what we are looking for is precisely the functional dependence of Λ on r_0. is actually a function of two variables, the distance r_0 from the BS and the with respect to some reference direction. For simplicity (and with no loss of g analysis can be done for any direction), throughout the paper this dependence c dropped. In the results, we take what is seemingly the worst-case direction, i.e. corner of the cell.

We note that, since the transmissions from BS_0 can be synchronized, the perfect orthogonality, whereas the transmissions from $BS_j, j = 1, \ldots, 18$, have ra relative to the receiver in the cell of interest. The parameter γ in Eq. (6) takes fact. If, as assumed in [4], there is no synchronization, $\gamma = 1$. If, on the other han there is perfect alignment of the sequences (i.e., the *bit periods* are synchronized i: be no correlation between different signals, and $\gamma = 0$. It must be noted that this true if the chip pulse shape were rectangular, whereas in the presence of a different the correlation of aligned sequences would be small, but could be nonzero. In the . consider the case in which the signals are synchronous, allowing γ to be a small (filtered chips) as well as 0 (rectangular chips). To justify the assumption of Gaus: it can be shown, as in [4], that the Liapounoff version of the central limit theorem a: of the interfering signals transmitted by the surrounding BS's. Also, we note th the number of signals is not very large (in fact, it is 18), we are interested in ve error rates (of the order of 10^{-1}), since we will use very powerful codes. Therefc not far out on the tail of the Gaussian distribution, our approximation turns out tc

If, given r_0, the pdf $f_\nu(\nu)$ of the r.v. ν were known, the bit error probability of a at distance r_0 from the base station could simply be found from (6) as

$$\overline{P}_e(\Lambda, r_0) = \int_0^\infty P_e(\Lambda, r_0, \nu) f_\nu(\nu) d\nu.$$

It is easy to show (see Appendix A) that the distribution of ν is given by [10]

$$\begin{aligned} F_\nu(a) &\triangleq P[\nu \le a] \\ &= e^{-W/a} \prod_{i=1}^{18} \left(\frac{1}{1 + \frac{1}{a}\left(\frac{r_i}{r_0}\right)^{-\eta}} \right), \end{aligned} \tag{12}$$

where W is defined in (7). Even though it is not explicitly indicated in the notation, $F_\nu(a)$ is dependent on the position of the mobile, r_0.

As indicated in the previous section, the optimal PCL is given by the solution of the following equation:

$$\overline{P}_e(\Lambda(r_0), r_0) = P_d, \quad \text{for all } r_0 \in (0, 1], \tag{13}$$

in which the cell radius is normalized to 1. Notice, from (8) that the function $\Lambda(r_0)$ is proportional to the PCL, according to the constant $3L/M$, which is still unknown. In order to determine it, recall that $E[\varphi(r_0)] = 1$; hence, from (8), we obtain

$$E[\Lambda(r_0)] = \frac{3L}{M}, \tag{14}$$

which also explicitly relates the function $\Lambda(r_0)$ to the system efficiency, i.e., the ratio of the number of admitted users M and the processing gain (spreading factor) L. In (13), P_d is the desired error probability, and the function $\Lambda(r_0)$ is the unknown. In (14), the expectation is taken over the random position of the mobile, r_0. Since $\Lambda(r_0)$ and $\varphi(r_0)$ differ only by a constant, in the following, when talking about the PCL, we will refer to either of them interchangeably.

It is worth noting that, in our notation, L is the processing gain *per channel symbol.* In the presence of coding, this is not equal to the processing gain *per information bit*, which we indicate by L_i. L_i is a parameter of the system, whereas L depends on the particular code being used. More precisely, when a code of rate R_c is employed, the actual transmission rate on the channel is increased by a factor $1/R_c$. Therefore,

$$L = L_i R_c. \tag{15}$$

In order to make a fair comparison between different choices, we refer to the ratio of the number of admitted users, M, and the processing gain *per information bit*, L_i. We define *system utilization* to be the ratio

$$\rho \triangleq \frac{M}{L_i} = R_c \frac{M}{L}; \tag{16}$$

it is taken as a measure of the efficiency of the transmission scheme.

An interesting case corresponds to the *absence of noise.* In Eqs. (6) and (9), this corresponds to $W = 0$, and the statistics of ν are dependent only on the propagation losses. Once γ is fixed, the effect of the spreading, the number of users and the PCL are summarized in the one parameter Λ. This means that the problem stated in Eq. (13) can be solved in general, and the same solution applies to systems with different processing gains. This is not true, in general, when noise is present.

It should be noted, however, that CDMA systems are typically *interference limited*, and therefore neglecting noise is a reasonable assumption. Moreover, as a proof of this intuitive argument, it will be shown later that the results obtained in the presence of moderate noise do not differ significantly from those obtained in its absence. Therefore, in the following, we assume $W = 0$.

4 Coding

Due to the severe propagation environment, the use of coding in mobile communication is unavoidable. In particular, in voice transmission, which requires very limited delays, ARQ strategies are typically not effective, and the use of FEC codes is a more reasonable choice. As to the analysis, in studying the performance of codes, it is convenient to distinguish two limiting situations: independent bits (corresponding to the use of perfect interleaving) and dependent bits (corresponding to no interleaving).

4.1 Block Codes

If an (n, k) block code with t error correction capability is used, the bit error probability P_b, after decoding, conditional on fading, can be approximated as

$$P_b(p) \simeq \sum_{i=t+1}^{n} \frac{i}{n} \binom{n}{i} p^i (1-p)^{n-i}, \tag{17}$$

in which p is the channel error probability. When interleaving is used, all bits experience independent fading, p is given by Eq. (11), and the error probability after decoding is

$$\overline{P}_b^{(i)} = P_b\left(\overline{P}_e(\Lambda, r_0)\right); \tag{18}$$

when interleaving is not used, all bits in the block fade together, $p = P_e(\Lambda, r_0, \nu)$ is the *conditional* error probability on the uncoded channel, and Eq. (17) provides the *conditional* bit error probability after decoding; this last probability must be averaged over $f_\nu(\nu)$, to get

$$\overline{P}_b^{(ni)} = \int_0^\infty P_b\left(P_e(\Lambda, r_0, \nu)\right) f_\nu(\nu) d\nu. \tag{19}$$

Due to the unfavorable propagation environment, poor performance can be expected in the absence of interleaving, since it is difficult to recover a faded packet (all bits fade at the same time, and the error correction is not very effective). Our results confirm this intuition, yielding a system utilization dramatically lower than in the presence of interleaving.

The results obtained for BCH codes of block length 63, 127 and 255, when perfect interleaving is assumed, $P_d = 10^{-3}$ (a typical value for voice), and intracell sequences are perfectly orthogonal

(i.e., $\gamma = 0$), are illustrated in Fig. 1a. The curves represent the system utilization, ρ, vs. the rate of the code, R_c, and are parametrized by the block length. This plot is repeated for $\gamma = 0.1$ in Figs. 1b. We note from Table I that, for $\gamma = 0.01$, the results obtained are almost the same as for $\gamma = 0$. The apparently strange behavior of the curves is due to the fact that the error capability of the codes is not a linear function of the number of parity digits; this accounts for "jumps" in the curves at various points. To be more specific, for a BCH code with block length $2^m - 1$, to increase the error correction capability from t to $t + 1$, we need to add m parity digits. In some instances, however, this would increase t by more than one (for more details see, for example, [11]). This discrete behavior can also explain why in Fig. 1, even though the longer code gives, in general, better performance than the shorter one, at some points the latter can outperform the former. The optimal $\varphi(r_0)$, as obtained by solving (13) and (14), is plotted vs. r_0 in Fig. 2, for the BCH (255,47) code, with perfect interleaving and $\gamma = 0$.

Since, in the system under study, we are interested primarily in voice transmission, the natural solution of increasing the block length to obtain better performance is, at some point, not feasible, due to the unacceptable increase in delay; we note that, due to the relatively low bit rates (tens of kbit/s), the complexity of the decoder, even in a portable unit, is not a major issue. As an example, assume we have an uncoded bit rate R (in bit/s) and a code rate R_c (information bits per symbol in the block). The delay D, assuming no processing delay, is roughly twice the duration of the block, times the degree of interleaving, a. Therefore, we can write

$$D \simeq 2 \frac{R_c}{R} a n. \tag{20}$$

For example, with $R_c \simeq 0.2$ (corresponding to maximum performance in our computations), and $R = 9.6$ kbit/s, we obtain

$$D \simeq 0.042\, n a \text{ ms.} \tag{21}$$

It is easy to see that for $n = 255$ and $a = 10$, the delay is greater than 100 ms, and becomes detectable.

To model the situation in which the interleaving is not perfect, we considered the following case: We assume that, after deinterleaving, adjacent pairs of code symbols fade in identical manners, but that different pairs of symbols fade independently [5]. If we denote by p_1 and p_2 the probability that either one or both of the two bits are in error, respectively, it is shown in Appendix B that the error probability can be approximated as

$$P_b \simeq \sum_{i=t+1}^{n} \frac{i}{n} \sum_{k=0}^{\lfloor i/2 \rfloor} \frac{\lfloor n/2 \rfloor !}{k!\,(i-2k)!\,(\lfloor n/2 \rfloor - i + k)!}\, p_2^k\, p_1^{i-2k}\, (1 - p_1 - p_2)^{\lfloor n/2 \rfloor - i + k}. \tag{22}$$

Eq. (22) is evaluated under the same conditions as Eq. (17). Comparing the results, presented in Table I, we note that the performance is slightly worse than in the case of perfect interleaving. As this model is generalized, and more than two symbols fade together, the performance is expected to become progressively worse. In this situation, however, using a binary BCH code may not be

the best choice. Rather, codes such as nonbinary BCH codes, Reed-Solomon codes or burst-error-correction codes should be used.

So far, we have neglected the thermal noise, even though it is always present; this is a reasonable assumption, due to the fact that the CDMA systems are inherently *interference limited.* To substantiate this intuitive argument, we evaluated the probabilities of error for the situation in which $W > 0$. More precisely, from (7) we obtain

$$W(r_0) = \frac{P_N}{P_0 K r_0^{-\eta}} \frac{3L}{M} = \frac{r_0^{\eta}}{SNR_0} \frac{3L}{M} \triangleq W_0 r_0^{\eta}, \tag{23}$$

where $SNR_0 \triangleq \frac{P_0 K}{P_N}$ is the signal-to-thermal-noise ratio at the boundary of the cell ($r_0 = 1$), without power control, and is a system parameter. From our evaluations, W_0 turns out to be rather small, generally considerably smaller than 1. Also, the transmitted power P_0 is left as a parameter, and can be chosen in such a way that the presence of the noise has in fact a negligible effect. In Table II, the results for $W_0 = 1$, 0.1 and 0.01 are shown, and should be compared with those in Table I, corresponding to $W_0 = 0$. We note that the significant degradation in performance (25-40%) for $W_0 = 1$, becomes much smaller (4-5%) as soon as W_0 takes values of 0.1 or less. As an example, assume the following values of the parameters: K = -108 dB, P_0 = 0 dBW, P_N = -134 dBW; we have

$$W_0 \simeq 0.0075\rho \tag{24}$$

and, for values of ρ in the range shown in the Tables, W_0 is less than 0.1. Therefore, neglecting the background noise, in this case, is legitimate.

4.2 Convolutional Codes

For convolutional codes, the bit error probability can be upper bounded as [12]

$$P_b \leq \sum_{d=d_{free}}^{\infty} \beta_d P(d), \tag{25}$$

in which d_{free} is the *minimum free distance* of the code, $P(d)$ is the *first-event error probability* and the weights β_d depend on the particular code (values of β_d for some codes of practical interest are tabulated in the literature, e.g., [13]). Assuming that the Viterbi algorithm with soft-decision decoding is used to decode, and in the presence of perfect interleaving, following an approach similar to [5] , the first-event error probability, conditioned on fading, is given by

$$P(d) = \Phi\left(-\sqrt{\frac{\Lambda\left(\sum_{l=1}^{d} \alpha_{0l}^2\right)^2}{W + \sum_{j=1}^{18} \rho_j \sum_{l=1}^{d} \alpha_{0l}^2 \alpha_{jl}^2}}\right), \tag{26}$$

where

$$\rho_j \triangleq \left(\frac{r_j}{r_0}\right)^{-\eta}, \; j = 1, \ldots, 18, \tag{27}$$

the other symbols have been already defined, and we assumed $\gamma = 0$. Note that the index l runs over the set of d coded symbols in which the two decoding paths differ, whereas the index j denotes the BS.

The expression in (26) should be averaged over the set of r.v.'s $\alpha_{jl}^2, j = 0, \ldots, 18, l = 1, \ldots, d$. This is clearly not feasible, unless we resort to some approximation. In particular, if we replace the denominator by its mean, conditioned upon $\alpha_{0l}^2, l = 1, \ldots, d$, we obtain

$$\begin{aligned} P(d) &\simeq \Phi\left(-\sqrt{\frac{\Lambda\left(\sum_{l=1}^{d}\alpha_{0l}^2\right)^2}{W + \sum_{j=1}^{18}\rho_j \sum_{l=1}^{d}\alpha_{0l}^2}}\right) \\ &= \Phi\left(-\sqrt{\frac{\Lambda S^2}{W + \left(\sum_{j=1}^{18}\rho_j\right) S}}\right), \end{aligned} \tag{28}$$

where

$$S \triangleq \sum_{l=1}^{d}\alpha_{0l}^2. \tag{29}$$

If noise can be neglected, i.e., $W = 0$, Eq. (28) can be further reduced to

$$P(d) \simeq \Phi\left(-\sqrt{\Gamma S}\right), \tag{30}$$

where

$$\Gamma \triangleq \frac{\Lambda}{\sum_{j=1}^{18}\rho_j} \tag{31}$$

These last two equations deserve some comments. First, we note that (30) is very easy to average, because the randomness is limited to S, which is a well-known *chi-square* distributed r.v.; a single integration (known in closed form [12]) is required. Given the required probability of error and a particular code, Γ needs to be computed from Eqs. (30) and (25) just once. Also, even though it is defined as the ratio of functions of r_0, Γ itself does not depend on r_0; once Γ has been found, the function $\Lambda(r_0)$ is simply given by

$$\Lambda(r_0) = \Gamma \sum_{j=1}^{18}\rho_j, \tag{32}$$

where the dependence on r_0 is concentrated in the ρ_j's. Eq. (14) can be rewritten as

$$\frac{3L}{M} = E[\Lambda(r_0)] = \Gamma E\left[\sum_{j=1}^{18}\rho_j\right]. \tag{33}$$

We remark that the expectation in the above equation, taken with respect to r_0, is a constant (whose value is approximately 0.625), and Γ depends only on the chosen code and the required error probability. The remaining operations, which are straightforward, are to compute the system utilization, ρ, and the PCL, $\varphi(r_0)$ (or, equivalently, $\Lambda(r_0)$), from Eqs. (33) and (32), respectively. For example, for a convolutional code of rate 1/3 and constraint length 8, this approach yields $\Gamma \simeq 1.4$, corresponding to $M/L = 3/(0.625\Gamma) \simeq 3.43$. Since the rate of the code is 1/3, the system utilization turns out to be $\rho = 114\%$. The PCL obtained from Eqs. (32) and (33) is plotted vs. r_0 in Fig. 3.

In the above, in order to be able to handle the analysis, we introduced two major assumption, which are to be discussed below. First, the summation in (25) involves an infinite number of terms, whereas only a few values of β_d are available in the literature. The obvious way to overcome this difficulty is to truncate the summation after a certain number of terms. This, of course, means that the general term of the sum must decrease significantly after few nonzero terms, so that the remaining tail of the series can be discarded. In Fig. 4, the error probability (25), evaluated using the probabilities (30), is plotted vs. Γ; the curves correspond to various numbers of nonzero terms that have been considered. It is clear that, even with 9 terms (the maximum number of weights seemingly available in the literature), the sum does not converge, at least for the value of interest of the probability of error, namely 10^{-3}. Thus, for a given error probability, the actual value of Γ is greater than the value obtained by considering the truncated sum. On the other hand, we remark that the curves decrease rapidly, and a small increase of Γ has a significant effect in reducing the probability of error, P_b. Therefore, the error committed by using the truncated sum in the computation leads to a moderate error on Γ, and thus on the evaluation of the capacity (in our judgement, of the order of 10-20%); in any event, the approximate evaluation is qualitatively valuable in studying how the performance of the system varies with the key parameters. Also, (25) is an upper bound and, qualitatively, it tends to be looser for larger values of the error probability; since it is precisely for those values that the convergence is slower, this has the effect of partially compensating for the error.

The second assumption was to replace the interference power by its mean, and this enabled us to reduce (28) to (30). Actually, the number of random variables in the sum in the denominator is not very large, and, further, they are not identically distributed, since the sum is a weighted sum. Thus, the applicability of the law of large numbers can be questioned. We computed the probabilities (26) via a Monte-Carlo simulation (10^5 points); the error probabilities are plotted in Fig. 5, and the system utilizations obtained for the code of rate 1/3 and constraint length 8, for the two methods, are presented in Table III, along with the maximum efficiency obtained when block codes are used. Perfect interleaving, $\gamma = 0$ and $W_0 = 0$ are assumed. As can be seen, the approximate approach yields the correct qualitative behavior, but is poor from a quantitative point of view. This is especially clear when Fig. 5 is compared with the corresponding analytical results in Fig. 4. On the other hand, the approximate approach can be viewed as valuable for at least two reasons: it provides an easy and fast approach, which is qualitatively correct and can be a good starting point; moreover, it provides insight into the PCL issue. Indeed, a PCL of the form of (32) works well even in the simulation approach, giving a probability of error fairly constant in

the range of interest. As an example, in Fig. 6, P_b is plotted vs. the location of the mobile, based on the PCL of (32). We note that P_b is fairly flat. That is, even though our definition of optimal power control law, Eq. (13), is no longer strictly valid, the approximate solution is not far from optimal. Also, from the point of view of the capacity, when the expectation in (14) is taken, the contribution of $\Lambda(r_0)$ for r_0 small is negligible if compared with that at the external region of the cell, and therefore the portion of the PCL which determines the system performance is for r_0 close to 1. These considerations suggest that a more refined solution, although feasible via the simulation approach, would yield practically the same results.

A comparison between the optimal PCL's for block codes and convolutional codes, as plotted in Figs. 2 and 3, respectively, shows that the optimal PCL's are very close to each other. This fact suggests that a PCL of the form (32) could be used for the block codes as well. And in fact, as it is shown in Fig. 7, this yields an error probability fairly constant with r_0, as for the convolutional code (Fig. 6). The difference is that, in the case of convolutional codes, the PCL tends to priviledge the users close to the BS, whereas, in the case of block codes, it tends to priviledge the users on the boundary of the cell. However, the difference in performance is very small.

5 Sensitivity Analysis

In this section, we study the sensitivity of the results obtained to both the number of interfering cells considered and to the propagation exponent, η. For simplicity, we illustrate the results for the block codes only, for which a completely analytical approach is feasible. The sensitivities to the presence of noise, W_0, and to the degree of orthogonality of the intracell interfering sequences, γ, have already been discussed in the previous section.

5.1 Number of Cells

Often, in the literature, only few cells are considered as a source of interference. We chose to include two tiers (i.e., 18 cells), following [2]. Considering fewer cells, e.g., the first tier only (i.e., 6 cells), or even only the 4 closest cells, as in [8], gives optimistic results. To quantify this, we computed the system utilization in both the above cases; the results are compared in Table IV. For $\gamma = 0$, when 6 and 4 cells, instead of 18, are considered, the utilization obtained is 11% and 16% higher, respectively, than what it is when 18 cells are considered.

5.2 Propagation power loss exponent

It is of interest to investigate the sensitivity of the results to the propagation power loss law exponent, η, since it depends on the specific environment. Table V shows the same results as before, but for various values of η. As η decreases, the performance becomes worse, since the

negative effect of stronger interfering signals outweighs the beneficial effect of a stronger intended signal. The corresponding decrease in the system capacity, limited to 8-10% for $\eta = 3.75$, can be as large as 35-40% for $\eta = 3$.

6 Conclusions

In this paper, we studied the mobile-to-base link of a cellular CDMA mobile radio system, and illustrated an analytical method to finding an optimal power control law and computing the resulting performance. This approach has proven to be most suitable for studying the coded performance when block codes are employed. For convolutional codes, the appoximations involved in the derivation of the final results make the results less accurate, even though the analysis provides insight and is qualitatively valuable, as confirmed by simulation. The results show that convolutional codes perform much better than block codes, yielding a system utilization almost three times as large. Also, we found that, in the same conditions (namely, perfectly orthogonal sequences and absence of noise), the optimal PCL can be approximated by means of a simple function of r_0, in a form holding for both block and convolutional codes. We remark that the results obtained do not take into account cell sectorization and voice activity, which are known to augment the capacity by about a factor of 6 [2]. Further investigation is required to include the effect of shadowing, which is particularly significant in metropolitan areas.

Appendices

A Derivation of Eq. (12)

In (9), the $\alpha_j^2, j = 0, \ldots, 18$ are independent and exponentially distributed r.v.'s with unit mean, whose distribution and density functions are, respectively,

$$F_{\alpha_j^2}(x) \triangleq P[\alpha_j^2 \leq x] = 1 - e^{-x} \tag{34}$$

and

$$f_{\alpha_j^2}(x) = e^{-x}. \tag{35}$$

Conditioned on the $\{r_j\}$, all other terms in (9) are deterministic. Therefore, the distribution function of ν is computed as follows:

$$F_\nu(a) \triangleq P[\nu \leq a] = P\left[\frac{\alpha_0^2}{W + \sum_{j=1}^{18} \alpha_j^2 \left(\frac{r_j}{r_0}\right)^{-\eta}} \geq \frac{1}{a}\right]$$

$$= \int_0^\infty dx_1 e^{-x_1} \ldots \int_0^\infty dx_{18} e^{-x_{18}} \exp\left[-\frac{1}{a}\left(W + \sum_{j=1}^{18} x_j \left(\frac{r_j}{r_0}\right)^{-\eta}\right)\right]$$

$$= e^{-W/a} \prod_{j=1}^{18} \int_0^\infty \exp\left[-\left(1 + \frac{1}{a}\left(\frac{r_j}{r_0}\right)^{-\eta}\right) x_j\right] dx_j.$$

This last expression yields Eq. (12).

B Derivation of Eq. (22)

In a block of length n there are $\lfloor n/2 \rfloor$ pairs of bits (this would be exactly true for n even, is an approximation for n odd); as in [5], we assume that the two bits in a pair fade identica whereas all pairs fade independently of each other. We denote by p_1 and p_2 the probabilities t one or both bits in a pair are detected erroneously, respectively. Therefore, i errors in a block c originate from different combinations of single and double errors. More precisely, we have

$$P[i \text{ errors in a block}] = \sum_{k=0}^{\lfloor i/2 \rfloor} P[k \text{ double errors and } (i-2k) \text{ single errors}]. \qquad (3$$

The error pattern in a block can be modeled by means of generalized Bernoulli trials [14], wit. probabilities

$$P[k_1 \text{ double errors and } k_2 \text{ single errors}] =$$

$$= \frac{\lfloor n/2 \rfloor !}{k_1!\, k_2!\, (\lfloor n/2 \rfloor - k_1 - k_2)!}\, p_2^{k_2}\, p_1^{k_1}\, (1 - p_1 - p_2)^{\lfloor n/2 \rfloor - k_1 - k_2}. \qquad (38)$$

Therefore, the error probability can be approximated as

$$P_b(p) \simeq \sum_{i=t+1}^{n} \frac{i}{n} P[i \text{ errors in the block}] \qquad (39)$$

which, using (37) and (38), yields Eq. (22).

References

[1] R.L. Pickholtz *et al.*, "Spread spectrum for mobile communications", *IEEE Trans. Veh. Tech.*, vol. VT-40, pp. 313-322, May 1991.

[2] K.S. Gilhausen *et al.*, "On the capacity of a cellular CDMA system", *IEEE Trans. Veh. Tech.*, vol. VT-40, pp. 303-312, May 1991.

[3] W.C.Y. Lee, "Overview of cellular CDMA", *IEEE Trans. Veh.* May 1991.

[4] L.B. Milstein *et al.*, "Performance evaluation for cellular CD *Commun.*, vol. SAC-10, pp. 680-689, May 1992.

[5] B.R. Vojcic *et al.*, "On the performance of CDMA operating over a link", submitted to *IEEE J. Select. Areas Commun.*

[6] G.L. Stuber, C. Kchao, "Analysis of a multiple-cell direct-seque radio", *IEEE J. Select. Areas Commun.*, vol. SAC-10, pp. 669-679

[7] R.V. Nettleton, H. Alavi, "Power control for a spread spectrum cell in *Proc. 33rd IEEE Veh. Tech. Conf.*, Toronto, ON, 1983, pp.242-2

[8] R.R. Gejji, "Forward-link-power control in CDMA cellular systems" vol. VT-41, pp. 532-536, Nov. 1992.

[9] M.B. Pursley, "Performance evaluation for phase-coded spread spect munication, Part I: System analysis," *IEEE Trans. Commun.*, vol. C(1977.

[10] M. Zorzi, S. Pupolin, "Performance of Slotted Aloha in fading chann *IEEE Trans. Veh. Tech.*

[11] G.C. Clark, J.B. Cain, *Error-correction coding for digital communicati* Press, 1981.

[12] J.G. Proakis, *Digital communications*, 2nd edition. New York: McGrav

[13] J. Conan, "The weight spectra of some short low-rate convolutional *Commun.*, vol. COM-32, pp. 1050-1053, Sep. 1984.

[14] A. Papoulis, *Probability, random variables and stochastic processes*, 2n McGraw-Hill, 1984.

Figures and Tables

Fig. 1: System utilization, ρ, vs. the rate of the block code, R_c, for block length $n = 63, 127, 255$, $\eta = 4$; perfect interleaving, no noise. (a) $\gamma = 0$, (b) $\gamma = 0.1$.

Fig. 2: Optimal $\varphi(r_0)$, vs. r_0, for the (255,47) BCH code. $\eta = 4$, perfect interleaving, $\gamma = 0$, no noise.

Fig. 3: Optimal power control law for the approximate analysis of the convolutional codes, $\varphi(r_0)$, vs. r_0. $\eta = 4$, perfect interleaving, $\gamma = 0$, no noise.

Fig. 4: Performance of the convolutional code of rate 1/3 and constraint length 8, vs. the parameter Γ; approximate analysis, optimal power control law; $\eta = 4$, $\gamma = 0$, perfect interleaving, no noise.

Fig. 5: Performance of the convolutional code of rate 1/3 and constraint length 8 at the boundary of the cell, vs. the parameter Γ; simulation results, optimal power control law, $\eta = 4$, perfect interleaving, $\gamma = 0$, no noise.

Fig. 6: BER of the convolutional code of rate 1/3 and constraint length 8 vs. the location of the mobile, r_0, for some values of Γ; simulation results, approximate power control law, $\eta = 4$, $\gamma = 0$, perfect interleaving, no noise.

Fig. 7: BER of the (255,47) BCH code vs. the location of the mobile, r_0, when the approximate PCL is used; $\eta = 4$, $\gamma = 0$, perfect interleaving, no noise.

Tab. I: Maximum system utilization, ρ, for different values of γ, with perfect and imperfect interleaving, and with no interleaving. BCH codes, $\eta = 4$, no noise.

Tab. II: Maximum system utilization, ρ, in the presence of noise, for different values of γ and W_0, with perfect and imperfect interleaving, BCH codes, $\eta = 4$.

Tab. III: Maximum system utilization, ρ, of the convolutional code of rate 1/3 and constraint length 8 (approximate approach and simulation), and maximum performance for BCH codes compared. Perfect interleaving, $\eta = 4$, $\gamma = 0$, no noise.

Tab. IV: Sensitivity of ρ, to the number of interfering cells considered: 18 cells (two whole tiers), 6 cells (first tier only), 4 cells (4 closest cells of the first tier). BCH codes, different values of γ, with perfect and imperfect interleaving, $\eta = 4$, no noise.

Tab. V: Sensitivity of ρ, to the propagation exponent, η. BCH codes, different values of γ, perfect interleaving, no noise.

Table I

	perfect interleaving	imperfect interleaving
$\gamma = 0$	32.7%	31.4%
$\gamma = 0.01$	32.5%	31.3%
$\gamma = 0.1$	29.8%	28.2%

Table II

	perfect interleaving			imperfect interleaving		
	$W_0 = 1$	$W_0 = 0.1$	$W_0 = 0.01$	$W_0 = 1$	$W_0 = 0.1$	$W_0 = 0.01$
$\gamma = 0$	20.2%	30.8%	32.5%	19.5%	29.6%	31.3%
$\gamma = 0.01$	20.2%	30.6%	32.4%	19.5%	29.5%	31.1%
$\gamma = 0.1$	19.1%	28.2%	29.6%	18.4%	27.2%	28.6%

Table III

convolutional code (approximate)	convolutional code (simulation)	block code
114%	92%	32.7%

Table IV

	perfect interleaving			imperfect interleaving		
	18 cells	6 cells	4 cells	18 cells	6 cells	4 cells
$\gamma = 0$	32.7%	36.4%	37.9%	31.4%	35.0%	36.3%
$\gamma = 0.01$	32.5%	36.2%	37.6%	31.3%	34.8%	36.1%
$\gamma = 0.1$	29.8%	32.8%	34.0%	28.8%	31.7%	32.8%

Table V

	$\eta = 3$	$\eta = 3.5$	$\eta = 3.75$	$\eta = 4$
$\gamma = 0$	20.5%	26.6%	29.7%	32.7%
$\gamma = 0.01$	20.5%	26.5%	29.5%	32.5%
$\gamma = 0.1$	19.3%	24.6%	27.2%	29.8%

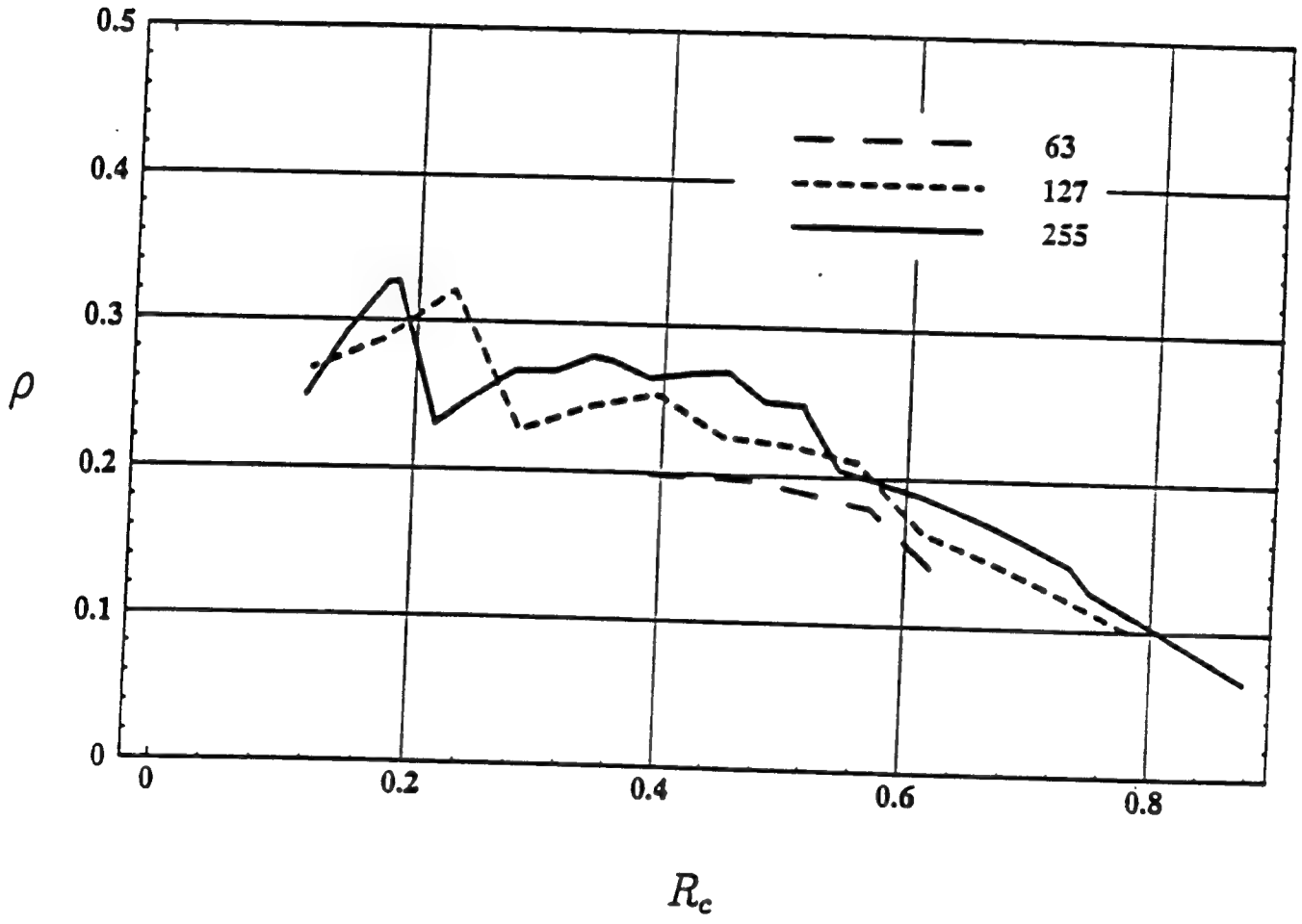

Fig. 1a: System utilization, ρ, vs. the rate of the block code, R_c, for block length $n = 63, 127, 255$, $\eta = 4$; perfect interleaving, no noise, $\gamma = 0$.

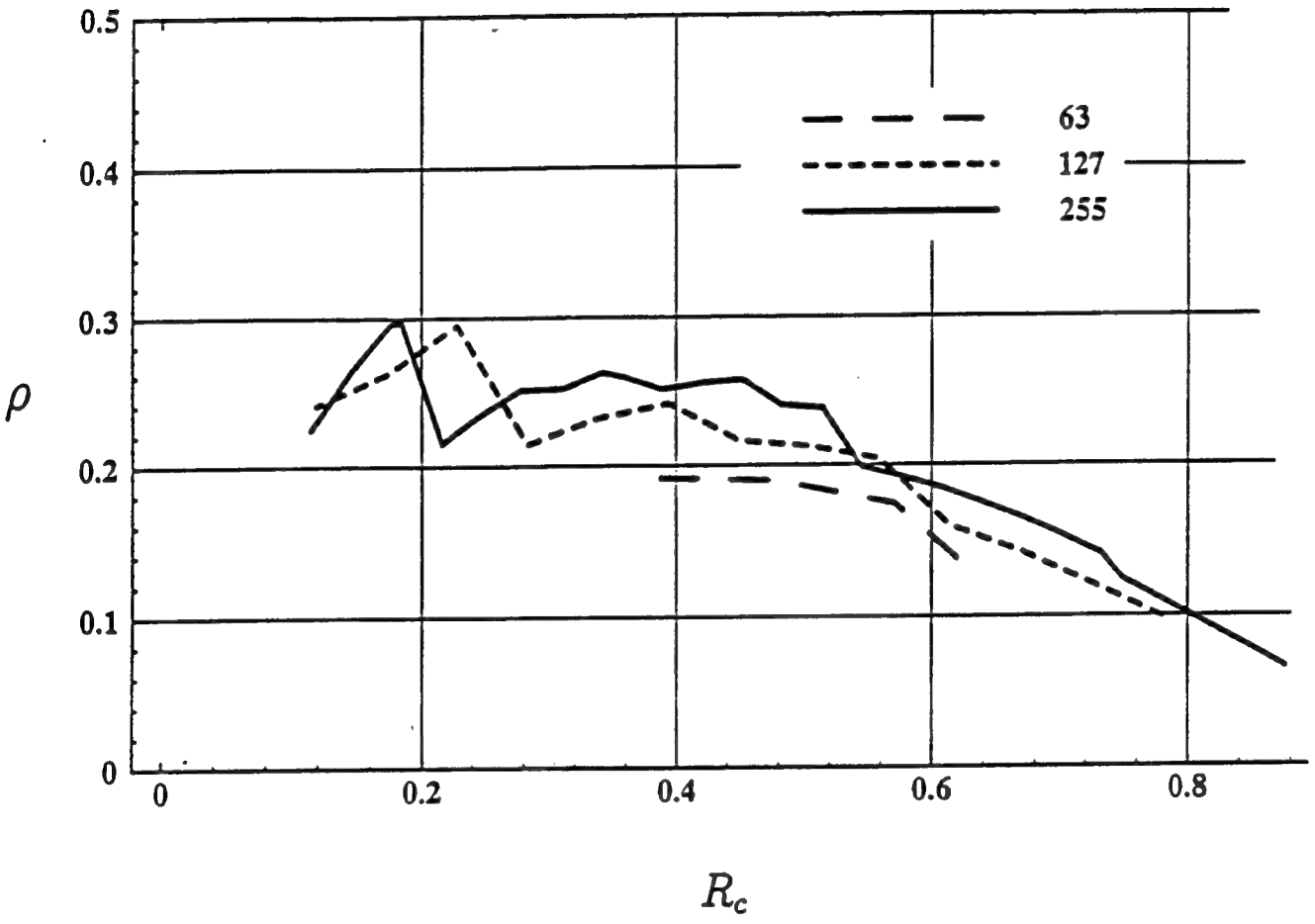

Fig. 1b: System utilization, ρ, vs. the rate of the block code, R_c, for block length $n = 63, 127, 255$, $\eta = 4$; perfect interleaving, no noise, $\gamma = 0.1$.

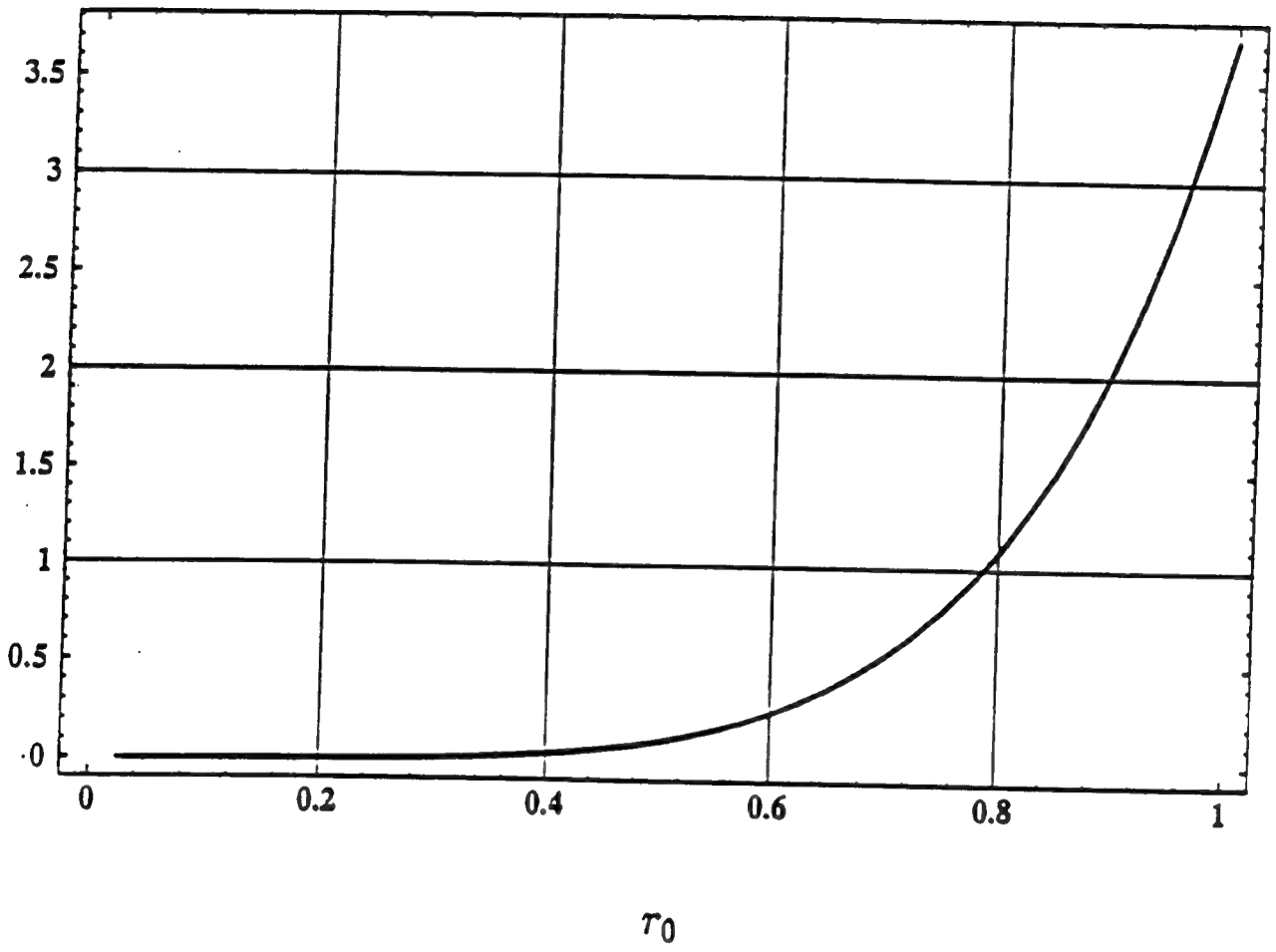

Fig. 2: Optimal $\varphi(r_0)$, vs. r_0, for the (255,47) BCH code. $\eta = 4$, perfect interleaving, $\gamma = 0$, no noise.

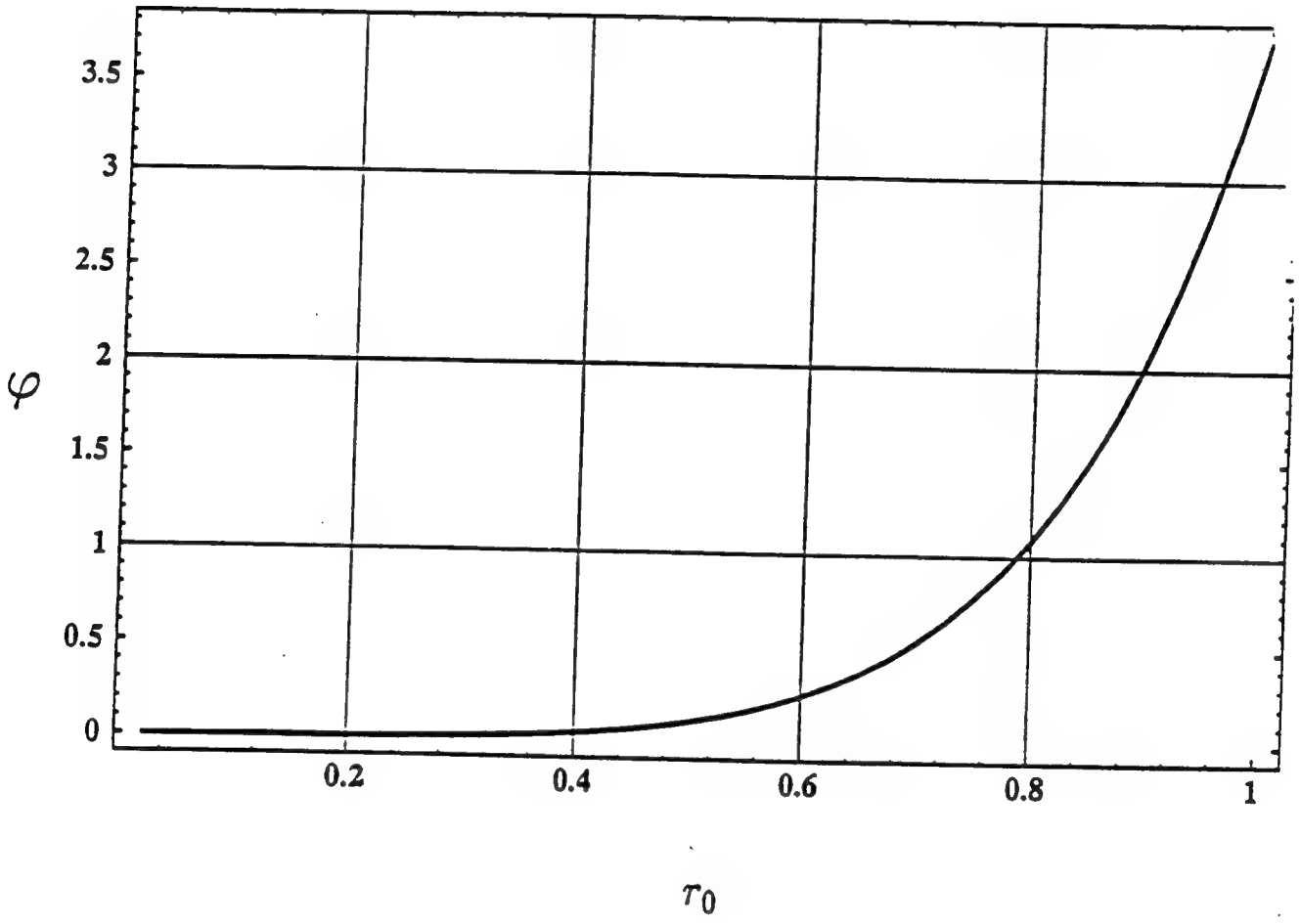

Fig. 3: Normalized optimal power control law for the approximate analysis of the convolutional codes, $\varphi(r_0)$, vs. r_0. $\eta = 4$, perfect interleaving, $\gamma = 0$, no noise.

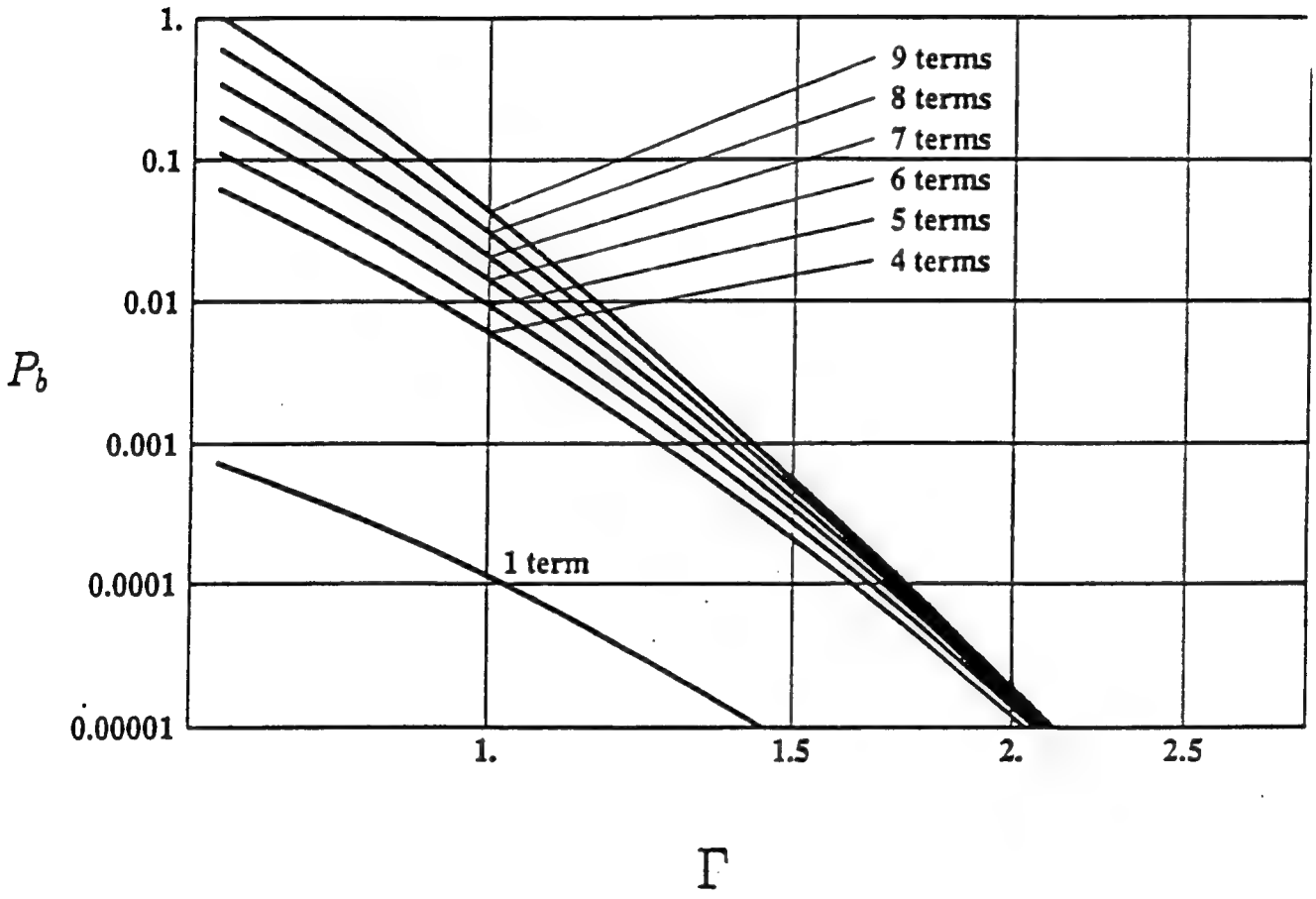

Fig. 4: Performance of the convolutional code of rate 1/3 and constraint length 8, vs. the parameter Γ; approximate analysis, optimal power control law; $\eta = 4$, $\gamma = 0$, perfect interleaving, no noise.

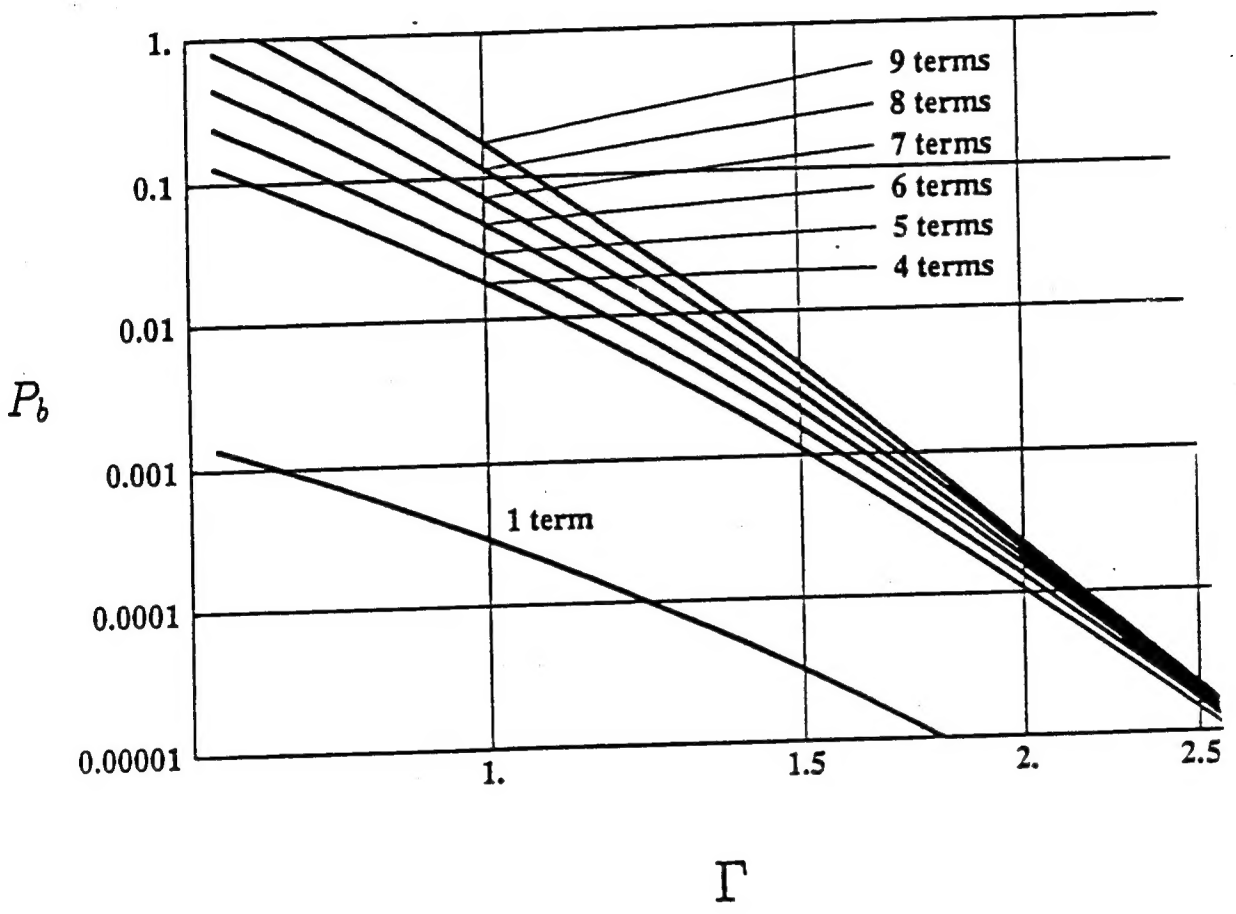

Fig. 5: Performance of the convolutional code of rate 1/3 and const. length 8 at the boundary of the cell, vs. the parameter Γ; simulation res optimal power control law, $\eta = 4$, perfect interleaving, $\gamma = 0$, no noise.

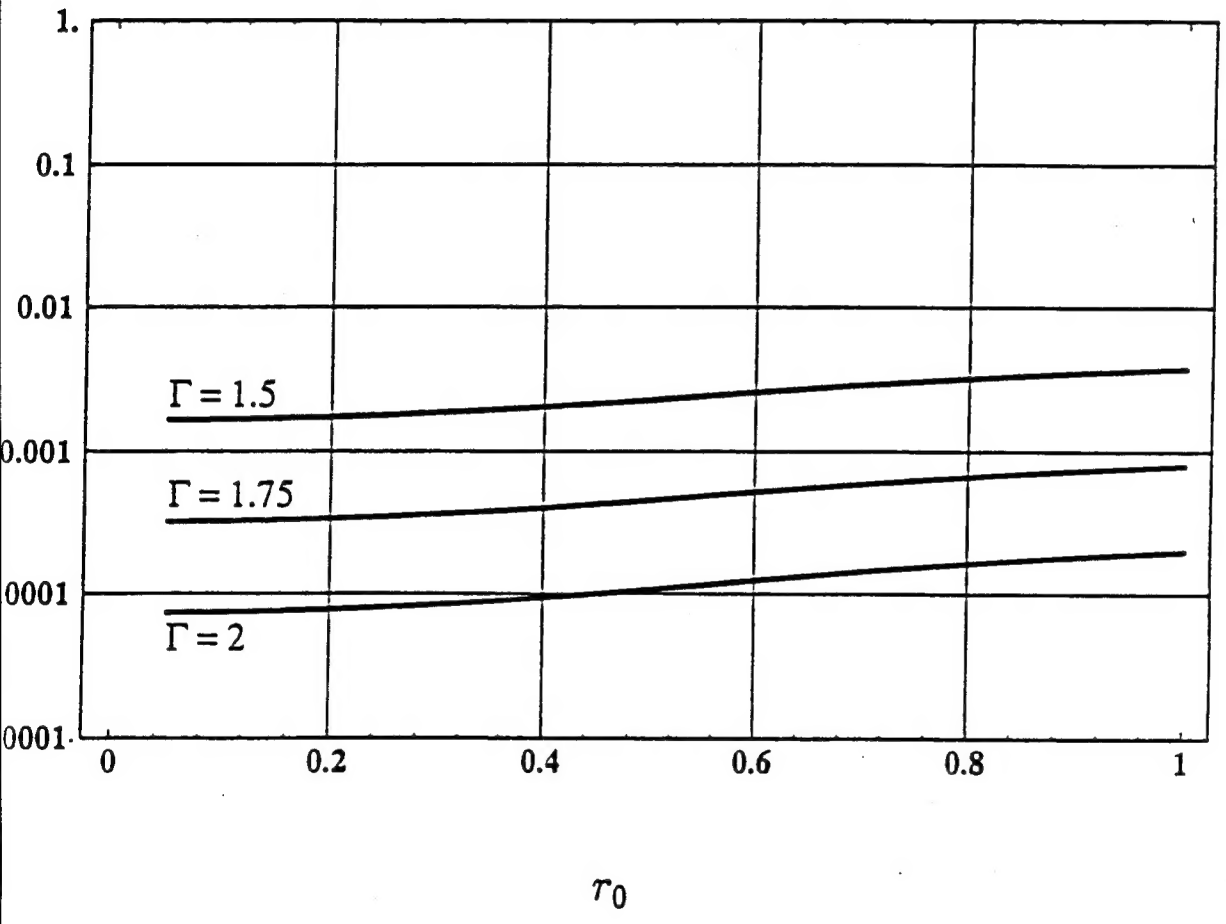

g. 6: BER of the convolutional code of rate 1/3 and constraint length 8 the location of the mobile, r_0, for some values of Γ; simulation results, proximate power control law, $\eta = 4$, $\gamma = 0$, perfect interleaving, no noise.

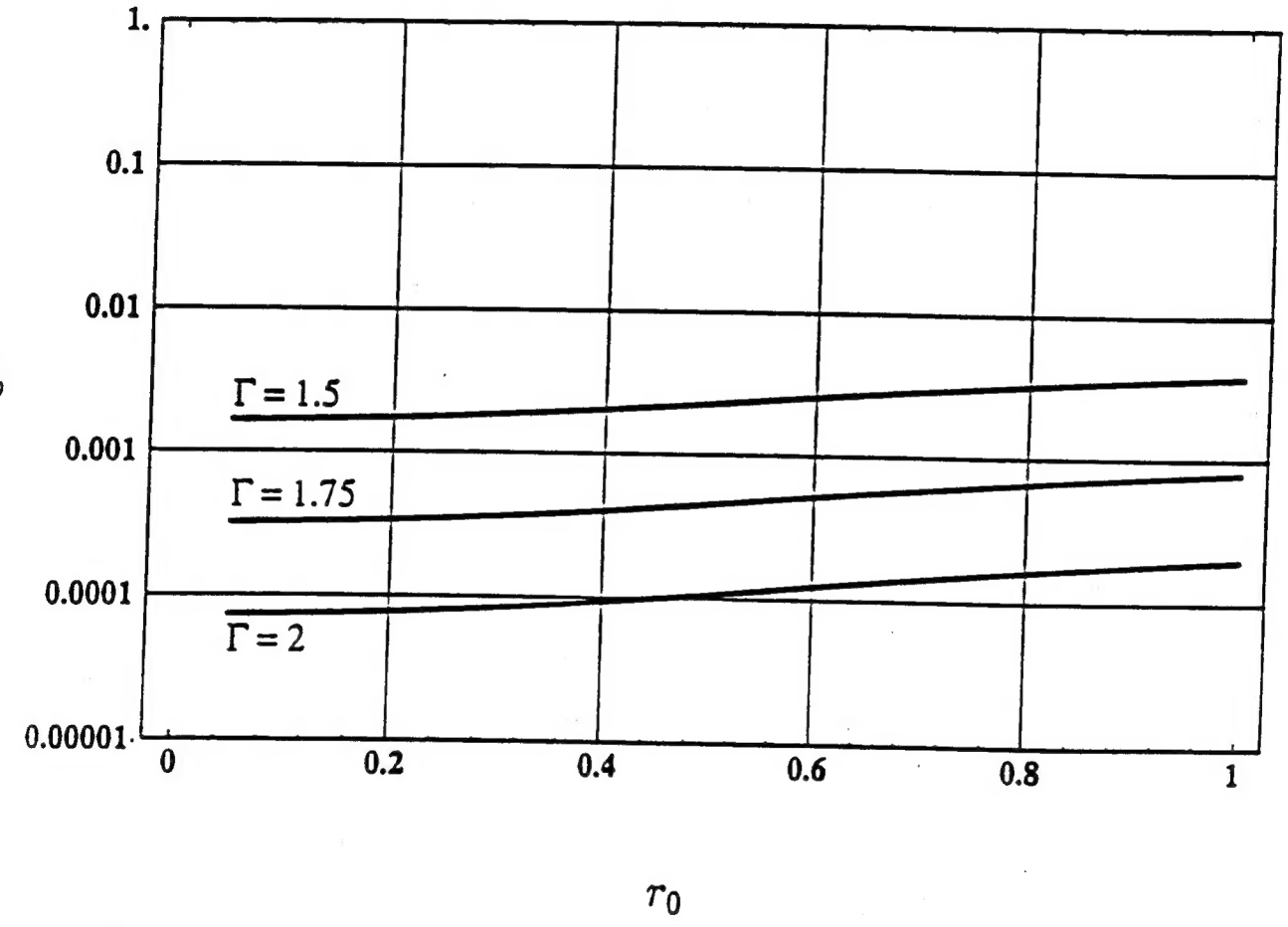

Fig. 6: BER of the convolutional code of rate 1/3 and constraint length 8 vs. the location of the mobile, r_0, for some values of Γ; simulation results, approximate power control law, $\eta = 4$, $\gamma = 0$, perfect interleaving, no noise.

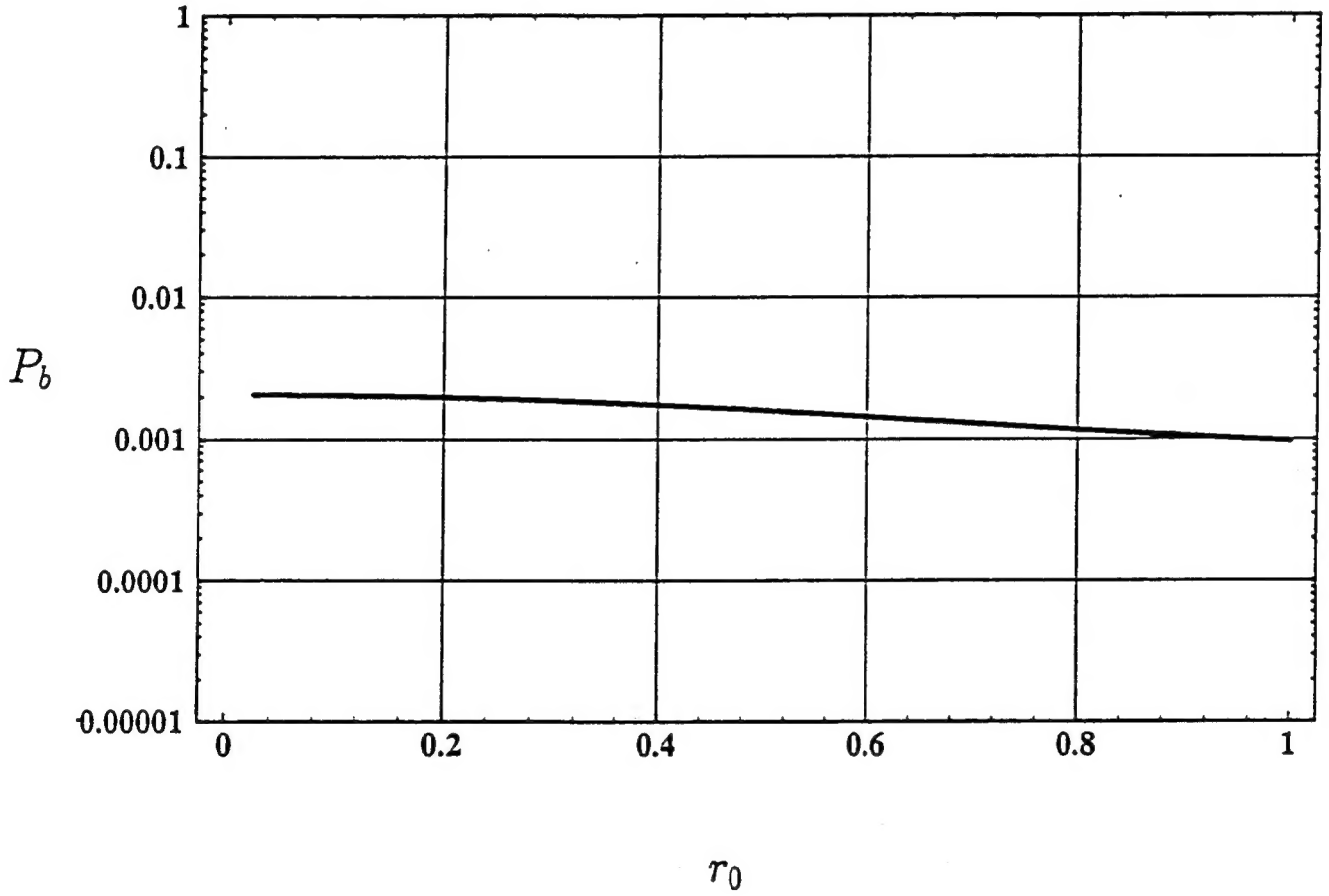

Fig. 7: BER of the (255,47) BCH code vs. the location of the mobile, r_0, when the approximate PCL is used; $\eta = 4$, $\gamma = 0$, perfect interleaving, no noise.